Oxidative Medicine and Cellular Longevity

Metal and Metalloid-Induced Oxidative Damage: Biological Importance of Potential Antioxidants

Lead Guest Editor: Maria F. H. Carneiro
Guest Editors: Gustavo R. M. Barcelos, Fernando Barbosa Jr., Joseph Adeyemi, and Glenda Gobe

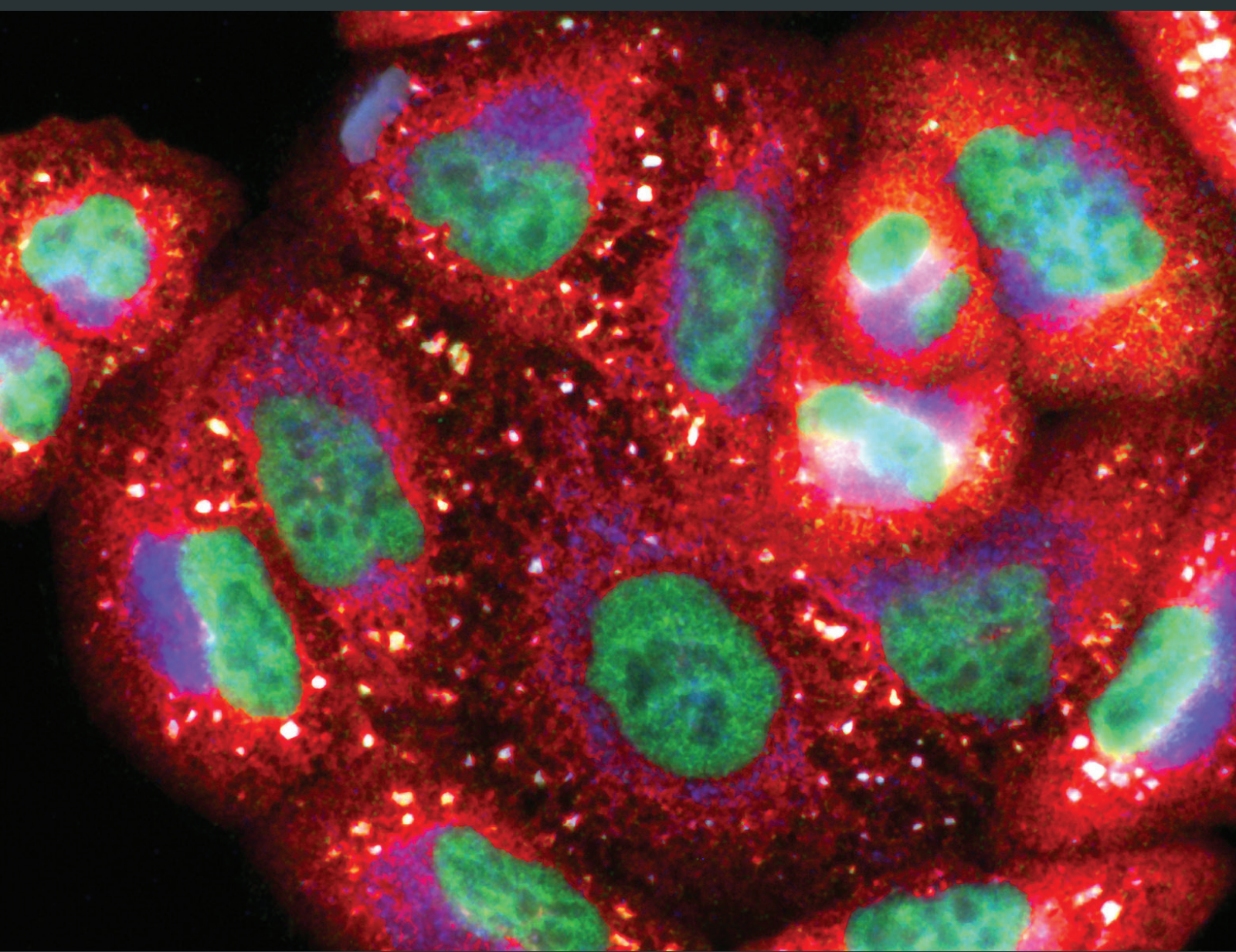

Metal and Metalloid-Induced Oxidative Damage: Biological Importance of Potential Antioxidants

Oxidative Medicine and Cellular Longevity

Metal and Metalloid-Induced Oxidative Damage: Biological Importance of Potential Antioxidants

Lead Guest Editor: Maria F. H. Carneiro
Guest Editors: Gustavo R. M. Barcelos, Fernando Barbosa Jr., Joseph Adeyemi, and Glenda Gobe

Editorial Board

Contents

Hindawi
Oxidative Medicine and Cellular Longevity
Volume 2018, Article ID 3586071, 2 pages
https://doi.org/10.1155/2018/3586071

Editorial

Metal and Metalloid-Induced Oxidative Damage: Biological Importance of Potential Antioxidants

Maria Fernanda Hornos Carneiro,[1] **Gustavo Rafael Mazzaron Barcelos**,[2] **Fernando Barbosa Jr.**,[1] **Joseph Adeyemi**,[3] **and Glenda Gobe**[4]

[1]*Department of Clinical Analysis, Toxicology and Food Science, School of Pharmaceutical Sciences of Ribeirao Preto, University of Sao Paulo, Ribeirão Preto, SP, Brazil*
[2]*Department of Biosciences, Institute of Health and Society, Federal University of Sao Paulo, Santos, SP, Brazil*
[3]*Department of Biology, School of Sciences, Federal University of Technology, Akure, Ondo State, Nigeria*
[4]*Kidney Disease Research Collaborative, Translational Research Institute, School of Biomedical Sciences, Faculty of Medicine, NHMRC CKD.QLD CRE, Royal Brisbane and Women's Hospital, University of Queensland, Brisbane, QLD, Australia*

Correspondence should be addressed to Maria Fernanda Hornos Carneiro; mafehoca@fcfrp.usp.br

Received 24 June 2018; Accepted 24 June 2018; Published 25 July 2018

A general disregard by industries and big corporations for the environment has meant that the natural environment has repeatedly been polluted, jeopardizing the well-being of all living organisms. The toxic effects of metals and metalloids have been recognized for quite some time to generate several free radicals and other reactive species that lead to cellular oxidative stress. Metals and metalloids are toxic elements at the top of the priority list of hazardous substances of the Agency for Toxic Substances and Disease Registry (ATSDR). Gaps of knowledge still exist that are related to their toxicity, mainly concerning the mechanisms of action. Due to their extreme potential to cause oxidative damage, the structural, functional, biochemical, and molecular effects of metals and metalloids on oxidative stress need description, and the identification of new potential competitive-protective agents is imperative. This special issue brings together the results of six papers covering several aspects of the toxicology of metals and metalloids in *in vitro* and *in vivo* experimental models. They provide a deeper understanding of the mechanisms involved in metal and metalloid toxicity and highlight the need to develop strategies to decrease exposure to metals, as well as identify substances that may help overcome the hazardous effects within the living body.

Carnosic acid, a natural benzenediol abietane diterpene found in rosemary (*Rosmarinus officinalis),* was explored to rescue the arsenite-induced oxidative stress in hepatic cells in *in vitro* and *in vivo* models in the study of S. Das et al. Carnosic acid was able to significantly rescue the activation of MAPK, NF-κB, p53, and intrinsic and extrinsic apoptotic signaling seen in arsenite-exposed hepatic cells. Carnosic acid could also significantly counteract with redox stress and ROS-mediated signaling, thereby attenuating arsenite-mediated hepatotoxicity. Other effects, such as arsenic bioaccumulation, DNA fragmentation, and hematological changes, were also reverted in models after coadministration with carnosic acid. The authors attributed the rescue to the antioxidant potential of carnosic acid which in their view had the potential to be a new therapeutic agent to counteract with arsenite-mediated toxic manifestations. In the same way, the study of A. Officioso et al. compared the beneficial effects of olive oil phenol hydroxytyrosol (HT) and 5-*S*-lipoylhydroxytyrosol (Lipo-HT) on oxidative alterations of human erythrocytes induced by exposure to inorganic mercury. Both HT and Lipo-HT decreased Hg-induced generation of ROS, hemolysis, and the depletion of intracellular GSH levels. At all doses tested, Lipo-HT exhibited a higher ability

to counteract Hg-induced cytotoxicity compared to HT. To explain that, the authors propose a model where Lipo-HT is more effective to chelate mercury ions and encourage the use of Lipo-HT in nutraceutical strategies to counteract heavy metal toxicity in humans.

Obesity- or diabetes-induced oxidative stress is discussed as a major risk factor for DNA damage. What has not been addressed yet is how vitamin E and many polyphenols exhibit antioxidative activities with consequences on epigenetic regulation of inflammation and DNA repair. To shed light on that, the study of K. Zappe et al. investigated the counteraction of oxidative stress by vitamin E in the colorectal cancer cell line Caco-2 under normal- and high-glucose cell culture condition. Results revealed a dose-dependent counteracting effect of vitamin E on malondialdehyde levels. Also, an induction in the expression of the genes of DNA repair *MutL homolog (MLH1)* and the *DNA methyltransferase 1 (DNMT1)* was noticed, accompanied by an increase in global methylation by LINE-1. The authors suggest that vitamin E supplementation has a high potential for treatment and might even be used as a possible approach in the prevention of diseases caused by obesity and diabetes.

Cadmium is one of the most poisonous environmental chemicals, causing toxicity in humans and experimental animals. The study of M. C. Cupertino et al. investigated the relationship between germ and Leydig cell death, testosterone, and adiponectin levels in cadmium-mediated acute toxicity. Dose-dependent cadmium accumulation in testes was identified. At the highest doses of exposure, animals exhibited marked inflammatory infiltrate and disorganization of the seminiferous epithelium. Although Leydig cells were morphologically resistant to Cd toxicity, massive germ cell death, DNA oxidation, and fragmentation were observed. Also, testosterone and adiponectin levels were significantly decreased by cadmium. The authors discuss the mechanisms behind the findings, but why germ cells are a primary target of cadmium-induced toxicity while Leydig cells remain resistant to death even when exposed to higher doses of this metal is still unclear.

Despite the undoubted advantages of titanium bone fixations such as high biotolerance, favorable mechanical properties, and osseointegration ability, their negative impact on the human body, both at the implant site and at the systemic level, is still debated. To contribute to the toxicological background in this emergent area, the study of J. Borys et al. evaluated the influence of Ti6Al4V titanium alloy on redox balance and oxidative damage in the periosteum surrounding the titanium miniplates and screws as well as in plasma and erythrocytes of patients with mandibular fractures. The occurrence of a redox imbalance as well as oxidative damage in the periosteum surrounding the Ti6Al4V titanium alloy was demonstrated. Changes in antioxidant potential in the patients treated with titanium implants were also observed in the plasma/erythrocytes. Results indicate the need to improve the miniplates and screws used for osteosynthesis by increasing the thickness of the passive TiO_2 layer or using new, biodegradable, and more biocompatible materials. The authors also suggest that supplementation with antioxidants could be tested as a therapeutic procedure in patients treated with titanium fixations.

Finally, S. R. Lee critically reviewed the role of zinc as either an antioxidant or a prooxidant. For instance, it functions as an antioxidant through the catalytic action of copper/zinc-superoxide dismutase, stabilization of membrane structure, protection of the protein sulfhydryl groups, and upregulation of the expression of metallothionein, which possesses a metal-binding capacity and exhibits antioxidant functions. Also, zinc can suppress anti-inflammatory responses that would otherwise augment oxidative stress. On the other hand, zinc deficiency and zinc excess cause cellular oxidative stress. The conditions behind the dual actions of zinc and the oxidative imbalance that occurs in zinc deficiency and zinc overload in conjunction with the intracellular regulation of free zinc are summarized in this review.

We hope that the new findings on the toxicity of metals and metalloids as well as on the identification of protective agents presented in this special edition can contribute to the development of science, to the environmental and health regulatory agency policies, and to more effective strategies to rescue toxicity.

Acknowledgments

We thank all the referees that have contributed their time and scientism to this special issue.

Maria Fernanda Hornos Carneiro
Gustavo Rafael Mazzaron Barcelos
Fernando Barbosa Jr.
Joseph Adeyemi
Glenda Gobe

Hindawi
Oxidative Medicine and Cellular Longevity
Volume 2018, Article ID 3714725, 10 pages
https://doi.org/10.1155/2018/3714725

Clinical Study

Exposure to Ti4Al4V Titanium Alloy Leads to Redox Abnormalities, Oxidative Stress, and Oxidative Damage in Patients Treated for Mandible Fractures

Jan Borys,[1] Mateusz Maciejczyk,[2] Bożena Antonowicz,[3] Adam Krętowski,[4] Danuta Waszkiel,[5] Piotr Bortnik,[1] Katarzyna Czarniecka-Bargłowska,[1] Magdalena Kocisz,[5] Julita Szulimowska,[6] Marek Czajkowski,[7] Napoleon Waszkiewicz,[8] and Anna Zalewska[5]

[1]*Department of Maxillofacial and Plastic Surgery, Medical University of Bialystok, Sklodowskiej M.C. 24, 15-274 Bialystok, Poland*
[2]*Department of Physiology, Medical University of Bialystok, Mickiewicza 2c Str., 15-233 Bialystok, Poland*
[3]*Department of Oral Surgery, Medical University of Bialystok, Sklodowskiej M.C. 24a Str., 15-276 Bialystok, Poland*
[4]*Clinical Research Centre, Medical University of Bialystok, Sklodowskiej M.C. 24a Str., 15-276 Bialystok, Poland*
[5]*Department of Conservative Dentistry, Medical University of Bialystok, Sklodowskiej M.C. 24a Str., 15-276 Bialystok, Poland*
[6]*Department of Pedodontics, Medical University of Bialystok, Sklodowskiej M.C. 24a Str., 15-276 Bialystok, Poland*
[7]*IPL Marek Czajkowski, Aleja Solidarności 6/77 Str., 15-751 Białystok, Poland*
[8]*Department of Psychiatry, Medical University of Bialystok, Brodowicza 1, 16-070 Choroszcz, Poland*

Correspondence should be addressed to Mateusz Maciejczyk; mat.maciejczyk@gmail.com

Received 16 December 2017; Revised 8 May 2018; Accepted 17 May 2018; Published 14 June 2018

Academic Editor: Gustavo R. M. Barcelos

Due to the high biotolerance, favourable mechanical properties, and osseointegration ability, titanium is the basic biomaterial used in maxillofacial surgery. The passive layer of titanium dioxide on the surface of the implant effectively provides anticorrosive properties, but it can be damaged, resulting in the release of titanium ions to the surrounding tissues. The aim of our work was to evaluate the influence of Ti6Al4V titanium alloy on redox balance and oxidative damage in the periosteum surrounding the titanium miniplates and screws as well as in plasma and erythrocytes of patients with mandibular fractures. The study included 31 previously implanted patients (aged 21–29) treated for mandibular fractures and 31 healthy controls. We have demonstrated increased activity/concentration of antioxidants both in the mandibular periosteum and plasma/erythrocytes of patients with titanium mandibular fixations. However, increased concentrations of the products of oxidative protein and lipid modifications were only observed in the periosteum of the study group patients. The correlation between the products of oxidative modification of the mandible and antioxidants in plasma/erythrocytes suggests a relationship between the increase of oxidative damage at the implantation site and central redox disorders in patients with titanium miniplates and screws.

1. Introduction

Jaw bone fractures are a frequent and significant problem in clinical practice. The most common types of injuries are mandibular fractures that lead to morphological and functional disorders of the stomatognathic system as well as aesthetic defects of the facial skeleton. The treatment of mandibular fractures is aimed at reconstructing the anatomical shape of the bones and occlusion from before the injury and restoring normal functions of the chewing organ and facial aesthetics [1]. The use of internal bone fixation systems with miniplates and screws allows not only to avoid long-term intermaxillary immobilization and dental splint insertion, which are troublesome for the patient, but also to cure fractures in case of contraindications for inoperative orthopaedic treatment [1]. Miniplates and screws made of titanium, due to the high biocompatibility of this metal and its alloys used in the production of such fixations, are commonly used in traumatology, maxillofacial oncology, and orthognathic surgery. Despite the undoubted advantages of

titanium bone fixations, their negative impact on the human body, both at the implant site and at the systemic level, is still debated [1, 2]. During the removal of titanium bone fixations, the presence of discoloured gray tissues surrounding the miniplates and screws was often observed [3, 4]. Some patients have also suffered from inflammatory symptoms around the anastomosis sites reported postoperatively both after several months and even years after osteosynthesis of the fractured mandible. Therefore, it is important to explore the impact of titanium miniplates and screws on the surrounding tissues [2]. The results of recent studies indicate that the cause of chronic inflammation around titanium bone fixations may be the increased production of oxygen-free radicals and reactive nitrogen species (RNS) [3, 5–7]. It is believed that overproduction of reactive oxygen species (ROS) and RNS can lead to the damage of cellular components by oxidation, thereby impairing normal cell functioning as a result of increased synthesis of proinflammatory mediators and affecting growth, differentiation, and apoptosis processes in the cells [8].

Although oxidative stress is one of the mechanisms of titanium toxicity [9], the kind (and extent) of oxidative damage it can cause is still unknown. What is more, the literature on the subject so far has not offered any study evaluating the effect of titanium bone fixation systems in patients with mandibular fractures on the redox balance both at the implant site and at the systemic level. Therefore, the aim of our work was to evaluate enzymatic and nonenzymatic antioxidant systems and oxidative damage of proteins, lipids, and DNA in the periosteum surrounding the bone fixations as well as in plasma and erythrocytes of patients treated for mandible fractures, compared to the control group.

2. Materials and Methods

2.1. Patients. The protocol of the study was approved by the Bioethics Committee of the Medical University of Bialystok, Poland (permission number R-I-002/3/2-16).

62 patients operated at the Department of Maxillofacial and Plastic Surgery, Medical University in Bialystok, Poland, were enrolled in the study. The study group included 31 previously implanted patients (11 women and 20 men aged 21–29, mean age: 24 years and 7 months) treated for mandibular fractures. The causes of the fractures in patients were beating (61.2%), sports (19.4%), traffic accident (12.9%), and fall from the stairs (6.5%). All patients were treated for bilateral fracture of the mandibular body. The fractured bone fragments in the mandible were fixed with two 4- or 6-hole miniplates and 4–6 screws (on the right and left side): in total 4 miniplates and 16–24 screws (MEDGAL Sp. z o.o., Księżyno, Poland).

Two months after implantation (every 2 weeks), and then, every month until the fixations were removed, the patients went to the hospital for follow-up examinations performed by one qualified surgeon (J.B.). In all patients from the study group, there were no signs of acute and chronic inflammation such as edema, inflammatory infiltration, purulent fistula, and redness of the mucous membrane or skin around the titanium fixations. In the physical examination, no enlargement of regional lymph nodes was also observed, which did not require specialized diagnostics in these group of patients. In the study group, there were also no clinical allergy signs like edema, changes on the skin, and mucous membranes.

The control group, selected by sex and age to match the study group, consisted of 31 generally healthy patients (11 women and 20 men aged 21–29, mean age: 24 years and 2 months) operated due to dentofacial deformities, whose periosteum and blood samples were taken immediately prior to the insertion of titanium implants.

2.1.1. Inclusion Criteria: Study Group

(i) Maxillary bone fixations after treatment for fractures of the mandibular body.

2.1.2. Inclusion Criteria: Control Group

(i) Generally healthy patients with dentofacial deformities before surgical treatment.

2.1.3. Inclusion Criteria: Study and Control Group

(i) Written informed consent for participation in the study,

(ii) Age 21–29,

(iii) $18.5 \leq \text{BMI} \geq 24.5$,

(iv) No former treatment for bone fracture or jaw osteotomies performed with titanium fixations,

(v) A noninflammation-induced healing process from insertion of fixations until their removal,

(vi) No craniocerebral traumas (hematomas),

(vii) Normal results of complete blood count (WBC $4.5–8.5 \times 10^3/\mu$L; RBC $3.6–5.4 \times 10^{12}$/L; HGB 12.0–16.0 g/dL; PLT $100–450 \times 10^9$/L; hematocrit 36–54%) and biochemical blood tests (CRP 0.1–5 mg/L; Na^+ 135.0–145.0 mmol/L; K^+ 3.8–5.0 mmol/L; international normalized ratio (INR), 0.9–1.3; activated partial thromboplastin time (APTT), 37.0–46.0 sec; prothrombin time (PT), 12.0–18.0 sec),

(viii) No systemic (insulin resistance, diabetes, hypertension, and coronary heart disease) and autoimmune disorders (psoriasis, multiple sclerosis, and rheumatoid arthritis), hyperlipidemia, liver, kidney, thyroid, lung, gastrointestinal and infectious (HCV and HIV infection) diseases, or gingivitis, periodontitis, and active odontogenic infection foci,

(ix) Nonsmokers,

(x) Nonalcohol drinkers,

(xi) No intake of antibiotics, nonsteroidal anti-inflammatory drugs (NSAIDs), glucocorticosteroids, dietary supplements, and vitamins.

2.1.4. Exclusion Criteria: Study and Control Group

(i) Another type of mandibular fracture (singular fracture, fracture of mandibular ramus or condyle),

(ii) Wounds of soft tissues, injury of the skull, brain, chest, abdomen, and extremities,

(iii) Inflammatory complications and jaw synostosis disorders after implantation,

(iv) Operations due to bone fractures in the past and for other reasons during the last year.

The clinical parameters of patients and control group are presented in Table 1.

2.2. Surgical Procedure. All patients were operated by the same qualified maxillofacial surgeon (J.B.). Two months before the surgery, patients in both groups were on a diet (2000 kcal, including 55% carbohydrates, 30% fat, and 15% protein) determined by a dietician. Miniplates and screws were removed under local anaesthesia of 2% lignocaine and epinephrine (Polfa, Warsaw, Poland) from 3 to 8 months (approx. 5 months) after the surgery. The research material was a gray-pigmented periosteum adhering to the titanium miniplates excised as a standard procedure during the removal of mandibular bone fixations. In the control group, healthy periosteum was taken separately from the mandible during bimaxillary osteotomy before implantation of the miniplates and screws. Gray-pigmented periosteum was aseptic (data not shown). The tissues were immediately frozen upon collection in liquid nitrogen and stored at −80°C until assayed.

2.3. Blood (Plasma and Erythrocytes). Before the surgery and after an overnight fast, 9 mL of venous blood samples were collected in plastic EDTA tubes (S-Monovette® K3 EDTA blood collection system, Sarstedt). To separate plasma samples and erythrocytes, the samples were centrifuged at 1500 ×g (4°C, 10 min; MPW 351, MPW Med. Instruments, Warsaw, Poland). Erythrocytes were washed three times in cold solution of 0.9% NaCl (w : v) and haemolysed by the addition of cold 50 mM phosphate buffer (pH 7.4) 1 : 9 (v : v) [10]. In order to prevent sample oxidation, 0.5 M butylated hydroxytoluene (Sigma-Aldrich, Germany; 100 μL/10 mL sample) was added [11]. All samples were stored at −80°C until use.

2.4. Tissue Homogenates. Before the biochemical determinations, fragments of periosteum were rinsed in ice-cold PBS (20 mM, pH 7.0), weighed and milled into small pieces that were homogenized on ice (Omni TH, Omni International, Kennesaw, GA, USA) in ice-cold PBS (1 : 15, w : v). 0.5 M butylated hydroxytoluene (10 μL/1 mL PBS) and the protease inhibitor (Complete Mini Roche, France; 1 tablet/10 mL PBS) were added to all the samples [12]. The tissue suspensions were sonicated on ice with an ultrasonic cell disrupter (UP 400S, Hielscher, Teltow, Germany; 1800 J/sample, 20 s x 3) and centrifuged (3500 ×g, 4°C, 20 min), and the resulting supernatants were analyzed on the same day.

2.5. Antioxidant Assays. Antioxidant enzymes (glutathione peroxidase (GPx), catalase (CAT), and superoxide dismutase-1 (SOD)) and total protein were analyzed in erythrocytes and tissue homogenates, while nonenzymatic antioxidants (reduced glutathione (GSH) and uric acid (UA)) and total protein were estimated both in plasma and tissue homogenates. The absorbance in all assays was measured with Infinite M200 PRO Multimode Microplate Reader, Tecan. The assays were performed in duplicates, except for the CAT (triplicate samples). Reagents for all the assays were obtained from Sigma-Aldrich, Germany (unless noted otherwise).

The activity of GPx (EC 1.11.1.9) was assessed colorimetrically by measuring the decrease in absorbance at 340 nm wavelength as a result of NADPH (chemically reduced form of nicotinamide adenine dinucleotide phosphate) oxidation. One unit of GPx activity was defined as the amount of the enzyme needed to catalyze the oxidation of 1 mmol NADPH per minute [13]. The results were expressed in units per mg of total protein.

The activity of CAT (EC 1.11.1.6) was determined colorimetrically by measuring the rate of hydrogen peroxide (H_2O_2) degradation at 240 nm [14]. One unit of CAT activity was defined as the amount of the enzyme needed to catalyze the decomposition of 1 mmol H_2O_2 per minute. CAT determination was performed in triplicate samples and the results were expressed in nmol H_2O_2 per mg of total protein.

The activity of SOD (EC 1.15.1.1) was analyzed colorimetrically by measuring the inhibition of adrenaline oxidation at 480 nm. One unit of SOD activity was defined as the amount of the enzyme needed to inhibit adrenaline oxidation by 50% [15]. The results were expressed as mU per mg of total protein.

The concentration of GSH was estimated colorimetrically by reaction with DTNB [5,5′-dithiobis-(2-nitrobenzoic acid)] to obtain a product with absorption maximum at 412 nm [16]. The results were expressed as μg per mg of total protein.

The concentration of UA was measured colorimetrically at 490 nm by reaction with 2,4,6-tripyridyl-s-triazine using the commercial kit QuantiChromTM Uric Acid Assay Kit DIUA-250 (BioAssay Systems, Hayward, CA, USA). The results were expressed as μg per mg of total protein.

The concentration of total protein was determined colorimetrically using the commercial kit Thermo Scientific PIERCE BCA Protein Assay (Rockford, IL, USA) with bovine serum album as a standard.

2.6. Total Antioxidant/Oxidant Status. Total antioxidant/oxidant status (total antioxidant capacity (TAC), ferric reducing ability of plasma (FRAP), and total oxidant status (TOS)) and total protein content were analyzed both in the plasma and tissue homogenates. The absorbance in all assays was measured with Infinite M200 PRO Multimode Microplate Reader, Tecan. All assays were performed in duplicate samples, excluding the TAC and TOS determination (triplicate samples).

The concentration of TAC was estimated at 660 nm by ABTS + [2,2′-azino-bis-(3-ethylbenzo-thiazoline-6-sulfonate)]-based colorimetric micromethod [17]. TAC determination

Table 1: Clinical characteristics of patients with titanium mandibular fixations and healthy controls.

Serum/plasma	Control group					Study group				
	Mean	SD	Geometric mean	Lower 95% CI of mean	Upper 95% CI of mean	Mean	SD	Geometric mean	Lower 95% CI of mean	Upper 95% CI of mean
WBC $\times 10^3/\mu$L	7.530	1.958	7.278	6.841	8.219	6.917	1.709	6.756	6.315	13.232
RBC $\times 10^6/\mu$L	5.207	0.411	5.193	5.062	5.352	5.070	0.264	5.064	4.977	10.047
HGB g/dL	15.270	1.027	15.240	14.908	15.632	15.320	0.720	15.300	15.067	30.387
HCT %	45.230	2.630	45.160	44.304	46.156	45.550	2.123	45.510	44.803	90.353
MCV fL	87.140	3.817	87.070	85.796	88.484	89.630	3.549	89.570	88.381	178.011
MCHC g/dL	33.760	0.918	33.750	33.437	34.083	33.650	1.524	33.620	33.114	66.764
PLT $\times 10^3/\mu$L	230.700	43.800	227.100	215.282	246.118	228.300	23.380	227.300	220.070	448.370
PT s	12.230	0.624	12.220	12.010	12.450	11.660	0.699	11.640	11.414	23.074
INR	0.935	0.077	0.933	0.908	0.962	0.908	0.072	0.906	0.883	1.791
APTT s	27.640	1.468	27.610	27.123	28.157	26.780	3.809	26.550	25.439	52.219
Na^+ mmol/L	140.700	1.890	140.700	140.035	141.365	139.800	1.184	139.800	139.383	279.183
K^+ mmol/L	4.363	0.317	4.353	4.251	4.475	4.390	0.215	4.386	4.314	8.704
CRP mg/L	1.050	0.370	1.002	0.920	1.180	1.000	0.548	0.880	0.807	1.807

*Statistical significance $p < 0.05$, study group *versus* control.

was performed in triplicate samples, and the results were expressed as μmol Trolox equivalent per mg of total protein.

The concentration of TOS was estimated bichromatically (560/800 nm) based on the ferrous ion oxidation to ferric ion in the presence of oxidants in the sample [18]. TOS determination was performed in triplicate samples, and the results were expressed in μmol H_2O_2 equivalent per mg of total protein.

Oxidative stress index (OSI) was expressed in % according to the formula: OSI = TOS/TAC × 100% [19].

The concentration of FRAP was analyzed colorimetrically at 593 nm, measuring the ferric reducing ability of the sample by reaction with 2,4,6-tripyridyl-s-triazine [20]. The results were expressed in μmol per mg of total protein.

2.7. Oxidative Damage Determination. Oxidative damage products (advanced glycation end products (AGEs), advanced oxidation protein products (AOPP), 4-hydroxynonenal (4-HNE) protein adducts, and 8-hydroxydeoxyguanosine (8-OHdG)) and total protein content were analyzed both in plasma and tissue homogenates. The absorbance/fluorescence in all assays was measured with Infinite M200 PRO Multimode Microplate Reader, Tecan. All the assays were performed in duplicate samples.

The levels of AOPP were assessed colorimetrically at 340 nm by measuring the total iodide ion oxidizing capacity of the sample [21]. The results were expressed in μmol per mg of total protein.

The content of AGE was determined fluorimetrically at 350/440 nm in 1 : 5 diluted plasma samples and tissue homogenates [21]. The results were expressed in fluorescence per mg of total protein.

The concentration of 4-HNE protein adducts as well as 8-OHdG was measured with the commercial ELISA kit according to the manufacturer's instructions (OxiSelect™ HNE Adduct Competitive ELISA, Cell Biolabs Inc., San Diego, CA, USA; USCN Life Science, Wuhan, China, resp.). The results were expressed in μg/pg per mg of total protein.

2.8. Statistical Analysis. Statistical analysis was performed using the Statistica 10.0 system (StatSoft, Cracow, Poland) and GraphPad Prism (GraphPad Software, La Jolla, USA). The D'Agostino-Pearson test and Shapiro-Wilk test were used to examine normal distribution. Since most of the data were normally distributed, the results were presented as a mean, standard deviations, geometric mean, and 95th confidence intervals of mean. In the case of normal distribution of the results, a Student's *t*-test was used. In the lack of normal distribution of the results, the Mann–Whitney *U* test was used. The associations between the measured parameters were analyzed by Pearson's correlation. The results were assumed to be statistically significant when $p < 0.05$.

3. Results

3.1. Antioxidant Defence. CAT activity was significantly lower in mandibular periosteum and considerably higher in erythrocytes of the study group compared to the control group. SOD activity was significantly higher in patients with a mandibular fracture compared to the controls, while no statistically relevant changes were observed in erythrocytes. The concentration of UA was significantly higher both in mandibular periosteum and plasma of the study group patients than in the controls. The activity of GPx in mandibular periosteum and erythrocytes and GSH concentration in mandibular periosteum and plasma showed similar values in patients in the study and control groups (Tables 2 and 3).

3.2. Total Antioxidant/Oxidant Status. There was a statistically significant increase in TAC level in the mandibular periosteum of patients in the study group compared to healthy controls. There was also a considerable increase in TOS in the posttraumatic mandibular periosteum of study group

Table 2: Enzymatic and nonenzymatic antioxidants, antioxidant/oxidant status, and oxidative damage in the mandible (Man) of patients with titanium mandibular fixations and healthy controls.

Man	Control group					Study group				
	Mean	SD	Geometric mean	Lower 95% CI of mean	Upper 95% CI of mean	Mean	SD	Geometric mean	Lower 95% CI of mean	Upper 95% CI of mean
CAT nmol H_2O_2/min/mg protein	1.435	0.349	0.973	1.312	2.747	0.605*	0.139	0.272	0.556	1.160
SOD mU/mg protein	136.500	20.240	119.400	129.375	265.875	282.000*	44.750	175.200	266.247	548.247
GPx IU/mg protein	0.024	0.003	0.022	0.022	0.046	0.027	0.006	0.025	0.025	0.052
UA μg/mg protein	0.155	0.024	0.125	0.146	0.301	0.285*	0.040	0.234	0.271	0.556
GSH μg/mg protein	1.496	0.299	1.178	1.391	2.887	1.121	0.242	0.810	1.036	2.157
TAC μmol/mg protein	67.420	9.123	57.140	64.209	131.629	252.700*	35.150	204.000	240.327	493.027
TOS μmol H_2O_2 Equiv./mg protein	1.088	0.186	0.895	1.023	2.111	1.953	0.632	1.202	1.730	3.683
OSI %	1.956	0.406	1.441	1.813	3.769	1.188	0.337	1.340	1.069	2.257
FRAP μg/mg protein	20.100	3.496	11.540	18.869	38.969	28.660*	4.034	22.820	27.240	55.900
AGE fluorescence/mg protein	91.410	13.390	77.730	86.697	178.107	197.500*	22.010	174.400	189.752	387.252
AOPP μmol/mg protein	1.911	0.242	1.743	1.826	3.737	2.607*	0.246	2.318	2.521	5.128
4-HNE μg/mg protein	234.900	43.450	210.700	219.605	454.505	405.000*	42.540	377.300	390.025	795.025
8-OHdG pg/mg protein	52.340	8.200	46.890	49.454	101.794	71.160	11.740	64.010	67.027	138.187
Total protein mg/mL	3094.000	288.400	2964.000	2992.480	6086.480	1948.000*	210.000	1145.000	1874.078	3822.078

4-HNE: 4-hydroxynonenal protein adducts; 8-OHdG: 8-hydroxydeoxyguanosine; AGE: advanced glycation end products; AOPP: advanced oxidation protein products; CAT: catalase; FRAP: ferric reducing ability of plasma; GPx: glutathione peroxidase; GSH: reduced glutathione; Man: mandible; OSI: oxidative stress index; SOD: superoxide dismutase-1; TAC: total antioxidant status; TOS: total oxidant status; UA: uric acid; *statistical significance $p < 0.05$, study group *versus* control.

Table 3: Enzymatic and nonenzymatic antioxidants, antioxidant/oxidant status, and oxidative damage in the erythrocytes/plasma of patients with titanium mandibular fixations and healthy controls.

Erythrocytes/plasma	Control group					Study group				
	Mean	SD	Geometric mean	Lower 95% CI of mean	Upper 95% CI of mean	Mean	SD	Geometric mean	Lower 95% CI of mean	Upper 95% CI of mean
CAT nmol H_2O_2/min/mg protein	6.900	1.047	5.127	6.531	13.431	48.830*	5.823	39.510	46.780	95.610
SOD mU/mg protein	153.600	7.930	149.600	150.809	304.409	154.800	11.270	145.500	150.833	305.633
GPx IU/mg protein	0.020	0.002	0.019	0.019	0.039	0.020	0.001	0.019	0.019	0.039
UA μg/mg protein	0.658	0.011	0.656	0.654	1.312	0.733*	0.012	0.730	0.729	1.462
GSH μg/mg protein	0.687	0.178	0.517	0.625	1.312	0.463	0.044	0.410	0.447	0.910
TAC μmol/mg protein	49.570	7.384	44.020	46.971	96.541	37.680	6.483	26.780	35.398	73.078
TOS μmol H_2O_2 Equiv./mg protein	0.629	0.186	0.508	0.564	1.193	0.382	0.055	0.316	0.363	0.745
OSI %	1.318	0.282	1.128	1.219	2.537	1.902	0.551	1.181	1.708	3.610
FRAP μg/mg protein	13.580	3.186	11.750	12.458	26.038	10.990	3.239	6.285	9.850	20.840
AGE fluorescence/mg protein	526.000	30.420	507.700	515.292	1041.292	603.500	180.100	365.200	540.103	1143.603
AOPP umol/mg protein	0.497	0.049	0.452	0.479	0.976	0.506	0.054	0.439	0.487	0.994
4-HNE μg/mg protein	80.890	12.860	70.980	76.363	157.253	108.500	17.570	93.980	102.315	210.815
8-OHdG pg/mg protein	27.350	4.247	21.110	25.855	53.205	32.750*	5.534	27.510	30.802	63.552
Total protein mg/mL	4444.000	109.400	4416.000	4405.490	8849.490	3445.000*	213.300	2712.000	3369.916	6814.916

4-HNE: 4-hydroxynonenal protein adducts; 8-OHdG: 8-hydroxydeoxyguanosine; AGE: advanced glycation end products; AOPP: advanced oxidation protein products; CAT: catalase; FRAP: ferric reducing ability of plasma; GPx: glutathione peroxidase; GSH: reduced glutathione; OSI: oxidative stress index; SOD: superoxide dismutase-1; TAC: total antioxidant status; TOS: total oxidant status; UA: uric acid; *statistical significance $p < 0.05$, study group *versus* control.

patients compared to the controls. The decreased OSI value in patients with mandibular fracture compared to the control group was also observed. The FRAP level in the mandibular periosteum of the study group patients was significantly higher than in the control group. No statistically relevant changes in plasma TAC, TOS, OSI, and FRAP between the groups were demonstrated (Tables 2 and 3).

3.3. Oxidative Damage Products. There was a statistically significant increase in AGE fluorescence in the mandibular periosteum of the study group compared to AGE fluorescence in the control group. AOPP concentration in the mandibular periosteum of the study group was considerably higher than in the control group. There was a statistically relevant increase in the level of 4-HNE in the mandibular periosteum of patients with mandibular fracture compared to healthy controls. The content of AGE, AOPP, 4-HNE, and 8-OHdG in plasma of the study and control group was similar. The concentration of 8-OHdG in the mandibular periosteum of the traumatic patients yielded similar values to those obtained in mandibular periosteum in the control group (Tables 2 and 3).

3.4. Correlations. The results of all statistically significant correlations are presented in Table 4. Importantly, we have demonstrated a positive correlation between TAC concentration in the mandibular periosteum and UA level in plasma of patients in the study group. In this group, TOS concentration in the mandibular periosteum was positively correlated with CAT activity in erythrocytes as well as 8-OHdG level in the mandibular periosteum with GPx activity in erythrocytes.

Table 4: Correlations of redox biomarkers in control group and patients with titanium mandibular fixations.

		r	p
Control group			
TOS Man	OSI Man	0.551	0.033
TAC Man	UA plasma	0.425	0.043
GPx erythrocytes	FRAP plasma	0.737	0.037
TAC plasma	GSH plasma	0.608	0.003
8-OHdG plasma	AOPP plasma	0.559	0.047
Study group			
UA Man	FRAP Man	0.519	0.019
TAC Man	AGE Man	0.450	0.031
4-HNE Man	OSI Man	0.592	0.043
8-OHdG Man	AGE Man	0.883	0.000
TOS Man	OSI Man	0.567	0.034
AGE Man	GPx erythrocytes	0.574	0.025
TOS Man	CAT erythrocytes	0.515	0.043
8-OHdG Man	GPx erythrocytes	0.781	0.002
TAC Man	UA plasma	0.425	0.043
4-HNE Man	GSH plasma	0.662	0.019
GSH Man	GSH plasma	0.417	0.048
SOD erythrocytes	AGE plasma	0.470	0.020
TAC plasma	AOPP plasma	0.695	0.000
TOS plasma	AOPP plasma	0.529	0.000
TOS plasma	GSH plasma	0.645	0.002
8-OHdG plasma	GSH plasma	0.589	0.044

4-HNE: 4-hydroxynonenal protein adducts; 8-OHdG: 8-hydroxydeoxyguanosine; AGE: advanced glycation end products; AOPP: advanced oxidation protein products; CAT: catalase; FRAP: ferric reducing ability of plasma; GPx: glutathione peroxidase; GSH: reduced glutathione; Man: mandible; OSI: oxidative stress index; SOD: superoxide dismutase-1; TAC: total antioxidant status; TOS: total oxidant status; UA: uric acid.

4. Discussion

Our findings point to an increased occurrence of redox homeostasis disorders and oxidative stress in patients with mandible fractures treated surgically with titanium miniplates and screws. Although exposure to Ti6Al4V titanium alloy does not alter the clinical picture, the periosteum that contacted the titanium fixations of the mandible showed significantly higher concentrations of oxidation protein products and more extensive lipid modification compared to the control group. We also observed significant changes in the activity/concentration of enzymatic and nonenzymatic antioxidants in the periosteum as well as in the plasma and erythrocytes of the study group.

Titanium is widely used in many fields of medicine and dentistry due to its good biotolerance (biocompatibility) and its osseointegration ability to foster the contact thickening of bones [22]. Titanium and its alloys are used in the production of joint implants and external stabilizers as well as other metal components such as plates, clamps, screws, clips, dental implants, artificial valves, and vascular stents [22]. Their unique advantage is that they do not require removal for at least 20 years. Titanium miniplates and screws are also basic biomaterials used in the surgical treatment of mandibular fractures. One of the most commonly used titanium fixations in maxillofacial surgery is the Ti6Al4V alloy containing, in addition to titanium, 6% aluminium (Al) and 4% vanadium (V) [23]. Ti6Al4V demonstrates high mechanical strength and corrosion resistance due to the presence of a tight protective passive layer of titanium dioxide (TiO_2) on the surface of the alloy [9, 24]. It is believed that the passive layer effectively protects the surface of the implant from the effects of corrosive agents present in the environment of body fluids [25]. However, there are reports stating that in the period from the implantation to the exploitation of the biomaterial, the TiO_2 layer may be damaged, resulting in the release of metal ions (such as titanium, aluminium, or vanadium) into the surrounding tissues and organs [9]. In physiological conditions, the body content of these trace elements is very low. Corrosion of the implant, however, raises their concentration and may thus interfere with the process of their natural degradation. The local interaction of metal ions or products of the corrosion of metallic materials with the body tissues is referred to as metallosis [26].

The mandible is the only moving bone of the facial part of the skull. In patients with titanium implants, mandibular movements triggered by strong muscles cause micromovements of the fixed bone fragments, which increases the friction between the miniplates and the screws. This

phenomenon is responsible for the corrosion of titanium fixations and the release of titanium ions to the tissues/organs surrounding the implants [3]. In our investigation, the deposition of titanium particles in the study group was observed in the form of gray periosteal discolourations adjacent to the titanium miniplates and screws (data not shown). Importantly, none of the patients had any symptoms of chronic and acute inflammation or healing disorders at the site of the fracture. All patients had their metal implants removed exclusively for reasons not connected to a health risk. Indeed, the most common reason for the removal of miniplates and screws (14 patients) was the desire to get rid of nonfunctional implants in order to avoid future reactions to a foreign body and to eliminate the risk of artefacts causing problems in the interpretation of CT and MRI.

Titanium belongs to the group of biocompatible elements that usually do not cause negative bodily reactions. However, in some people, titanium triggers allergic symptoms (local eczema, rush, and pruritus) [27] and is responsible for the periapical reaction (in the implant-tissue interlayer), which may lead to the destabilization of implants [28]. However, the mechanisms of titanium toxicity in the body are still not well known. Titanium is believed to be responsible for an increased production of oxygen-free radicals and RNS [9, 29]. This element may thus contribute to the induction of oxidative stress as well as structural and functional damage of the cells by the oxidation reaction. Oxidative stress results from overproduction of ROS and/or inadequate activity of the body's antioxidant systems [8, 30]. The products of the oxidative modification of proteins, lipids, and nucleic acids that emerge due to oxidative stress are directly responsible for the damage to the tissues and organs of the body [8]. A significant role in the prevention of oxidative stress is attributed to enzymatic (CAT, SOD, and GPx) and nonenzymatic antioxidants (e.g., UA, reduced glutathione, and vitamin C). These compounds inhibit the formation of free oxygen radicals and/or participate in their conversion into nonreactive derivatives [31]. The antioxidant enzymes are characterized by a greater selectivity of action, while the remaining antioxidants scavenge free radicals in a nonselective manner and/or interrupt the oxidation reaction in the cell [32]. Additionally, nonenzymatic antioxidants may affect the activity of antioxidant enzymes so that the action of one group of antioxidants depends on the other and vice versa [33]. SOD is responsible for the dismutation of the superoxide anion to hydrogen peroxide, which is then broken down by CAT and GPx enzymes. An important role in the defence against free radical overproduction is also carried out by UA, the main blood antioxidant, which constitutes 70–80% of the total antioxidant capacity [34].

The increased activity/concentration of antioxidants (↑SOD, ↑UA, ↑TAC, and ↑FRAP) in the mandibular periosteum of patients with titanium mandibular fixations, compared to the controls, suggests an adaptive reaction of the body in response to excessive ROS production (↑TOS) due to exposure to Ti6Al4V titanium alloy and its wear products. As Wang et al. [25] demonstrated, titanium ions released from implants may stimulate phagocytes (mainly macrophages) and osteoclasts to produce increased amounts of ROS and RNS. By participating in phagocytosis, they can also increase the activity of NADPH oxidase (NOX) [35] which is the main source of free radicals in the cell. High concentrations of ROS can initiate inflammation at the implantation site (by increasing the production of proinflammatory cytokines), which additionally (by positive feedback) increases the production of free oxygen radicals [5, 9, 29]. In our study, the induction of antioxidant defence mechanisms was observed not only in the periosteum but also in the plasma (↑UA) and erythrocytes (↑CAT) of the patients in the study group. These changes point not only to redox imbalances in the implantation site (mandibular periosteum) but also to systemic disorders (blood). A positive correlation found between TAC levels in the mandibular periosteum and the UA concentration in the plasma in the patients from the study group may indicate a relationship between the local and the central antioxidant response. These observations, however, require further research, especially on a larger number of patients with titanium mandibular fixations. The assessment of white cell populations and cytokines produced by oxidative stress may also be helpful for clarifying the systemic etiology of redox imbalance in these patients.

Interestingly, we have observed a significantly lower CAT activity in the periosteum of the patients in the study group versus healthy controls. The decrease in CAT activity may be explained by the exhaustion of the ability to neutralize hydrogen peroxide in the conditions of an overproduction of this tissue. In patients with titanium fixations of the mandible, a higher production of H_2O_2 may occur as the direct effect of titanium on the periosteal cells [5, 6, 33] or due to an increase in SOD activity that produces a large amount of hydrogen peroxide as a by-product of the dismutation reaction. This is confirmed by the results of our study (↑SOD in the mandible of the patients in the study group) and may be partially explained by the lack of changes in GPx specific activity.

Despite the increased defence capacity of the antioxidant systems (↑SOD, ↑UA, ↑TAC, and ↑FRAP), we can observe an increased oxidative damage of proteins (↑AGE and ↑AOPP) and lipids (↑4-HNE) in the mandibular periosteum contacting Ti6Al4V titanium alloy. These changes suggest that the body is not able to protect itself effectively against oxidative stress and free radical damage of cells at the site of implantation of miniplates and screws. Importantly, the observed increase in oxidative stress biomarkers did not depend on the time span between osteosynthesis and the removal of the mandibular fixations.

Redox balance disorders as well as products of oxidative damage to the cell components can have a negative impact on the bone remodelling process in patients with mandibular fractures [9, 36]. The proper healing of a fracture depends on the recruitment and differentiation of osteoprogenitor cells towards osteoblasts and osteoclasts. Therefore, this process depends on the production of components of the extracellular matrix of the bone, particularly collagen proteins [37]. It is well known that bone tissue, periosteum, bone marrow, and surrounding soft tissues are involved in the healing of bone fractures; however, a particular role is

attributed to the periosteum [38, 39]. Microscopically, the periosteum consists of two layers: the external fibrous layer and the inner layer adhering to the bone (cambium) [40, 41]. In the outer fibrous layer, two sublayers can be distinguished: a superficial layer containing mainly collagen fibers with fibroblasts, which is rich in blood vessels and nerve fibers, and a deeper layer containing a lot of elastic fibers and collagen, a small number of cells and blood vessels. The outer fibrous layer provides elasticity and flexibility [40, 41]. The cambial layer (cambium) is composed of 3-4 cell layers of mainly osteoblasts and preosteoblastic cells and has osteogenic properties. This layer is responsible for the appearance of lamellar bone during growth and creation of woven bone after a fracture [40–42]. In our investigation, all the patients in the study group were treated surgically using an anatomical setting of bone fragments with miniplates and screws. In the case of surgical treatment of fractures, little or no periosteal response is observed [38, 39]. Therefore, it may be assumed that the observed periosteal changes are mainly caused by exposure to titanium implants after fractures.

Oxidative damage to proteins and lipids that occurs due to the overproduction of ROS is responsible for the structural and functional changes of these biomolecules, and this in turn disrupts normal cellular and tissue homeostasis [36, 43]. Titanium ions and cytokines released by macrophages under the influence of the products of titanium implants degradation cause the generation and activation of fibroblasts and osteoclasts, stimulating osteolysis processes [44, 45]. They may also induce genomic instability in human fibroblast cells, which is of particular importance in young people [26], and can inhibit type I collagen synthesis by osteoblasts [46]. In the case of fracture healing, this condition may lead to an inadequate formation of the organic matrix of the bone and thus impair its biomechanical properties. As shown by Sheikhi et al. [47], oxidized lipids lead to osteoblastogenesis and simultaneously stimulate osteoclast activity.

We did not detect oxidative damage to the cell components in the plasma and erythrocytes of the study group patients, which indicates that, excluding the implantation site, the body is capable of preventing free radical damage caused by oxidative stress. A positive correlation between TOS Man and CAT erythrocytes as well as 8-OHdG Man and GPx erythrocytes proves that there is a correlation between the increased oxidative damage in the mandibular periosteum and the central redox disorders in patients with titanium miniplates and screws.

In conclusion, we have demonstrated the occurrence of redox imbalance as well as oxidative damage in the periosteum surrounding the Ti6Al4V titanium alloy. Changes in antioxidant efficiency in the patients treated with titanium implants were also observed in the plasma/erythrocytes, which proves both local and systemic influence of titanium on the human body. The obtained results indicate the need to improve the miniplates and screws used for osteosynthesis by increasing the thickness of the passive TiO_2 layer or using new, biodegradable, and biocompatible materials (for instance based on magnesium and its alloys). Supplementation with antioxidants would also be helpful in patients treated with titanium fixations; however, further research is needed in this area.

Our work, apart from the undoubted advantages (careful selection of the group of young people (aged 21–29) with similar types of jaw fractures), also had some limitations. We evaluated only the most commonly used biomarkers of oxidative stress; therefore, the assessment of other parameters may lead to different observations and conclusions. It should also be borne in mind that changes in antioxidant defence as well as increased generation of the products of oxidative damage of proteins and lipids may indicate not only the body's response to the introduction of titanium miniplates and screws but also an ongoing callus remodelling in the course of mandibular fracture healing and the related increased protein metabolism.

Conflicts of Interest

Authors declare no conflict of interest.

Acknowledgments

This work was supported by the Medical University of Bialystok, Poland (Grant nos. N/ST/ZB/17/001/1109, N/ST/ZB/17/002/1109, N/ST/ZB/17/003/1109, N/ST/ZB/17/004/1109, and N/ST/MN/16/002/1109).

References

[1] M. A. Kuriakose, M. Fardy, M. Sirikumara, D. W. Patton, and A. W. Sugar, "A comparative review of 266 mandibular fractures with internal fixation using rigid (AO/ASIF) plates or mini-plates," *The British Journal of Oral & Maxillofacial Surgery*, vol. 34, no. 4, pp. 315–321, 1996.

[2] J. O'Connell, C. Murphy, O. Ikeagwuani, C. Adley, and G. Kearns, "The fate of titanium miniplates and screws used in maxillofacial surgery: a 10 year retrospective study," *International Journal of Oral and Maxillofacial Surgery*, vol. 38, no. 7, pp. 731–735, 2009.

[3] J. Borys, M. Maciejczyk, A. J. Krętowski et al., "The redox balance in erythrocytes, plasma, and periosteum of patients with titanium fixation of the jaw," *Frontiers in Physiology*, vol. 8, 2017.

[4] G. Voggenreiter, S. Leiting, H. Brauer et al., "Immuno-inflammatory tissue reaction to stainless-steel and titanium plates used for internal fixation of long bones," *Biomaterials*, vol. 24, no. 2, pp. 247–254, 2003.

[5] K. Peters, R. E. Unger, A. M. Gatti, E. Sabbioni, R. Tsaryk, and C. J. Kirkpatrick, "Metallic nanoparticles exhibit paradoxical effects on oxidative stress and pro-inflammatory response in endothelial cells *in vitro*," *International Journal of Immunopathology and Pharmacology*, vol. 20, no. 4, pp. 685–695, 2007.

[6] D. G. Olmedo, D. R. Tasat, P. Evelson, M. B. Guglielmotti, and R. L. Cabrini, "Biological response of tissues with macrophagic activity to titanium dioxide," *Journal of Biomedical Materials Research Part A*, vol. 84A, no. 4, pp. 1087–1093, 2008.

[7] M.-C. Lee, F. Yoshino, H. Shoji et al., "Characterization by electron spin resonance spectroscopy of reactive oxygen species generated by titanium dioxide and hydrogen peroxide," *Journal of Dental Research*, vol. 84, no. 2, pp. 178–182, 2005.

[8] M. Valko, D. Leibfritz, J. Moncol, M. T. D. Cronin, M. Mazur, and J. Telser, "Free radicals and antioxidants in normal physiological functions and human disease," *The International Journal of Biochemistry & Cell Biology*, vol. 39, no. 1, pp. 44–84, 2007.

[9] R. Tsaryk, M. Kalbacova, U. Hempel et al., "Response of human endothelial cells to oxidative stress on Ti6Al4V alloy," *Biomaterials*, vol. 28, no. 5, pp. 806–813, 2007.

[10] M. Choromańska, A. Klimiuk, P. Kostecka-Sochoń et al., "Antioxidant defence, oxidative stress and oxidative damage in saliva, plasma and erythrocytes of dementia patients. Can salivary AGE be a marker of dementia?," *International Journal of Molecular Sciences*, vol. 18, no. 10, p. 2205, 2017.

[11] U. Kolodziej, M. Maciejczyk, A. Miasko et al., "Oxidative modification in the salivary glands of high fat-diet induced insulin resistant rats," *Frontiers in Physiology*, vol. 8, 2017.

[12] U. Kołodziej, M. Maciejczyk, W. Niklińska et al., "Chronic high-protein diet induces oxidative stress and alters the salivary gland function in rats," *Archives of Oral Biology*, vol. 84, pp. 6–12, 2017.

[13] D. E. Paglia and W. N. Valentine, "Studies on the quantitative and qualitative characterization of erythrocyte glutathione peroxidase," *The Journal of Laboratory and Clinical Medicine*, vol. 70, no. 1, pp. 158–169, 1967.

[14] H. Aebi, "[13] Catalase *in vitro*," *Methods in Enzymology*, vol. 105, pp. 121–126, 1984.

[15] H. P. Misra and I. Fridovich, "The role of superoxide anion in the autoxidation of epinephrine and a simple assay for superoxide dismutase," *The Journal of Biological Chemistry*, vol. 247, no. 10, article 4623845, pp. 3170–3175, 1972.

[16] M. S. Moron, J. W. Depierre, and B. Mannervik, "Levels of glutathione, glutathione reductase and glutathione S-transferase activities in rat lung and liver," *Biochimica et Biophysica Acta (BBA) - General Subjects*, vol. 582, no. 1, pp. 67–78, 1979.

[17] O. Erel, "A novel automated direct measurement method for total antioxidant capacity using a new generation, more stable ABTS radical cation," *Clinical Biochemistry*, vol. 37, no. 4, pp. 277–285, 2004.

[18] O. Erel, "A new automated colorimetric method for measuring total oxidant status," *Clinical Biochemistry*, vol. 38, no. 12, pp. 1103–11111, 2005.

[19] M. Knaś, M. Maciejczyk, K. Sawicka et al., "Impact of morbid obesity and bariatric surgery on antioxidant/oxidant balance of the unstimulated and stimulated human saliva," *Journal of Oral Pathology & Medicine*, vol. 45, no. 6, pp. 455–464, 2016.

[20] I. F. F. Benzie and J. J. Strain, "The ferric reducing ability of plasma (FRAP) as a measure of "antioxidant power": the FRAP assay," *Analytical Biochemistry*, vol. 239, no. 1, pp. 70–76, 1996.

[21] M. Kalousová, J. Skrha, and T. Zima, "Advanced glycation end-products and advanced oxidation protein products in patients with diabetes mellitus," *Physiological Research*, vol. 51, no. 6, pp. 597–604, 2002.

[22] R. Branemark, P.-I. Branemark, B. Rydevik, and R. R. Myers, "Osseointegration in skeletal reconstruction and rehabilitation: a review," *Journal of Rehabilitation Research and Development*, vol. 38, no. 2, pp. 175–181, 2001.

[23] Z. Cai, T. Shafer, I. Watanabe, M. E. Nunn, and T. Okabe, "Electrochemical characterization of cast titanium alloys," *Biomaterials*, vol. 24, no. 2, pp. 213–218, 2003.

[24] P. Tengvall, H. Elwing, L. Sjöqvist, I. Lundström, and L. M. Bjursten, "Interaction between hydrogen peroxide and titanium: a possible role in the biocompatibility of titanium," *Biomaterials*, vol. 10, no. 2, pp. 118–120, 1989.

[25] J. Wang, G. Zhou, C. Chen et al., "Acute toxicity and biodistribution of different sized titanium dioxide particles in mice after oral administration," *Toxicology Letters*, vol. 168, no. 2, pp. 176–185, 2007.

[26] N. Coen, M. A. Kadhim, E. G. Wright, C. P. Case, and C. E. Mothersill, "Particulate debris from a titanium metal prosthesis induces genomic instability in primary human fibroblast cells," *British Journal of Cancer*, vol. 88, no. 4, pp. 548–552, 2003.

[27] M. Goutam, C. Giriyapura, S. K. Mishra, and S. Gupta, "Titanium allergy: a literature review," *Indian Journal of Dermatology*, vol. 59, no. 6, p. 630, 2014.

[28] A. Tawse-Smith, S. Ma, A. Siddiqi, W. J. Duncan, L. Girvan, and H. M. Hussaini, "Titanium particles in peri-implant tissues: surface analysis and histologic response," *Clinical Advances in Periodontics*, vol. 2, no. 4, pp. 232–238, 2012.

[29] M. Kalbacova, S. Roessler, U. Hempel et al., "The effect of electrochemically simulated titanium cathodic corrosion products on ROS production and metabolic activity of osteoblasts and monocytes/macrophages," *Biomaterials*, vol. 28, no. 22, pp. 3263–3272, 2007.

[30] M. Maciejczyk, B. Mikoluc, B. Pietrucha et al., "Oxidative stress, mitochondrial abnormalities and antioxidant defense in ataxia-telangiectasia, bloom syndrome and Nijmegen breakage syndrome," *Redox Biology*, vol. 11, pp. 375–383, 2017.

[31] A. M. Pisoschi and A. Pop, "The role of antioxidants in the chemistry of oxidative stress: a review," *European Journal of Medicinal Chemistry*, vol. 97, pp. 55–74, 2015.

[32] T. Konopka, A. Gmyrek-Marciniak, Z. Kozłowski, U. Kaczmarek, and J. Wnukiewicz, "Antioxidative potential of saliva with peridontitis and squamous cell carcinoma of lower oral cavity," *Dental and Medical Problems*, vol. 43, pp. 354–362, 2006.

[33] P. Żukowski, M. Maciejczyk, and D. Waszkiel, "Sources of free radicals and oxidative stress in the oral cavity," *Archives of Oral Biology*, vol. 92, pp. 8–17, 2018.

[34] M. Knaś, M. Maciejczyk, D. Waszkiel, and A. Zalewska, "Oxidative stress and salivary antioxidants," *Dental and Medical Problems*, vol. 50, pp. 461–466, 2013.

[35] A. Federico, F. Morgillo, C. Tuccillo, F. Ciardiello, and C. Loguercio, "Chronic inflammation and oxidative stress in human carcinogenesis," *International Journal of Cancer*, vol. 121, no. 11, pp. 2381–2386, 2007.

[36] F. Wauquier, L. Leotoing, V. Coxam, J. Guicheux, and Y. Wittrant, "Oxidative stress in bone remodelling and disease," *Trends in Molecular Medicine*, vol. 15, no. 10, pp. 468–477, 2009.

[37] J. Borys, S. Z. Grabowska, B. Antonowicz, D. Dryl, A. Citko, and F. Rogowski, "Collagen type I and III metabolism in assessment of mandible fractures healing," *Roczniki Akademii Medycznej w Bialymstoku*, vol. 49, pp. 237–245, 2004.

[38] R. Dimitriou, E. Tsiridis, and P. V. Giannoudis, "Current concepts of molecular aspects of bone healing," *Injury*, vol. 36, no. 12, pp. 1392–1404, 2005.

[39] T. A. Einhorn, "The cell and molecular biology of fracture healing," *Clinical Orthopaedics and Related Research*, vol. 355S, article 9917622, pp. S7–S21, 1998.

[40] J. R. Dwek, "The periosteum: what is it, where is it, and what mimics it in its absence?," *Skeletal Radiology*, vol. 39, no. 4, pp. 319–323, 2010.

[41] G. Augustin, A. Antabak, and S. Davila, "The periosteum. Part 1: anatomy, histology and molecular biology," *Injury*, vol. 38, no. 10, pp. 1115–1130, 2007.

[42] Y. V. Kuzenko, A. M. Romaniuk, and D. Horobchenko, "Periodontitis and atherosclerosis – mechanisms of association through matrix metalloproteinase 1 expression," *Dental and Medical Problems*, vol. 51, pp. 187–192, 2014.

[43] B. Halliwell, M. V. Clement, and L. H. Long, "Hydrogen peroxide in the human body," *FEBS Letters*, vol. 486, no. 1, pp. 10–13, 2000.

[44] S. Y. Yang, B. Wu, L. Mayton et al., "Protective effects of IL-1Ra or vIL-10 gene transfer on a murine model of wear debris-induced osteolysis," *Gene Therapy*, vol. 11, no. 5, pp. 483–491, 2004.

[45] T. Koreny, M. Tunyogi-Csapó, I. Gál, C. Vermes, J. J. Jacobs, and T. T. Glant, "The role of fibroblasts and fibroblast-derived factors in periprosthetic osteolysis," *Arthritis and Rheumatism*, vol. 54, no. 10, pp. 3221–3232, 2006.

[46] C. Vermes, R. Chandrasekaran, J. J. Jacobs, J. O. Galante, K. A. Roebuck, and T. T. Glant, "The effects of particulate wear debris, cytokines, and growth factors on the functions of MG-63 osteoblasts," *The Journal of Bone and Joint Surgery*, vol. 83, no. 2, pp. 201–211, 2001.

[47] M. Sheikhi, R. K. L. Bouhafs, K.-J. Hammarstrom, and C. Jarstrand, "Lipid peroxidation caused by oxygen radicals from Fusobacterium-stimulated neutrophils as a possible model for the emergence of periodontitis," *Oral Diseases*, vol. 7, no. 1, pp. 41–46, 2001.

Hindawi
Oxidative Medicine and Cellular Longevity
Volume 2018, Article ID 1421438, 24 pages
https://doi.org/10.1155/2018/1421438

Research Article

Carnosic Acid, a Natural Diterpene, Attenuates Arsenic-Induced Hepatotoxicity via Reducing Oxidative Stress, MAPK Activation, and Apoptotic Cell Death Pathway

Sonjit Das,[1] Swarnalata Joardar,[1] Prasenjit Manna,[2] Tarun K. Dua,[1] Niloy Bhattacharjee,[1] Ritu Khanra,[1] Shovonlal Bhowmick,[3] Jatin Kalita,[2] Achintya Saha,[3] Supratim Ray,[4] Vincenzo De Feo,[5] and Saikat Dewanjee[1]

[1]*Advanced Pharmacognosy Research Laboratory, Department of Pharmaceutical Technology, Jadavpur University, Kolkata 700032, India*
[2]*Biological Science and Technology Division, CSIR-North East Institute of Science and Technology, Jorhat, Assam 785006, India*
[3]*Department of Chemical Technology, University of Calcutta, Kolkata 700009, India*
[4]*Department of Pharmaceutical Sciences, Assam University, Silchar 788011, India*
[5]*Department of Pharmacy, University of Salerno, Fisciano 84084, Italy*

Correspondence should be addressed to Vincenzo De Feo; defeo@unisa.it and Saikat Dewanjee; s.dewanjee@yahoo.com

Received 4 October 2017; Revised 19 December 2017; Accepted 14 March 2018; Published 2 May 2018

Academic Editor: Maria F. H. Carneiro

The present studies have been executed to explore the protective mechanism of carnosic acid (CA) against $NaAsO_2$-induced hepatic injury. CA exhibited a concentration dependent (1–4 μM) increase in cell viability against $NaAsO_2$ (12 μM) in murine hepatocytes. $NaAsO_2$ treatment significantly enhanced the ROS-mediated oxidative stress in the hepatic cells both in *in vitro* and *in vivo* systems. Significant activation of MAPK, NF-κB, p53, and intrinsic and extrinsic apoptotic signaling was observed in $NaAsO_2$-exposed hepatic cells. CA could significantly counteract with redox stress and ROS-mediated signaling and thereby attenuated $NaAsO_2$-mediated hepatotoxicity. $NaAsO_2$ (10 mg/kg) treatment caused significant increment in the As bioaccumulation, cytosolic ATP level, DNA fragmentation, and oxidation in the liver of experimental mice ($n = 6$). The serum biochemical and haematological parameters were significantly altered in the $NaAsO_2$-exposed mice ($n = 6$). Simultaneous treatment with CA (10 and 20 mg/kg) could significantly reinstate the $NaAsO_2$-mediated toxicological effects in the liver. Molecular docking and dynamics predicted the possible interaction patterns and the stability of interactions between CA and signal proteins. ADME prediction anticipated the drug-likeness characteristics of CA. Hence, there would be an option to employ CA as a new therapeutic agent against As-mediated toxic manifestations in future.

1. Introduction

Arsenic (As) is a toxic metalloid, which raises much disquiet in the health standpoints for human and animals [1]. The primary natural pools of As are rocks, from which As is mobilized through natural different processes [2]. Besides the natural sources, industrial outcomes can also cause the release and mobilization of As to soil, water, and air in various forms [2, 3]. Organic As compounds are not the concern for health risks [4]. Inorganic trivalent arsenicals (arsenites, AsO_2^-) are most potent toxicants [5]. Drinking water contaminated with arsenites is thought to be the major root of As calamity affecting >140 million people in ~70 countries [4]. Following ingestion, As is absorbed through the gastrointestinal tract and bioaccumulated into various organs [6]. It can also enter into the body through the respiratory system and dermis [7]. Intake of arsenites > 30 μg per day has been reported to exert arsenicosis to the critical organs [4, 6, 8]. Earlier investigations revealed that As reduces mitochondrial integrity, resulting in random formation of superoxide radical which subsequently potentiates a cascade of radical reactions and enhances the secondary generation of other

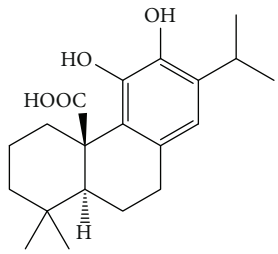

Figure 1: Structure of carnosic acid.

ROS [6, 7, 9, 10]. On the other hand, As further promotes oxidative stress by reacting with -SH group and thereby deactivates the defense mechanism of several antioxidant enzymes and glutathione system [5]. The excess of ROS triggers wide ranges of pathological occurrences including damages to the structural components of cells, alteration in the expressions of genes, DNA damage, and apoptosis [6, 7]. Despite As is a major threat to the global health, the development of a suitable therapy is still underway. The primary therapeutic strategy includes the treatment with chelating agents; however, the adverse effects like removal of essential metals and redistribution of As largely restricted their clinical usefulness [6]. The biological half-life of inorganic As is ~10 h [11], which also argues against the employment of chelating agent as therapeutic negotiator. As-mediated augmented oxidative stress has been considered to be the principle etiology of arsenicosis. Therefore, it would be worthy to exploit the role of natural antioxidants to counteract As-mediated toxic manifestations.

Carnosic acid (CA), (4aR,10aS)-5,6-dihydroxy-1,1-dimethyl-7-propan-2-yl-2,3,4,9,10,10a-hexahydrophenanthrene-4a-carboxylic acid, is a naturally occurring phenolic diterpene (Figure 1). CA is commonly found in *Rosmarinus officinalis* and *Salvia officinalis* [12, 13]. CA has been reported to possess antioxidant [14, 15], neuroprotective [16], antiobesity [17], and anti-inflammatory [18] activities. Considering the antioxidant and radical scavenging effects of CA, the present studies have been undertaken to evaluate the possible therapeutic role of CA against As-induced hepatotoxicity.

2. Material and Methods

2.1. Chemicals. CA, bovine serum albumin (BSA), Dulbecco's modified Eagle's medium (DMEM), fetal bovine serum (FBS), Bradford reagent, and collagenase type I were procured from Sigma-Aldrich Chemical Company, MO, USA. Antibodies for immunoblotting were bought from Novus Biologicals, CO, USA. The solvents (HPLC grade) were obtained from Merck, Mumbai, India. Kits for the measurement of different biochemical parameters were procured from Span Diagnostics Ltd., India. 1-Chloro-2,4-dinitrobenzene, $(NH_4)_2SO_4$, $NaAsO_2$, 2,4-dinitrophenylhydrazine, ethylenediaminetetraacetic acid, 5,5-dithiobis(2-nitrobenzoic acid), N-Ethylmaleimide, nitro blue tetrazolium, NADH, KH_2PO_4, phenazine methosulphate, $Na_4P_2O_7$, GSH, NaN_3, thiobarbituric acid, 5-thio-2-nitrobenzoic acid, and CCl_3 COOH were obtained from Sisco Research Laboratory, Mumbai, India.

2.2. Animals. Healthy Swiss albino mice (♂, ~2 month old, 25 ± 5 g) were procured from Chakraborty Enterprise, Kolkata, India and were housed in standard polypropylene cages ($29 \times 22 \times 14$ cm) in the animal house of the Department of Pharmaceutical Technology, Jadavpur University, India. The mice were maintained with temperature (22 ± 2°C), humidity (40 ± 10%), and 12 h light–dark cycle [19]. The mice were fed standard diet and water ad libitum. The *in vivo* experiment has been permitted (Ref number AEC/PHARM/1701/09/2017) by the animal ethical committee, Jadavpur University (Reg. number: 0367/01/C/CPCSEA, UGC, India), and the principles of laboratory animal care were followed during the experiment [20]. The animals were acclimatized for a period of 2 weeks before the execution of the *in vivo* experiment.

2.3. In Vitro Assays

2.3.1. Determination of Cytotoxic Effect of $NaAsO_2$. Hepatocytes were isolated from the liver of immediately sacrificed albino mice by two-step in situ collagenase perfusion as described by Dua et al. [6]. The hepatocytes were passaged at least a couple of times before the execution of *in vitro* experiment. Concentration-dependent cytotoxic effect of $NaAsO_2$ was determined. Briefly, hepatocytes ($\sim 2 \times 10^6$ cells/well) were seeded in tissue culture plate and incubated at 37°C and 5% CO_2 for 24 h to form uniform monolayer of hepatocytes in the wells of culture plate. The cells were exposed to different concentrations of $NaAsO_2$ for 2 h, and the cell viability was determined employing MTT (3-(4,5-dimethylthiazolyl-2)-2, 5-diphenyltetrazolium bromide) assay [6]. The experiments were performed in triplicate. $NaAsO_2$ exhibited IC_{50} value of ~12 μM in murine hepatocytes.

2.3.2. Determination of Effect of CA on Murine Hepatocytes. To determine the effect of CA on hepatocytes, hepatocytes ($\sim 2 \times 10^6$ cells/set) were exposed to CA (1, 2, 4, 6, and 10 μM). The experiments were performed in triplicate. The cell viability was measured employing MTT assay at different intervals up to 4 h [6].

2.3.3. Assessment of Cytoprotective Role of CA. To determine the cytoprotective effect of CA, hepatocytes ($\sim 2 \times 10^6$ cells/set) were exposed to $NaAsO_2$ (12 μM) along with CA (1, 2, 4, 6 and 10 μM). The experiments were performed in triplicate. The cell viability was measured employing MTT assay at different intervals up to 4 h [6]. One set of hepatocytes exposed to $NaAsO_2$ (12 μM) was kept as toxic control, while an untreated set of hepatocytes was maintained as untreated control.

2.3.4. Hoechst Staining. Hoechst 33258 nuclear staining has been executed to study the cytotoxic events [21]. Briefly, hepatocytes (~2000 cells/well) were exposed to $NaAsO_2$ (12 μM) and $NaAsO_2$ (12 μM) along with CA (4 μM) for 2 h at 37°C and 5% CO_2. One set of hepatocytes without any treatment was kept as normal control. After 4 h, hepatocytes were fixed with paraformaldehyde (4%) in phosphate buffer saline (PBS) of pH 7.4 for 20 min. The fixed hepatocytes were exposed to Hoechst 33258 (5 μg/ml in PBS) for

15 min followed by washing with PBS. Fluorescent nuclei and nuclear pattern were recorded. The experiments were performed in triplicate.

2.3.5. Flow Cytometric Analysis. The flow cytometric study has been performed to accomplish the nature of cell death. Briefly, hepatocytes were exposed to $NaAsO_2$ (12 μM) and $NaAsO_2$ (12 μM) along with CA (4 μM) for 2 h at 37°C and 5% CO_2. One set of hepatocytes without any treatment was kept as normal control. After 2 h, different sets of hepatocytes were treated with propidium iodide (PI) and FITC-labeled annexin V for 30 min at 37°C [21]. The excess of PI and annexin V was washed out, and the cells were fixed for analyzing in a flow cytometer using FACSCalibur (Becton Dickinson, Mountain View, USA) equipped with 488 nm argon laser light source; 515 nm band pass filter for FITC fluorescence and 623 nm band pass filter for PI fluorescence using CellQuest software, USA. The scatter plots of PI fluorescence (y-axis) versus FITC fluorescence (x-axis) were prepared for different sets of hepatocytes. The experiments were performed in triplicate.

2.3.6. Assays for Redox Markers. Different sets of hepatocytes, each containing 1 ml of suspension (~2×10^6 cells/ml), were used in experiments. The prophylactic role of CA against $NaAsO_2$ intoxication was analyzed by incubating hepatocytes with CA (4 μM) and $NaAsO_2$ (12 μM) together for 2 h at 37°C. One set of hepatocytes incubated with $NaAsO_2$ (12 μM) served as toxic control. One set of hepatocytes without any treatment was kept as normal control. The intracellular ROS production was estimated by measuring the fluorescence of 2,7-dichlorofluorescein diacetate (DCF) in a fluorescence spectrometer (Olympus 1X70, Japan) following the method as described by Manna and Jain [22]. The levels of lipid peroxidation, protein carbonylation, reduced glutathione (GSH), and the levels of endogenous antioxidant enzymes, namely superoxide dismutase (SOD), catalase (CAT), glutathione peroxidase (GPx), glutathione-S-transferase (GST), and glutathione reductase (GR), were quantified employing reputable protocols [23]. The experiments were performed in triplicate.

2.3.7. Western Blotting of Signal Proteins in the Hepatocytes. The protein samples of hepatocytes for specific cellular components namely whole cell, cytosolic, and mitochondrial fractions were separated following standard sequential fractionation procedure as described by Baghirova and coworkers [24]. The sample proteins (20 μg) were resolved in 12% SDS-PAGE gel electrophoresis and transferred into nitrocellulose membrane [25, 26]. The membrane was blocked by blocking buffer (containing 5% nonfat dry milk) for 1 h and subsequently incubated with primary antibody at 4°C overnight. After primary antibody treatment, the membrane was washed with tris-buffered saline (TBST; containing 0.1% tween 20). The membrane was then treated with suitable HRP-conjugated secondary antibody at room temperature for 1 h. The blots were developed by ECL substrate (Millipore, MA, USA) to detect the expressions of proteins in a ChemiDoc Touch Imaging System (Bio-Rad, USA). The densitometric analysis was performed using Image Lab software (Bio-Rad, USA). Normalization of expression was done employing β-actin as a loading protein. The membranes were then subjected to mild stripping using stripping buffer containing 1% SDS (pH 2.0) and glycine (25 mM), followed by treatments with respective primary and secondary antibodies for detecting the expressions of other proteins in the same membrane. The expressions of Bcl-2, Bax, cytochrome C, Apaf-1, cleaved caspase 9, cleaved caspase 3, Bid, Fas, cleaved caspase 8, total JNK, phospho-JNK (Tyr 183/Tyr 185), total-p38, phospho-p38 (Tyr 180/Tyr 182), p53, phospho-IκBα (Ser 32), and total IκBα, phospho-NF-κB (p65) (Ser 536) were estimated. The experiments were performed in triplicate.

2.4. In Vivo Bioassay

2.4.1. Experimental Setup. The *in vivo* experiment was performed following established protocol by our group [6.7]. Twenty-four Swiss albino mice (♂) were divided into four groups ($n = 6$) and were treated as follows:

Gr I: normal control, mice received only 1% tween 80 in distilled water (1 ml, *p.o.*, once daily) for 15 days.

Gr II: toxic control, mice were treated with $NaAsO_2$ (10 mg/kg body weight, *p.o.*, once daily) for 10 days.

Gr III: animals were treated with CA (10 mg/kg body weight, *p.o.*, once daily for 15 days) began 5 days prior to the beginning of exposure to $NaAsO_2$ (10 mg/kg body weight, *p.o.*, once daily for 10 days), totalizing 15 days treatment period.

Gr IV: animals were treated with CA (20 mg/kg body weight, *p.o.*, once daily for 15 days) began 5 days prior to the beginning of exposure to $NaAsO_2$ (10 mg/kg body weight, *p.o.*, once daily for 10 days), totalizing 15 days treatment period.

The doses of CA were selected on the basis of *in vitro* observation, subacute toxicity studies, preliminary *in vivo* study (with limited number of animals). In subacute toxicity studies, CA (10 and 20 mg/kg body weight, *p.o.*, once daily for 30 days) did not show any significant change in haematological, biochemical, and histological parameters when compared with normal mice (Supplementary Table 2 and Supplementary Figure 2).

The food intake and water intake were monitored on a daily basis. After 15 days, the mice were fasted overnight and were sacrificed by cervical dislocation under CO_2 anesthesia. Before sacrificing the mice, body weight was recorded. For measurements of haematological parameters and biochemical markers in the sera, blood samples were collected from retro-orbital venous plexus after applying tetracaine (0.5%, one drop) ophthalmic anesthetic drop to the eyes. The livers were excised and cleaned with PBS. The weight of liver was recorded. The organs were homogenized immediately in Tris–HCl (0.01 M) + EDTA (0.001 M) buffers of pH 7.4 and centrifuged (12,000g) at 4°C for 30 min to obtain tissue homogenate. Urine samples were collected from the bladder and immediately stored at −80°C [27]. A schematic overview of the *in vivo* assay has been depicted in Figure 2.

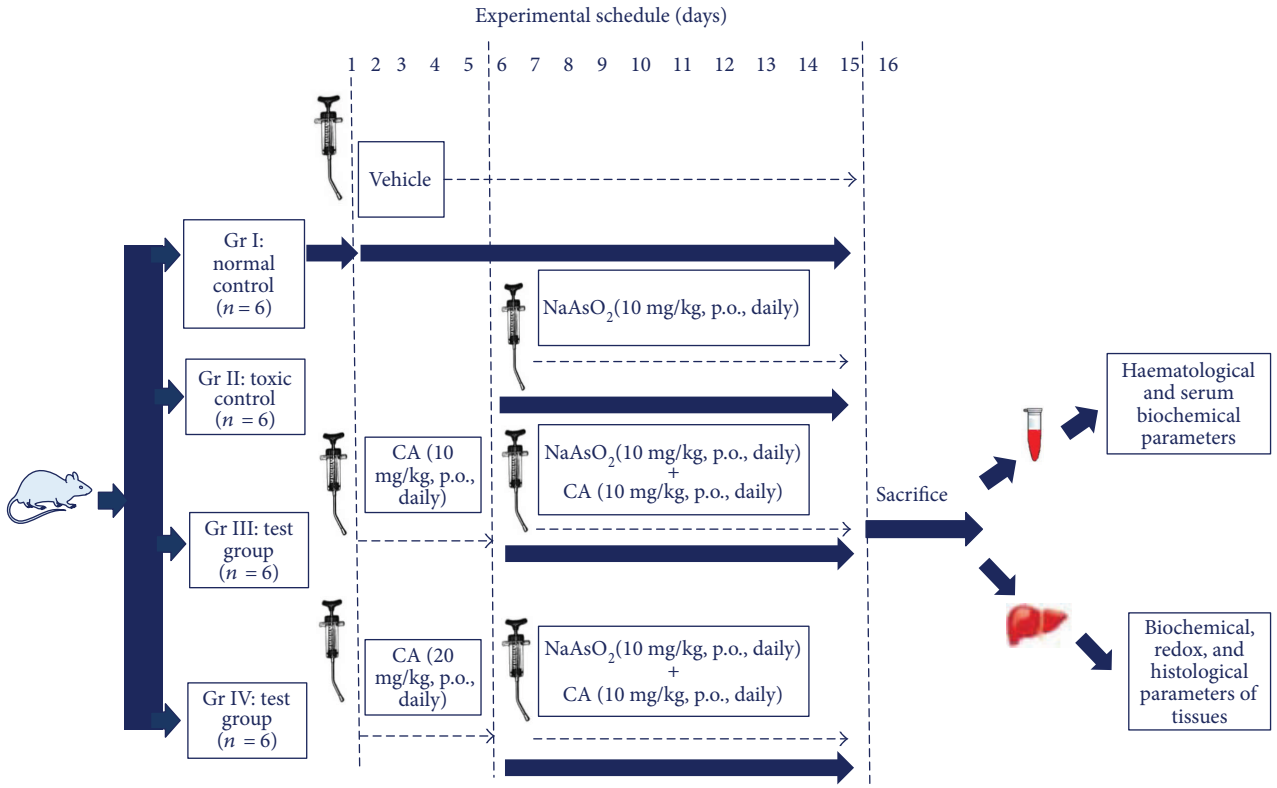

Figure 2: A schematic outline of *in vivo* experimental protocol.

2.4.2. Estimation of Haematological and Serum Biochemical Parameters. Total erythrocyte count was measured using a haemocytometer and haemoglobin content was estimated using a haemoglobinometer. The levels of alanine aminotransferase (ALT), aspartate aminotransferase (AST), creatine kinase (CK), and lactate dehydrogenase (LDH) in the sera were estimated by commercially available kits (Span Diagnostics Limited, India) following manufacturer's protocol.

2.4.3. Assays for Hepatic and Urinary As. The As contents in liver and urine of experimental animals were analyzed following the method of Das et al. [28], using hydride generation system in atomic absorption spectrophotometer (Perkin Elmer model number 3100, USA).

2.4.4. Assays for Biochemical and Redox Markers in Liver. Cytosolic fractions from livers of experimental mice were isolated following subcellular fractionation protocol employing centrifugation methods mentioned by Abcam, Cambridge, MA, USA. Cytosolic ATP level in the hepatic tissue was estimated by the commercially available assay kit (Abcam, Cambridge, MA, USA) following manufacturer's protocol. The extent of DNA fragmentation was measured by the diphenylamine reaction as described by Lin et al. [29]. Briefly, the hepatic tissue was lysed with hypotonic lysing buffer (10 mM Tris, pH 8.0, 1 mM EDTA, 0.5% triton X-100), and the lysates were centrifuged to separate intact and fragmented fractions. Then the pellet and the supernatant were separately precipitated with 12.5% trichloroacetic acid. The DNA precipitates were heated to 90°C for 10 min in 5% trichloroacetic acid and quantitatively estimated by colorimetric reaction with diphenylamine [29]. DNA oxidation was evaluated by RP-HPLC analysis and was represented as 7,8-hydroxy-2′-deoxyguaosine/2′-deoxyguaosine (8-OHdG/2-dG) ratio [30, 31]. Briefly, DNA was isolated from hepatic tissue by pronase-ethanol method followed by enzymatic digestion as the protocol by Chepelev et al. [31]. 8-OHdG stock solution (35 mmol/l) was prepared in water, while 2-dG stock solution (37 mmol/l) was prepared in 0.5 mol/l NH_4OH [30]. The aliquots of 8-OHdG and 2-dG stock solutions were adequately diluted first in water and finally in digested DNA samples to obtain working spiked solutions. Quantitative estimation was done in Dionex UltiMate 3000 HPLC system (Dionex, Germany), using a C-18 column (250 × 4.6 mm, particle size 5 μ) and electrochemical detector. The columns were preconditioned with 1 ml acetonitrile, followed by 1 ml water, and 1 ml 100 mM NaH_2PO_4 (pH 6.0). For 8-OHdG analysis, the mobile phase (pH 3.0) contained formic acid (0.1 mol/l), citric acid (1.0 mmol/l), NaN_3 (7.7 mmol/l), EDTA (0.5 mmol/l), diethylamine (24.0 mmol/l), and 4% acetonitrile. For 2-dG analysis, the mobile phase comprised NaH_2PO_4 (50.0 mmol/l) (pH 4.5) and 4% acetonitrile. A flow rate of 1.0 ml/min was used. The applied potentials at the first and second electrodes for 8-OHdG were 0.0 and+0.5 volts, respectively. While the applied potentials for 2-dG were +0.4 and +0.8 volts at the first and second electrodes, respectively. The intercellular ROS, TBARS level, protein carbonylation, endogenous antioxidant enzymes, and GSH levels were assayed following established protocols [23].

2.4.5. Western Blotting of Signaling Proteins in Liver. The protein samples of liver for specific cellular components, namely cytosolic, mitochondrial, and nuclear fractions, were separated, employing sequential fractionation process [24]. The sample proteins (20 μg) were resolved in 12% SDS-PAGE gel electrophoresis and immunoblotted as mentioned in the earlier section. The expressions of Bcl-2, Bax, cytochrome C, Apaf-1, cleaved caspase 9, cleaved caspase 3, Bid, Fas, cleaved caspase 8, total JNK, phospho-JNK (Tyr 183/Tyr 185), total-p38, phospho-p38 (Tyr 180/Tyr 182), p53, phospho-IκBα (Ser 32), total IκBα, and phospho-NF-κB (p65) (Ser 536) were estimated.

2.4.6. Histological Studies. The livers from the experimental mice were immediately fixed in 10% buffered formalin and were processed for paraffin sectioning. Sections (~5 μm) were stained with hematoxylin and eosin (H & E) for studying the histology of hepatic tissues [32].

2.4.7. Statistical Analysis. The experimental data were denoted as mean ± SD. The data were statistically examined by one-way ANOVA followed by Dunnett's *t*-test using computerized GraphPad InStat (version 3.05), GraphPad software, USA. The values were considered significant when $p < 0.05$ or 0.01.

2.5. In Silico Prediction

2.5.1. Absorption, Distribution, Metabolism, and Excretion (ADME) Prediction. In silico ADME properties of CA were predicted using QikProp module of Maestro Schrödinger software [33]. Lipinski's rule of five (molecular weight < 500, number of hydrogen bond donors < 5, number of hydrogen bond acceptors < 10, log$P$ < 5) was also assessed, which helped in distinguishing between drug-like or non-drug-like profiles of a candidate molecule. Furthermore, some important ADME profiles, like oral absorptions, cell permeability, blood brain barrier, and so on of CA, were predicted in silico.

2.5.2. Molecular Docking and Postdocking Simulation Analysis. The high-resolution X-ray crystallographic structures of proteins were retrieved from Protein Data Bank (PDB) accessed on June 2017 [34]. The protein crystal structures for Bax (PDB ID: 4BD2), Bcl-2 (PDB: 4LXD), cytochrome C (PDB: 3ZCF), Apaf-1 (PDB: 1Z6T), caspase 9 (PDB: 2AR9), caspase 3 (PDB: 5I9B), Fas (PDB: 3EZQ), caspase 8 (PDB: 4PRZ), Bid (PDB: 4QVE), IκB (PDB: 4KIK), JNK (PDB: 4E73), NF-κB (PDB: 4IDV), p53 (PDB: 2XWR), and p38 (PDB: 3S3I) were downloaded in PDB format. To perform molecular docking, all proteins were prepared in Protein Preparation Wizard using Maestro in the Schrödinger suite [33] for addition of hydrogen atoms and to repair the faults like missing loops and steric clashes. Hence, protonation state was selected to be consistent in physiological pH. To obtain the minimum energy structure, system was subjected to a restrained minimization using the OPLS2005 force field in Impact Refinement module (Impref). The ligand, CA, was processed in LigPrep module of Schrödinger [33]. Using the Receptor Grid generation panel, the receptor grid was generated. During the grid generation step, the binding site was defined by a rectangular box surrounding the cocrystallized ligand. The position and size of the active site were also determined. Molecular docking was performed using standard precision (SP) method of docking using Glide module [33] to evaluate the binding affinity between protein and ligand.

Following molecular docking, the protein-ligand complex was subjected to molecular dynamics (MD) simulation study using the Desmond program (Desmond Molecular Dynamics System and Maestro-Desmond Interoperability Tools, Schrödinger) [33]. The complex was neutralized by appropriate number of ions and surrounded by an orthorhombic shape of water box solvated by TIP3P (transferable intermolecular potential 3P) water model [35]. By adopting the SHAKE algorithm, bond lengths to H atoms and internal geometry of H_2O molecules were constrained [36]. The simulation was carried out for each complex in equilibrated system of NPT ensemble at maximum 40 ns using the Nose-Hoover chain thermostat temperature at 300 K and Martyna-Tobias-Klein barostat bar pressure at 1.013 with a relaxation time of 1.0 ps and 2.0 ps, respectively. Energy of system and atomic coordinate data were recorded in every 1.2 ps time intervals.

3. Results

3.1. Effect of CA against $NaAsO_2$ Intoxication In Vitro

3.1.1. Dose-Dependent Effect of $NaAsO_2$-Induced Cytotoxicity. Reduction of cell viability is the index of cytotoxicity. In search of the cytotoxic effect of $NaAsO_2$, hepatocytes were incubated with $NaAsO_2$ at different concentrations for 2 h. The cell viability was reduced by $NaAsO_2$ in a concentration-dependent manner (Figure 3(a)). The IC_{50} value has been found to be 11.6 μM (~12 μM). Based on the observed IC_{50} value, subsequent *in vitro* experiments were executed using $NaAsO_2$ (12 μM) as a toxic control.

3.1.2. Effect of CA on Murine Hepatocytes. The hepatocytes incubated with CA (1–6 μM) did not show any significant change in the cell viability up to 4 h of experimental duration when compared with normal/untreated hepatocytes (~95.2% at 4 h). However, cell viability was slightly/insignificantly reduced (~89.2% at 4 h) with CA (10 μM). The data were included as supplementary Figure 1.

3.1.3. Concentration-Dependent Cytoprotective Role of CA against $NaAsO_2$-Induced Cytotoxicity. $NaAsO_2$ (12 μM, ~IC_{50}) exposed hepatocytes exhibited significant ($p < 0.01$) reduction in cell viability up to 4 h (Figure 3(b)). Simultaneous treatment of hepatocytes with CA (1–10 μM) and $NaAsO_2$ (12 μM) significantly ($p < 0.05$–0.01) prevented the reduction in cell viability in a concentration-dependent manner up to 4 μM. However, cytoprotective effect of CA was further reduced >4 μM concentration when compared with CA (4 μM). Based on the observation, the concentration of CA and the incubation time have been standardized to 4 μM and 2 h, respectively, for subsequent *in vitro* experiments. The CA (4 μM) alone did not show any significant difference in redox parameters in isolated murine hepatocytes (Supplementary Table 1).

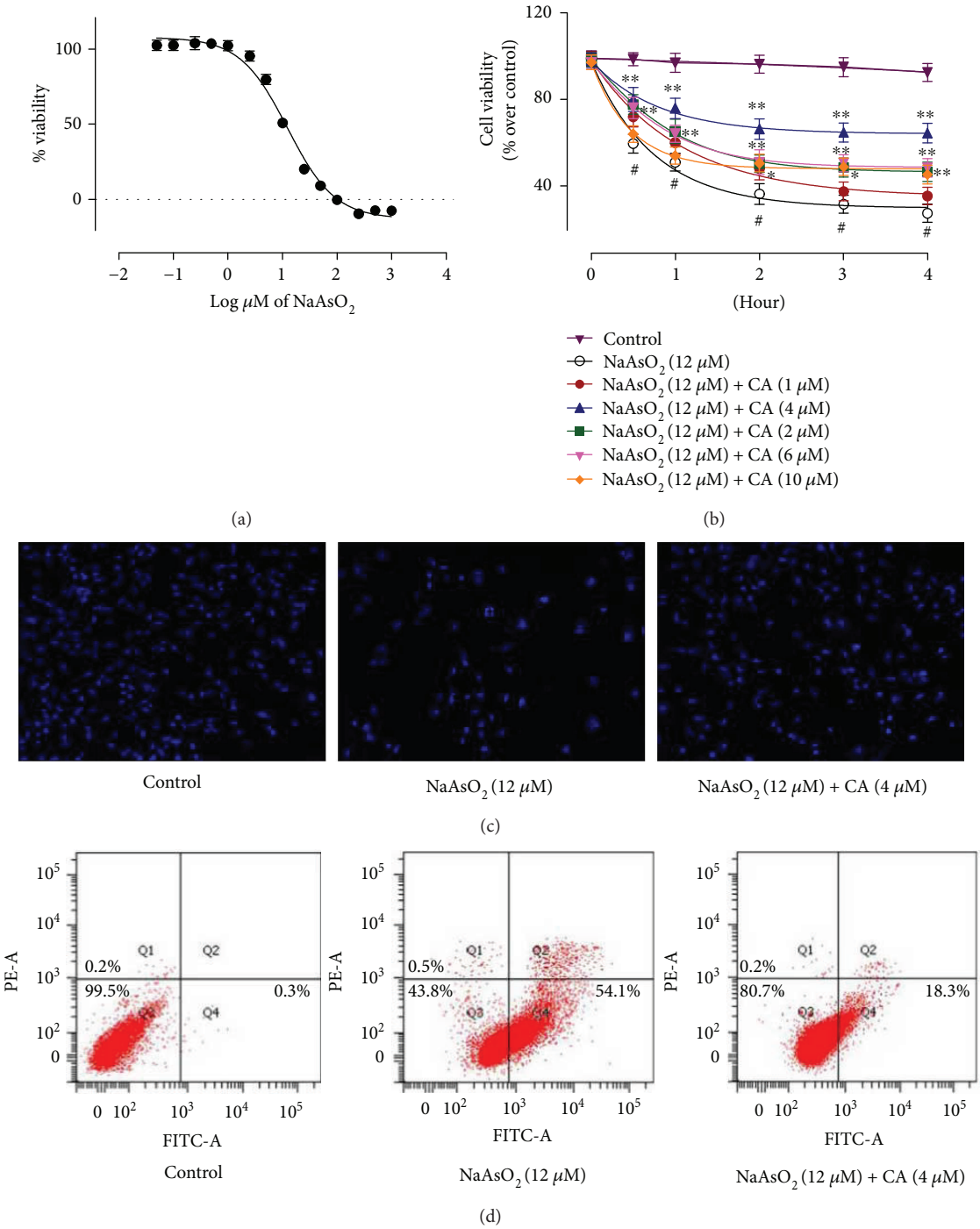

Figure 3: The cell viability, image, and flow cytometric assays in the absence ($NaAsO_2$) and presence of CA ($NaAsO_2 + CA$) *in vitro* employing isolated murine hepatocytes. (a) Effect of $NaAsO_2$ at different concentrations on cell viability in isolated murine hepatocytes. Values are represented as mean ± SD ($n = 3$). (b) Effect on cell viability in the absence ($NaAsO_2$) and presence of CA ($NaAsO_2 + CA$). Values are represented as mean ± SD ($n = 3$). $^{\#}$Values significantly ($p < 0.01$) differ from normal control. *Values significantly ($p < 0.05$) differ from toxic control. **Values significantly ($p < 0.01$) differ from toxic control. (c) Hoechst staining of hepatocytes in the absence ($NaAsO_2$) and presence of CA ($NaAsO_2 + CA$). (d) Percentage distribution of apoptotic and necrotic cells in the absence ($NaAsO_2$) and presence of CA ($NaAsO_2 + CA$) analyzed by flow cytometric assay.

3.1.4. Effect on Hoechst Staining. The cytoprotective effect of CA has been estimated by Hoechst staining following visualization through fluorescence microscope (Figure 3(c)) of hepatocytes under different treatments. $NaAsO_2$ (12 μM) treated hepatocytes exhibited significant reduction of visible nuclei; however, the visible nuclei exhibited explicit patterns of morphological changes, condensation, fragmentation of the nuclei, and chromatin condensation. Simultaneous

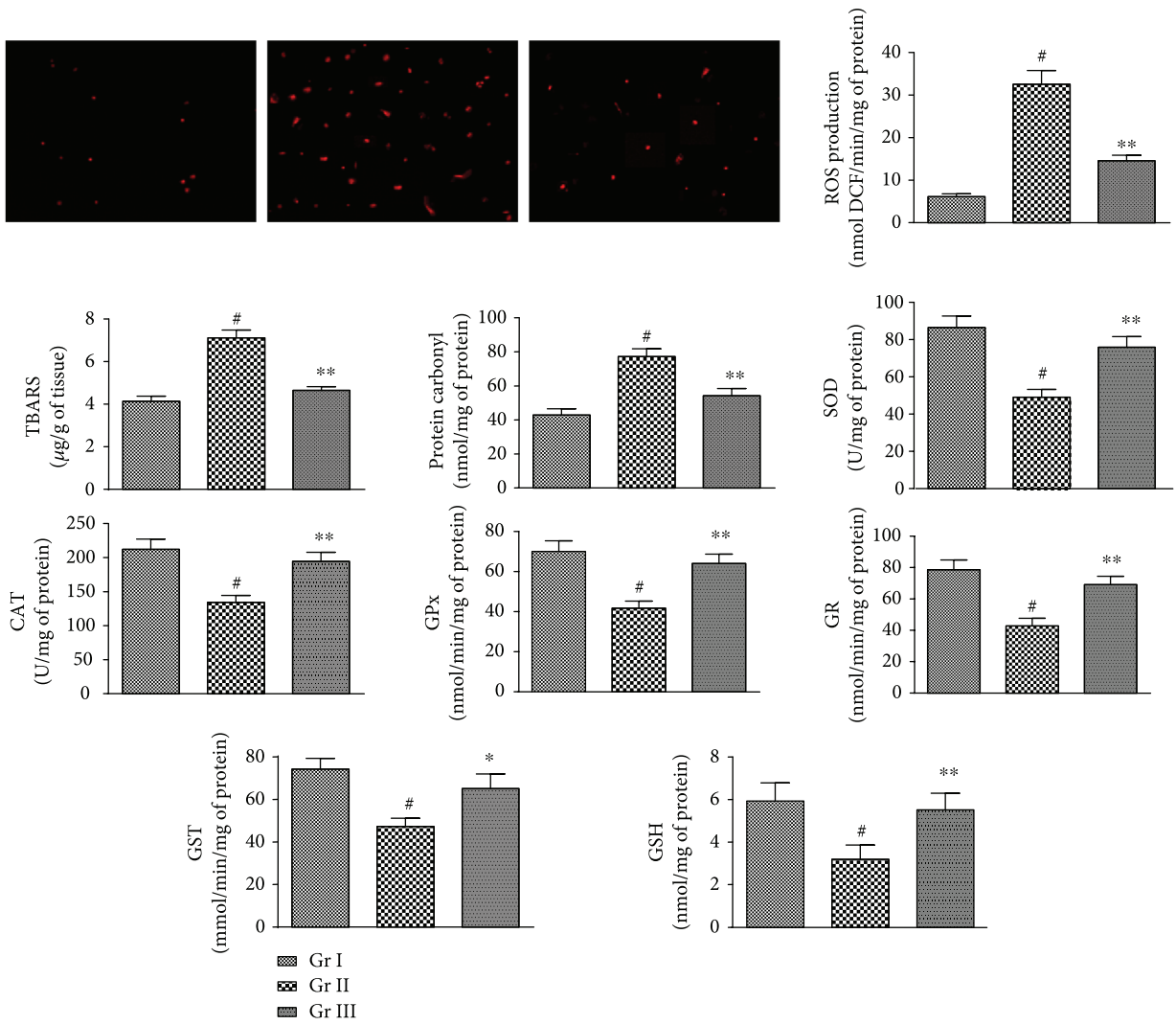

FIGURE 4: The effect on ROS accumulation, lipid peroxidation, protein carbonylation, and endogenous redox systems in the absence ($NaAsO_2$) and presence of CA ($NaAsO_2$ + CA) in isolated murine hepatocytes. Values are represented as mean ± SD ($n = 3$). #Values significantly ($p < 0.01$) differ from normal control. *Values significantly ($p < 0.05$) differ from toxic control. **Values significantly ($p < 0.01$) differ from toxic control. SOD unit, "U" is defined as inhibition (μ moles) of NBT-reduction/min. CAT unit "U" is defined as H_2O_2 consumption/min. Gr I: normal control; Gr II: toxic control; Gr III: hepatocytes incubated with $NaAsO_2$ (12 μM) along with CA (4 μM).

incubation of hepatocytes with CA (4 μM) and $NaAsO_2$ (12 μM) could significantly attenuate the cytotoxic effect of $NaAsO_2$ (12 μM) and could restore nuclear morphology to near-normal status.

3.1.5. Flow Cytometric Analysis. To investigate the nature of cell death, hepatocytes under different treatments were assessed by flow cytometric analysis. Flow cytometric data (Figure 3(d)) revealed that $NaAsO_2$ (12 μM) treated hepatocytes exhibited very low PI staining (~0.5%) with very high annexin V-FITC binding (~54.1%) indicating majority of apoptotic cells. Simultaneous treatment of hepatocytes with CA (4 μM) and $NaAsO_2$ (12 μM) resulted significant reduction in the count of the apoptotic cells (~18.3%) indicating a possible cytoprotective effect of CA against $NaAsO_2$ (12 μM) induced cytotoxicity. The control group showed very little apoptotic (~0.3%) and necrotic (~0.2%) cells as compared with viable cells (~99.5%).

3.1.6. Effects on $NaAsO_2$-Induced Alteration in Redox Status in Hepatocytes. The prophylactic effects of CA on $NaAsO_2$-induced oxidative stress in isolated murine hepatocyte have been depicted in Figure 4. Overproduction of ROS is an index of redox-challenged cellular atmosphere. In this study, $NaAsO_2$ (12 μM) incubated hepatocytes revealed significant ($p < 0.01$) enhance in ROS production in the hepatocytes as ostensible from fluorescence of DCF measured in fluorescence microscope. CA (4 μM) could significantly ($p < 0.01$) reduce the $NaAsO_2$ (12 μM) mediated ROS production in the hepatocytes. Overproduction of ROS causes oxidative damage of cellular macromolecules. In this study, $NaAsO_2$ (12 μM) exposed hepatocytes exhibited significantly ($p < 0.01$) high level of thiobarbituric acid reactive substances

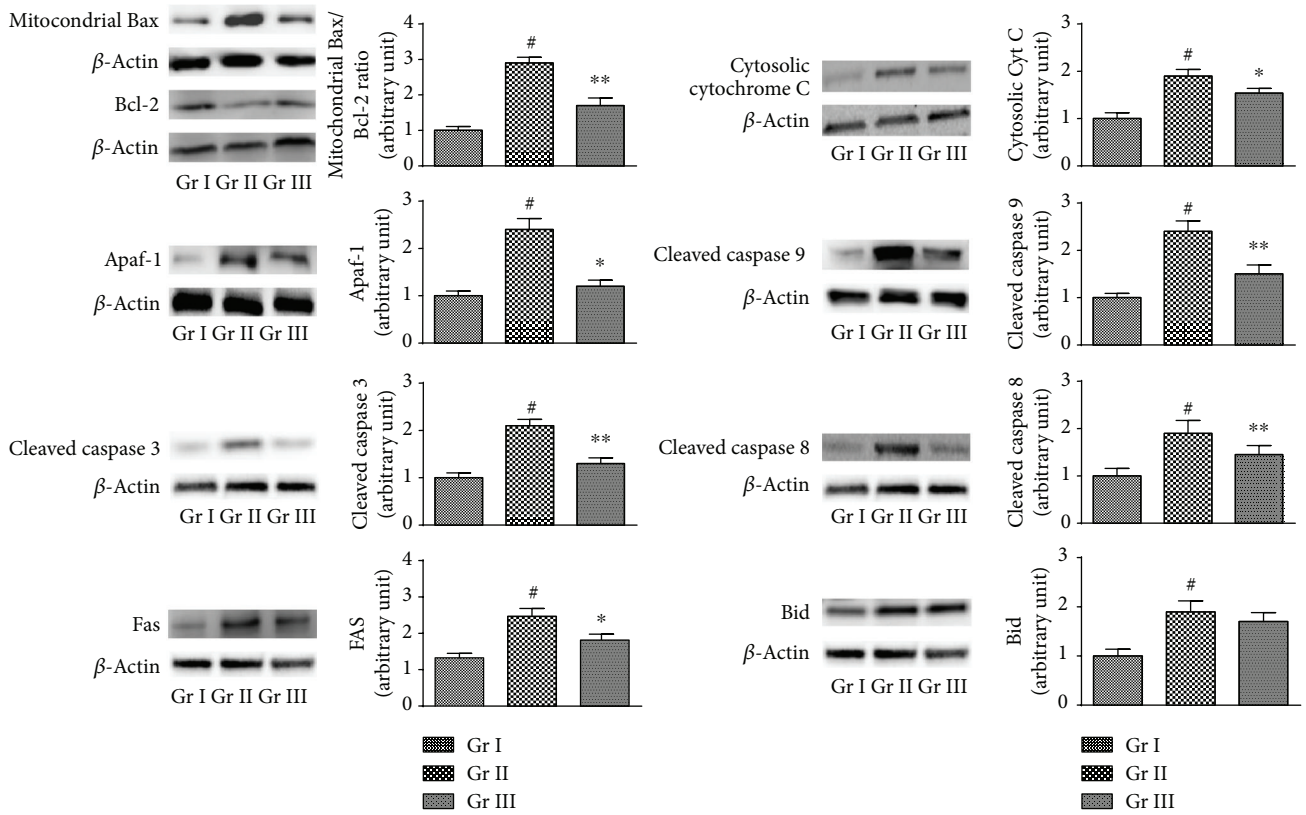

FIGURE 5: The effect on intrinsic and extrinsic apoptotic signaling in the absence ($NaAsO_2$) and presence of CA ($NaAsO_2$ + CA) *in vitro*. The relative band intensities were assessed and the normal control band was allotted a random value of 1. β-actin served as loading control. Values are expressed as mean ± SD ($n = 3$). #Values significantly ($p < 0.01$) differ from normal control. *Values significantly ($p < 0.05$) differ from toxic control. **Values significantly ($p < 0.01$) differ from toxic control. Gr I: normal control; Gr II: toxic control; Gr III: hepatocytes incubated with $NaAsO_2$ (12 μM) along with CA (4 μM).

(TBARS) level. TBARS, a by-product of lipid peroxidation, is used as a marker to estimate the extent of lipid peroxidation. $NaAsO_2$ (12 μM) exposed hepatocytes showed significant ($p < 0.01$) escalation in the level of carbonylated protein. However, simultaneous treatment with CA (4 μM) could significantly attenuate $NaAsO_2$ mediated the lipid peroxidation (<0.01) and protein carbonylation (<0.01). $NaAsO_2$ (12 μM) intoxication concomitantly creates a redox-challenged cellular environment via significant (<0.01) depletion in the levels of endogenous antioxidant enzymes (SOD, CAT, GPx, GST, and GR) and GSH. However, treatment with CA (4 μM) along with $NaAsO_2$ (12 μM) could significantly reverse the $NaAsO_2$-mediated changes in the levels of antioxidant enzymes ($p < 0.05$–0.01) and GSH ($p < 0.01$) in the murine hepatocytes.

3.1.7. Effects on Apoptotic Events in Hepatocytes. The prophylactic effects of CA on $NaAsO_2$-induced intrinsic and extrinsic apoptotic signaling have been shown in Figure 5. Oxidative stress further promotes apoptosis via downregulation and upregulation in the transcriptions of antiapoptotic and proapoptotic signal proteins, respectively. In this study, the Western blot analysis revealed that $NaAsO_2$ (12 μM) caused significant upregulation in the expression of the Bax (proapoptotic) protein in mitochondria with concomitant downregulation in the expression of Bcl-2 (antiapoptotic) protein, resulting a significant ($p < 0.01$) increase in Bax/Bcl-2 ratio in the hepatocytes. $NaAsO_2$ (12 μM) exposure further promoted the release of cytochrome C to the cytosol evidenced from significant upregulation ($p < 0.01$) in the expression of cytosolic cytochrome C in murine hepatocytes. $NaAsO_2$ (12 μM) treatment significantly ($p < 0.01$) activated Apaf-1 expression in the cytosol of murine hepatocytes, which further endorsed the cleavage of procaspases. Significant upregulations ($p < 0.01$) in the expressions of cleaved caspase 9 and cleaved caspase 3 were observed in $NaAsO_2$ (12 μM) exposed hepatocytes. However, CA (4 μM) cotreatment could significantly ($p < 0.05$–0.01) reinstate the expressions of aforementioned intrinsic apoptotic proteins to near-normal status. In search of the effect on extrinsic pathway of apoptosis (mitochondria independent), Western blot analysis of FAS, cleaved caspase 8, and Bid were performed. $NaAsO_2$ (12 μM) exposed hepatocytes exhibited significant ($p < 0.01$) upregulations in the expressions of FAS, cleaved caspase 8, and Bid. CA (4 μM) cotreatment could significantly restore the expressions of FAS ($p < 0.05$) and cleaved caspase 8 ($p < 0.01$) to near-normal status. However, CA (4 μM) was not found to be effective against Bid.

To investigate the proapoptotic effect of NF-κB, the signal proteins were immunoblotted (Figure 6). $NaAsO_2$ (12 μM) treatment could significantly ($p < 0.01$) stimulate the phosphorylation of cytosolic IκBκ and thereby could

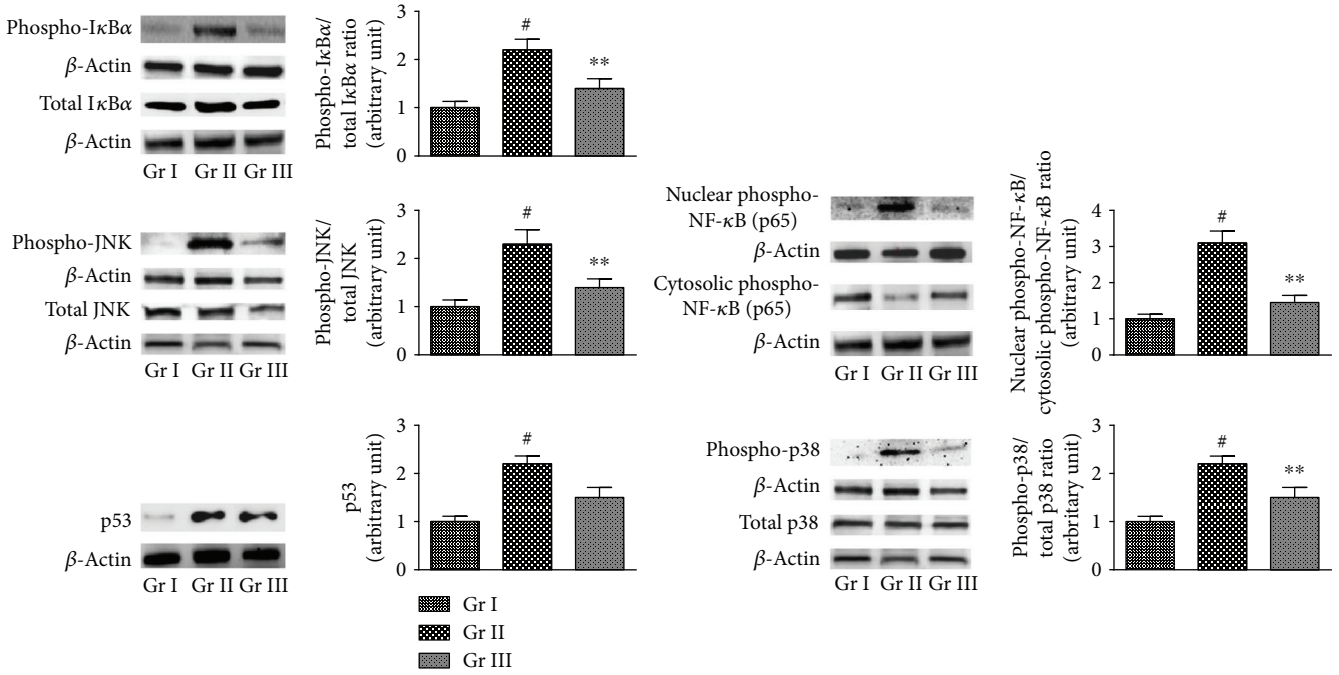

Figure 6: The effect on IκBα, NF-κB, JNK, p38, and p53 signaling in the absence ($NaAsO_2$) and presence of CA ($NaAsO_2$ + CA) *in vitro*. The relative band intensities were assessed and the normal control band was allotted a random value of 1. β-actin served as loading control. Values are expressed as mean ± SD ($n = 3$). #Values significantly ($p < 0.01$) differ from normal control. *Values significantly ($p < 0.05$) differ from toxic control. **Values significantly ($p < 0.01$) differ from toxic control. Gr I: normal control; Gr II: toxic control; Gr III: hepatocytes incubated with $NaAsO_2$ (12 μM) along with CA (4 μM).

Table 1: Effects on body weight, liver weight, hepatic As content, and urinary As content in the absence ($NaAsO_2$) and presence of CA (CA + $NaAsO_2$) in mice.

Parameters	Gr I	Gr II	Gr III	Gr IV
Body weight (g)	28.16 ± 3.11	21.77 ± 2.08#	26.08 ± 3.01*	26.92 ± 3.33*
Liver weight (g)	1.24 ± 0.21	1.15 ± 7.29	1.17 ± 0.13	1.22 ± 0.25
Liver As (μg/g of tissue)	0.06 ± .0001	0.51 ± 0.04#	0.35 ± 0.04*	0.32 ± 0.02*
Urinary As (μg/g of creatinine)	2.34 ± 0.31	19.65 ± 2.17#	23.67 ± 2.98*	26.01 ± 3.22**

Values are expressed as mean ± SD ($n = 6$). #Values differ significantly from normal control ($p < 0.01$). *Values differ significantly from $NaAsO_2$ control ($p < 0.05$). **Values differ significantly from $NaAsO_2$ control ($p < 0.01$). Gr I: normal control; Gr II: toxic control; Gr III: CA (10 mg/kg) + $NaAsO_2$ (10 mg/kg); Gr IV: CA (20 mg/kg) + $NaAsO_2$ (10 mg/kg).

activate NF-κB (p65) signaling. A significant ($p < 0.01$) translocation of NF-κB (p65) to the nucleus was visualized in $NaAsO_2$ (12 μM) exposed hepatocytes. However, CA (4 μM) could significantly ($p < 0.01$) attenuate the aforementioned NF-κB signaling pathway within the hepatocytes. ROS can also trigger the mitogen-activated protein kinases (MAPK). In this study, $NaAsO_2$ (12 μM) could significantly ($p < 0.01$) stimulate the phosphorylation of JNK and p38 (Figure 6). However, CA (4 μM) could significantly ($p < 0.01$) downregulate the $NaAsO_2$ (12 μM) mediated phosphorylation of JNK and p38. On the other hand, $NaAsO_2$ (12 μM) could significantly ($p < 0.01$) upregulate p53 signaling, while CA (4 μM) was not found to be effective against p53.

3.2. Effects of CA against $NaAsO_2$ Intoxication In Vivo

3.2.1. Effect on Body Weight, Liver Weight, Hepatic As Content, and Urinary As Content. During the tenure of experiment, no significant change in food and water intake was recorded in the animals of either of experimental group. $NaAsO_2$ (10 mg/kg) treated mice exhibited significant ($p < 0.01$) reduction in the body weight; however, simultaneous administration of CA (10 and 20 mg/kg) along with $NaAsO_2$ (10 mg/kg) could significantly ($p < 0.05$) restore the body weight to near-normal status (Table 1). No significant difference in liver weight was observed in the experimental mice of either group. $NaAsO_2$ (10 mg/kg) exposed mice exhibited significant ($p < 0.01$) increase in the accumulation of As in the liver coupled with significantly ($p < 0.01$) poor urinary clearance of As when compared with normal mice. On the other hand, simultaneous administration of CA (10 and 20 mg/kg) along with $NaAsO_2$ (10 mg/kg) could significantly ($p < 0.05$–0.01) promote the As clearance resulting significantly ($p < 0.05$) low hepatic As content.

Table 2: Effects on haematological and serum biochemical parameters in the absence ($NaAsO_2$) and presence of CA (CA + $NaAsO_2$) in mice.

Parameters	Gr I	Gr II	Gr III	Gr IV
Total erythrocyte count ($\times 10^6/mm^3$)	6.28 ± 0.42	$3.22 \pm 0.34^{\#}$	$4.04 \pm 0.25^{*}$	$5.19 \pm 0.67^{**}$
Haemoglobin (g/dl)	8.76 ± 0.72	$4.89 \pm 0.43^{\#}$	$6.12 \pm 0.48^{*}$	$6.88 \pm 0.87^{**}$
ALT (IU/I)	68.54 ± 5.81	$112.98 \pm 9.63^{\#}$	$89.85 \pm 7.62^{**}$	$82.17 \pm 6.15^{**}$
AST (IU/I)	58.12 ± 4.63	$82.91 \pm 7.29^{\#}$	$73.62 \pm 5.82^{*}$	$64.57 \pm 5.51^{**}$
CK (IU/mg protein)	10.87 ± 1.05	$18.65 \pm 1.24^{\#}$	$14.22 \pm 0.98^{**}$	$13.78 \pm 1.33^{**}$
LDH (U/l)	171.34 ± 13.42	$252.67 \pm 21.50^{\#}$	$198.33 \pm 20.12^{**}$	$187.54 \pm 17.72^{**}$

Values are expressed as mean ± SD ($n = 6$). $^{\#}$Values differ significantly from normal control ($p < 0.01$). *Values differ significantly from $NaAsO_2$ control ($p < 0.05$). **Values differ significantly from $NaAsO_2$ control ($p < 0.01$). Gr I: normal control; Gr II: toxic control; Gr III: CA (10 mg/kg) + $NaAsO_2$ (10 mg/kg); Gr IV: CA (20 mg/kg) + $NaAsO_2$ (10 mg/kg).

3.2.2. Effects on Blood Parameters. Blood parameters give crucial impression of pathological state within the system. The effects of CA on blood parameters of experimental mice were reported in Table 2. $NaAsO_2$ (10 mg/kg) treated mice exhibited significant ($p < 0.01$) reduction in erythrocyte counts and haemoglobin level. However, simultaneous administration of CA (10 and 20 mg/kg) along with $NaAsO_2$ (10 mg/kg) could significantly ($p < 0.05$–0.01) restore the erythrocyte counts and haemoglobin level ($p < 0.01$) to near-normal status. $NaAsO_2$ (10 mg/kg) treatment caused significant ($p < 0.01$) increase in ALT, AST, LDH, and CK levels in the sera of experimental mice. However, concurrent administration of CA (10 and 20 mg/kg) along with $NaAsO_2$ (10 mg/kg) could significantly ($p < 0.05$–0.01) revert the serum biochemical parameters to near-normal status.

3.2.3. Effects on Redox Status in Liver. In *in vivo* assay, $NaAsO_2$ (10 mg/kg) treated mice exhibited significant ($p < 0.01$) elevation in the level of intracellular ROS within the hepatic tissue (Figure 7). However, simultaneous administration of CA (10 and 20 mg/kg) along with $NaAsO_2$ (10 mg/kg) could significantly ($p < 0.01$) attenuate intracellular ROS production in the liver (Figure 6). Significant ($p < 0.01$) upregulations in lipid peroxidation and protein carbonylation were observed in the liver of $NaAsO_2$ (10 mg/kg) exposed mice. On the other hand, CA (10 and 20 mg/kg) treatment could significantly ($p < 0.05$–0.01) reinstate lipid peroxidation and protein carbonylation in the hepatic tissue of the experimental mice to near-normal status (Figure 7). $NaAsO_2$ (10 mg/kg) further potentiated oxidative stress via significant ($p < 0.01$) depletion in the levels of GSH and endogenous antioxidant enzymes (SOD, CAT, GPx, GR, and GST) in the hepatic tissue (Figure 7). However, simultaneous administration of CA (10 and 20 mg/kg) along with $NaAsO_2$ (10 mg/kg) could significantly ($p < 0.05$–0.01) revert GSH and endogenous antioxidant enzymes to near-normal status (Figure 7).

3.2.4. Effects in the Expressions of Signal Proteins in the Liver. In this study, the expressions of different apoptotic proteins in the liver of experimental mice were assessed by Western blotting (Figure 8). Significant upregulations ($p < 0.01$) in the expressions of proapoptotic Bax protein in the mitochondria and concomitant downregulations ($p < 0.01$) in the expressions of antiapoptotic-Bcl-2 protein in the cellular fraction were observed in the liver of $NaAsO_2$ (10 mg/kg) treated mice. In this study, significant ($p < 0.01$) high mitochondrial Bax/Bcl-2 ratio was observed in the hepatic tissue of $NaAsO_2$ (10 mg/kg) treated mice. However, treatment with CA (10 and 20 mg/kg) along with $NaAsO_2$ (10 mg/kg) could significantly ($p < 0.05$–0.01) reciprocate As-mediated alteration of Bax/Bcl-2 ratio in the liver of experimental animals. $NaAsO_2$ (10 mg/kg) treated mice revealed significant ($p < 0.01$) upregulation of cytosolic cytochrome C in the hepatic tissue, which suggested the release of cytochrome C into cytosol from mitochondria. On other hand, treatment with CA (10 and 20 mg/kg) along with $NaAsO_2$ (10 mg/kg) could significantly ($p < 0.05$) attenuate As-provoked cytochrome C release to cytosol. Significant upregulations ($p < 0.01$) in the expressions of Apaf-1 were recorded in the liver of $NaAsO_2$-exposed mice. CA (20 mg/kg) treatment along with $NaAsO_2$ (10 mg/kg) could significantly ($p < 0.05$) downregulate the expression of Apaf-1 in the hepatic tissue of experimental mice. $NaAsO_2$ (10 mg/kg) treated mice exhibited significant ($p < 0.01$) upregulation in the expressions of cleaved caspases 3 and 9 in the liver of experimental mice. However, treatment with CA (10 and 20 mg/kg) along with $NaAsO_2$ (10 mg/kg) could significantly reciprocate the expressions of cleaved caspases 3 ($p < 0.05$–0.01) and 9 ($p < 0.01$) in the liver of experimental mice. To study the effect of $NaAsO_2$ on death receptor-mediated apoptosis, immunoblot analysis of FAS, Bid and cleaved caspase 8 was performed. $NaAsO_2$ (10 mg/kg) treated mice exhibited significant ($p < 0.01$) upregulation in the expressions of the FAS, Bid, and cleaved caspase 8 in the hepatic tissue, which advocated simultaneous engrossment of the extrinsic pathway of apoptosis. Treatment with CA (10 and 20 mg/kg) along with $NaAsO_2$ (10 mg/kg) could significantly reciprocate the As-mediated alteration in the expressions of FAS ($p < 0.05$) and cleaved caspase 8 ($p < 0.01$). However, CA (10 and 20 mg/kg) treatment did not exhibit any significant change in As-provoked Bid expression in the liver of experimental animals.

To investigate the effect on NF-κB, the signaling, $NaAsO_2$ (10 mg/kg) treatment could significantly ($p < 0.01$) stimulate

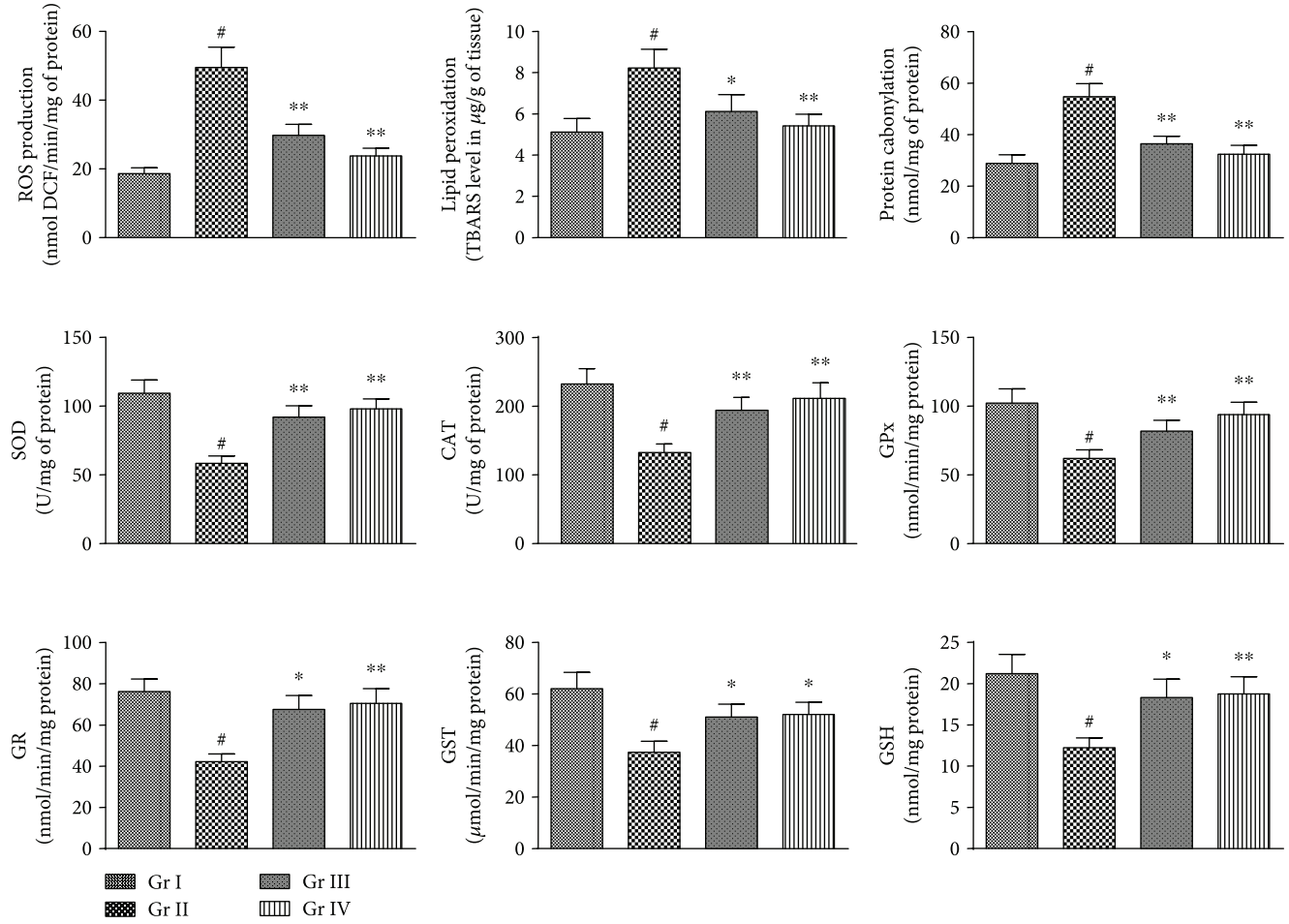

Figure 7: The effect on ROS accumulation, lipid peroxidation, protein carbonylation, and endogenous redox systems in the absence ($NaAsO_2$) and presence of CA ($NaAsO_2$ + CA) *in vivo* in the liver of experimental mice. Values are represented as mean ± SD ($n = 6$). #Values significantly ($p < 0.01$) differ from normal control. #Values significantly ($p < 0.01$) differ from normal control. *Values significantly ($p < 0.05$) differ from toxic control. **Values significantly ($p < 0.01$) differ from toxic control. SOD unit "U" is defined as inhibition (μ moles) of NBT-reduction/min. CAT unit "U" is defined as H_2O_2 consumption/min. Gr I: normal control; Gr II: toxic control; Gr III: CA (10 mg/kg) + $NaAsO_2$ (10 mg/kg), Gr IV: CA (20 mg/kg) + $NaAsO_2$ (10 mg/kg).

the phosphorylation of cytosolic IκBα and thereby could significantly trigger the translocation of phosphorylated NF-κB (p 65) ($p < 0.01$) to the nucleus (Figure 9). However, CA (10 and 20 mg/kg) along with $NaAsO_2$ (10 mg/kg) could significantly ($p < 0.05$–0.01) attenuate the aforementioned NF-κB signaling pathway in the liver of experimental mice (Figure 9). In this study, $NaAsO_2$ (10 mg/kg) could significantly ($p < 0.01$) upregulate the phosphorylation of JNK and p38 (Figure 9). The treatment with CA (10 and 20 mg/kg) along with $NaAsO_2$ (10 mg/kg) could significantly ($p < 0.01$) reciprocate the phosphorylation of JNK and p38 in the hepatic tissue of experimental mice (Figure 9). However, CA (10 and 20 mg/kg) could not counteract with the $NaAsO_2$ (10 mg/kg) mediated p53 upregulation in the liver of experimental mice (Figure 9).

3.2.5. Effects on ATP Levels, DNA Fragmentation, and DNA Oxidation in the Liver. In this study, $NaAsO_2$ (10 mg/kg) treatment caused significant ($p < 0.01$) elevation in the level of cytosolic ATP in the hepatic tissue of experimental mice (Figure 10). The experimental observation could be substantiated with the establishment of apoptotic incidence within the liver. $NaAsO_2$ (10 mg/kg) mediated significant ($p < 0.01$) upregulations of DNA fragmentation and oxidation further confirmed the establishment of As-mediated cytotoxic events within the hepatic tissue of mice (Figure 10). On the other hand, concomitant treatment with CA (10 and 20 mg/kg) along with $NaAsO_2$ (10 mg/kg) could significantly ($p < 0.05$–0.01) reduce cytosolic ATP level, DNA fragmentation, and DNA oxidation in the hepatic tissue of experimental mice close to the normal status (Figure 10).

3.2.6. Effects on the Histology of the Liver. The histological sections of livers of experimental mice were depicted in Figures 11(a) and (b). The liver section of $NaAsO_2$ (10 mg/kg) exposed mice exhibited diffused portal veins (red arrows), damaged hepatocytes with infiltrating leukocytes (green arrows), vacuolated cytoplasm (blue arrows), and induction of apoptosis (yellow arrows) when compared with the liver section of normal mice. However,

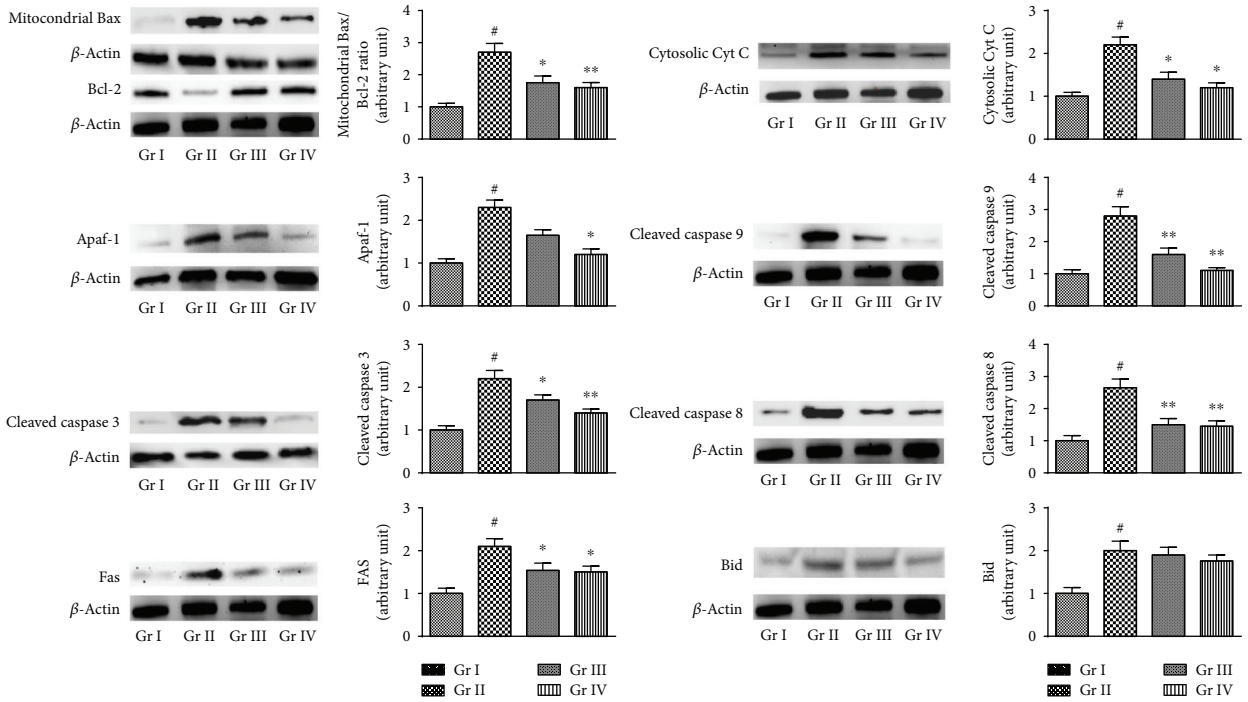

FIGURE 8: The effect on intrinsic and extrinsic apoptotic signaling in the absence ($NaAsO_2$) and presence of CA ($NaAsO_2$ + CA) *in vivo* in the liver of experimental mice. The relative band intensities were assessed and the normal control band was allotted a random value of 1. β-actin served as loading control. Values are expressed as mean ± SD ($n = 6$). #Values significantly ($p < 0.01$) differ from normal control. *Values significantly ($p < 0.05$) differed from toxic control. **Values significantly ($p < 0.01$) differed from toxic control. Gr I: normal control; Gr II: toxic control; Gr III: CA (10 mg/kg) + $NaAsO_2$ (10 mg/kg), Gr IV: CA (20 mg/kg) + $NaAsO_2$ (10 mg/kg).

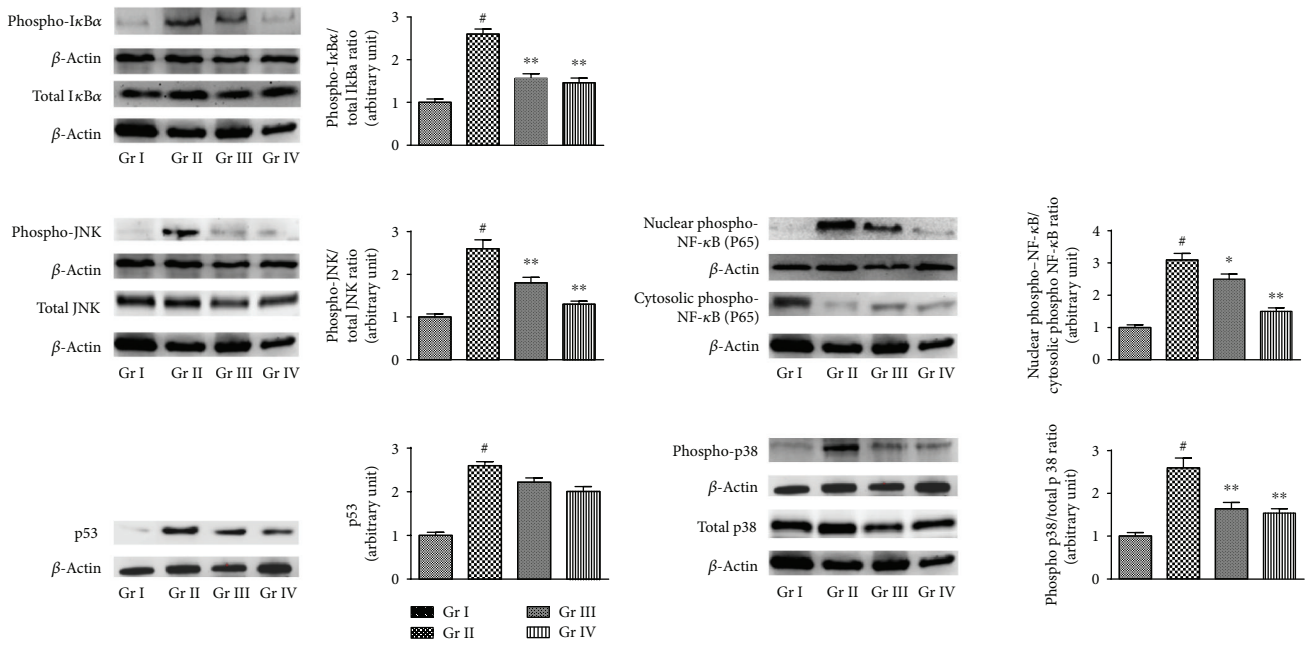

FIGURE 9: The effect on IκBα, NF-κB, JNK, p38, and p53 signaling in the absence ($NaAsO_2$) and presence of CA ($NaAsO_2$ + CA) *in vivo* in the liver of experimental mice. The relative band intensities were assessed and the normal control band was allotted a random value of 1. β-actin served as loading control. Values are expressed as mean ± SD ($n = 6$). #Values significantly ($p < 0.01$) differ from normal control. *Values significantly ($p < 0.05$) differed from toxic control. **Values significantly ($p < 0.01$) differed from toxic control. Gr I: normal control; Gr II: toxic control; Gr III: CA (10 mg/kg) + $NaAsO_2$ (10 mg/kg), Gr IV: CA (20 mg/kg) + $NaAsO_2$ (10 mg/kg).

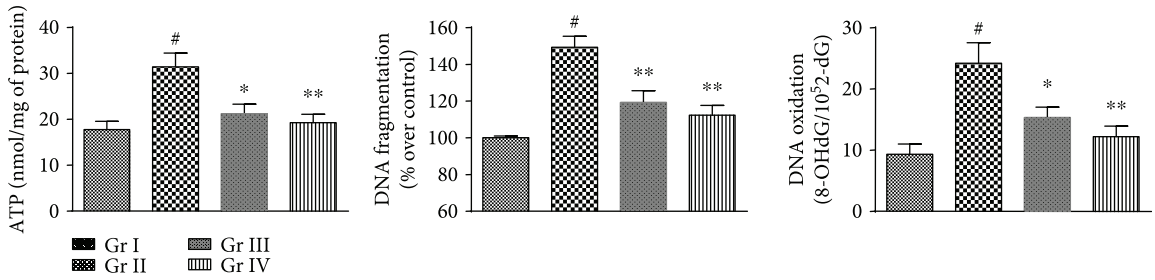

FIGURE 10: The effect on ATP, DNA fragmentation and DNA oxidation in the absence ($NaAsO_2$) and presence of CA ($NaAsO_2$ + CA) *in vivo* in the liver of experimental mice. Values are expressed as mean ± SD ($n = 6$). #Values significantly ($p < 0.01$) differ from normal control. *Values significantly ($p < 0.05$) differ from toxic control. **Values significantly ($p < 0.01$) differ from toxic control. Gr I: normal control; Gr II: toxic control; Gr III: CA (10 mg/kg) + $NaAsO_2$ (10 mg/kg), Gr IV: CA (20 mg/kg) + $NaAsO_2$ (10 mg/kg).

CA (10 and 20 mg/kg) treatment could reinstate $NaAsO_2$ (10 mg/kg) mediated the aforementioned pathological changes and restored the histology of liver to near-normal status.

3.3. In Silico Studies

3.3.1. ADME Analysis. The drug-likeness and pharmacokinetic properties of CA was evaluated using QikProp module of Schrödinger. Drug-likeness and physicochemical properties were found to be as molecular weight = 332.4, H-bond donor = 3, H-bond acceptor = 3.5, predicted water partition coefficient = 3.7, aqueous solubility = −4.4, and total solvent accessible surface area = 575.8. The pharmacokinetic profiles, such as predicted brain/blood partition coefficient = −0.7, predicted apparent Caco-2 cell permeability = 182.7, number of likely metabolic reactions = 4, and human oral absorption = 89.3%, are significantly compliant with recommended values of drug-likeness. In Table 3, some other important predicted ADME parameters of CA were presented. The better drug-likeness with acceptable biopharmaceutical properties clearly indicated that CA may be a potential drug candidate.

3.3.2. Molecular Docking. Molecular docking analysis was attempted to dig into the possible binding patterns and interactions of CA with the selective signal proteins. Generated docking poses were ranked on the basis of Glide score. The lowest scored conformer was considered to be the best docking pose. Glide score represents the most capable best fit for a ligand in the active site of the target protein. In this study, Apaf-1 (PDB: 1Z6T), cytochrome C (PDB: 3ZCF), Bid (PDB: 4QVE), Fas (PDB: 3EZQ), and p53 (PDB: 2XWR) did not demonstrate significant docked pose after docking with CA; therefore, these proteins were discarded for further in silico analysis. Hydrogen bond (H-bond) interactions with the catalytic amino acid residues along with Glide score and Emodel values of other proteins were presented in Table 4. Molecular docking of Bax protein with the CA revealed three types of molecular interactions, namely H-bond, cation-π, and π-π stacking (Figure 12(a)). It was observed that H-bond interactions are fit into the Bax hydrophobic groove of Leu 122 residue and with the side chain of positively charged Arg 37 residue. The cation-π and π-π stacking interactions were also found with the same charged Arg 37 residue. In case of Bcl-2 protein, no single H-bond interaction was found to be formed with the catalytic residues. However, H-bond was predicted into ligand itself in the presence of H_2O molecule through intramolecular H-bond interaction (Figure 12(b)). This intramolecular H-bond formation was also highlighted in the cocrystal structure of Bcl-2 (PDB: 4LXD). Docking analysis of caspase 9 revealed that Arg 355 residue participates to form H-bond with CA along with the formation of π-π stacking and salt bridge (Figure 12(c)). Since H-bond interaction with Arg 355 was also found with the ligand of X-ray crystal structure of caspase 9 (PDB: 2AR9), therefore, this interaction may be considered as a constraint to play a dynamic role in the biological phenomenon. The binding interactions of caspase 3 revealed that Thr 62 and Arg 207 residues are involved in H-bond formation with CA (Figure 12(d)). However, Thr 62 residue interacted through H_2O-bridge formation. Caspase 8 was found to interact with two amino acid residues, Glu 396 and Thr 467, to form H-bond interaction with CA (Figure 12(e)). The same Glu 396 residue has been found to participate in H-bond formation in cocrystallized ligand of the PDB (4PRZ).

The binding interactions of CA with IκB showed involvement of two residues, backbone atom of Leu 21 and side chain atom of Asp 103 in H-bond formation (Figure 13(a)). When comparing interaction with the cocrystallized structure of IκB (PDB: 4KIK), it has been found that different amino acid residues (Glu 149, Glu 97, and Cys 99) were involved in H-bond formation. The docking analysis also revealed the predicted interaction for IκB with negatively charged Asp 103 residue that might be important for the activation of the receptor. The H-bond interaction with two amino acids, Arg 416 (side chain) and Leu 472 (backbone), was observed between NF-κB protein and CA along with π-π stacking interaction with Arg 408 residue (Figure 13(b)). The cocrystallized structure of NF-κB (PDB: 4IDV) exhibited that Leu 472 residue is found to participate in H-bond interaction. Docking analysis of JNK exhibited a single H-bond interaction between Asn 114 and CA; however, the crystal structure of JNK (PDB: 4E73) specified the involvement of Met 111 in the interaction (Figure 13(c)). The interaction with Asn 114 might highlight that JNK has

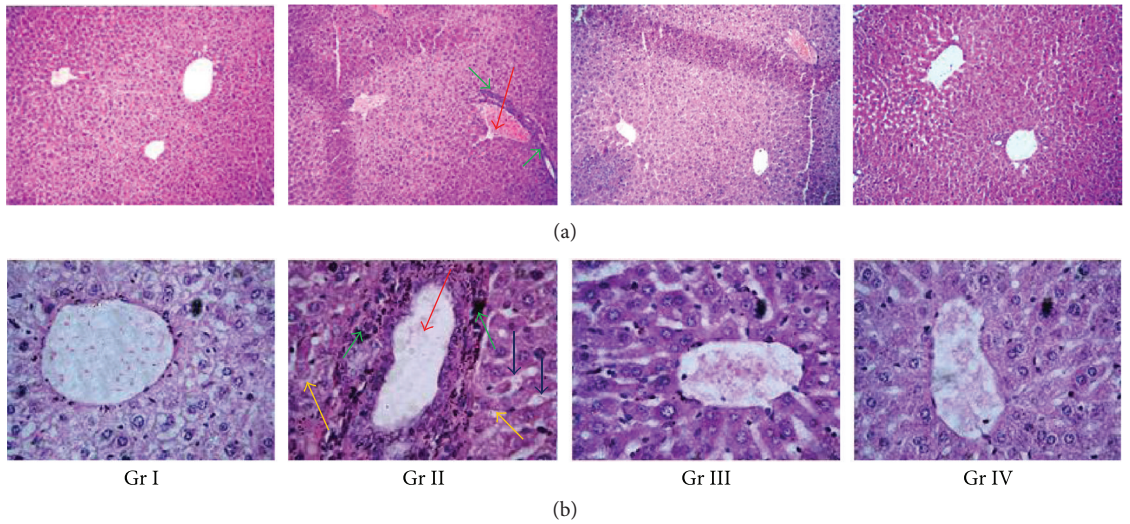

Figure 11: Histological sections 100x (a) and 400x (b) of the livers of experimental mice in the absence ($NaAsO_2$) and presence of CA ($NaAsO_2$ + CA). The liver sections of normal mice revealed normal portal vein and hepatocytes. $NaAsO_2$-exposed liver section exhibited dilated portal vein (red arrow), vacuolated cytoplasm (blue arrows), apoptosis (yellow arrows), and leucocytes infiltration (green arrows) when compared with the section of normal control liver. CA treatment could reinstate $NaAsO_2$ mediated the aforementioned pathological changed. Gr I: normal control; Gr II: toxic control; Gr III: CA (10 mg/kg) + $NaAsO_2$ (10 mg/kg), Gr IV: CA (20 mg/kg) + $NaAsO_2$ (10 mg/kg).

Table 3: Prediction of drug-likeness and ADME profiles of CA.

Sl. number	Descriptors	Predicted values for CA	Recommended values (based on properties of 95% of known drugs)
1.	Molecular weight	332.4	130.0 to 725.0
2.	SASA	575.8	300.0 to 1000.0
3.	WPSA	0.0	0.0 to 175.0
4.	H-bond donor	3.0	0.0 to 6.0
5.	H-bond acceptor	3.5	2.0 to 20.0
6.	glob	0.8	0.75 to 0.95
7.	QPlogPo/w	3.7	−2.0 to 6.5
8.	QPlogS	−4.4	−6.5 to 0.5
9.	QPlogHERG	−1.9	Concern below −5
10.	QPPCaco	182.7	25 poor; >500 great
11.	QPlogBB	−0.7	−3.0 to 1.2
12.	QPPMDCK	100.2	<25 poor, >500 great
13.	QPlogKp	−3.2	−8.0 to −1.0
14.	#metab	4.0	1.0 to 8.0
15.	QPlogKhsa	0.3	−1.5 to 1.5
16.	% of human oral absorption	89.3	>80% is high; <25% is poor

SASA: total solvent accessible surface area; WPSA: weakly polar component of the SASA; glob: globularity descriptor; QPlogPo/w: predicted octanol/water partition coefficient; QPlogS: predicted aqueous solubility; QPlogHERG: predicted IC_{50} value for blockage of HERG K+ channels; QPPCaco: predicted apparent Caco-2 cell permeability; QPlogBB: predicted brain/blood partition coefficient; QPPMDCK: predicted apparent MDCK cell permeability in nm/sec; QPlogKp: predicted skin permeability; #metab: number of likely metabolic reactions; QPlogKhsa: prediction of binding to human serum albumin.

another binding site where CA interacted to form H-bond. For the protein p38, no H-bond interaction was observed but possessed moderate dock score of −5.608 kcal/mol in docking. Although, a number of lofty hydrophobic amino acids (Val 38, Ala 51, Val 52, Leu 75, Leu 104, Val 105, Leu 108, etc.) have been found to interact between CA and p38 (Figure 13(d)).

3.3.3. Molecular Dynamics. The MD simulation was carried out for further refinement and stabilization of the docked complexes in dynamic environment to evaluate the most energetically stable binding conformation. The simulation time range of 20–40 ns was used to allow and permit reorganization of the interaction configuration of protein-ligand complex. In the simulation study, the compactness of each

Table 4: Dock score, Emodel value, and interacting residues in molecular docking analysis.

Sl. number	Proteins	Glide scores (Kcal/mol)	Glide Emodel values	Interacting residues in H-bond interaction	Other interactions
1.	Bax	−3.115	−15.341	Arg 37, Leu 122	Cation-π, π-π stacking with Arg 37
2.	Bcl-2	−4.986	−29.586	—	H-bond with H_2O
3.	Caspase 9	−3.596	−23.725	Arg 355	π-π stacking, salt bridge with Arg 355
4.	Caspase 3	−4.263	−30.352	Arg 207, Thr 62	—
5.	Caspase 8	−4.060	−19.905	Glu 396, Thr 467	—
6.	IκB	−6.524	−33.382	Asp 103, Leu 21	—
7.	NF-κB	−6.042	−36.121	Arg 416, Leu 472	π-π stacking with Arg 408
8.	JNK	−4.642	−17.079	Asn 114	—
9.	p38	−5.608	−30.359	—	—

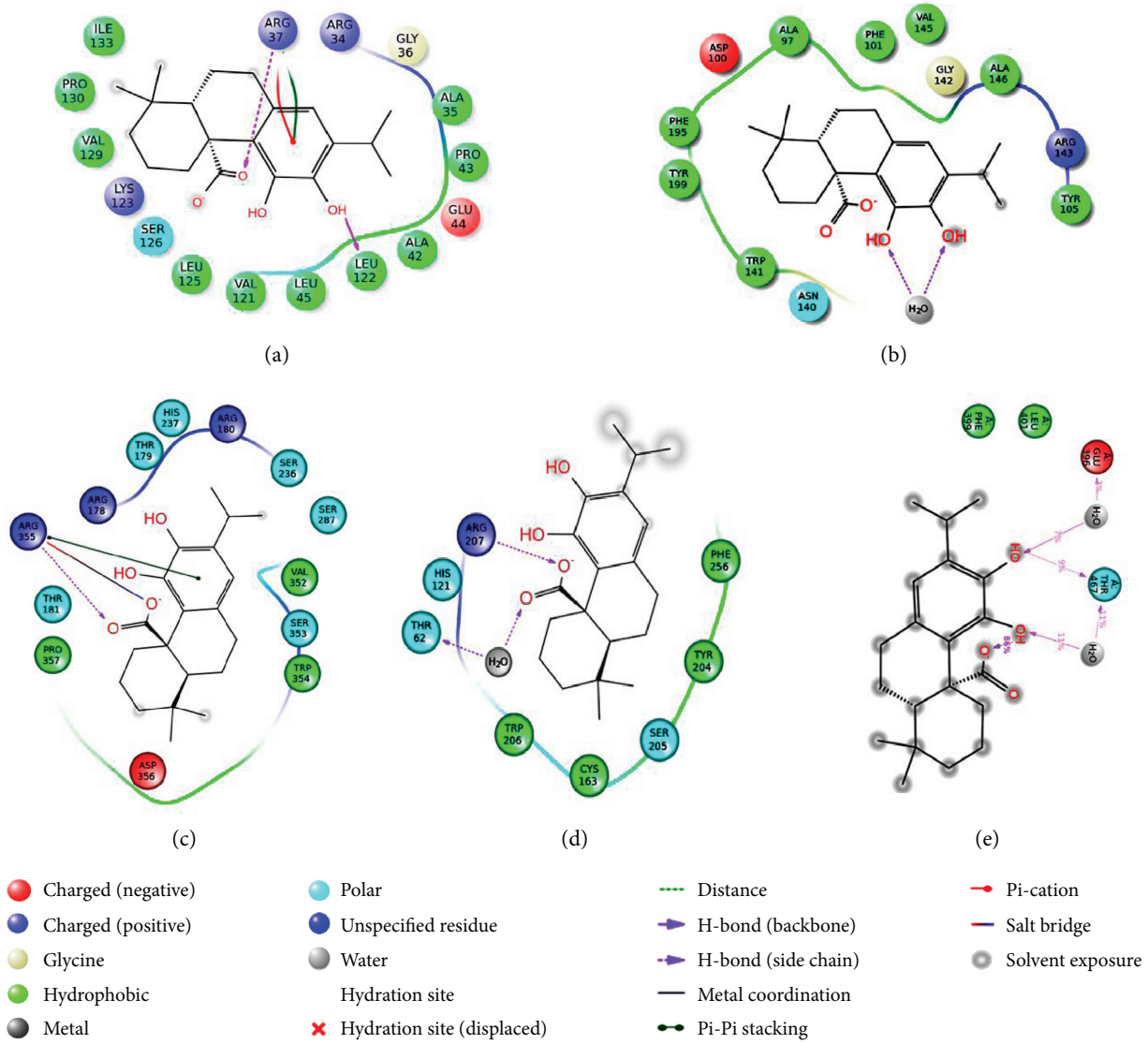

Figure 12: Docking interactions of CA with Bax (a), Bcl-2 (b), caspase 9 (c), caspase 3 (d), and caspase 8 (e) proteins.

simulated complex has been analyzed through root-mean-square deviation (RMSD), root-mean-square fluctuation (RMSF), radius of gyration, and the secondary structure elements (SSE) of CA ligand interactions with the selective protein along with stable H-bond and hydrophobic interactions. The RMSD plot of Bax-CA complex showed that there

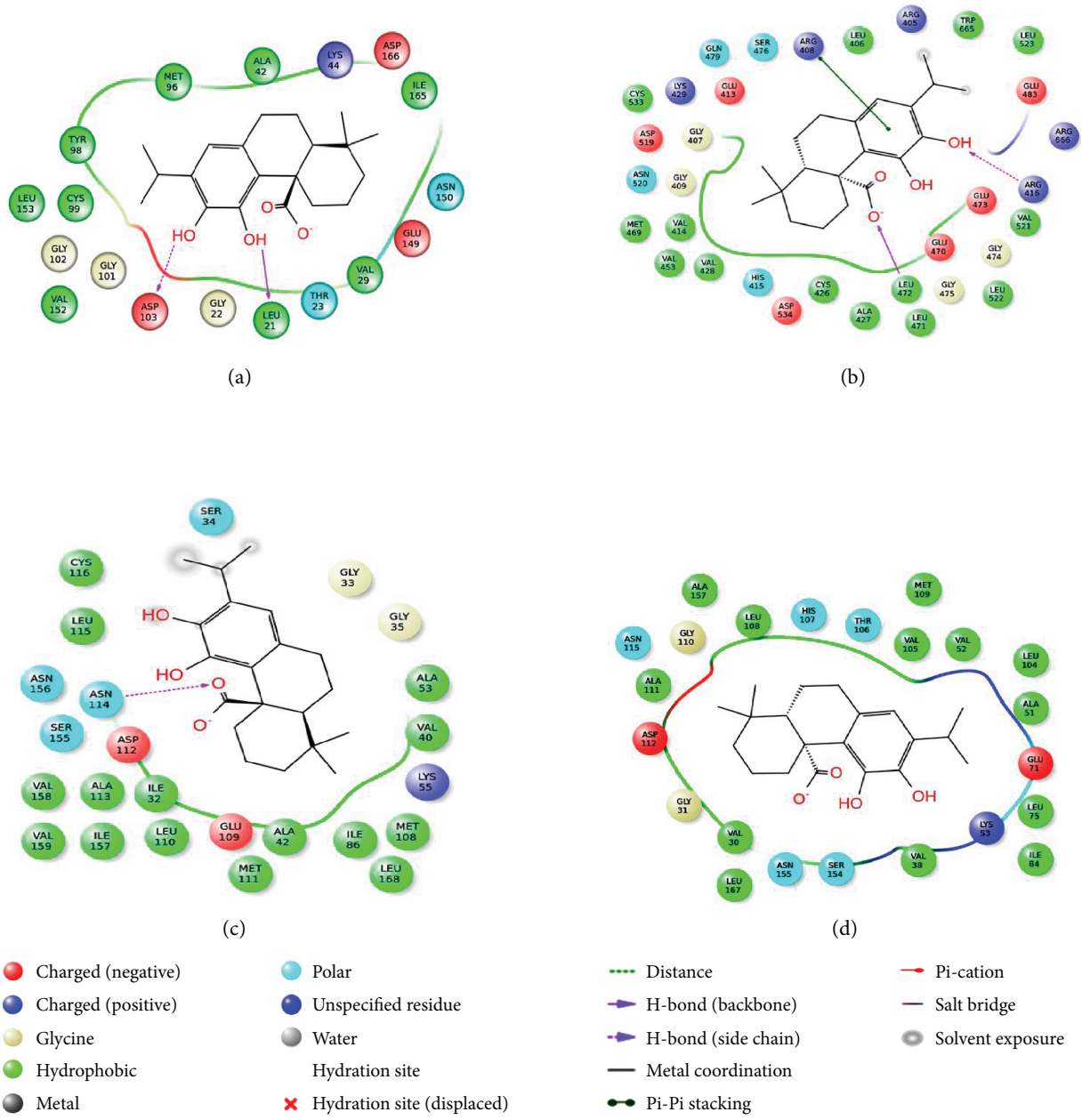

Figure 13: Docking interactions of CA with IκB (a), NF-κB (b), JNK (c), and p38 (d) proteins.

is significant deviation till 30 ns of run. However, the complex was thereafter found to be appropriately stable and consistent until reaching to the end of the run (Figure 14(a)). The modeling analysis clearly appeared that the regions comprising catalytic amino acids of Bax protein interacting with CA exhibited adequate conformational stabilities. During the simulation run of Bcl-2-CA complex, the dynamic nature of interaction has been witnessed at 20 ns. The protein-ligand RMSD plot for Bcl-2-CA complex showed equilibrated simulation complex and stabilized at RMSD value of around 3 Å for protein backbone (Figure 14(b)). However, when the protein-ligand complex was first aligned on the protein backbone, the rearrangement of conformation explained a high deviation in RMSD of ligand with respect to time. Analysis of MD features of caspase 9-CA complex revealed the RMSD plot of MD complex with high fluctuation at the initial stage; however, after 32 ns, the complex become stabilizes gradually (Figure 14(c)). Analysis of the protein SSE, it has been noticed that a total of around 40.74% SSE contributed to the overall protein stability for caspase 9-CA complex. To realize the behavior of caspase 3-CA complex in dynamic environment, the MD simulation was carried out at 40 ns to study the molecular interaction pattern of the simulated complex. It has been observed in the RMSD plot (Figure 14(d)) that most stable time period for caspase 3-CA complex is 30–40 ns of the simulation run. For the production of binding orientation of caspase 8-CA complex in MD-simulated state, the simulation was

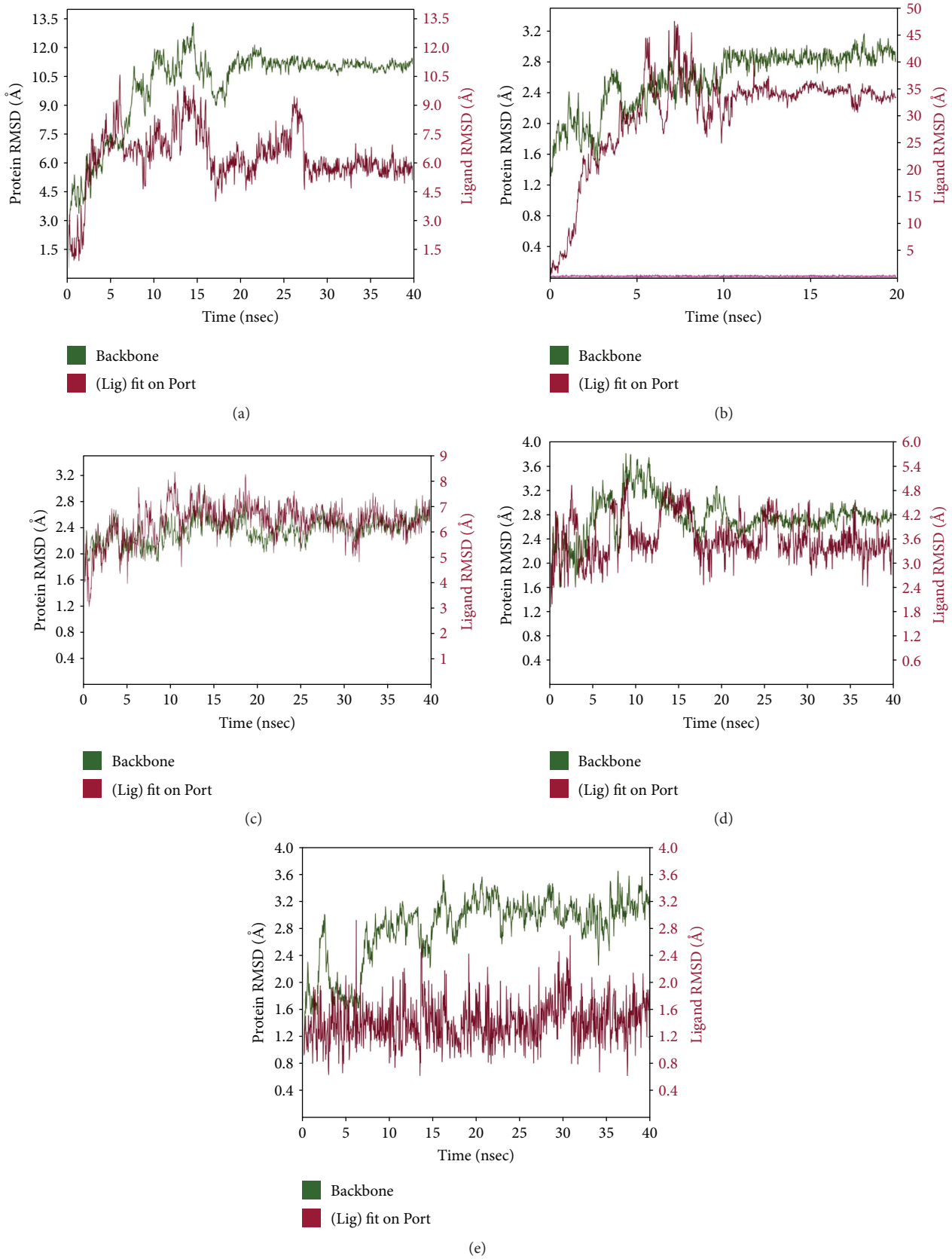

Figure 14: MD-simulated RMSD plot of Bax (a), Bcl-2 (b), caspase 9 (c), caspase 3 (d), and caspase 8 (e) backbones and CA ligand complex.

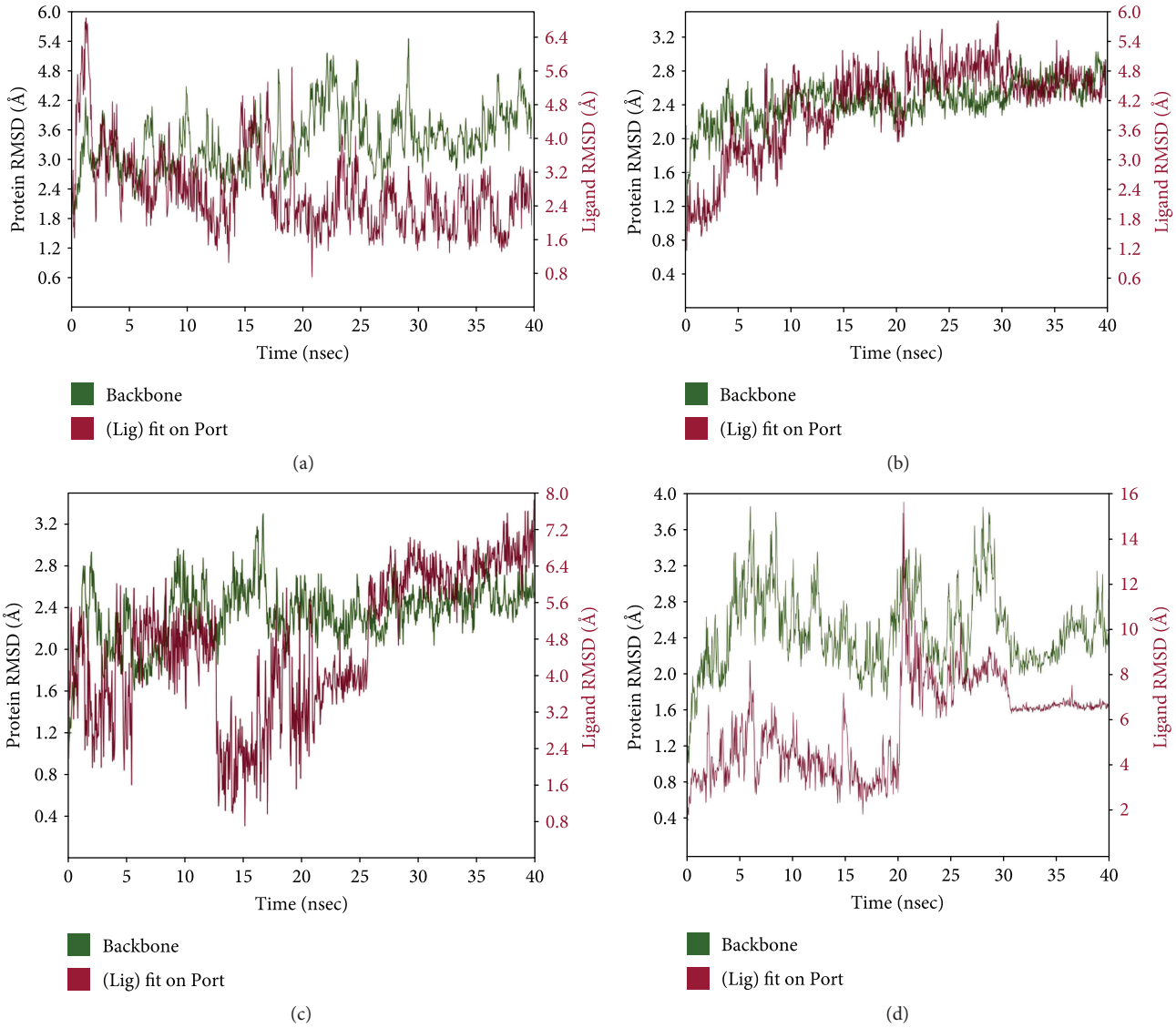

Figure 15: MD-simulated RMSD plot of IκB (a), NF-κB (b), JNK (c), and p38 (d) backbones and CA ligand complex.

executed at 40 ns. It has been noted that the complex is sufficiently stable in the long run (7–40 ns). It was exhibited by RMSDs of about 3.2 and 2.0 Å for protein backbone and ligand, respectively (Figure 14(e)). The MD simulation of IκB-CA ligand bound complex was performed up to 40 ns. The RMSD plot (Figure 15(a)) showed minimal fluctuations during simulation run; however, a consistent interaction has been observed across the MD simulation trajectory after 25 ns. In protein SSE, α-helices (45.15%) and β-strands (7.41%) were monitored throughout the simulation. An interaction pattern at different time points of MD simulation for NF-κB and CA complex has been recorded for 40 ns (Figure 15(b)). Although fluctuation in the RMSDs plot has been observed up to 30 ns of run, but the fluctuation was reduced during the run at 30–40 ns. It suggested that complex is undergoing a large conformational change and it leads to the equilibrated state during the simulation. The MD simulation run at 40 ns for the JNK-CA complex has not shown the consistent interaction across the MD simulation trajectory, as depicted in RMSD plot (Figure 15(c)). To evaluate the dynamic stability of p38-CA complex subjected to MD simulation for 40 ns, the RMSD plot showed higher congeneric fluctuation followed by small and large peaks in between (Figure 15(d)). The fluctuation-differentiate extended throughout the conformational arrangement as supported by docked complex which has not generated any bond interaction.

4. Discussion

Arsenites-contaminated drinking water has been regarded as a major hazard over 70 countries in the world [4]. Inorganic arsenicals have been shown to induce cytotoxic effect to the various organs through generation of excess of intracellular ROS coupled with downregulation of endogenous redox defense [4]. Therefore, employing an antioxidant would be

a therapeutic strategy to counteract with As-mediated toxic exhibitions. CA, a naturally occurring phenolic diterpene, has been reported to possess significant ROS scavenging and antioxidant activities [14, 15]. It is one of the antioxidant food additives. Dried rosemary is used as a food component in various recipes. Dried rosemary (0.4–2.5 g/serving) corresponds to 0.05–0.4 mg/kg of CA [37]. Rosemary extract (0.01–2 g/kg) is also used as flavouring in processed foods. Rosemary extract containing variable amount of CA (5–20%) was classified as a food additive by the European Commission [37, 38]. Through various rosemary supplements up to 1-2 mg/kg of CA is consumed by human per day [37].

Present studies have been executed to evaluate the probable prophylactic role of CA against As intoxication in the liver of experimental mice employing established *in vitro* and *in vivo* preclinical assays. Despite the mouse has a higher metabolic turnover than human, the mouse has similar metabolite profile as human adults [39]. The absorption, distribution, and excretion of trivalent As follow similar patterns in both mouse and human. Trivalent As follow similar metabolic pattern like arsenite → monomethylarsonate → dimethylarsenite in both human and mouse [40]. Besides, As-mediated dysfunction in hepatic endothelial cells follows similar redox signaling in both mouse and human [41]. Considering the association in phenotypic anchors namely adsorption, arsenic burden in tissues, metabolism, excretion, and altered gene expression between the As-exposed human and mouse [41], mouse model has been employed in this study.

Haematological and serum biochemical status give primary indications of toxicological proceedings within the body and/or in the precise organs. In this study, $NaAsO_2$ exposure significantly reduced erythrocyte count and thereby exhibited a significant reduction in haemoglobin level in mice. As-induced oxidative haematotoxicity has been reported in earlier literatures [6, 42]. As experiences biotransformation in the hepatic tissues through binding with thiol group of proteins and thereby interferes with the integrity of the membrane of hepatocytes following leakage of AST and ALT into the sera [6]. Therefore, AST and ALT are accepted to be the markers for hepatotoxicity [6]. In this study, significant raise in the AST and ALT levels was observed in the sera of $NaAsO_2$-exposed mice. Similarly, the high levels of LDH and CK in the sera confirmed the loss of membrane integrity due to $NaAsO_2$ intoxication. The high levels of aforementioned tissue-specific enzymes confirmed the induction of hepatotoxicity by $NaAsO_2$. On the other hand, CA treatment could significantly reinstate the levels of aforementioned tissue-specific enzymes in the sera, which primarily gave an impression of hepatoprotective effect of the compound.

The earlier explanations revealed that $NaAsO_2$ exposure significantly promoted intracellular ROS generation in both *in vitro* and *in vivo* systems [7, 15, 43]. ROS have multiple targets to initiate and propagate toxicological events namely oxidative destruction of cellular macromolecules, assuaging the endogenous redox defense and endorsing the apoptotic event via transformation in the normal transcriptions of different signaling proteins [26]. In this study, $NaAsO_2$ exposure caused significant production and accumulation of intracellular ROS, which finally exerted significant extent of cytotoxic effect. The ROS in excess directly expose peroxidative injury to the membrane lipids, carbonylation of cellular proteins, and oxidation of nucleic acids [21]. However, CA could significantly attenuate the ROS-mediated toxicosis to the cellular biomolecules. The experimental observation would be correlated to the restriction of ROS production and/or ROS scavenging effect by CA.

Cellular redox defense systems play an imperative role to neutralize oxidative stress [44]. Cellular antioxidant enzymes and GSH constitute endogenous redox defense reservoir [44]. $NaAsO_2$ exposure further endorse redox stress through significant inhibition of endogenous redox defense systems, which was in accordance to the previous observations [1, 6, 7]. Decrease in the levels of SOD and CAT could be accounted to an overproduction of superoxide anion during As metabolism [45]. Arsenites have high affinity toward thiol group [46], which would be corroborated to the depletion of cellular GSH levels. GSH acts as the substrate for the enzymes, specifically GR, GPx, and GST. The downregulation in the activities of GR, GPx, and GST would be correlated to the strong affinity of arsenites toward thiol group. Besides, GSH is also known to be a key intracellular reductant for As methylation and transport and thereby facilitate the removal of As from the body [47]. GSH-As complexes act as substrates for the ATP-binding cassette membrane transporters, which facilitate active efflux of As from the cells [48]. Depletion of hepatic GSH helps accumulation of As in the liver and promotes oxidative stress. On the other hand, CA along with $NaAsO_2$ could significantly improve the cellular redox defense via augmenting the levels of endogenous antioxidant enzymes and GSH. CA treatment also promoted As clearance from hepatic tissue, which would be correlated with the CA-mediated upregulation of hepatic GSH level. The probable mechanism of CA has been proposed to be the conversion of catechol type-CA to quinone type-CA through donation of a pair of electrons to oxygen radicals to become electrophilic [49]. This quinone type-CA has been reported to form adducts with the -SH of GSH and/or other protein/enzymes and thereby activate antioxidant-responsive element. This antioxidant-responsive element further induces phase 2 enzymes and increases GSH level [49].

ROS has been reported to endorse apoptosis via alteration in the expressions of different signal proteins from their normal transcriptional levels [26]. ATP supplies the required energy for this programmed cell death [26]. In this study, a significantly high level of cytosolic ATP in the hepatic tissue followed by $NaAsO_2$ exposure revealed the favorable cellular atmosphere for the cleavages of caspases in the cytosol. The augmentation of cytosolic ATP may be correlated to that of $NaAsO_2$-mediated downregulation of microsomal ATPases in the liver [50]. Apoptosis is usually governed by the complex reciprocity between the pro- and antiapoptotic events via the transcription of respective signal proteins. Bax is a proapoptotic member of Bcl-2 family, which regulates apoptosis through mitochondrial stress. Translocation

of Bax protein into mitochondria from cytosol initiates intrinsic apoptotic signaling [51]. In this study, $NaAsO_2$ intoxication caused activation of proapoptotic signaling and mitigation, which was apparent from significant upregulation of Bax protein in mitochondria. Besides, $NaAsO_2$ could significantly inhibit the expression of Bcl-2 in cytosol, which is a member of antiapoptotic protein [21]. The Bax translocation further opens the transition pores in the mitochondrial membranes resulting with the release of cytochrome C into the cytosol [26]. Cytochrome C release would be further potentiated through the downregulation of Bcl-2 in the cytosol [52]. In this study, a significant upregulation in the expression of cytochrome C in the cytosol was observed in $NaAsO_2$-exposed hepatic cells. The release of cytochrome C into cytosol provides a key signal for the intrinsic pathway of apoptosis [52]. Through the interaction with Apaf-1, cytochrome C potentiates the downstream apoptotic signaling cascades via cleavages of caspases 9 and 3 into their respective cleaved/active forms in cytosol [52, 53]. It has been regarded that cytochrome C release is distal to caspase 8 activation in Fas-mediated apoptosis [52]. Earlier investigation revealed that, ROS can potentiate the death-receptor mediated apoptosis through receptor clustering and establishment of lipid raft-derived signaling platforms [54]. The Fas signaling is one of the key processes in extrinsic/death receptor-mediated apoptosis. In the extrinsic pathway of apoptosis, the activation of FAS resulted in the cleavage of procaspase 8 into its cleaved/active form followed by activation of Bid signaling [55]. In this study, significant upregulation in the expressions of FAS, cleaved caspase 8, and Bid were observed in $NaAsO_2$-exposed hepatic cells. CA treatment could significantly attenuate the intrinsic and extrinsic pathways of apoptosis via reciprocating the expression of the involved transcription factors except Bid. NF-κB is one of the redox-sensitive transcription proteins. ROS significantly contributes in signal-transduction pathways of NF-κB [21]. The NF-κB signaling is initiated with the phosphorylation of IκBα on Ser 32 followed by translocation of phospho-NF-κB (Ser 536) to the nucleus [56]. Nuclear translocation of phospho-NF-κB can trigger proapoptotic event via promotion of Bax translocation to mitochondria. NF-κB can also potentiate the expression of Fas-ligand and thereby exert a proapoptotic role [57]. In this study, $NaAsO_2$ significantly upregulated NF-kB signaling and that could be attenuated by CA treatment. Among the many signaling pathways, mitogen-activated protein kinase (MAPK) family proteins are crucial for the maintenance of cells. C-Jun N-terminal kinase (JNK) and p38 are stress responsive signal proteins involved in apoptosis [58]. MAPK member proteins are also redox sensitive [21]. Strong functional interactions exist between the p53 and MAPK [59]. The activation of p53 can lead to cell cycle arrest [60]. Earlier observation revealed that, p38, JNK, and p53 significantly contribute in arsenite-induced apoptosis via activation of proapoptotic signaling in the mitochondria [60, 61]. In this study, significant upregulation in the p38, JNK, and p53 signaling was observed in $NaAsO_2$-exposed hepatic cells. CA could significantly attenuate $NaAsO_2$-mediated p38 and JNK signaling via preventing their phosphorylation. However, CA did not show significant control on p53 signaling in the hepatic cells of mice. Experimental observation revealed that CA exerted antiapoptotic effect through inhibition of MAPK activation, imbalance of pro- and antiapoptotic factors, and inhibition of caspase cleavage.

Utilizing chemometric analysis, valuable information on molecular basis has been elucidated for different protein-ligand complex structures in silico. In this study, Bax, Bcl-2, caspase 9, caspase 3, caspase 8, IκB, NF-κB, JNK, and p38 demonstrated significant interactions with CA in silico, which were in accordance to our observation in *in vitro* and *in vivo* studies. On the other hand, Apaf-1, cytochrome C, Bid, Fas, and p53 did not demonstrate significant docked pose. In our experiment, we did not observe any effect of CA on Bid and p53 expressions. However, CA has been found to regulate the expressions of Apaf-1, cytochrome C, and Fas *in vitro* and *in vivo*. The H-bond formation which is a key interaction to explicate the stability of the CA inside the binding pocket has been observed for most of the proteins, except Bcl-2 and p38. The π-π stacking, a noncovalent interaction, has been observed with Bax, caspase 9, and NF-κB proteins. It might play vital roles in stabilization of protein structures and therefore important in many aspects of macromolecular study. The π-π stacking arrangement has been previously observed in many protein crystal structures as this arrangement is conserved in some families of enzymes. The occurrence of cation-π interaction, another type of noncovalent bonding, has been identified with positively charged residue in Bax protein. This interaction has been regarded as the most important interaction in structural biology. It plays a vital role in molecular recognition and signaling. MD simulations for all the complexes indicate that most interactions appeared in docking analysis are stable during MD simulation except JNK and p38. Thus, CA may be considered as a potential drug candidate having a wide range of bioactivity and may provide multitherapeutic benefits.

5. Conclusion

$NaAsO_2$-mediated production and accumulation of oxidative free radicals play significant role in the As-induced hepatotoxicity. The present study demonstrated that $NaAsO_2$ can elicit hepatocellular apoptosis by triggering NF-κB, MAPK, p53, and intrinsic and extrinsic apoptotic signaling. On the other hand, treatment with the CA could significantly attenuate $NaAsO_2$-mediated hepatotoxicity by counteracting with oxidative stress, promoting endogenous redox defense, accelerating As clearance and downstream regulation of apoptotic signaling cascades as observed in *in vitro* and *in vivo* preclinical assays (Figure 16). In silico molecular docking studies predicted the possible interactions between CA and the active sites of signal proteins. In silico ADME prediction revealed that CA supports the drug-likeness character ostensible from Lipinski's rule of five. Therefore, CA would have a good possibility to be a new therapeutic agent to counteract with As-mediated toxic manifestations.

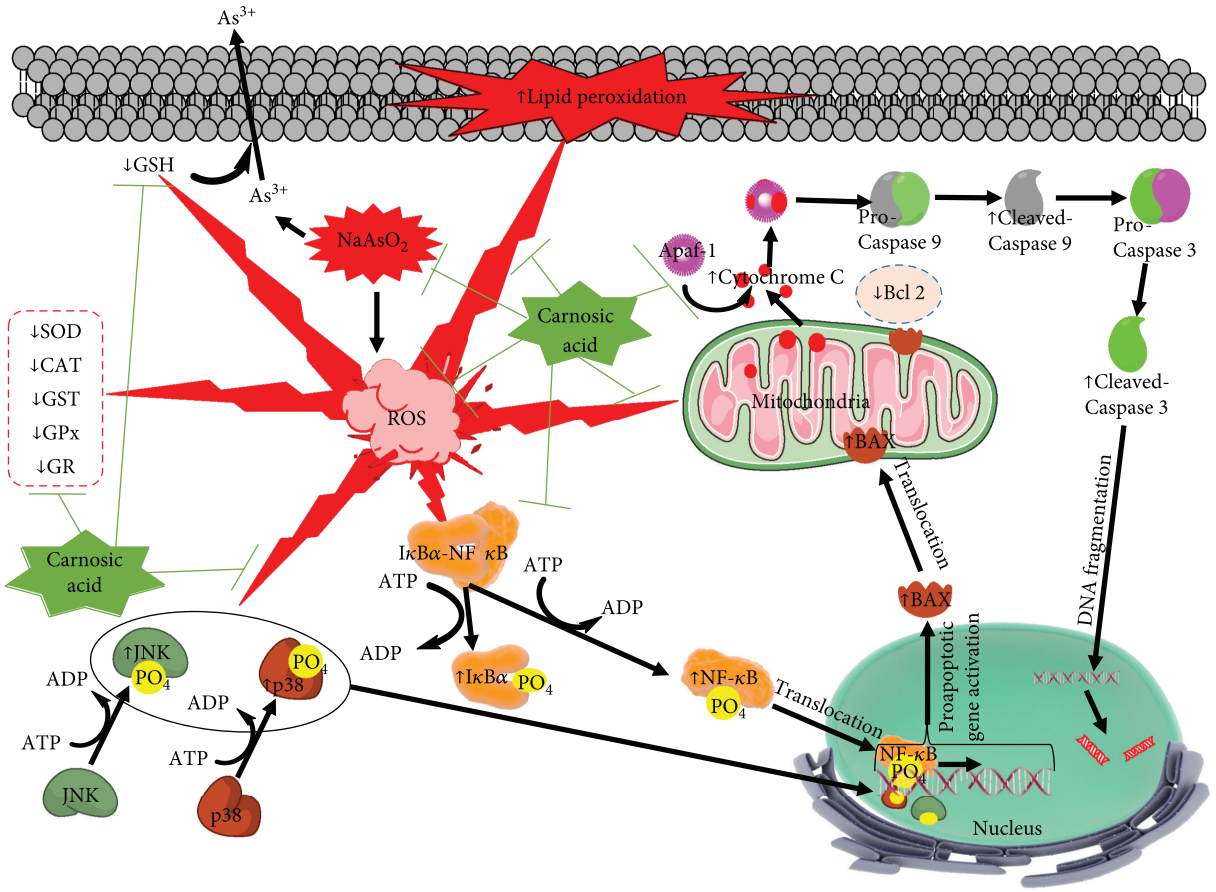

FIGURE 16: Schematic presentation probable protective mechanism of CA against $NaAsO_2$-mediated hepatic injury. The red lightning bolts indicated the pathological events involved within $NaAsO_2$-exposed hepatic cells. The green lines denoted the activity restricted by CA.

Conflicts of Interest

The authors declare that there is no conflict of interests.

Authors' Contributions

Saikat Dewanjee, Prasenjit Manna, Supratim Ray, and Vincenzo De Feo designed the experiments. Saikat Dewanjee and Prasenjit Manna supervised the work. Swarnalata Joardar, Prasenjit Manna, and Jatin Kalita performed *in vitro* assays. Niloy Bhattacharjee performed flow cytometric analysis and image assay. Sonjit Das, Tarun K. Dua, Swarnalata Joardar, and Ritu Khanra performed *in vivo* assay. Sonjit Das and Swarnalata Joardar performed immunoblot analysis for *in vivo* assay. Shovonlal Bhowmick, Supratim Ray, and Achintya Saha performed in silico analysis. Saikat Dewanjee and Prasenjit Manna compiled and analyzed the data. Saikat Dewanjee, Prasenjit Manna, and Vincenzo De Feo wrote the manuscript. Sonjit Das and Swarnalata Joardar contributed equally to this work.

Acknowledgments

The authors gratefully acknowledge the University Grants Commission (UGC), New Delhi, India, for providing the Rajiv Gandhi National Fellowship (Ref. no. F1-17.1/2013-14/RJNF-2013-14-SC-ASS-52029 (SA-III/Website) dated 06.02.3014) to Mister Sonjit Das. The authors are thankful to the Department of Biotechnology (DBT), Ministry of Science and Technology, Government of India, for providing the Ramalingaswami Re-Entry Fellowship (Grant no. BT/RLF/Re-Entry/34/2013) to Dr. Prasenjit Manna. The authors are thankful to Jadavpur University, Kolkata, India, and the Director, CSIR-NEIST for providing necessary facilities for this study. The authors are thankful to Ms. Cassandra Warden, Vanderbilt University Medical Center, Department of Ophthalmology, USA, for excellent editing of this manuscript.

Supplementary Materials

Supplementary Figure 1: effect of $NaAsO_2$ at different concentrations on cell viability in isolated murine hepatocytes. Values are expressed as mean ± SD ($n = 3$). Supplementary Figure 2: effect of CA to the histological structure of livers of experimental mice. Supplementary Table 1: the effect of CA (4 μM) on ROS accumulation, lipid peroxidation, protein carbonylation, and endogenous redox systems in isolated murine hepatocytes. Supplementary Table 2: effects of CA (10 and 20 mg/kg) on haematological, serum biochemical, and redox parameters in mice. *(Supplementary Materials)*

References

[1] A. K. Das, S. Bag, R. Sahu et al., "Protective effect of *Corchorus olitorius* leaves on sodium arsenite-induced toxicity in experimental rats," *Food and Chemical Toxicology*, vol. 48, no. 1, pp. 326–335, 2010.

[2] P. Roy and A. Saha, "Metabolism and toxicity of arsenic: a human carcinogen," *Current Science*, vol. 82, no. 1, pp. 38–45, 2002.

[3] R. N. Ratnaike, "Acute and chronic arsenic toxicity," *Postgraduate Medical Journal*, vol. 79, no. 933, pp. 391–396, 2003.

[4] A. K. Das, S. Dewanjee, R. Sahu, T. K. Dua, M. Gangopadhyay, and M. K. Sinha, "Protective effect of *Corchorus olitorius* leaves against arsenic-induced oxidative stress in rat brain," *Environmental Toxicology and Pharmacology*, vol. 29, no. 1, pp. 64–69, 2010.

[5] A. K. Das, R. Sahu, T. K. Dua et al., "Arsenic-induced myocardial injury: protective role of *Corchorus olitorius* leaves," *Food and Chemical Toxicology*, vol. 48, no. 5, pp. 1210–1217, 2010.

[6] T. K. Dua, S. Dewanjee, M. Gangopadhyay, R. Khanra, M. Zia-Ul-Haq, and V. De Feo, "Ameliorative effect of water spinach, *Ipomea aquatica*(Convolvulaceae), against experimentally induced arsenic toxicity," *Journal of Translational Medicine*, vol. 13, no. 1, p. 81, 2015.

[7] T. K. Dua, S. Dewanjee, and R. Khanra, "Prophylactic role of *Enhydra fluctuans* against arsenic-induced hepatotoxicity via antiapoptotic and antioxidant mechanisms," *Redox Report*, vol. 21, no. 4, pp. 147–154, 2016.

[8] J. J. Stevens, B. Graham, A. M. Walker, P. B. Tchounwou, and C. Rogers, "The effects of arsenic trioxide on DNA synthesis and genotoxicity in human colon cancer cells," *International Journal of Environmental Research and Public Health*, vol. 7, no. 5, pp. 2018–2032, 2010.

[9] L. Li, P. Qiu, B. Chen et al., "Reactive oxygen species contribute to arsenic-induced EZH2 phosphorylation in human bronchial epithelial cells and lung cancer cells," *Toxicology and Applied Pharmacology*, vol. 276, no. 3, pp. 165–170, 2014.

[10] K. Jomova, Z. Jenisova, M. Feszterova et al., "Arsenic: toxicity, oxidative stress and human disease," *Journal of Applied Toxicology*, vol. 31, no. 2, pp. 95–107, 2011.

[11] T. Rossman, "Arsenic," in *Environmental and Occupational Medicine*, W. Rom and S. Markowitz, Eds., pp. 1006–1017, Lippincott Williams & Wilkins, Hagerstown, MD, 4th edition, 2007.

[12] K. Schwarz and W. Ternes, "Antioxidative constituents of *Rosmarinus officinalis* and *Salvia officinalis*," *Zeitschrift für Lebensmittel-Untersuchung und Forschung*, vol. 195, no. 2, pp. 99–103, 1992.

[13] S. Manoharan, S. Balakrishnan, V. Vinothkumar, and S. Silvan, "Anti-clastogenic potential of carnosic acid against 7, 12-dimethylbenz (a) anthracene (DMBA) -induced clastogenesis," *Pharmacological Reports*, vol. 62, no. 6, pp. 1170–1177, 2010.

[14] A. I. Kuzmenko, R. P. Morozova, I. A. Nikolenko, G. V. Donchenko, S. L. Richheimer, and D. T. Bailey, "Chemiluminescence determination of the *in vivo* and *in vitro* antioxidant activity of RoseOx® and Carnosic acid," *Journal of Photochemistry and Photobiology B*, vol. 48, no. 1, pp. 63–67, 1999.

[15] O. I. Aruoma, B. Halliwell, R. Aeschbach, and J. Löligers, "Antioxidant and prooxidant properties of active rosemary constituents: carnosol and carnosic acid," *Xenobiotica*, vol. 22, no. 2, pp. 257–268, 1992.

[16] J. A. Park, S. Kim, S.-Y. Lee et al., "Beneficial effects of carnosic acid on dieldrin-induced dopaminergic neuronal cell death," *Neuroreport*, vol. 19, no. 13, pp. 1301–1304, 2008.

[17] K. Ninomiya, H. Matsuda, H. Shimoda et al., "Carnosic acid, a new class of lipid absorption inhibitor from sage," *Bioorganic and Medicinal Chemistry Letters*, vol. 14, no. 8, pp. 1943–1946, 2004.

[18] J. Reuter, A. Jocher, S. Hornstein, J. Mönting, and C. Schempp, "Sage extract rich in phenolic diterpenes inhibits ultraviolet-induced erythema *in vivo*," *Planta Medica*, vol. 73, no. 11, pp. 1190-1191, 2007.

[19] S. Dewanjee, R. Sahu, S. Karmakar, and M. Gangopadhyay, "Toxic effects of lead exposure in Wistar rats: involvement of oxidative stress and the beneficial role of edible jute (*Corchorus olitorius*) leaves," *Food and Chemical Toxicology*, vol. 55, no. 1, pp. 78–91, 2013.

[20] Public Health Service [PHS], *Public Health Service Policy on Human Care and Use of Laboratory Animals*, US Department of Health and Human Services, National Institute of Health, Office of Laboratory Animal welfare, Washington, DC, 2015.

[21] S. Dewanjee, S. Joardar, N. Bhattacharjee et al., "Edible leaf extract of Ipomoea aquatica Forssk. (*Convolvulaceae*) attenuates doxorubicin-induced liver injury via inhibiting oxidative impairment, MAPK activation and intrinsic pathway of apoptosis," *Food and Chemical Toxicology*, vol. 105, pp. 322–336, 2017.

[22] P. Manna and S. K. Jain, "L-cysteine and hydrogen sulfide increase PIP3 and AMPK/PPARγ expression and decrease ROS and vascular inflammation markers in high glucose treated human U937 monocytes," *Journal of cellular Biochemistry*, vol. 114, no. 10, pp. 2334–2345, 2013.

[23] P. Manna, J. Das, J. Ghosh, and P. C. Sil, "Contribution of type 1 diabetes to rat liver dysfunction and cellular damage via activation of NOS, PARP, IkappaBalpha/NF-kappaB, MAPKs, and mitochondria-dependent pathways: prophylactic role of arjunolic acid," *Free Radical Biology and Medicine*, vol. 48, no. 11, pp. 1465–1484, 2010.

[24] S. Baghirova, B. G. Hughes, M. J. Hendzel, and R. Schulz, "Sequential fractionation and isolation of subcellular proteins from tissue or cultured cells," *MethodsX*, vol. 2, pp. 440–445, 2015.

[25] S. Dewanjee, T. K. Dua, R. Khanra et al., "Water spinach, *Ipomoea aquatica* (Convolvulaceae), ameliorates lead toxicity by inhibiting oxidative stress and apoptosis," *PLoS One*, vol. 10, no. 10, article e0139831, 2015.

[26] N. Bhattacharjee, T. K. Dua, R. Khanra et al., "Protocatechuic acid, a phenolic from *Sansevieria roxburghiana* leaves, suppresses diabetic cardiomyopathy via stimulating glucose metabolism, ameliorating oxidative stress, and inhibiting inflammation," *Frontiers in Pharmacology*, vol. 8, 2017.

[27] R. Khanra, N. Bhattacharjee, T. K. Dua et al., "Taraxerol, a pentacyclic triterpenoid, from *Abroma augusta* leaf attenuates diabetic nephropathy in type 2 diabetic rats," *Biomedicine and Pharmacotherapy*, vol. 94, pp. 726–741, 2017.

[28] D. Das, A. Chatterjee, B. K. Mandal, G. Samanta, D. Chakraborti, and B. Chanda, "Arsenic in ground water in six districts of West Bengal, India: the biggest arsenic calamity in the world. Part 2. Arsenic concentration in drinking water, hair, nails, urine, skin-scale and liver tissue (biopsy) of the affected people," *Analyst*, vol. 120, no. 3, pp. 917–924, 1995.

[29] K. T. Lin, J. Y. Xue, F. F. Sun, and P. Y. K. Wong, "Reactive oxygen species participate in peroxynitrite-induced apoptosis in HL-60 Cells," *Biochemical and Biophysical Research Communications*, vol. 230, no. 1, pp. 115–119, 1997.

[30] A. Bolner, M. Pilleri, V. De Riva, and G. P. Nordera, "Plasma and urinary HPLC-ED determination of the ratio of 8-OHdG/2-dG in Parkinson's disease," *Clinical Laboratory*, vol. 57, no. 11-12, pp. 859–866, 2011.

[31] N. L. Chepelev, D. A. Kennedy, R. Gagné et al., "HPLC measurement of the DNA oxidation biomarker, 8-oxo-7,8-dihydro-2′-deoxyguanosine, in cultured cells and animal tissues," *Journal of Visualized Experiments*, vol. 102, article e52697, 2015.

[32] S. Dewanjee, M. Gangopadhyay, R. Sahu, and S. Karmakar, "Cadmium induced pathophysiology: prophylactic role of edible jute (*Corchorus olitorius*) leaves with special emphasis on oxidative stress and mitochondrial involvement," *Food and Chemical Toxicology*, vol. 60, no. 1, pp. 188–198, 2013.

[33] L. Schrödinger, 2014, http://www.schrodinger.com.

[34] H. M. Berman, J. Westbrook, Z. Feng et al., "The protein data bank," *Nucleic Acids Research*, vol. 28, no. 1, pp. 235–242, 2000.

[35] P. Mark and L. Nilsson, "Structure and dynamics of the TIP3P, SPC, and SPC/E water models at 298 K," *Journal of Physical Chemistry A*, vol. 105, no. 43, pp. 9954–9960, 2001.

[36] J.-P. Ryckaert, G. Ciccotti, and H. J. C. Berendsen, "Numerical integration of the cartesian equations of motion of a system with constraints: molecular dynamics of n-alkanes," *Journal of Computational Physics*, vol. 23, no. 3, pp. 327–341, 1977.

[37] S. Birtić, P. Dussort, F.-X. Pierre, A. C. Bily, and M. Roller, "Carnosic acid," *Phytochemistry*, vol. 115, pp. 9–19, 2015.

[38] F. Aguilar, H. Autrup, S. Barlow et al., "Use of rosemary extracts as a food additive-scientific opinion of the panel on food additives, flavourings, processing aids and materials in contact with food," *The EFSA Journal*, vol. 721, no. 1, pp. 1–29, 2008.

[39] L. Demetrius, "Of mice and men," *EMBO Reports*, vol. 6, pp. S39–S44, 2005.

[40] M. Vahter and G. Concha, "Role of metabolism in arsenic toxicity," *Pharmacology & Toxicology*, vol. 89, no. 1, pp. 1–5, 2001.

[41] J. C. States, A. Barchowsky, I. L. Cartwright, J. F. Reichard, B. W. Futscher, and R. C. Lantz, "Arsenic toxicology: translating between experimental models and human pathology," *Environmental Health Perspectives*, vol. 119, no. 10, pp. 1356–1363, 2011.

[42] N. C. Sumedha and S. Miltonprabu, "Arsenic induced oxidative hematotoxicity in rats and its protection by diallyl trisulfide," *International Journal of Biological and Pharmaceutical Research*, vol. 4, no. 7, pp. 507–515, 2013.

[43] Z. Zhang, P. Pratheeshkumar, A. Budhraja, Y.-O. Son, D. Kim, and X. Shi, "Role of reactive oxygen species in arsenic-induced transformation of human lung bronchial epithelial (BEAS-2B) cells," *Biochemical and Biophysical Research Communications*, vol. 456, no. 2, pp. 643–648, 2015.

[44] S. Dewanjee, A. K. Das, R. Sahu, and M. Gangopadhyay, "Antidiabetic activity of *Diospyros peregrina* fruit: effect on hyperglycemia, hyperlipidemia and augmented oxidative stress in experimental type 2 diabetes," *Food and Chemical Toxicology*, vol. 47, no. 10, pp. 2679–2685, 2009.

[45] A. J. Searle and R. L. Willson, "Glutathione peroxidase: effect of superoxide, hydroxyl and bromine free radicals on enzyme activity," *International Journal of Radiation Biology and Related Studies in Physics, Chemistry and Medicine*, vol. 37, no. 2, pp. 213–217, 1980.

[46] S. Shen, X.-F. Li, W. R. Cullen, M. Weinfeld, and X. C. Le, "Arsenic binding to proteins," *Chemical Reviews*, vol. 113, no. 10, pp. 7769–7792, 2013.

[47] H. V. Aposhian, "Enzymatic methylation of arsenic species and other new approaches to arsenic toxicity," *Annual Review of Pharmacology and Toxicology*, vol. 37, no. 1, pp. 397–419, 1997.

[48] E. M. Leslie, A. Haimeur, and M. P. Waalkes, "Arsenic transport by the human multidrug resistance protein 1 (MRP1/ABCC1) evidence that a tri-glutathione conjugate is required," *Journal of Biological Chemistry*, vol. 279, no. 31, pp. 32700–32708, 2004.

[49] B. D. Sahu, K. K. R. Rentam, U. K. Putcha, M. Kuncha, G. M. N. Vegi, and R. Sistla, "Carnosic acid attenuates renal injury in an experimental model of rat cisplatin-induced nephrotoxicity," *Food and Chemical Toxicology*, vol. 49, no. 12, pp. 3090–3097, 2011.

[50] O. O. Odunuga, G. W. Okunade, and O. O. Olorunsogo, "Reversal of sodium arsenite inhibition of rat liver microsomal Ca^{2+} pumping ATPase by vitamin C," *Bioscience Reports*, vol. 19, no. 1, pp. 11–15, 1999.

[51] T. Satoh, M. Izumi, Y. Inukai et al., "Carnosic acid protects neuronal HT22 Cells through activation of the antioxidant-responsive element in free carboxylic acid- and catechol hydroxyl moieties-dependent manners," *Neuroscience Letters*, vol. 434, no. 3, pp. 260–265, 2008.

[52] J. Cai, J. Yang, and D. P. Jones, "Mitochondrial control of apoptosis: the role of cytochrome c," *Biochimica et Biophysica Acta (BBA) - Bioenergetics*, vol. 1366, no. 1-2, pp. 139–149, 1998.

[53] G. W. Wang, J. B. Klein, and Y. J. Kang, "Metallothionein inhibits doxorubicin induced mitochondrial cytochrome c release and caspase-3 activation in cardiomyocytes," *Journal of Pharmacology and Experimental Therapeutics*, vol. 298, no. 2, pp. 461–468, 2001.

[54] M. L. Circu and T. Y. Aw, "Reactive oxygen species, cellular redox systems and apoptosis," *Free Radical Biology and Medicine*, vol. 48, no. 6, pp. 749–762, 2010.

[55] P. E. Czabotar, G. Lessene, A. Strasser, and J. M. Adams, "Control of apoptosis by the BCL-2 protein family: implications for physiology and therapy," *Nature Reviews Molecular Cell Biology*, vol. 15, no. 1, pp. 49–63, 2014.

[56] M. J. Morgan and Z.-G. Liu, "Crosstalk of reactive oxygen species and NF-κB signaling," *Cell Research*, vol. 21, no. 1, pp. 103–115, 2011.

[57] M. Barkett and T. D. Gilmore, "Control of apoptosis by Rel/NF-κB transcription factors," *Oncogene*, vol. 18, no. 49, pp. 6910–6924, 1999.

[58] T. Wada and J. M. Penninger, "Mitogen activated protein kinases in apoptosis regulation," *Oncogene*, vol. 23, no. 16, pp. 2838–2849, 2004.

[59] G. S. Wu, "The functional interactions between the MAPK and p53 signaling pathways," *Cancer Biology & Therapy*, vol. 3, no. 2, pp. 156–161, 2014.

[60] N. Bhattacharjee, S. Barma, N. Konwar, S. Dewanjee, and P. Manna, "Mechanistic insight of diabetic nephropathy and its pharmacotherapeutic targets: an update," *European Journal of Pharmacology*, vol. 791, no. 1, pp. 8–24, 2016.

[61] A. Yoda, K. Toyoshima, Y. Watanabe et al., "Arsenic trioxide augments Chk2/p53-mediated apoptosis by inhibiting oncogenic Wip1 phosphatase," *Journal of Biological Chemistry*, vol. 283, no. 27, pp. 18969–18979, 2008.

Hindawi
Oxidative Medicine and Cellular Longevity
Volume 2018, Article ID 9042192, 9 pages
https://doi.org/10.1155/2018/9042192

Research Article

Comparative Analysis of the Effects of Olive Oil Hydroxytyrosol and Its 5-*S*-Lipoyl Conjugate in Protecting Human Erythrocytes from Mercury Toxicity

Arbace Officioso,[1] Lucia Panzella,[2] Fabiana Tortora,[1] Maria Laura Alfieri,[2] Alessandra Napolitano,[2] and Caterina Manna[1]

[1]*Department of Biochemistry, Biophysics and General Pathology, University of Campania "Luigi Vanvitelli", Naples, Italy*
[2]*Department of Chemical Sciences, University of Naples "Federico II", Naples, Italy*

Correspondence should be addressed to Alessandra Napolitano; alesnapo@unina.it
and Caterina Manna; caterina.manna@unicampania.it

Received 20 September 2017; Accepted 4 March 2018; Published 12 April 2018

Academic Editor: Glenda Gobe

Oxidative stress is one of the underlying mechanisms of the toxic effects exerted by mercury (Hg) on human health. Several antioxidant compounds, including the olive oil phenol hydroxytyrosol (HT), were investigated for their protective action. Recently, we have reported that 5-*S*-lipoylhydroxytyrosol (Lipo-HT) has shown increased antioxidant activities compared to HT and exerted potent protective effects against reactive oxygen species (ROS) generation and oxidative damage in human hepatocellular carcinoma HepG2 cell lines. In this study, the effects of Lipo-HT and HT on oxidative alterations of human erythrocytes induced by exposure to 40 μM $HgCl_2$ were comparatively evaluated. When administered to the cells, Lipo-HT (5–20 μM) proved nontoxic and it decreased the Hg-induced generation of ROS, the hemolysis, and the depletion of intracellular GSH levels. At all tested concentrations, Lipo-HT exhibited higher ability to counteract Hg-induced cytotoxicity compared to HT. Model studies indicated the formation of a mercury complex at the SH group of Lipo-HT followed by a redox reaction that would spare intracellular GSH. Thus, the enhanced erythrocyte protective action of Lipo-HT from Hg-induced damage with respect to HT is likely due to an effective chelating and reducing ability toward mercury ions. These findings encourage the use of Lipo-HT in nutraceutical strategies to contrast heavy metal toxicity in humans.

1. Introduction

Hydroxytyrosol (HT) is a dietary phenolic antioxidant compound, naturally present in virgin olive oil, contributing to its great oxidative stability and prolonged shelf life [1]. HT is endowed with several pharmacological properties [2–4], including anti-inflammatory [5], antiatherogenic [6], and anticancer activities [7]. Mechanisms underlying HT biological effects include both radical scavenging properties and metal chelating activity [8–11]. Cytoprotective effects of HT against xenobiotic compounds have been reported, including protection from acrolein-induced DNA damage [12], acrylamide-induced mitochondrial dysfunction [13], and carbon tetrachloride-induced oxidative stress [14].

Mercury (Hg) is a highly toxic, redox-active heavy metal which represents one of the main agents responsible for environmental pollution [15, 16]. The health consequences of human exposure to Hg can be severe [17, 18] and include renal injury [19] and neuronal disorders [20]. In this respect, Hg is considered a potential contributing factor to Alzheimer's and Parkinson's diseases [21]. Red blood cells (RBC) may also represent an important target of Hg toxicity. This metal, indeed, preferentially accumulates in these cells and induces morphological changes which increase their procoagulant activity [22–24]. Finally, an

increasing body of data suggests a positive correlation between Hg exposure and the onset of cardiovascular diseases [25].

The increased formation of reactive oxygen species (ROS) is generally agreed to be one of the key mechanisms responsible for Hg-induced toxicity [26–28]. Mercury is endowed with high affinity for sulfhydryl groups, and it is therefore able to react with low-molecular-weight thiols, including glutathione (GSH) [29, 30].

Indeed, the cellular levels of GSH have been shown to significantly decrease following Hg exposure, with consequent impairment of the antioxidant defence system [31]. Following the oxidative stress hypothesis of Hg toxicity, a number of antioxidants [32, 33], including phenolic compounds [34–36], have been proposed and tested for their protective action. In this connection, we recently provided experimental evidence that HT has the potential to modulate cytotoxicity and the oxidative stress induced in human RBC by Hg treatment [37, 38]. Using the scanning electron microscopy technique, we also showed that HT treatment significantly reduces echinocyte formation [37], a morphological RBC alteration reported to correlate with increased coagulability of these cells [39]. Furthermore, a recent study by Mohan et al. highlighted the efficacy of HT in preventing methylmercury-induced genotoxicity and apoptosis in IMR-32 human neuroblastoma cells. HT was shown to inhibit methylmercury-induced neuronal cell dysfunction as highlighted by the decrease in ROS formation and maintenance of an efficient endogenous defence system, including GSH levels and superoxide dismutase and catalase activities [40].

In the last few years, several HT derivatives with enhanced antioxidant and pharmacological properties have been described [41–46]. Among these, 5-S-lipoylhydroxytyrosol (Lipo-HT), synthesized by conjugation of HT with the biologically relevant thiol dihydrolipoic acid, showed increased antioxidant activities compared to HT in several chemical assays and exerted potent protective effects against ROS generation and oxidative cell damage in human hepatocellular carcinoma HepG2 cell lines (Figure 1) [47, 48]. Insertion of the sulfur-containing chain was found to exert a crucial influence on the reactivity of the adjacent catechol system conferring a more pronounced lipophilic character on the core system and resulting in an overall potentiation of the antioxidant activity of HT. This effect was also demonstrated in the case of other naturally occurring catechols [49, 50]. Because of the peculiar combination in its molecular scaffold of a number of redox-active groups, Lipo-HT exerts a multidefence antioxidant action through different mechanisms, including H-atom release, ferric and cupric ion reduction, and OH radical scavenging [48].

The aim of this study was to test the ability of Lipo-HT to prevent human RBC from the oxidative alterations induced by Hg treatment in comparison with the parent HT. These cells are a unique cellular model for *in vitro* studies which investigate oxidative stress-related alterations as well as Hg toxicity [23, 24, 37, 38]. Mercury(II)chloride ($HgCl_2$) was selected for running the experiments since mercury is a well-known oxidative stress inducer [51].

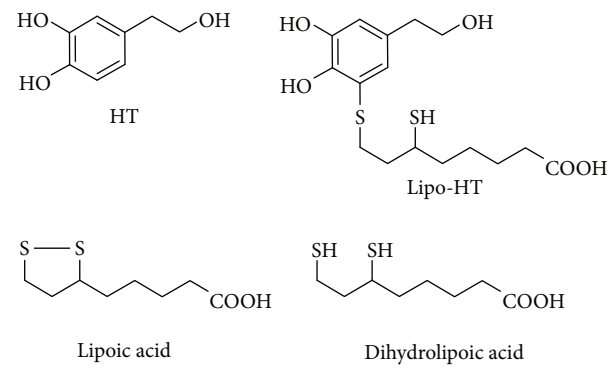

Figure 1

The rationale of testing Lipo-HT in this toxicity model system stems from the possibility of exploiting, in addition to the antioxidant power of the catechol moiety activated by the adjacent thioalkyl group, the free SH group of dihydrolipoic acids capable of effectively chelating Hg. Cytoprotective effects were indeed observed in the case of this conjugate, whose mechanisms were initially investigated at the molecular level by model experiments.

2. Materials and Methods

2.1. Chemicals. 2′,7′-Dichlorodihydrofluorescein diacetate (DCFH-DA), mercuric chloride ($HgCl_2$), tyrosol, lipoic acid, 5,5′-dithiobis(2-nitrobenzoic acid) (DTNB) (Ellman's reagent), and HT were from Sigma Chemical Co. All other chemicals used were of the highest purity grade available.

2.2. Methods. UV/Vis spectra were recorded on a Jasco V-730 spectrophotometer. HPLC analysis was carried out on an Agilent instrument equipped with a UV detector set at 254 nm. The chromatographic separation was achieved on a Phenomenex SphereClone ODS column (250 mm × 4.6 mm, 5 μm) using binary gradient elution conditions as follows: 0.1% trifluoroacetic acid (solvent A) and acetonitrile (solvent B), from 5% to 90% B, 0–45 min, and flow rate 0.7 mL/min. LC/MS analyses were run on a LC/MS ESI-TOF 1260/6230DA Agilent instrument operating in positive ionization mode in the following conditions: nebulizer pressure 35 psig; drying gas (nitrogen) 8 L/min, 325°C; capillary voltage 3500 V; and fragmentor voltage 175 V. An Eclipse Plus C18 column, 150 × 4.6 mm, 5 μm, at a flow rate of 0.4 mL/min was used, with the same mobile phase as above.

2.3. Synthesis of 5-S-Lipoylhydroxytyrosol (Lipo-HT). The procedure previously described was adopted [48]. The reaction was carried out on tyrosol (1.0 g) affording Lipo-HT in about 30% yield. The purity of the compound was evaluated (>95%) by HPLC and ^{1}H NMR analysis.

2.4. Preparation of RBC and Treatment with Hg. The RBC fraction was obtained from whole blood obtained from human healthy volunteers deprived of leucocytes and platelets by filtration on a nylon net, washed twice with isotonic saline solution (0.9% NaCl), and finally resuspended with buffer A (5 mM Tris-HCl containing 0.9%

NaCl, 1 mM $MgCl_2$, and 2.8 mM glucose, pH 7.4) to obtain a 10% hematocrit. Intact RBC were incubated at 37°C with 40 μM $HgCl_2$ for 4 h. For the experiments with Lipo-HT or HT, stock solutions (100 mM) were prepared in DMSO. Just before the experiments, these solutions were diluted to 1 mM with the isotonic saline solution and added to the incubation medium to obtain the desired concentration 5 min before addition of Hg. As a control, the effects of the highest volume of DMSO used on RBC in the presence of Hg were also evaluated and found to be negligible. RBC from each donor were used for a single assay in triplicate. Each experiment was repeated on RBC obtained from three different donors.

2.5. Determination of Hemolysis. The extent of hemolysis was determined spectrophotometrically, according to Tagliafierro et al. [37]. At the end of the incubation, the reaction mixture was centrifuged at 1100g for 5 min and the hemoglobin (Hb) released was evaluated by measuring the absorption of the supernatant at 540 nm. Packed RBC were hemolyzed with ice-cold distilled water at 40 : 1 v/v, the lysate was centrifuged at 1500g for 10 minutes, and the supernatant (B) was absorbed at 540 nm. The percentage of hemolysis was calculated as the ratio of the readings (A/B) × 100.

2.6. Determination of ROS. To quantify ROS generation, the dichlorofluorescein (DCF) assay was used according to Tagliafierro et al. [37]. Intact RBC were incubated with DCFH-DA at 10 μM final concentration for 15 min at 37°C. After centrifugation at 1200g for 5 min, the supernatant was removed and the hematocrit value was adjusted to 10% with buffer A. RBC were then treated with $HgCl_2$ in the dark. At the end of incubation, 20 μL of RBC were diluted in 2 mL of water and the fluorescence intensity of the oxidized derivative DCF was recorded (λ_{ex} 502 nm; λ_{em} 520 nm). The results were expressed as fluorescent intensity/mg of Hb.

2.7. Quantification of Intracellular GSH. The intracellular GSH content was determined spectrophotometrically by reaction with DTNB reagent, according to van den Berg et al. [52]. The samples (0.25 mL) described above were centrifuged, the supernatants were removed, and RBC were lysed by the addition of 0.6 mL of ice-cold water. Proteins were precipitated by the addition of 0.6 mL ice-cold metaphosphoric acid solution (1.67 g metaphosphoric acid, 0.2 g EDTA, and 30 g NaCl in 100 mL of water). After incubation at 4°C for 5 min, the protein precipitate was removed by centrifugation at 18000g for 10 min and 0.45 mL of the supernatant was mixed with an equal volume of 0.3 M Na_2HPO_4. 100 μL of DTNB solution (20 mg DTNB plus 1% of sodium citrate in 100 mL of water) was then added to the sample, and after a 10 min incubation at room temperature, the absorbance of the sample was read against the blank at 412 nm.

2.8. Reaction of Lipo-HT or HT with Hg^{2+} Ions. 5 μL of a 100 mM $HgCl_2$ solution was added to 5 mL of buffer (pH 7.4), followed by 5 μL of a 50 mM DMSO solution of Lipo-HT or HT (100 μM and 50 μM final concentrations for Hg^{2+} and Lipo-HT or HT, resp.). The reaction mixture was taken under stirring and periodically analyzed by HPLC, LC/MS, and UV/Vis spectroscopy. When required, the reaction mixture was taken to pH 3 with 4 M HCl before analysis. In other experiments, aliquots (1.5 mL) of the reaction mixture of Lipo-HT were periodically withdrawn, added with 11 μL of a 10 mM Ellman's reagent solution in 0.1 M phosphate buffer (pH 7.4), and after 15 min the absorbance at 412 nm was read. In other experiments, the reaction was run: (i) in the absence of $HgCl_2$ and (ii) under an argon atmosphere. Methanooxocinobenzodioxinone derivatives were obtained by tyrosinase-catalyzed oxidation of HT as previously described [53].

2.9. Statistical Analysis. Data are shown as means ± SE. The significance of differences was determined by one-way ANOVA followed by a post hoc Dunnett multiple comparison test with significance set at $p < 0.05$. GraphPad Prism 5 was used for statistical analysis.

3. Results and Discussion

3.1. Cytoprotective Effects of Lipo-HT and HT on Hg-Induced Oxidative Alterations in RBC. The ability of natural and biobased phenolic antioxidants to counteract Hg-induced cytotoxicity was investigated using olive oil HT and its conjugate with dihydrolipoic acid, Lipo-HT, which in *in vitro* tests proved highly efficient in counteracting the action of ROS and associated cellular damage [48]. Lipo-HT was prepared from tyrosol and dihydrolipoic acid according to a procedure previously developed [48].

Intact RBC were exposed *in vitro* to 40 μM $HgCl_2$. Based on our previous results [37] on the dose-dependency of Hg toxic effects in RBC, the concentration of 40 μM was taken as the optimal dose to study the oxidative stress-mediated cytotoxicity in our *in vitro* model. Moreover, it is worth noting that comparable concentrations have been found in the blood of individuals exposed to peculiar working environments like gold mines [16]. Cellular lysis, ROS formation, and intracellular GSH levels were evaluated in RBC following 4 h incubation.

Prolonged Hg treatment is associated with severe hemolysis; therefore, cell lysis was evaluated by measuring hemoglobin release in the medium upon cell exposure to $HgCl_2$. Data in Figure 2 show a dramatic increase in the hemolytic process confirming the cytotoxicity resulting from exposure of cells to $HgCl_2$. Both compound Lipo-HT and HT are effective in preventing the toxic effect of the heavy metal as highlighted by the decrease in hemolysis. At all tested concentrations, Lipo-HT shows an enhanced ability over HT on Hg-induced cytotoxicity. Comparable protective effects are provided by Lipo-HT at concentrations halved with respect to those of HT in a statistically significant mode.

Figure 3 reports ROS production in the presence of Hg^{2+} and varying amounts of Lipo-HT or HT in the concentration range 5–20 μM as determined by DCF fluorescence assay. The Hg-induced ROS generation is dose-dependently prevented in the presence of increasing concentrations of either Lipo-HT or HT, a significant effect being observable starting

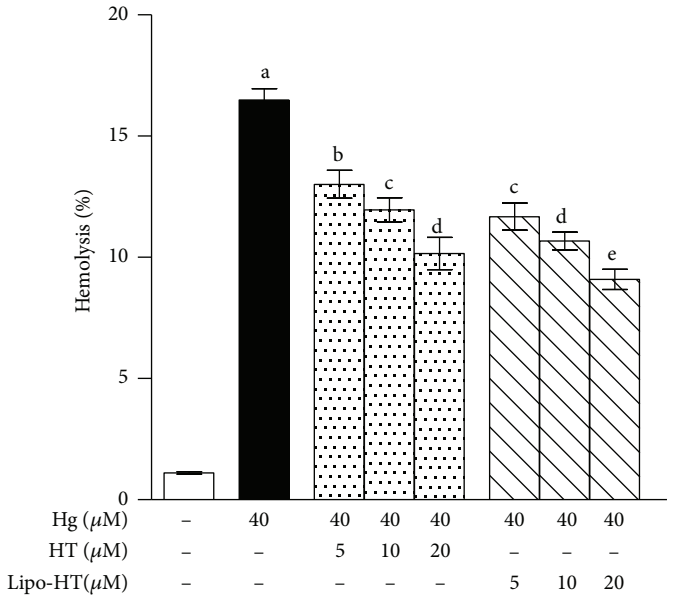

Figure 2: Effect of HT and Lipo-HT on Hg-induced hemolysis. Cells were treated with $HgCl_2$ at 40 μM for 24 h in the presence of increasing concentrations of the selected compounds. Data are the means ± SE ($n = 9$). Statistical analysis was performed with one-way ANOVA followed by Dunnett's test ($p < 0.05$). Means with different letters are significantly different.

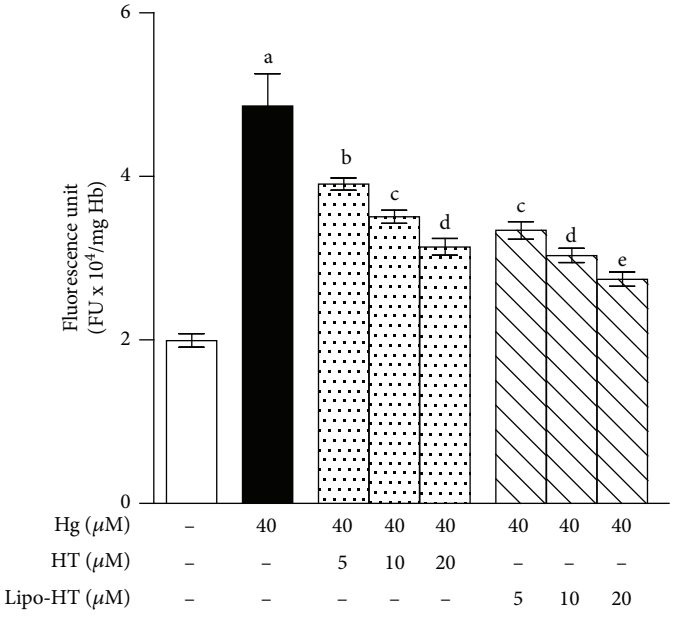

Figure 3: Effect of HT and Lipo-HT on Hg-induced ROS production in RBC. Cells were treated with $HgCl_2$ at 40 μM for 4 h in the presence of increasing concentrations of the selected compounds. ROS production was evaluated by means of the fluorescent probe DCF. Data are the means ± SE ($n = 9$). Statistical analysis was performed with one-way ANOVA followed by Dunnett's test ($p < 0.05$). Means with different letters are significantly different.

from a concentration as low as 5 μM. Interestingly, Lipo-HT appears more effective than HT, producing a 57% decrease of ROS production with respect to the basal level at 5 μM versus an only 34% decrease for HT at the same concentration.

To confirm the observed markedly protective action of Lipo-HT on the specific events that ultimately result in Hg toxicity, the effect of the compounds under study on GSH intracellular concentrations was evaluated. Hg^{2+} specifically binds to biological thiols, including GSH, and is able to induce their oxidation with consequent depletion of the intracellular levels. This is generally regarded as a most critical corollary of Hg toxicity, resulting in the impairment of the antioxidant defence system. Data in Figure 4 refer to the levels of GSH in RBC as determined spectrophotometrically by Ellman's assay. Following cell exposure to Hg^{2+}, the GSH level is significantly reduced with respect to the control

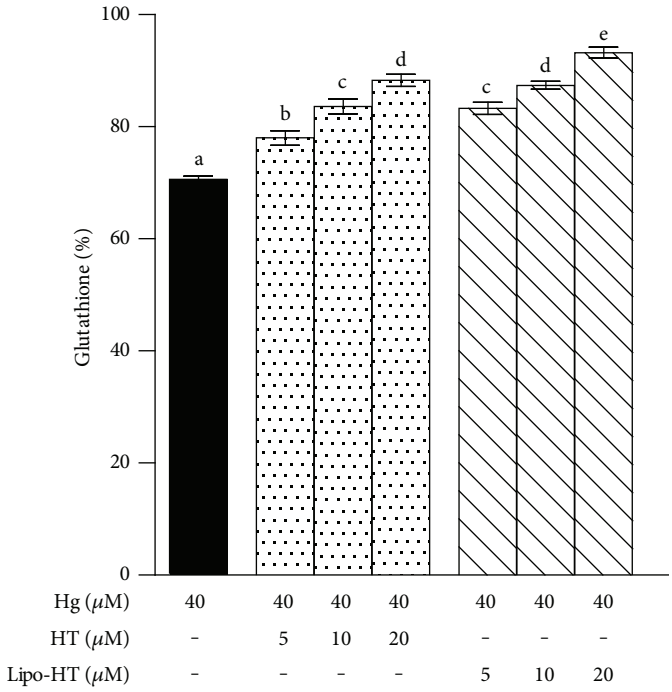

FIGURE 4: Effect of HT and Lipo-HT on Hg-induced GSH decrease in RBC. Cells were treated with 40 μM $HgCl_2$ for 4 h in the presence of increasing concentrations of the selected compounds. Data are the means ± SE ($n = 9$). Statistical analysis was performed with one-way ANOVA followed by Dunnett's test ($p < 0.05$). Means with different letters are significantly different.

RBC. Also in this case, coincubation with Lipo-HT at 5 μM prevents GSH depletion by about 30%, an effect that is obtained with 10 μM HT.

To assess the role of the lipoyl side chain in the observed protective action of Lipo-HT, in other experiments the effects of lipoic acid on Hg-induced toxicity in RBC were investigated. It is clear that this compound could not fully model dihydrolipoic acid that, however, was not possible to include in the controls due to its high instability. Lipoic acid proved to be quite efficient in controlling the Hg-induced increase of ROS levels with effects at 20 μM statistically comparable to those of HT at the same concentration and those exerted by Lipo-HT at 10 μM. On the other hand, at 5 and 10 μM, lipoic acid did not restore the levels of GSH compared to the control in a statistically significant manner and only at the highest dose tested (20 μM) did it produce effects statistically comparable to those obtained with HT at 5 μM.

3.2. Analysis of the Reaction of Lipo-HT and HT with Hg^{2+} Ions at pH 7.4. In order to obtain information about the mechanisms responsible for the protective effect of Lipo-HT against the damage induced to RBC by Hg ions, in other experiments the course of the reaction of Lipo-HT (50 μM) with Hg^{2+} (100 μM) at pH 7.4 was followed by HPLC and LC/MS. An almost complete consumption of Lipo-HT was observed after 5 min, with concomitant formation of two major products eluted at about 22 and 25 min (Figure 5(a)). This latter showed pseudomolecular ion peaks $[M+H]^+$, $[M+Na]^+$, and $[M+K]^+$ at m/z 921, 943, and 959, in that order, suggestive of a 2 : 1 complex of Lipo-HT with Hg. Consistently with the presence of the seven stable isotopes of Hg (with ^{202}Hg being the most abundant at 29.86%), these peaks showed a distinct isotopic pattern (Figure 5(b)), which provided further evidence for the formation of the complex [54]. Ellman's assay [55] indicated a more than 90% abatement of sulfhydryl groups in the reaction mixture after 5 min, pointing to the involvement of the thiolate moiety rather than the catechol unit in Hg-complex formation.

The MS spectrum of the compound eluted at 22 min was characterized by pseudomolecular ion peaks $[M+Na]^+$ and $[M+K]^+$ at m/z 381 and 397, respectively. A $[M\text{-}H_2O+H]^+$ at m/z 341 together with $[2M+Na]^+$ and $[3M+K]^+$ at m/z 739 and 1113, respectively, were also present (Figure 5(c)). These data were suggestive of an oxidation product of Lipo-HT, likely a thioketone as shown in Figure 6. HPLC and LC/MS analysis of the mixture at 1 h reaction time revealed that the Lipo-HT/Hg complex had disappeared, and it also revealed the presence of thioketone as the only residual product.

In control experiments run in the absence of Hg, only a 20% consumption of Lipo-HT was observed after 1 h, and no other product could be detected, apart from traces of thioketone and of the disulfide of Lipo-HT [48]. Moreover, a complete consumption of Lipo-HT, together with the formation of the products eluted at 22 and 25 min, was observed even when the reaction was run under an argon atmosphere, ruling out a possible role of oxygen in the oxidation reaction.

Based on all these observations, a mechanism for the reaction of Lipo-HT with Hg^{2+} was proposed as depicted in Figure 6. This involves the rapid formation of the Lipo-HT/Hg^{2+} complex, followed by oxidation with formation of a thioketone, likely coupled with the reduction of Hg^{2+}. Hence,

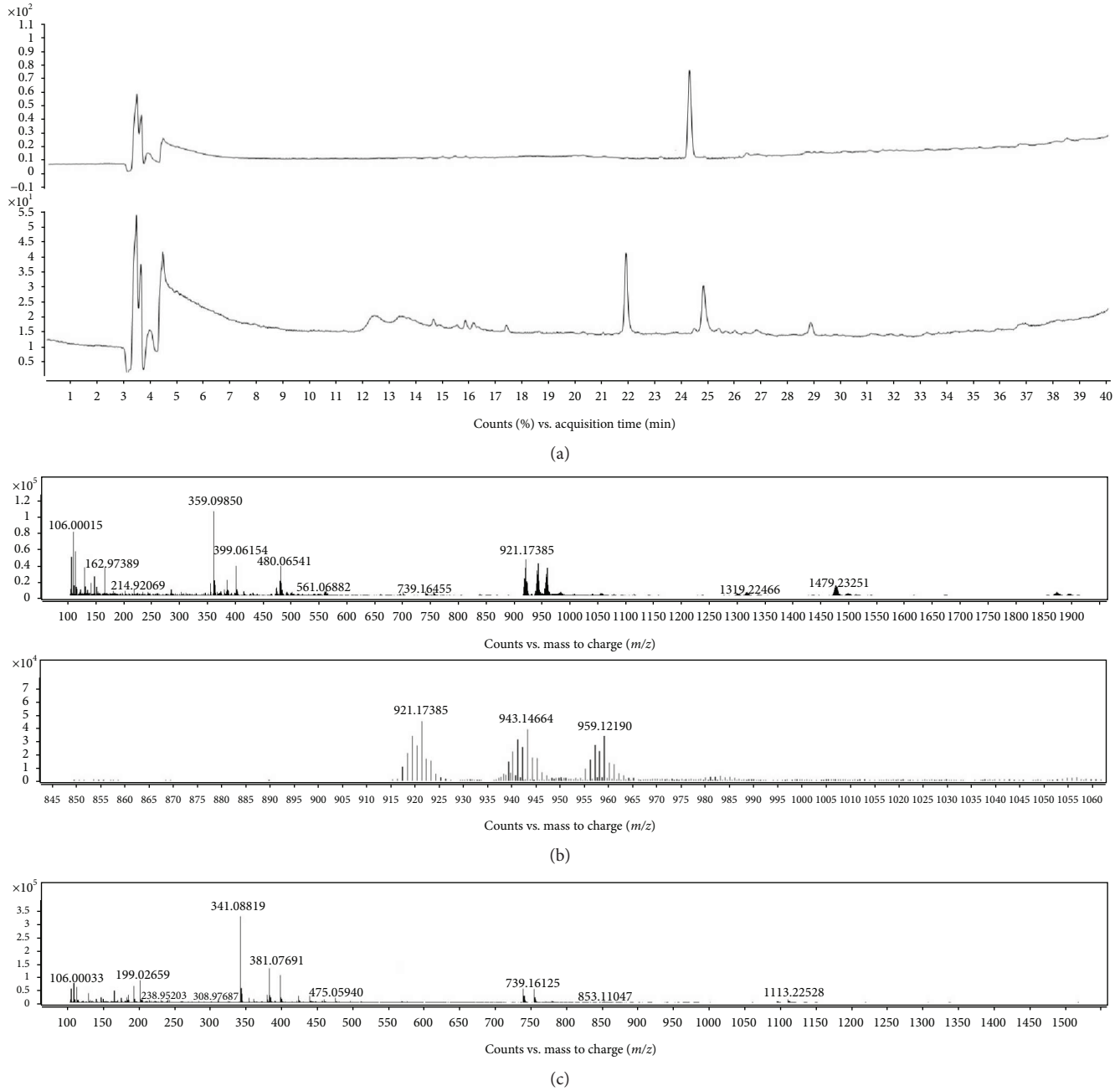

Figure 5: Analysis of the reaction mixture of Lipo-HT with Hg^{2+} ions at pH 7.4. (a) Total ion current (TIC) chromatograms of the reaction mixture of Lipo-HT (50 μM) with Hg^{2+} (100 μM) at pH 7.4 (top: before addition of Hg^{2+}, bottom: 5 min after addition of Hg^{2+}). (b) Top: MS spectrum of the product eluted at 25 min; bottom: inset showing the Hg isotopic signatures of the complex. (c) MS spectrum of the product eluted at 22 min.

Lipo-HT would act as both a chelating and a reducing agent toward Hg ions, thus limiting their capacity to induce oxidative damage in biological compartments. Notably, under the same reaction conditions, HT underwent about 30% consumption after 1 h, giving rise to the methanooxocinobenzodioxinone derivatives identified by comparison of the chromatographic behavior and mass spectra with those of authentic samples [53]. LC/MS analysis of the mixture in the early stages of the reaction revealed the formation of an oxidation product of HT, likely *o*-quinone; accordingly, the UV/Vis spectrum of the reaction mixture at the same time showed an absorption maximum at 390 nm, in close agreement with that reported for the *o*-quinone of HT [49]. No Hg complex formation could be observed, either by UV/Vis or by LC/MS analysis.

As to the relevance of the results of this model experiment to the effects observed in RBC, it should be noted that both Hg^{2+} and Lipo-HT and HT concentrations used were higher but comparable to those chosen for the cellular assays. This however does not allow us to extend tout court these

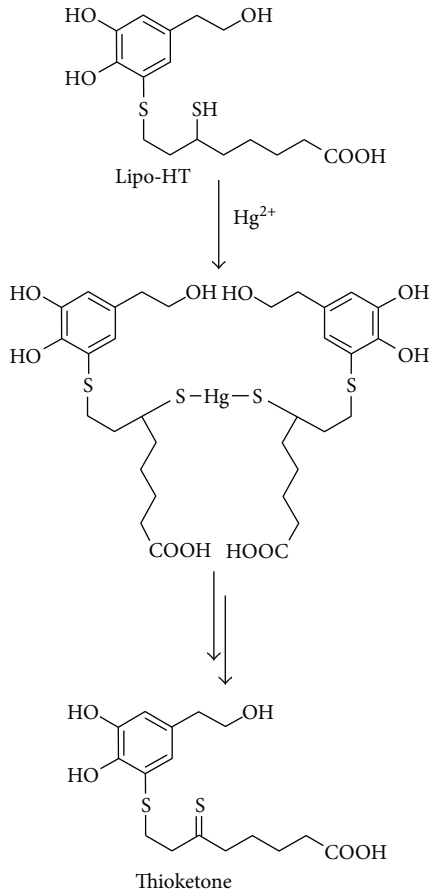

Figure 6: Mechanism proposed for the reaction of Lipo-HT with Hg^{2+} at pH 7.4.

findings to the *in vivo* environment where other species occurring at higher levels may compete with Lipo-HT for Hg binding.

4. Conclusion

The use of natural compounds of plant origin with a potential to control the oxidative cellular alterations associated with Hg exposure is a strategy that is gaining increasing interest to counteract the toxicity of this and other heavy metal pollutants [56]. In this connection, the present investigation provides a significant contribution showing the potency of a derivative of the olive oil polyphenol HT, which contains the active sulfhydryl moiety of dihydrolipoic acid in the molecular scaffold, in controlling the oxidation events triggered by Hg ions and in protecting the intracellular homeostasis warranted by GSH levels. The effects observed can be ascribed to formation of a Hg complex involving the free secondary SH group followed by a redox reaction that would spare intracellular GSH. It can therefore be concluded that the greater ability of Lipo-HT to protect RBC from Hg-induced damage compared to HT is likely due to the more effective chelating and reducing capacity toward Hg ions, in agreement with the higher reducing power toward iron and copper ions previously reported [48]. Although the catechol moiety of Lipo-HT does not seem to be involved in the Hg complex formation, it may play a role as a scavenger of ROS generated following Hg^{2+}-induced metabolic alterations in the cell. Finally, it should be emphasized that the concentrations of HT and its derivative used in this study (5–20 μM) are in the range of plasma concentrations of HT in individuals who adhere to the Mediterranean dietary habit and consume moderate quantities of extra virgin olive oil (25 mL/day). Although further experiments on animal models are clearly needed before the therapeutic use of Lipo-HT against mercury toxicity may be considered, and additional data concerning its absorption, plasma-half-life, and metabolism should be obtained, the results of the present work will expectedly stimulate further studies towards exploitation of this compound in nutraceutical strategies.

Abbreviations

Lipo-HT:	5-*S*-Lipoylhydroxytyrosol
HT:	Hydroxytyrosol
RBC:	Red blood cells
ROS:	Reactive oxygen species
DCFH-DA:	2′,7′-Dichlorodihydrofluorescein diacetate
Hb:	Hemoglobin
DCF:	Dichlorofluorescein
DTNB:	5,5′-Dithiobis(2-nitrobenzoic acid) (Ellman's reagent)
TIC:	Total ion current
MS:	Mass spectrometry.

Conflicts of Interest

The authors declare that they have no conflicts of interest.

Authors' Contributions

The manuscript was written through contributions of all authors. All authors have given approval to the final version of the manuscript.

Acknowledgments

This work was supported by Research Grants from the University of Campania.

References

[1] G. del Monaco, A. Officioso, S. D'Angelo et al., "Characterization of extra virgin olive oils produced with typical Italian varieties by their phenolic profile," *Food Chemistry*, vol. 184, pp. 220–228, 2015.

[2] F. Echeverría, M. Ortiz, R. Valenzuela, and L. Videla, "Hydroxytyrosol and cytoprotection: a projection for clinical interventions," *International Journal of Molecular Sciences*, vol. 18, no. 12, p. 930, 2017.

[3] H. Poudyal, N. Lemonakis, P. Efentakis et al., "Hydroxytyrosol ameliorates metabolic, cardiovascular and liver changes in a rat model of diet-induced metabolic syndrome: pharmacological and metabolism-based investigation," *Pharmacological Research*, vol. 117, pp. 32–45, 2017.

[4] V. Zappia, P. Galletti, C. Manna et al., "Chapter 136 – effects of hydroxytyrosol on cyclosporine nephrotoxicity," in *Olives Olive Oil Health Disease Prevention*, pp. 1245–1252, Academic Press, San Diego, CA, USA, 2010.

[5] E. Bigagli, L. Cinci, S. Paccosi, A. Parenti, M. D'Ambrosio, and C. Luceri, "Nutritionally relevant concentrations of resveratrol and hydroxytyrosol mitigate oxidative burst of human granulocytes and monocytes and the production of pro-inflammatory mediators in LPS-stimulated RAW 264.7 macrophages," *International Immunopharmacology*, vol. 43, pp. 147–155, 2017.

[6] S. Bulotta, M. Celano, S. M. Lepore, T. Montalcini, A. Pujia, and D. Russo, "Beneficial effects of the olive oil phenolic components oleuropein and hydroxytyrosol: focus on protection against cardiovascular and metabolic diseases," *Journal of Translational Medicine*, vol. 12, no. 1, p. 219, 2014.

[7] R. Fabiani, "Anti-cancer properties of olive oil secoiridoid phenols: a systematic review of in vivo studies," *Food & Function*, vol. 7, no. 10, pp. 4145–4159, 2016.

[8] C. Manna, L. Tagliafierro, I. Scala, B. Granese, G. Andria, and V. Zappia, "The role of iron toxicity in oxidative stress-induced cellular degeneration in down syndrome: protective effects of phenolic antioxidants," *Current Nutrition & Food Science*, vol. 8, no. 3, pp. 206–212, 2012.

[9] A. Napolitano, M. De Lucia, L. Panzella, and M. d'Ischia, "Chapter 134 – The chemistry of tyrosol and hydroxytyrosol: implications for oxidative stress," in *Olives and Olive Oil in Health and Disease Prevention*, pp. 1225–1232, Academic Press, San Diego, CA, USA, 2010.

[10] H. K. Obied, P. D. Prenzler, I. Konczak, A. U. Rehman, and K. Robards, "Chemistry and bioactivity of olive biophenols in some antioxidant and antiproliferative in vitro bioassays," *Chemical Research in Toxicology*, vol. 22, no. 1, pp. 227–234, 2009.

[11] A. Napolitano, L. Panzella, M. Savarese et al., "Acid-induced structural modifications of unsaturated fatty acids and phenolic olive oil constituents by nitrite ions: a chemical assessment," *Chemical Research in Toxicology*, vol. 17, no. 10, pp. 1329–1337, 2004.

[12] Z. Liu, L. Sun, L. Zhu et al., "Hydroxytyrosol protects retinal pigment epithelial cells from acrolein-induced oxidative stress and mitochondrial dysfunction," *Journal of Neurochemistry*, vol. 103, no. 6, pp. 2690–2700, 2007.

[13] X. Zhang, J. Cao, L. Jiang, C. Geng, and L. Zhong, "Protective effect of hydroxytyrosol against acrylamide-induced cytotoxicity and DNA damage in HepG2 cells," *Mutation Research/Fundamental and Molecular Mechanisms of Mutagenesis*, vol. 664, no. 1-2, pp. 64–68, 2009.

[14] Y. Y. Lee, C. Crauste, H. Wang et al., "Extra virgin olive oil reduced polyunsaturated fatty acid and cholesterol oxidation in rodent liver: is this accounted for hydroxytyrosol-fatty acid conjugation?," *Chemical Research in Toxicology*, vol. 29, no. 10, pp. 1689–1698, 2016.

[15] C. O. R. Okpala, G. Sardo, S. Vitale, G. Bono, and A. Arukwe, "Hazardous properties and toxicological update of mercury: from fish food to human health safety perspective," *Critical Reviews in Food Science and Nutrition*, pp. 1–16, 2017.

[16] C. T. Driscoll, R. P. Mason, H. M. Chan, D. J. Jacob, and N. Pirrone, "Mercury as a global pollutant: sources, pathways, and effects," *Environmental Science & Technology*, vol. 47, no. 10, pp. 4967–4983, 2013.

[17] K. Sundseth, J. Pacyna, E. Pacyna, N. Pirrone, and R. Thorne, "Global sources and pathways of mercury in the context of human health," *International Journal of Environmental Research and Public Health*, vol. 14, no. 1, p. 105, 2017.

[18] V. Branco, S. Caito, M. Farina, J. Teixeira da Rocha, M. Aschner, and C. Carvalho, "Biomarkers of mercury toxicity: past, present, and future trends," *Journal of Toxicology and Environmental Health, Part B*, vol. 20, no. 3, pp. 119–154, 2017.

[19] S. Miller, S. Pallan, A. S. Gangji, D. Lukic, and C. M. Clase, "Mercury-associated nephrotic syndrome: a case report and systematic review of the literature," *American Journal of Kidney Diseases*, vol. 62, no. 1, pp. 135–138, 2013.

[20] A. Carocci, N. Rovito, M. S. Sinicropi, and G. Genchi, "Mercury toxicity and neurodegenerative effects," *Reviews of Environmental Contamination and Toxicology*, vol. 229, pp. 1–18, 2014.

[21] M. Chin-Chan, J. Navarro-Yepes, and B. Quintanilla-Vega, "Environmental pollutants as risk factors for neurodegenerative disorders: Alzheimer and Parkinson diseases," *Frontiers in Cellular Neuroscience*, vol. 9, p. 124, 2015.

[22] J. Rooney, "Aplastic anemia, membranous nephropathy and mercury," *Indian Journal of Nephrology*, vol. 23, no. 6, pp. 467-468, 2013.

[23] G. I. Harisa, A. D. Mariee, O. M. Abo-Salem, and S. M. Attiaa, "Erythrocyte nitric oxide synthase as a surrogate marker for mercury-induced vascular damage: the modulatory effects of naringin," *Environmental Toxicology*, vol. 29, no. 11, pp. 1314–1322, 2014.

[24] K. Eisele, P. A. Lang, D. S. Kempe et al., "Stimulation of erythrocyte phosphatidylserine exposure by mercury ions," *Toxicology and Applied Pharmacology*, vol. 210, no. 1-2, pp. 116–122, 2006.

[25] J. K. Virtanen, T. H. Rissanen, S. Voutilainen, and T.-P. Tuomainen, "Mercury as a risk factor for cardiovascular diseases," *The Journal of Nutritional Biochemistry*, vol. 18, no. 2, pp. 75–85, 2007.

[26] S. Omanwar and M. Fahim, "Mercury exposure and endothelial dysfunction," *International Journal of Toxicology*, vol. 34, no. 4, pp. 300–307, 2015.

[27] Z. Chen, X. Wu, H. Luo et al., "Acute exposure of mercury chloride stimulates the tissue regeneration program and reactive oxygen species production in the *Drosophila* midgut," *Environmental Toxicology and Pharmacology*, vol. 41, pp. 32–38, 2016.

[28] H. Ghizoni, V. de Souza, M. R. Straliotto, A. F. de Bem, M. Farina, and M. A. Hort, "Superoxide anion generation and oxidative stress in methylmercury-induced endothelial toxicity in vitro," *Toxicology In Vitro*, vol. 38, pp. 19–26, 2017.

[29] J. P. K. Rooney, "The role of thiols, dithiols, nutritional factors and interacting ligands in the toxicology of mercury," *Toxicology*, vol. 234, no. 3, pp. 145–156, 2007.

[30] P. D. Oram, X. Fang, Q. Fernando, P. Letkeman, and D. Letkeman, "The formation constants of mercury(II)-glutathione complexes," *Chemical Research in Toxicology*, vol. 9, no. 4, pp. 709–712, 1996.

[31] L. E. Hernández, J. Sobrino-Plata, M. B. Montero-Palmero et al., "Contribution of glutathione to the control of cellular redox homeostasis under toxic metal and metalloid stress," *Journal of Experimental Botany*, vol. 66, no. 10, pp. 2901–2911, 2015.

[32] Y. Elseady and E. Zahran, "Ameliorating effect of β-carotene on antioxidant response and hematological parameters of mercuric chloride toxicity in Nile tilapia (*Oreochromis niloticus*)," *Fish Physiology and Biochemistry*, vol. 39, no. 4, pp. 1031–1041, 2013.

[33] Y. Deng, Z. Xu, W. Liu, H. Yang, B. Xu, and Y. Wei, "Effects of lycopene and proanthocyanidins on hepatotoxicity induced by mercuric chloride in rats," *Biological Trace Element Research*, vol. 146, no. 2, pp. 213–223, 2012.

[34] W. R. García-Niño and J. Pedraza-Chaverrí, "Protective effect of curcumin against heavy metals-induced liver damage," *Food and Chemical Toxicology*, vol. 69, pp. 182–201, 2014.

[35] Y. J. Shin, J. J. Kim, Y. J. Kim et al., "Protective effects of quercetin against $HgCl_2$-induced nephrotoxicity in Sprague-Dawley rats," *Journal of Medicinal Food*, vol. 18, no. 5, pp. 524–534, 2015.

[36] J. L. Franco, H. C. Braga, J. Stringari et al., "Mercurial-induced hydrogen peroxide generation in mouse brain mitochondria: protective effects of quercetin," *Chemical Research in Toxicology*, vol. 20, no. 12, pp. 1919–1926, 2007.

[37] L. Tagliafierro, A. Officioso, S. Sorbo, A. Basile, and C. Manna, "The protective role of olive oil hydroxytyrosol against oxidative alterations induced by mercury in human erythrocytes," *Food and Chemical Toxicology*, vol. 82, pp. 59–63, 2015.

[38] A. Officioso, K. Alzoubi, F. Lang, and C. Manna, "Hydroxytyrosol inhibits phosphatidylserine exposure and suicidal death induced by mercury in human erythrocytes: possible involvement of the glutathione pathway," *Food and Chemical Toxicology*, vol. 89, pp. 47–53, 2016.

[39] K. M. Lim, S. Kim, J. Y. Noh et al., "Low-level mercury can enhance procoagulant activity of erythrocytes: a new contributing factor for mercury-related thrombotic disease," *Environmental Health Perspectives*, vol. 118, no. 7, pp. 928–935, 2010.

[40] V. Mohan, S. Das, and S. B. S. Rao, "Hydroxytyrosol, a dietary phenolic compound forestalls the toxic effects of methylmercury-induced toxicity in IMR-32 human neuroblastoma cells," *Environmental Toxicology*, vol. 31, no. 10, pp. 1264–1275, 2016.

[41] C. Manna, V. Migliardi, F. Sannino, A. De Martino, and R. Capasso, "Protective effects of synthetic hydroxytyrosol acetyl derivatives against oxidative stress in human cells," *Journal of Agricultural and Food Chemistry*, vol. 53, no. 24, pp. 9602–9607, 2005.

[42] M. V. Sepporta, M. Á. López-García, R. Fabiani, I. Maya, and J. G. Fernández-Bolaños, "Enhanced chemopreventive activity of hydroxytyrosol on HL60 and HL60R cells by chemical conversion into thio derivatives," *European Journal of Pharmaceutical Sciences*, vol. 48, no. 4-5, pp. 790–798, 2013.

[43] R. Bernini, M. S. Gilardini Montani, N. Merendino, A. Romani, and F. Velotti, "Hydroxytyrosol-derived compounds: a basis for the creation of new pharmacological agents for cancer prevention and therapy," *Journal of Medicinal Chemistry*, vol. 58, no. 23, pp. 9089–9107, 2015.

[44] I. Fernandez-Pastor, A. Fernandez-Hernandez, F. Rivas, A. Martinez, A. Garcia-Granados, and A. Parra, "Synthesis and antioxidant activity of hydroxytyrosol alkyl-carbonate derivatives," *Journal of Natural Products*, vol. 79, no. 7, pp. 1737–1745, 2016.

[45] M. H. Gordon, F. Paiva-Martins, and M. Almeida, "Antioxidant activity of hydroxytyrosol acetate compared with that of other olive oil polyphenols," *Journal of Agricultural and Food Chemistry*, vol. 49, no. 5, pp. 2480–2485, 2001.

[46] I. Medina, S. Lois, D. Alcantara, R. Lucas, and J. C. Morales, "Effect of lipophilization of hydroxytyrosol on its antioxidant activity in fish oils and fish oil-in-water emulsions," *Journal of Agricultural and Food Chemistry*, vol. 57, no. 20, pp. 9773–9779, 2009.

[47] R. Amorati, L. Valgimigli, L. Panzella, A. Napolitano, and M. d'Ischia, "5-*S*-lipoylhydroxytyrosol, a multidefense antioxidant featuring a solvent-tunable peroxyl radical-scavenging 3-thio-1,2-dihydroxybenzene motif," *Journal of Organic Chemistry*, vol. 78, no. 19, pp. 9857–9864, 2013.

[48] L. Panzella, L. Verotta, L. Goya et al., "Synthesis and bioactivity profile of 5-*S*-lipoylhydroxytyrosol-based multidefense antioxidants with a sizeable (poly)sulfide chain," *Journal of Agricultural and Food Chemistry*, vol. 61, no. 8, pp. 1710–1717, 2013.

[49] M. De Lucia, L. Panzella, A. Pezzella, A. Napolitano, and M. d'Ischia, "Plant catechols and their *S*-glutathionyl conjugates as antinitrosating agents: expedient synthesis and remarkable potency of 5-*S*-glutathionylpiceatannol," *Chemical Research in Toxicology*, vol. 21, no. 12, pp. 2407–2413, 2008.

[50] M. d'Ischia, A. Napolitano, P. Manini, and L. Panzella, "Secondary targets of nitrite-derived reactive nitrogen species: nitrosation/nitration pathways, antioxidant defense mechanisms and toxicological implications," *Chemical Research in Toxicology*, vol. 24, no. 12, pp. 2071–2092, 2011.

[51] D. Yang, X. Tan, Z. Lv et al., "Regulation of Sirt1/Nrf2/TNF-α signaling pathway by luteolin is critical to attenuate acute mercuric chloride exposure induced hepatotoxicity," *Scientific Reports*, vol. 6, no. 1, article 37157, 2016.

[52] J. J. M. van den Berg, J. A. F. op den Kamp, B. H. Lubin, B. Roelofsen, and F. A. Kuypers, "Kinetics and site specificity of hydroperoxide-induced oxidative damage in red blood cells," *Free Radical Biology & Medicine*, vol. 12, no. 6, pp. 487–498, 1992.

[53] D. Vogna, A. Pezzella, L. Panzella, A. Napolitano, and M. d'Ischia, "Oxidative chemistry of hydroxytyrosol: isolation and characterisation of novel methanooxocinobenzodioxinone derivatives," *Tetrahedron Letters*, vol. 44, no. 45, pp. 8289–8292, 2003.

[54] X. Lin, J. Brooks, M. Bronson, and M. Ngu-Schwemlein, "Evaluation of the association of mercury(II) with some dicysteinyl tripeptides," *Bioorganic Chemistry*, vol. 44, pp. 8–18, 2012.

[55] M. Farid, H. Khan, H. Khan, R. Z. Paracha, and G. M. Khan, "Effect of mercuric chloride on glutathione (GSH) level in plasma and cytosolic fraction of human blood," *Jordan Journal of Pharmaceutical Science*, vol. 2, no. 1, pp. 22–31, 2008.

[56] P. Manini, L. Panzella, T. Eidenberger et al., "Efficient binding of heavy metals by black sesame pigment: toward innovative dietary strategies to prevent bioaccumulation," *Journal of Agricultural and Food Chemistry*, vol. 64, no. 4, pp. 890–897, 2016.

Hindawi
Oxidative Medicine and Cellular Longevity
Volume 2018, Article ID 3734250, 13 pages
https://doi.org/10.1155/2018/3734250

Research Article

Counteraction of Oxidative Stress by Vitamin E Affects Epigenetic Regulation by Increasing Global Methylation and Gene Expression of *MLH1* and *DNMT1* Dose Dependently in Caco-2 Cells

Katja Zappe,[1] Angelika Pointner,[1] Olivier J. Switzeny,[2] Ulrich Magnet,[1] Elena Tomeva,[1] Jutta Heller,[1] George Mare,[1] Karl-Heinz Wagner,[1] Siegfried Knasmueller,[3] and Alexander G. Haslberger[1]

[1]*Department of Nutritional Sciences, University of Vienna, 1090 Vienna, Austria*
[2]*Department of Toxicology, University Medical Center of the Johannes Gutenberg University Mainz, 55131 Mainz, Germany*
[3]*Institute of Cancer Research, Department of Medicine I, Medical University of Vienna, 1090 Vienna, Austria*

Correspondence should be addressed to Alexander G. Haslberger; alexander.haslberger@univie.ac.at

Received 27 October 2017; Revised 18 January 2018; Accepted 29 January 2018; Published 22 March 2018

Academic Editor: Joseph Adeyemi

Obesity- or diabetes-induced oxidative stress is discussed as a major risk factor for DNA damage. Vitamin E and many polyphenols exhibit antioxidative activities with consequences on epigenetic regulation of inflammation and DNA repair. The present study investigated the counteraction of oxidative stress by vitamin E in the colorectal cancer cell line Caco-2 under normal (1 g/l) and high (4.5 g/l) glucose cell culture condition. Malondialdehyde (MDA) as a surrogate marker of lipid peroxidation and reactive oxygen species (ROS) was analyzed. Gene expression and promoter methylation of the DNA repair gene *MutL homolog 1* (*MLH1*) and the *DNA methyltransferase 1* (*DNMT1*) as well as global methylation by *LINE-1* were investigated. Results revealed a dose-dependent counteracting effect of vitamin E on H_2O_2-induced oxidative stress. Thereby, 10 μM vitamin E proved to be more efficient than did 50 μM in reducing MDA. Further, an induction of *MLH1* and *DNMT1* gene expression was noticed, accompanied by an increase in global methylation. Whether *LINE-1* hypomethylation is a cause or effect of oxidative stress is still unclear. In conclusion, supplementation of exogenous antioxidants like vitamin E *in vitro* exhibits beneficial effects concerning oxidative stress as well as epigenetic regulation involved in DNA repair.

1. Introduction

Lifestyle-associated diseases, such as cancer and cardiovascular, respiratory, and metabolic diseases, comprise most of the noncommunicable diseases and account for more than two-thirds of the worldwide deaths [1]. Natural bioactive nutritional compounds like vitamin E play a major role in nutrition-based disease improvements as well as in its prevention [2].

Vitamin E is a collective term including α, β, γ, and δ isomers of saturated tocopherols [3] and unsaturated tocotrienols [4]. Beneficial and harmful effects on human health by vitamin E were observed, and therefore usefulness of vitamin E is highly controversial. Intervention studies showed anti-inflammatory effects, a delay of the aging process [5, 6], anticancer properties [7, 8], antidiabetic and eye disease protective potential [9], and cardiovascular protective [10] features. Adjuvant vitamin E treatment of patients suffering from different cancer types led to controversial effects [11, 12]. A meta-analysis revealed an increased all-cause mortality by a high dose of vitamin E [13], while other studies found promising synergistic effects between vitamin E and administered drugs, especially anticancerous effects [14, 15]. Most studies are based on different isoforms of vitamin E or mixture ratios, or synthetic racemic or natural *R*-, *E*-configurated isomers, all leading to different biological effective doses.

One important mechanism of all vitamin E forms is the nonenzymatic antioxidative, radical scavenging potential by donating hydrogen from the phenolic group on the chromanol ring [16]. Reactive oxygen species (ROS), a group of reactive metabolic by-products affecting the redox balance, are essential for signaling pathways, detoxification, and host defense [17, 18]. Furthermore, they are known for modulating gene expression and regulating growth signals and therefore having a significant impact on the sustained proliferation of cancer. High levels of ROS occurring as a response to oxidative stressors such as exogenous agents including tobacco smoke, alcohol consumption, and infections or various inflammatory processes damage DNA, lipids, and proteins were found to upregulate oncogenes. Inflammation processes and aging per se are fueled by ROS [17, 18].

The major initial endogenous ROS is superoxide ($O_2^{\bullet -}$), which is generated from oxygen under NADH consumption or by NADPH oxidases (NOX) and xanthine oxidase (XO) [19]. It reacts spontaneously with nitric oxide ($NO^{\bullet}$) to peroxynitrite ($ONOO^-$) or is disproportionated by superoxide dismutase (SOD) to hydrogen peroxide (H_2O_2) [19]. *In vitro* studies showed that exogenous H_2O_2 is linked with increased cell proliferation attended by moderate ROS concentrations [20]. Downstream ROS deriving as singlet oxygen $^1O_2$ are able to oxidize aliphatic chains to fatty acids, which are substrates for the hydroxyl radical to generate fatty acid peroxide radicals [21]. Peroxidation of polyunsaturated fatty acids (PUFAs) leads to the formation of small aldehydes such as malondialdehyde (MDA) and trans-4-hydroxy-2-nonenal (4-HNE) [22]. Both are considerably involved in cellular signaling, affecting chromatin modifications [23].

Long-term oxidative stress leads to chronic changes in enzymatic, transcriptional, epigenetic, and genomic regulation by inducing a new steady-state level of oxidants and antioxidants [18]. In cancer development, ROS-generating processes are generally upregulated and promote cell proliferation by altering metabolism and cell control mechanisms, consequently sustaining DNA damage, genomic instability, and inflammation [24].

Emerging studies reveal that only 5–10% of cancer incidences are exclusively caused by genetic factors [25]. In most other cases, epigenetic alterations play an important part [26]. Linkages of epigenetics with oxidative stress, nutritional effects, and cell signaling underline its importance [27]. Among epigenetic mechanisms, DNA methylation at the 5-position of cytosines in cytosine-guanine sequences (CpGs) in promoter regions is a key control mechanism of gene expression [28]. A global surrogate marker for estimating the genomic DNA methylation constitutes mobile element *long interspersed nuclear element-1* (*LINE-1*) with a frequency of 17% of the human genome and an estimated total genomic methylation content of 1/3 [29, 30]. Genome-wide loss of DNA methylation leads to genomic instability and results in a higher chance of mitotic recombination [31]. Therefore, *LINE-1* is suggested as an indicator of genomic stability [32]. The key enzymes involved in DNA methylation constitute the family of DNA methyltransferases (DNMTs) mediating the transfer of methyl groups to cytosines. DNMT overexpression or activation participates in tumor suppressor silencing [33, 34]. Tumors also often show aberrant high promoter methylation of the mismatch repair (MMR) gene *MutL homolog 1* (*MLH1*), which further boosts genomic instability [35]. Moreover, synergistic oxidative DNA damage repair plays a crucial role to protect the genome and to ensure its stability. It further reveals the complex interplay of the individual repair systems [36]. MMR was reported to contribute to base excision repair (BER) of 8-oxo-2′-deoxyguanosine (8-oxo-dG) [37] as well as to nucleotide excision repair (NER) of the MDA adduct with deoxyguanosine (M1dG) [38, 39]. MMR proteins, especially MLH1, were found to interact with DNMTs, the NAD-dependent deacetylase sirtuin-1 (SIRT1) and poly(ADP-ribose) polymerase 1 (PARP1) to prevent altered gene transcripts from the damaged site and induce cell death, when damage exceeds the repair capacity [40, 41].

The focus of this study was to investigate epigenetic effects of vitamin E in counteracting H_2O_2-induced ROS production and lipid peroxidation. Therefore, colorectal adenocarcinoma Caco-2 cells in normoglycemic and hyperglycemic media were treated with a mixture of tocopherols and tocotrienols in combination with different doses of H_2O_2 as well as ROS inhibitor *N*-acetylcysteine (NAC) [42] and NOX inhibitor VAS2870 [43]. Our aim was to identify concentrations of H_2O_2 and vitamin E, which are worth further investigation in higher repetition. Thus, total ROS, superoxide level, and MDA levels were assessed. To evaluate epigenetic alterations in genes linked with oxidative stress, chromosomal integrity, and DNA repair, global methylation by *LINE-1* promoter methylation as well as promoter methylation and expression of *MLH1* and *DNMT1* were determined.

2. Material and Methods

2.1. Cell Culture. The adherent human colorectal adenocarcinoma cell line Caco-2 (DSMZ, Germany) was cultured as monolayer in Dulbecco's modified Eagle medium (DMEM) high glucose (4.5 g/l) supplemented with 0.584 g/l L-glutamine, 5% (w/v) penicillin/streptomycin, and 10% (v/v) FBS at 37°C in a humidified atmosphere of 95% air and 5% CO_2. Cells were passaged before reaching confluency, using 1x PBS and Accutase® solution. A fraction of these cells was adjusted by stepwise reduction of D-glucose through addition of DMEM normal glucose (1.0 g/l, supplemented like the high glucose DMEM) to, finally, 1.0 g/l D-glucose. In the first step, D-glucose concentration was reduced by 1.75 g/l and cultivated for 14 days. The second and third reductions were by 0.875 g/l with cultivation for 8 and at least 23 days, respectively. Cultivation after each reduction was performed to give the cells time to adapt to the new condition, especially before the analyses (all chemicals from Sigma-Aldrich, Vienna).

2.2. Cell Treatments. Cells were seeded in 6-well plates in media with respective glucose concentration. The untreated control was incubated 72 h to reach 90% confluency. For treatment, after 24 h of growth, cells were treated for 48 h

with 0, 25, 50, 250, or 500 μM H_2O_2 (Sigma-Aldrich, Vienna) and cotreated with 0, 10, or 50 μM vitamin E (Aqua-E® supplement YASOO Health Inc., Nicosia) in all combinations. Vitamin E comprised a mixture of micellized *d*-α-tocopherol 20 IU/ml, other tocopherols 15 mg/ml, and tocotrienols 2 mg/ml from natural origin. Media without phenol red were used to avoid interference in treatments for ROS/superoxide and MDA detection. To investigate the contribution of ROS as a potential modulator of epigenetic alterations, cells were treated with 1 mM NAC (Enzo Life Science, Lausen) dissolved in sterile deionized water (QIAGEN, Hilden) or 2 μM VAS2870 (Sigma-Aldrich, Vienna) dissolved in DMSO (Sigma-Aldrich, Vienna). Further, after 1 h pretreatment with either NAC or VAS2870, 250 μM H_2O_2 was applied. Controls were treated with the corresponding solvent only. For analyzing the impact of the treatments, cells were harvested using 1x PBS and Accutase solution.

2.3. MDA as Marker for Lipid Peroxidation. Harvested cells were counted, and MDA levels were determined via HPLC with fluorescent detection at 533 nm as previously described [44, 45]. All chemicals were purchased from Sigma-Aldrich, Vienna, and all organic solvents used were of HPLC grade and purchased from Rathburn Chemicals Ltd., Walkerburn. Resulting MDA levels were expressed in MDA concentration per cell number. For run comparison, MDA levels were related to high glucose untreated control and corresponding media control for analysis of treatment impact.

2.4. Total ROS and Superoxide Level. 1×10^5 treated cells per well of a 96-well plate with black walls and transparent flat bottom were seeded by centrifugation at 40 ×g, 3 min with lowest acceleration (acc. 1) and second lowest deceleration (dcl. 2) (Jouan BR4i Multifunction Centrifuge, Thermo Fisher Scientific). All other steps were performed according to ROS/superoxide detection kit ENZ-51010 (Enzo Life Science, Lausen) manufacturers' instructions except after adding 1x wash buffer, an additional centrifugation step (same conditions as described above) was conducted to bring loosened cells down to the bottom. For the 60 min staining, a 1 : 2500 dilution of each dye in respective (glucose) DMEM was used. The negative assay control was generated by ROS scavenging activity for 60 min with 5 mM NAC and the positive assay control by ROS induction with 400 μM pyocyanin for 20 min of untreated cells. Plates were read at 37°C with FLUOstar Optima microplate reader (BMG Labtech, Ortenberg) using 4 mm orbital averaging, 6 cycles with 10 flashes per well, and cycle and fluorescence filters with ex 485 nm/em 520 nm and ex 544 nm/em 612 nm. Fluorescence levels were calculated over the same measurement time for all plates. Corresponding ROS/superoxide levels were related to high glucose untreated control for run comparisons and corresponding media control for analysis of treatment impact.

2.5. RNA/gDNA Extraction and Bisulfite Conversion. RNA and gDNA were extracted simultaneously from treated cells using RNAprotect® Cell Reagent, AllPrep DNA/RNA Mini Kit with additional reagent DX for lysis and proteinase K, and RNase-free DNase for cleanup (all QIAGEN, Hilden) according to manufacturer's protocols for cell culture. Homogenization step was performed using stainless steel beads (QIAGEN, Hilden) with Precellys® 24 (Bertin Technologies, Montigny-le-Bretonneux) at 1600 ×g (5000 rpm), 2x 15 s with a 10 s break in between. Bisulfite conversion of unmethylated cytosines in DNA was performed according to EpiTect® Fast Bisulfite Conversion Kit (QIAGEN, Hilden) manufacturer's instructions using bisulfite reaction setup for high-concentration samples and extension of both 60°C incubation times to 20 min. RNA and DNA concentrations were determined with Pico100 UV/Vis spectrophotometer (Picodrop Limited, Hinxton).

2.6. Gene Expression Analysis. Reverse transcription and cDNA amplification were done either with 1 μg RNA using the RT^2 First Strand Kit (QIAGEN, Hilden) or with the following modifications for the RT^2 HT First Strand Kit for 96 samples (QIAGEN, Hilden). GE2 buffer and RT mix were immediately aliquoted and stored for later use at −20°C. 8 μl of RNA solution was mixed with 6 μl GE2 buffer in a PCR tube and incubated in the thermocycler with preheated lid for 15 min at 42°C and then 5 min at 95°C. 6 μl RT mix was added and incubated in the thermocycler with preheated lid for 5 min at 37°C. After mixing with 91 μl nuclease-free distilled water, the cDNA was stored at −20°C.

Real-Time PCR was performed using *GAPDH* as housekeeping gene and *DNMT1* and *MLH1* as genes of interest according to RT^2 qPCR Primer Assays and RT^2 SYBR Green ROX qPCR Mastermix manufacturer's protocol (all QIAGEN, Hilden) in the real-time thermocycler StepOnePlus™ (Applied Biosystems, Vienna). PCR conditions were an initial PCR activation step of 10 min at 95°C and a 40x repeated 2-step cycling of 15 s denaturation at 95°C, and 1 min annealing and extension at 60°C followed by a melt curve analysis from 60°C to 95°C in 0.3°C steps. For comparisons of runs, an untreated control of each culture media was used on every plate. Relative expression was calculated using $\Delta\Delta C_T$ method and was expressed as $2^{-\Delta\Delta C_T}$.

2.7. Standard Synthesis for Methylation-Sensitive High-Resolution Melting (MS-HRM). For synthesis of unmethylated DNA standards, purified gDNA from untreated Caco-2 (high glucose media) was amplified according to the REPLI-g® Mini Kit (QIAGEN, Hilden) handbook using 5 μl template DNA and 16 h incubation with Master Mix at 30°C. Amplified gDNA was purified by precipitation with sodium acetate according to QIAGEN FAQ ID-305. Therefore, 1/10 volume of 3 M sodium acetate (Sigma-Aldrich, Vienna), pH 5.2, and 2–2.5 volumes ice-cold 96% ethanol (analysis grade, VWR Chemicals, Vienna) were mixed with the gDNA and precipitated for 1 h at −20°C. After centrifugation at 4°C for 20 min with 21200 ×g, the alcohol was pipetted off, and the pellet was washed twice at room temperature with 70% ethanol and was air dried. The purified DNA was dissolved according to pellet size in about 50–100 μl sterile TE buffer (AppliChem, Darmstadt). A part of the unmethylated standard was methylated according to the manufacturer's protocol for CpG Methyltransferase M.SssI 20 U/μl using 640 μM *S*-adenosyl-L-

methionine (SAM) and 10x NEBuffer 2 (all NEB, Frankfurt). Methylation at 37°C was performed for 4 h with addition of fresh SAM in between. The methylated standard was purified with sodium acetate as the unmethylated one. Unmethylated cytosines in standard DNA were bisulfite converted according to EpiTect Bisulfite Kit handbook (QIAGEN, Hilden) using 0.63–2 μg DNA.

2.8. DNA Methylation Analysis by MS-HRM. MS-HRM was performed according to the EpiTect HRM™ PCR handbook (QIAGEN, Hilden) using the Rotor-Gene® Q (QIAGEN, Hilden). The 10 μl reaction mix for PCR contained 5 μl 2x EpiTect HRM PCR Master Mix (QIAGEN, Hilden), 5 ng bisulfite converted DNA, and RNase-free water (QIAGEN, Hilden). Further PCR conditions were optimized for every primer set (http://biomers.net GmbH, Ulm). For *MLH1*, 500 nM of each primer (Table 1) was used. Initial PCR activation step 5 min at 95°C was followed by 40x repeated 3-step cycling of 15 s denaturation at 95°C, 30 s annealing at 50°C, and 20 s extension at 72°C. After 1 min denaturation at 95°C and 1 min heteroduplex formation at 40°C, HRM analysis was performed from 55°C to 95°C in 0.2°C steps. For *DNMT1*, 750 nM of each primer (Table 1) and 0.29 mM additional $MgCl_2$ were used. Initial PCR activation step 5 min at 95°C was followed by 40x repeated 3-step cycling of 15 s denaturation at 95°C, 30 s annealing at 50°C, and 20 s extension at 72°C. After 1 min at 95°C and 1 min at 40°C, HRM analysis was performed from 55°C to 95°C in 0.2°C steps. For *LINE-1*, 750 nM of each primer was used (Table 1). The initial hot-start polymerase activation step 5 min at 95°C was followed by 45x repeated 3-step cycling of 30 s denaturation at 95°C, 45 s annealing at 54°C, and 30 s extension at 72°C. After 1 min at 95°C and 1 min at 45°C, HRM analysis was performed from 60°C to 95°C in 0.1°C steps. DNA methylation standards were checked for every primer pair for either complete demethylation or methylation by comparison to EpiTect PCR Control DNA set standards (QIAGEN, Hilden). For comparison of all MS-HRM runs, unmethylated and methylated standards were mixed and used from the same mixture aliquots to generate the calibration curves at each run.

MS-HRM data were analyzed with Rotor-Gene Q Series Software version 2.3.1 according to Rotor-Gene Q User Manual (QIAGEN, Hilden). Normalized curves were analyzed based on curve interpolation as published by Spitzwieser et al. [46] based on Migheli et al. [47] and via the standardized fluorescence (SF) for the maximal temperature span in which the curves still differ. Calibration curve fitting was performed using TableCurve 2D and SigmaPlot (both Systat Software Inc.) for identifying the most suitable simple equation for each gene.

2.9. Statistical Analysis. Data are represented as mean ± standard deviation (SD). All experiments were performed in duplicates, if not indicated otherwise. Data presentation and statistical analysis were performed with SPSS® Statistics version 23 (IBM). Two-tailed Student's *t*-test for independent samples (CI = 0.95) without Welch correction was used for comparison with the untreated control (c) or respective H_2O_2 treatment (h). Two-way ANOVA was used for comparison of the different treatments (t) in the context of different glucose concentrations (g). Pearson correlation was performed between the measured parameters. Differences were considered statistically significant at a p value ≤ 0.05.

3. Results

3.1. Effects of Glucose Concentration. Cells were grown in normoglycemic media (1 g/l) as well as hyperglycemic conditions (4.5 g/l D-glucose), reflecting severe diabetic blood level [48], to elucidate the influence of the glucose concentration. Glucose concentration significantly ($p \leq 0.01$) increased MDA levels in cells grown under hyperglycemic compared to those in normoglycemic conditions (Figure 1). ROS levels were significantly decreased in relation to normoglycemic untreated control ($p \leq 0.001$). However, superoxide level was not affected by the hyperglycemic condition.

MLH1 expression as well as its mean promotor methylation was not affected by the glucose concentration alone (Figures 1 and 2). *DNMT1* expression was significantly increased by glucose in treated cells ($p \leq 0.001$) (Figure 1). *LINE-1* promoter methylation was not affected by different glucose concentrations (Figure 2).

Consequently, for analysis of the treatment effects in the following sections, relative comparison to respective untreated glucose control was used to minimize the effects of the glucose level. Furthermore, it would be of interest to investigate these observed changes by glucose reduction. Further investigation by measuring ROS, MDA levels, and *DNMT1* expression during smaller reductions steps based on these findings might reveal the mechanisms behind in more detail.

3.2. Effects of Vitamin E on Oxidative Stress

3.2.1. MDA. Incubation with 250 μM as well as 500 μM H_2O_2 provoked a significant increase in MDA levels at both glycemic conditions ($p \leq 0.01$) (Figure 3). Addition of 10 μM or 50 μM vitamin E could alleviate this effect. Interestingly, a dose of 10 μM vitamin E was more effective and completely prevents H_2O_2-induced MDA. In the normoglycemic condition, significant higher MDA levels compared to those in the untreated controls were measured after incubation with 250 μM H_2O_2 + 50 μM vitamin E ($p \leq 0.05$), whereas both vitamin E concentrations at high glucose levels in combination with 250 μM H_2O_2 led to the equal MDA levels.

The ROS scavenger NAC as well as the NOX inhibitor VAS2870 was able to reduce the MDA levels following 250 μM H_2O_2 treatments. A single treatment with NAC or VAS2870 had no significant effect on the MDA level.

Treatment with 10 μM or 50 μM vitamin E alone led to increased MDA levels under normoglycemic conditions (Figure 3(a)). Under hyperglycemic conditions, 10 μM or 50 μM vitamin E alone led to reduced MDA levels (Figure 3(b)). However, the latter was not significant.

3.2.2. ROS/Superoxide. Treatment with the assay controls pyocyanin or NAC resulted in the expected ROS/superoxide alterations. 48 h incubation with H_2O_2, vitamin E, or ROS/

Table 1: Primer sequences used for MS-HRM analysis. *LINE-1*-rv contains an additional 5′ biotin residue for possible pyrosequencing use. Primer sequences were taken from literature as indicated. Amplicon length and CpG content were determined using BiSearch version 2.53 [65] and Ensembl release 86 database [66].

Primer	Sequence (5′-3′) for MS-HRM	Reference	Amplicon (bp)	CpGs
MLH1-fw	TTTTTTTAGGAGTGAAGGAGG	[67]	123	13
MLH1-rv	AACRCCACTACRAAACTAAA			
DNMT1-fw	GGTATCGTGTTTATTTTTTAGTAA	[68]	115	6
DNMT1-rv	ACGAAACCAACCATACCCAA			
LINE-1-fw	TTTTGAGTTAGGTGTGGGATATA	[69]	~143–148	~1–10
LINE-1-rv	AAAATCAAAAAATTCCCTTTC			

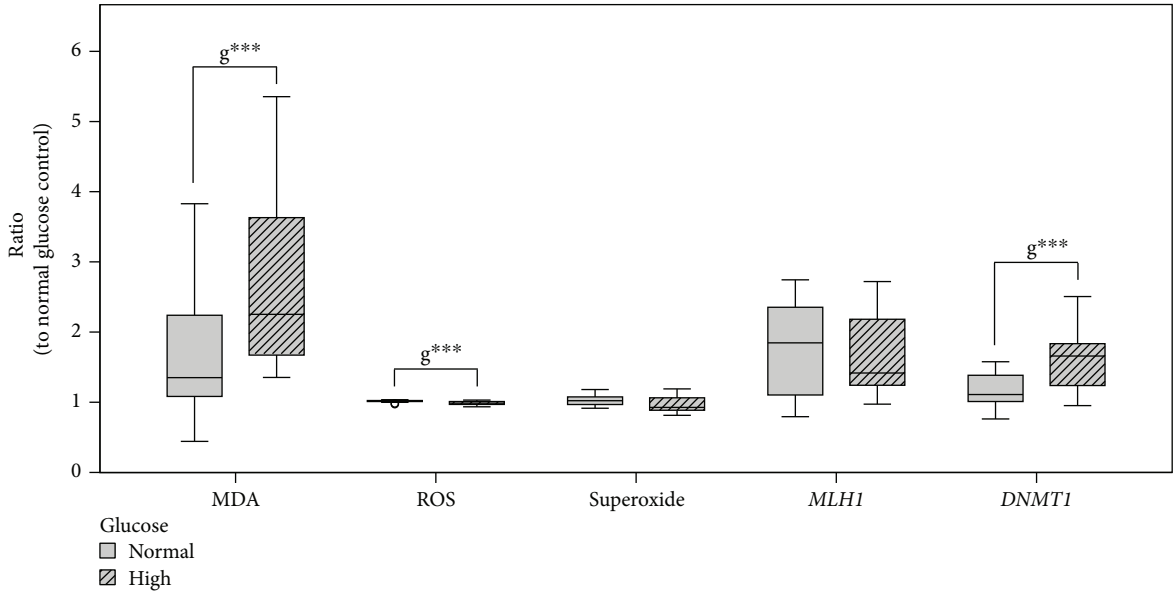

Figure 1: Impact of glucose level and shared 48 h treatments (Table 2) in Caco-2 on lipid peroxidation (MDA level) $n = 52$, ROS $n = 39$, and superoxide $n = 39$ formation and on *MLH1*$n = 36$ and *DNMT1*$n = 36$ gene expression. Data are displayed as ratio to normal glucose untreated control and grouped by normal and high glucose growing conditions. Differences between groups are statistically analyzed by two-way ANOVA on ratios except for gene expression, where analysis is based on $\Delta\Delta C_T$ to normal glucose untreated control. Significance by glucose (g) is marked with $***$ for $p \leq 0.001$.

NOX inhibitors had no significant impact on ROS or superoxide levels at both glycemic conditions (Figure 4), indicating that no stable changes were generated.

3.3. Treatment on MLH1 and DNMT1 Gene Regulation and LINE-1 Methylation

3.3.1. MLH1 Expression. There was no significant effect on *MLH1* expression after an exclusive treatment with H_2O_2 at various concentrations under both glycemic conditions (Figure 5). Incubation with solely 10 μM (not significant) or 50 μM ($p \leq 0.05$) vitamin E resulted in an elevated expression of *MLH1*.

Furthermore, a combined treatment of vitamin E and H_2O_2 in normoglycemic media significantly increased *MLH1*. A similar enhancing effect could be observed under hyperglycemic conditions, where combinations of 10 or 50 μM vitamin E with 25 to 500 μM H_2O_2 resulted in a significantly higher expression of *MLH1* ($p \leq 0.05$). Concerning treatment with 500 H_2O_2 + 50 μM vitamin E only, data from one sample could be obtained as this concentration was highly cytotoxic.

Inhibitor studies with NAC or VAS2870 combined with H_2O_2 performed in the hyperglycemic condition both showed a significant increase of *MLH1* expression.

3.3.2. DNMT1 Expression. In cells grown under normoglycemic conditions, 10 μM vitamin E increased *DNMT1* expression, while 50 μM showed no effect (Figure 6(a)). At hyperglycemic conditions, both vitamin E concentrations increased *DNMT1* expression, which was significant for 10 μM ($p \leq 0.05$) (Figure 6(b)). In contrast, H_2O_2 alone scarcely affected *DNMT1* expression level.

Combined incubation of vitamin E and H_2O_2 increased *DNMT1* expression under both glycemic conditions and was significant under hyperglycemic conditions ($p \leq 0.05$). Thereby, high H_2O_2 concentrations (250 μM, 500 μM) increased *DNMT1* expression less than did moderate ones (25 μM, 50 μM).

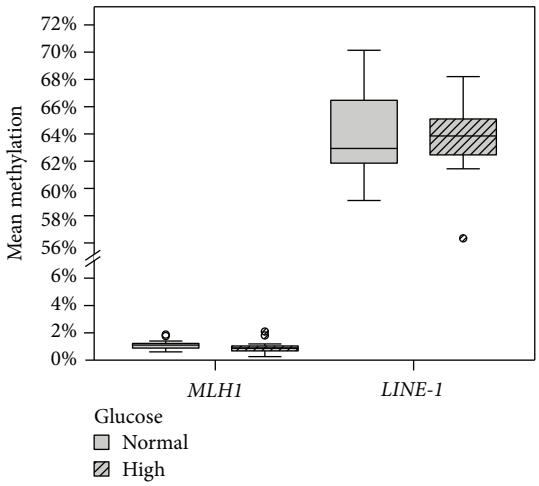

Figure 2: Impact of glucose levels and shared 48 h treatments (Table 2) in Caco-2 cells on the mean *MLH1* promoter $n = 36$ and global methylation (*LINE-1* promoter region) $n = 36$ grouped by normal and high glucose conditions. Differences between groups were statistically analyzed on mean promoter methylation by two-way ANOVA. No significance by glucose (g) was found.

A significant increase to the corresponding H_2O_2 treatment control was also detected for combinations of 10 μM vitamin E with 50 μM and 250 μM H_2O_2 ($p \leq 0.05$) and for 250 μM H_2O_2 + 50 μM vitamin E ($p \leq 0.01$).

NAC and VAS2870, when incubated with 250 μM H_2O_2, both showed a trend towards an upregulation compared to untreated and H_2O_2 treatment controls, which was more pronounced and significant with NAC ($p \leq 0.05$).

3.3.3. Promoter Methylation of MLH1, DNMT1, and LINE-1. Promoters of *MLH1* and *DNMT1* were both unmethylated in all treatments within a range of 0.4%–2.7% and 0.8%–1.2% methylation degree, respectively (Figure 7).

Consistently for both genes, no correlations between gene expression and methylation level were found. However, both gene expression levels themselves correlated positively ($r = 0.488$, $p \leq 0.01$, $n = 28$). Furthermore, a positive correlation was observed for MDA level and *MLH1* methylation ($r = 0.514$, $p \leq 0.05$, $n = 16$).

Caco-2 featured higher genomic instability as seen by low *LINE-1* promoter methylation level in the normoglycemic (62.4%) and hyperglycemic (64.7%) untreated controls (Figure 8). Treatment of 25 μM H_2O_2 under normoglycemic conditions led to a significant increase in *LINE-1* methylation ($p \leq 0.05$), which was reduced by a combined treatment with 50 μM vitamin E ($p \leq 0.05$) (Figure 7(a)). Under hyperglycemic conditions, H_2O_2 tended to reduce *LINE-1* methylation with a concentration of 500 μM causing a clear decrease ($p \leq 0.05$). The combination of 25 μM or 500 μM H_2O_2 with 10 μM vitamin E caused a significant increase in global methylation compared to corresponding H_2O_2 treatment ($p \leq 0.05$).

Incubation with NAC or VAS2870 under hyperglycemic conditions showed a trend to further decrease *LINE-1* methylation. However, when combined with H_2O_2, *LINE-1* methylation was higher compared to respective treatments of inhibitors alone.

4. Discussion

Obesity is one of the leading causes of type 2 diabetes, clinically characterized by chronic hyperglycemia. Both medical conditions often entail numerous comorbidities including cancer, metabolic syndrome, and cardiovascular and neurodegenerative diseases, resulting in an increased mortality risk [49]. Obesity and diabetes have been consistently associated with higher levels of oxidative stress, with hyperglycemia as one primary discussed contributor. Accumulation of ROS is a central mediator of cellular damage and intracellular signaling pathways, playing a pivotal role in the progression of diabetes and development of complications [50, 51].

Plants can synthesize a wide range of nonenzymatic antioxidants such as polyphenols or vitamins to scavenge ROS. Supplementation of exogenous antioxidants constitutes a potential means to counteract ROS-induced oxidative damage [16, 17]. Despite already discussed possible adverse effects, vitamin E exhibits strong antioxidative activities and impacts multiple regulatory pathways with consequences on epigenetic regulation of genes involved in the processes of inflammation and DNA repair [18, 52].

4.1. Effect of Glucose Level. The comparison of Caco-2 cells grown under normoglycemic media or under the frequently used hyperglycemic cell culture media in this study elucidated potential effects of severe diabetic glucose blood level [48] and further revealed possible influence of glucose level on treatments with H_2O_2 and/or vitamin E. A previous study has already remarked on the effects of high glucose on multiple signaling pathways targeting cell growth and maintenance, cell cycle, and cell proliferation in human hepatocellular carcinoma cell lines [53]. In our study, we could observe glucose-induced elevated *DNMT1* expression as well as an increase in lipid peroxidation assessed by MDA level during treatments (Figure 1). In contrast to studies on rats and diabetic patients [54], in our study on Caco-2 cells, increased MDA levels were accompanied by a reduction of ROS. One possible explanation for this finding might be the Warburg effect, an altered metabolism in cancer cells. This mechanism is characterized by an increased demand of glucose by higher glycolysis and pentose-phosphate pathway (PPP) rate, resulting in increased NADPH levels, which in turn drive down ROS levels to prevent oxidative stress-induced cell death [24, 55].

4.2. Treatment Effects on Lipid Peroxidation. We could demonstrate that vitamin E was able to reduce H_2O_2-induced lipid peroxidation dose dependently in both glucose conditions with 10 μM vitamin E being more potent than 50 μM. The difference in effects between vitamin E concentrations could be explained by the prooxidative potential of vitamin E in higher doses as reported previously [13]. When applied alone under hyperglycemic conditions, vitamin E was able to decrease MDA levels. These were still higher than those of the normoglycemic untreated control. In contrast, under

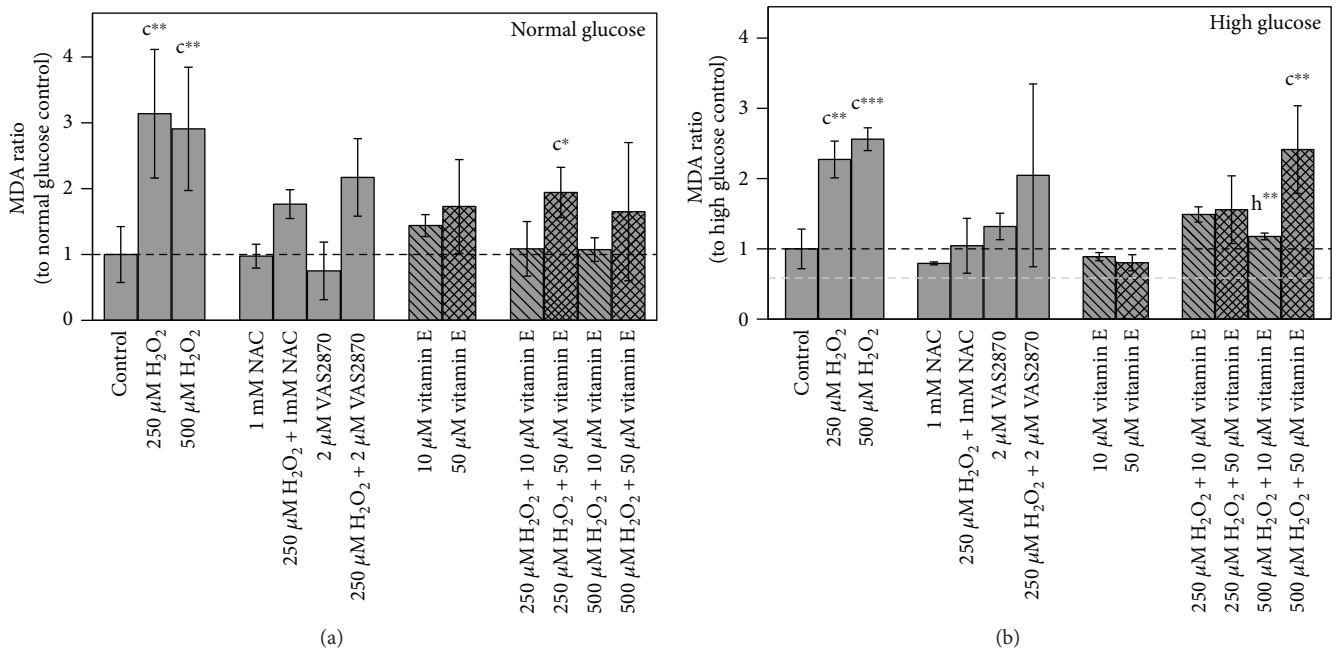

Figure 3: Impact of 48 h treatments on lipid peroxidation in Caco-2 cells grown in (a) normal and (b) high glucose media. Bar charts display the mean ± SD of MDA ratio to respective glucose untreated control. The gray dashed line represents the level of normal glucose untreated control in relation to high glucose untreated control. Differences to the respective controls are statistically analyzed by Student's *t*-test. Significance to untreated control (c) and respective H_2O_2 treatment (h) is marked with $*$ for $p \leq 0.05$, $**$ for $p \leq 0.01$, and $***$ for $p \leq 0.001$. Untreated controls are $n = 5$ due to assay controls.

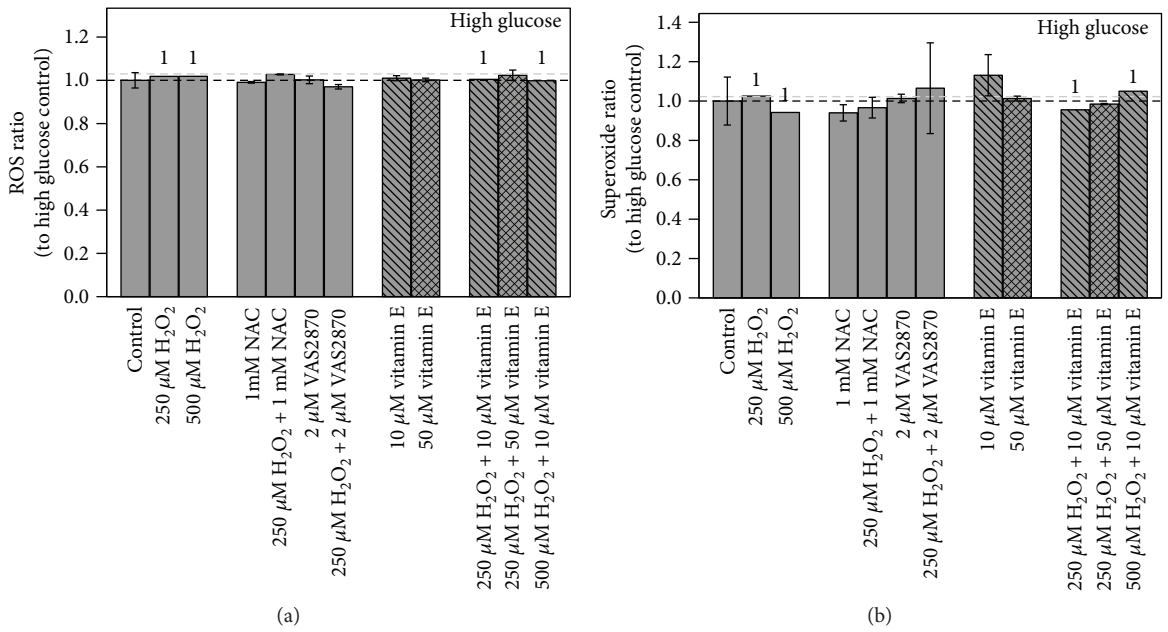

Figure 4: Impact of 48 h treatments on (a) ROS and (b) superoxide levels in high glucose grown Caco-2 cells. Bar charts display the mean ratio ± SD to high glucose untreated controls. The gray dashed line represents the level of normal glucose untreated control in relation to high glucose untreated control. Differences to respective controls are statistically analyzed by Student's *t*-test. 1 indicates lacking replicate, $n = 1$. Untreated controls are $n = 4$ due to assay controls.

normoglycemic conditions, vitamin E slightly increased MDA levels. Assuming that normoglycemic conditions led to low absolute ROS levels, addition of vitamin E might cause a redox misbalance by an excess of antioxidants.

4.3. Treatment Effects on DNA Damage Repair. MDA is not merely a by-product of lipid peroxidation but is also responsible for signaling and forms DNA adducts, such as M1dG, which, if not repaired, becomes mutagenic [23].

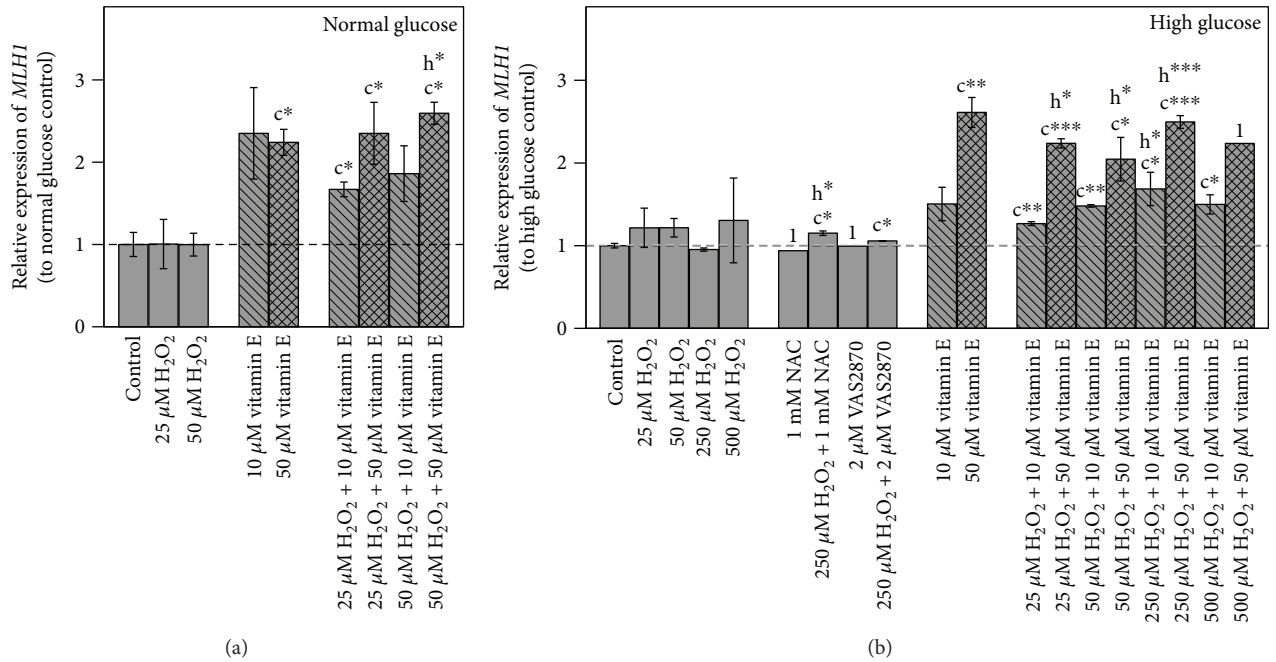

Figure 5: Impact of 48 h treatments on *MLH1* gene expression in (a) normal and (b) high glucose grown Caco-2 cells. Bar charts display the mean ± SD to respective glucose untreated control. The gray dashed line represents the level of normal glucose untreated control in relation to high glucose untreated control. Differences to respective controls are statistically analyzed on $\Delta\Delta C_T$ to normal glucose untreated control by Student's *t*-test. Significance to untreated control (c) and respective H_2O_2 treatment (h) is marked with $*$ for $p \leq 0.05$, $**$ for $p \leq 0.01$, and $***$ for $p \leq 0.001$. 1 indicates lacking replicate, $n = 1$.

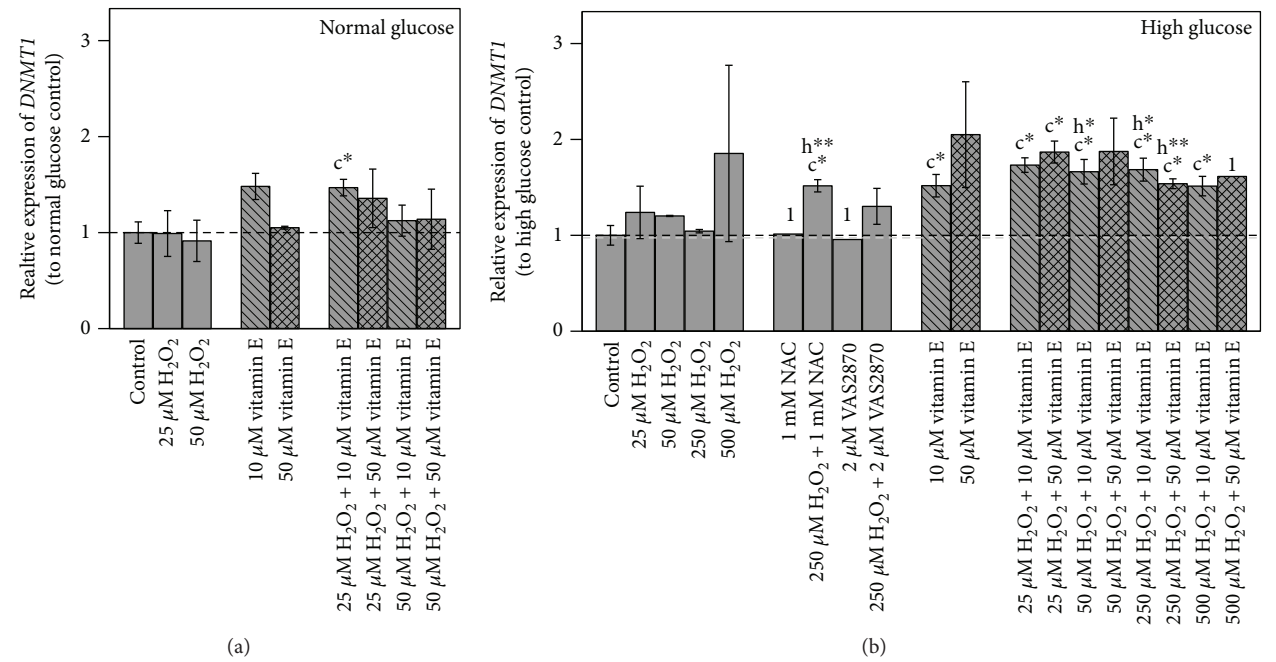

Figure 6: Impact of 48 h treatments on *DNMT1* gene expression in (a) normal and (b) high glucose grown Caco-2 cells. Bar charts display the mean ± SD to respective glucose untreated control. The gray dashed line represents the level of normal glucose untreated control in relation to high glucose untreated control. Differences to respective controls are statistically analyzed on $\Delta\Delta C_T$ to normal glucose untreated control by Student's *t*-test. Significance to untreated control (c) and respective H_2O_2 treatment (h) is marked with $*$ for $p \leq 0.05$ and $**$ for $p \leq 0.01$. 1 indicates lacking replicate, $n = 1$.

Table 2: Shared 48 h treatments by both glucose conditions per parameter.

	MDA	ROS	Superoxide	Expression		Methylation	
				MLH1	*DNMT1*	*MLH1*	*LINE-1*
Control	+	+	+	+	+	+	+
25 μM H_2O_2				+	+	+	+
50 μM H_2O_2				+	+	+	+
250 μM H_2O_2	+	+	+				
500 μM H_2O_2	+	+	+				
1 mM NAC	+	+	+				
250 μM H_2O_2 + 1 mM NAC	+	+	+				
2 μM VAS2870	+	+	+				
250 μM H_2O_2 + 2 μM VAS2870	+	+	+				
10 μM vitamin E	+	+	+	+	+	+	+
50 μM vitamin E	+	+	+	+	+	+	+
25 μM H_2O_2 + 10 μM vitamin E				+	+	+	+
25 μM H_2O_2 + 50 μM vitamin E				+	+	+	+
50 μM H_2O_2 + 10 μM vitamin E				+	+	+	+
50 μM H_2O_2 + 50 μM vitamin E				+	+	+	+
250 μM H_2O_2 + 10 μM vitamin E	+	+	+				
250 μM H_2O_2 + 50 μM vitamin E	+	+	+				
500 μM H_2O_2 + 10 μM vitamin E	+	+	+				
500 μM H_2O_2 + 50 μM vitamin E	+						

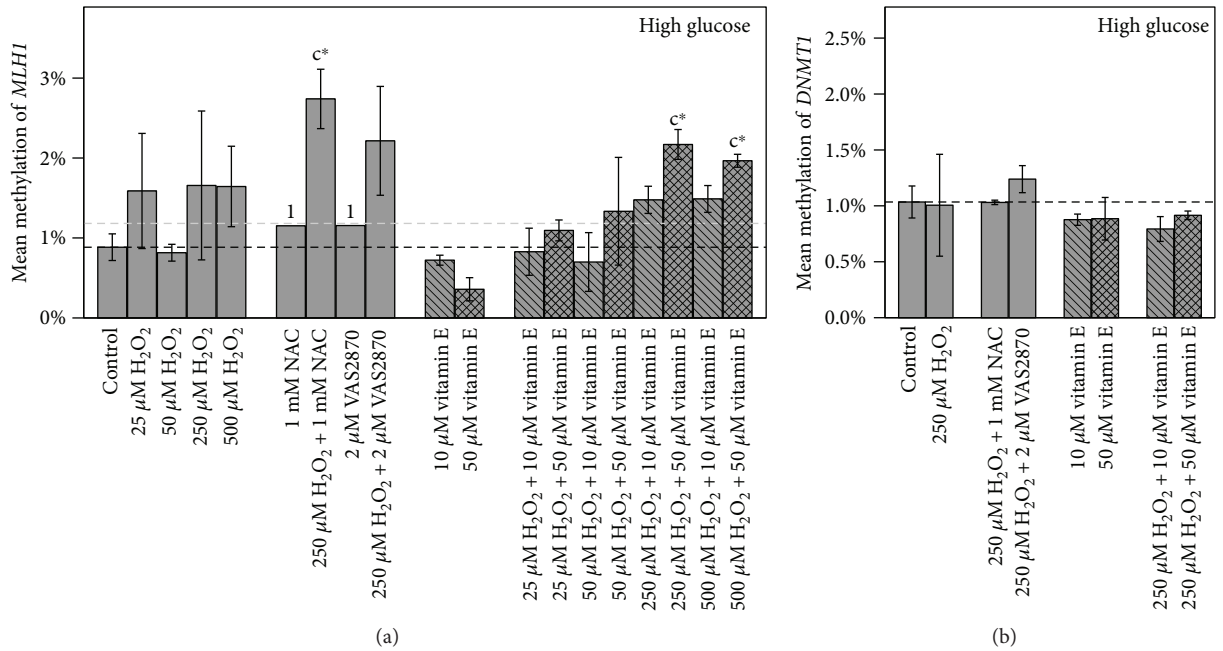

Figure 7: Impact of 48 h treatments with vitamin E on (a) *MLH1* and (b) *DNMT1* mean promoter methylation in high glucose grown Caco-2 cells. Bar charts display the mean ratio ± SD to high glucose untreated control. The gray dashed line represents the level of normal glucose untreated control. Differences to respective controls are statistically analyzed by Student's *t*-test. Significance to untreated control (c) is marked with $*$ for $p \leq 0.05$. 1 indicates lacking replicate, $n = 1$.

Consequently, at higher MDA levels, an increased DNA repair, for example, via an upregulation of the repair gene *MLH1*, is of advantage and might be cancer protective [38, 39].

Our results showed that such an effect was not caused by increased oxidative stress induced by the H_2O_2 treatments, which did not alter *MLH1* expression despite the highest MDA levels. In contrast, vitamin E was rather effective in this

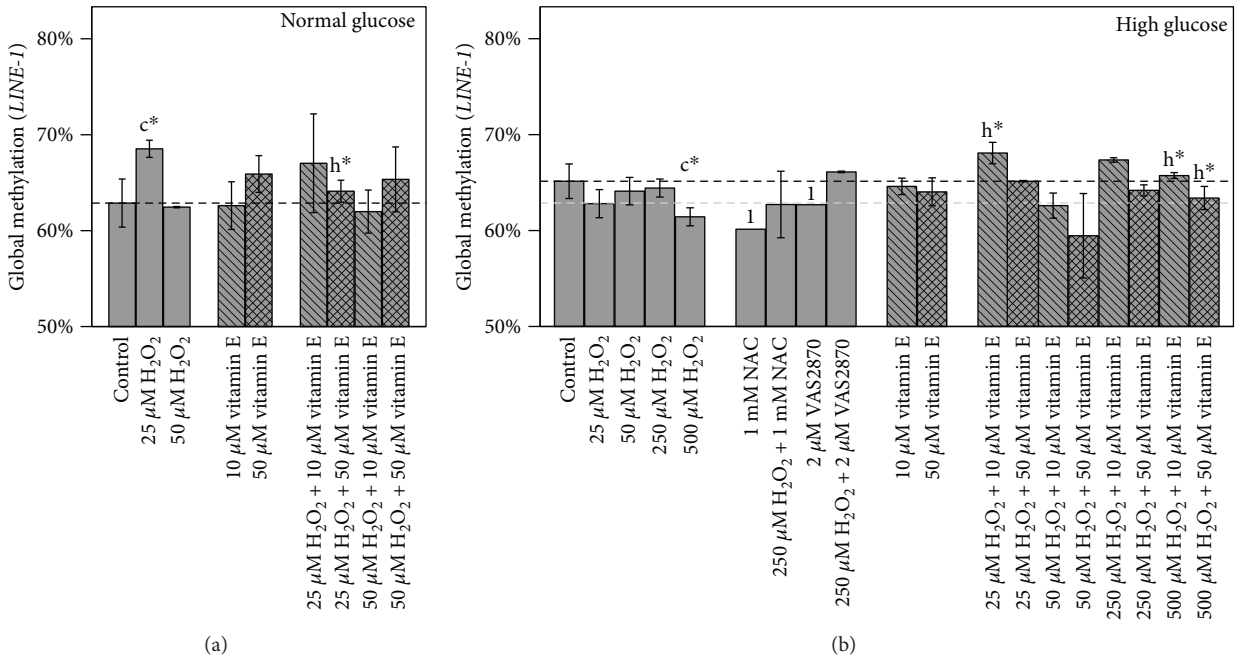

Figure 8: Impact of 48 h treatments on global methylation in (a) normal and (b) high glucose grown Caco-2 cells. Bar charts display the mean ± SD of *LINE-1* methylation levels. The gray dashed line represents the level of normal glucose untreated control in relation to high glucose untreated control. Differences to respective controls are statistically analyzed by Student's *t*-test. Significance to untreated control (c) and respective H_2O_2 treatment (h) is marked with $*$ for $p \leq 0.05$.

regard, showing a significant induction of *MLH1* over all treatments. It would be of interest to assess oxidative DNA damage level in further studies, to elucidate if vitamin E-induced *MLH1* expression was solely concentration dependent or stimulated by increased DNA damage.

MLH1 is reported to show aberrant high methylation patterns in so-called CIMP- (CpG island methylator phenotype-) positive tumors, first identified in colorectal cancer. [35]. CIMP-negative Caco-2 cells [56] displayed very low methylation rates (0.4%–2.7%) over all treatments, suggesting that regulation of *MLH1* expression in non-CIMP cancer types rather lies beyond DNA methylation. Consequently, our results showed no correlation between gene expression and methylation level of *MLH1* as previously also reported [57]. Moreover, *MLH1* promoter methylation was not affected by increased *DNMT1* expression. However, a positive correlation was observed for MDA level and *MLH1* methylation. This could indicate that high amounts of damage and induced ROS might provoke development towards CIMP.

4.4. Treatment Effects on DNMT1. We could demonstrate that H_2O_2 treatment combined with inhibitors as well as vitamin E led to an elevated *DNMT1* expression, though exclusive treatment with H_2O_2 scarcely affected *DNMT1* expression. These effects were more pronounced under hyperglycemic conditions, suggesting a significant glucose-induced impact.

Our results further showed a positive correlation between *DNMT1* and *MLH1* expression. Their proteins are reported to interact with each other [40, 41] and these genes to be controlled in a cell cycle-dependent manner with a gene expression restricted to S-phase for *DNMT1* [58] and an upregulated one for *MLH1* [59]. Furthermore, vitamin E compounds are known to be potent cell cycle modulators [15, 60].

These studies support our findings that the modulation of *DNMT1* and *MLH1* in Caco-2 by vitamin E might be based on a S-phase block. Cell cycle arrest with increased expression of DNA repair genes following DNA damage responses is thereby of particular advantage [61].

Consistently, the additional incubation with high H_2O_2 concentrations that enhanced *MLH1* expression more and *DNMT1* expression less than did moderate concentrations could be observed. ROS, triggering proliferation by the redox regulated cell cycle [24, 62], might promote S-phase transit despite the increased damage. Further experiments could clarify our assumptions on the cell cycle arrest in S-phase as causing a cell cycle arrest in the mutant p53 Caco-2 cells [63] by an independent mechanism provides a potential treatment to combat p53-defective cancer types.

4.5. Treatment Effects on LINE-1. DNA methylation of repetitive elements such as *LINE-1* can serve as a surrogate marker for global genomic DNA methylation, as it occurs with a frequency of at least 17% [29] in the human genome. Global DNA hypomethylation is reported to play a crucial role in genomic instability and, consequently, carcinogenic processes [31, 32]. However, our results could not show any correlation between *LINE-1* methylation and *MLH1* or *DNMT1* expression, respectively. Previously, it was demonstrated in bladder cancer cells that *LINE-1* methylation was significantly decreased after treatment with H_2O_2 and reestablished after pretreatment with tocopherol acetate [64]. Similar

effects could also be observed in our study under hyperglycemic conditions, where H_2O_2 tended to reduce *LINE-1* methylation provoking chromosomal instability. Though exclusive treatments with vitamin E could not reveal significant alterations, the combination of 25 μM or 500 μM H_2O_2 with 10 μM vitamin E resulted in a significant increase in global methylation as compared to H_2O_2 treatment control. In line with our results on reduction of H_2O_2-induced MDA, these findings underline the exciting beneficial effects of the lower vitamin E concentration in counteracting oxidative stress, while acting cancer protective. However, whether *LINE-1* hypomethylation is a cause or effect of oxidative stress is surely a worthwhile focus for future research. Additional studies with other immortalized but also primary cell lines treated with further natural substances bearing antioxidative potential such as (−)-epigallocatechin gallate (Pointner et al. 2017, submitted for publication) are of great interest to assess cell line and substance-specific characteristics.

Taken together, we could demonstrate that vitamin E reduced H_2O_2-induced lipid peroxidation in a dose-dependent manner as well as caused lower increase of the DNA repair gene *MLH1*. Furthermore, *DNMT1* expression and global methylation were positively affected, all of them underlining the exciting beneficial effects of the lower concentration of vitamin E in counteracting oxidative stress. Moreover, our study revealed an influence by glucose concentration on MDA and ROS level as well as *DNMT1* expression, which is suggested to be linked to metabolic pathways. Thereby neither NAC nor the NOX inhibitor was able to alter all investigated parameters in the same way as vitamin E did. However, the assumed ROS induction and scavenging effect through one-time treatment was very likely to act in the short term. Furthermore, the highly reactive exogenous redox active compounds were neutralized after 48 h.

5. Conclusions

Antioxidative processes clearly affect main epigenetic enzymes regulation and presumably chromatin modification. Different impacts of glucose concentration indicate that physiological glucose levels need to be respected when analyzing interactions between antioxidative mechanisms and epigenetics. Vitamin E, especially in low concentrations, showed beneficial effects *in vitro* concerning oxidative stress as well as epigenetic alterations, revealing its cancer protective potential. Supplementation of exogenous antioxidants like vitamin E constitutes an effective means to counteract hyperglycemia-induced oxidative damage. Therefore, it bears a great potential for treatment and might even be used as possible approach in prevention of diseases such as obesity and diabetes.

Abbreviations

BER: Base excision repair
CIMP: CpG island methylation phenotype
CpG: Cytosine-guanine sequence
DNMT: DNA methyltransferase
LINE-1: Long interspersed nuclear element-1
M1dG: MDA deoxyguanosine adduct
MDA: Malondialdehyde
MLH1: MutL homolog 1
MMR: Mismatch repair
MS-HRM: Methylation-sensitive high-resolution melting
NAC: *N*-Acetylcysteine
NAD(P)H: Reduced form of nicotinamide adenine dinucleotide (phosphate)
NER: Nucleotide excision repair
NOX: NADPH oxidases
ROS: Reactive oxygen species.

Conflicts of Interest

The authors declare that they have no conflicts of interest.

Acknowledgments

The work was funded by the Austrian Science Fund (FWF; AP2658721).

References

[1] WHO, *World Health Statistics 2016: Monitoring Health for the SDGs*, World Health Organization, Geneva, Switzerland, 2016.

[2] N. P. Gullett, A. R. M. Ruhul Amin, S. Bayraktar et al., "Cancer prevention with natural compounds," *Seminars in Oncology*, vol. 37, no. 3, pp. 258–281, 2010.

[3] E. Fernholz, "On the constitution of α-tocopherol," *Journal of the American Chemical Society*, vol. 60, no. 3, pp. 700–705, 1938.

[4] J. Bunyan, D. McHale, J. Green, and S. Marcinkiewicz, "Biological potenices of ε- and ζ1-tocopherol and 5-methyltocol," *The British Journal of Nutrition*, vol. 15, no. 2, pp. 253–257, 1961.

[5] M. Meydani, "Vitamin E," *The Lancet*, vol. 345, no. 8943, pp. 170–175, 1995.

[6] E. Mocchegiani, L. Costarelli, R. Giacconi et al., "Vitamin E-gene interactions in aging and inflammatory age-related diseases: implications for treatment. A systematic review," *Ageing Research Reviews*, vol. 14, pp. 81–101, 2014.

[7] P. Kong, Q. Cai, Q. Geng et al., "Vitamin intake reduce the risk of gastric cancer: meta-analysis and systematic review of randomized and observational studies," *PLoS One*, vol. 9, no. 12, article e116060, 2014.

[8] S. Das Gupta and N. Suh, "Tocopherols in cancer: an update," *Molecular Nutrition & Food Research*, vol. 60, no. 6, pp. 1354–1363, 2016.

[9] H. Y. Peh, W. S. D. Tan, W. Liao, and W. S. F. Wong, "Vitamin E therapy beyond cancer: tocopherol versus tocotrienol," *Pharmacology & Therapeutics*, vol. 162, pp. 152–169, 2016.

[10] Z. A. Daud, B. Tubie, M. Sheyman et al., "Vitamin E tocotrienol supplementation improves lipid profiles in chronic hemodialysis patients," *Vascular Health and Risk Management*, vol. 9, pp. 747–761, 2013.

[11] The alpha-Tocopherol Beta Carotene Cancer Prevention Study Group, "The effect of vitamin E and beta carotene on the incidence of lung cancer and other cancers in male smokers," *The New England Journal of Medicine*, vol. 330, no. 15, pp. 1029–1035, 1994.

[12] S. M. Lippman, E. A. Klein, P. J. Goodman et al., "Effect of selenium and vitamin E on risk of prostate cancer and other cancers," *JAMA*, vol. 301, no. 1, pp. 39–51, 2009.

[13] E. R. Miller III, R. Pastor-Barriuso, D. Dalal, R. A. Riemersma, L. J. Appel, and E. Guallar, "Meta-analysis: high-dosage vitamin E supplementation may increase all-cause mortality," *Annals of Internal Medicine*, vol. 142, no. 1, pp. 37–46, 2005.

[14] J. Emami, M. Rezazadeh, M. Rostami et al., "Co-delivery of paclitaxel and α-tocopherol succinate by novel chitosan-based polymeric micelles for improving micellar stability and efficacious combination therapy," *Drug Development and Industrial Pharmacy*, vol. 41, no. 7, pp. 1137–1147, 2015.

[15] T. Eitsuka, N. Tatewaki, H. Nishida, K. Nakagawa, and T. Miyazawa, "Synergistic anticancer effect of tocotrienol combined with chemotherapeutic agents or dietary components: a review," *International Journal of Molecular Sciences*, vol. 17, no. 12, article e1605, 2016.

[16] E. Serbinova, V. Kagan, D. Han, and L. Packer, "Free radical recycling and intramembrane mobility in the antioxidant properties of alpha-tocopherol and alpha-tocotrienol," *Free Radical Biology & Medicine*, vol. 10, no. 5, pp. 263–275, 1991.

[17] T. Rahman, I. Hosen, M. M. T. Islam, and H. U. Shekhar, "Oxidative stress and human health," *Advances in Bioscience and Biotechnology*, vol. 3, no. 7, pp. 997–1019, 2012.

[18] M. Sthijns, A. Weseler, A. Bast, and G. Haenen, "Time in redox adaptation processes: from evolution to hormesis," *International Journal of Molecular Sciences*, vol. 17, no. 12, article e1649, 2016.

[19] S. K. Powers, L. L. Ji, A. N. Kavazis, and M. J. Jackson, "Reactive oxygen species: impact on skeletal muscle," *Comprehensive Physiology*, vol. 1, pp. 941–969, 2011.

[20] J. Wang, D. Lin, H. Peng, Y. Huang, J. Huang, and J. Gu, "Cancer-derived immunoglobulin G promotes tumor cell growth and proliferation through inducing production of reactive oxygen species," *Cell Death & Disease*, vol. 4, no. 12, article e945, 2013.

[21] M. J. Davies, "Protein oxidation and peroxidation," *The Biochemical Journal*, vol. 473, no. 7, pp. 805–825, 2016.

[22] H. Esterbauer, K. H. Cheeseman, M. U. Dianzani, G. Poli, and T. F. Slater, "Separation and characterization of the aldehydic products of lipid peroxidation stimulated by ADP-Fe^{2+} in rat liver microsomes," *The Biochemical Journal*, vol. 208, no. 1, pp. 129–140, 1982.

[23] A. Ayala, M. F. Muñoz, and S. Argüelles, "Lipid peroxidation: production, metabolism, and signaling mechanisms of malondialdehyde and 4-hydroxy-2-nonenal," *Oxidative Medicine and Cellular Longevity*, vol. 2014, Article ID 360438, 31 pages, 2014.

[24] E. Panieri and M. M. Santoro, "ROS homeostasis and metabolism: a dangerous liason in cancer cells," *Cell Death & Disease*, vol. 7, no. 6, article e2253, 2016.

[25] P. Anand, A. B. Kunnumakara, C. Sundaram et al., "Cancer is a preventable disease that requires major lifestyle changes," *Pharmaceutical Research*, vol. 25, no. 9, pp. 2097–2116, 2008.

[26] S. B. Baylin and P. A. Jones, "A decade of exploring the cancer epigenome—biological and translational implications," *Nature Reviews Cancer*, vol. 11, no. 10, pp. 726–734, 2011.

[27] M. Daniel and T. O. Tollefsbol, "Epigenetic linkage of aging, cancer and nutrition," *The Journal of Experimental Biology*, vol. 218, no. 1, pp. 59–70, 2015.

[28] E. Li and Y. Zhang, "DNA methylation in mammals," *Cold Spring Harbor Perspectives in Biology*, vol. 6, no. 5, article a019133, 2014.

[29] E. S. Lander, L. M. Linton, B. Birren et al., "Initial sequencing and analysis of the human genome," *Nature*, vol. 409, no. 6822, pp. 860–921, 2001.

[30] A. S. Yang, M. R. Estécio, K. Doshi, Y. Kondo, E. H. Tajara, and J. P. Issa, "A simple method for estimating global DNA methylation using bisulfite PCR of repetitive DNA elements," *Nucleic Acids Research*, vol. 32, no. 3, article e38, 2004.

[31] H.-H. Cheung, T.-L. Lee, O. M. Rennert, and W.-Y. Chan, "DNA methylation of cancer genome," *Birth Defects Research Part C: Embryo Today: Reviews*, vol. 87, no. 4, pp. 335–350, 2009.

[32] H. H. Kazazian Jr. and J. L. Goodier, "LINE drive. Retrotransposition and genome instability," *Cell*, vol. 110, no. 3, pp. 277–280, 2002.

[33] P. M. Vertino, R. W. Yen, J. Gao, and S. B. Baylin, "De novo methylation of CpG island sequences in human fibroblasts overexpressing DNA (cytosine-5-)-methyltransferase," *Molecular and Cellular Biology*, vol. 16, no. 8, pp. 4555–4565, 1996.

[34] M. Fatemi, A. Hermann, H. Gowher, and A. Jeltsch, "Dnmt3a and Dnmt1 functionally cooperate during de novo methylation of DNA," *European Journal of Biochemistry*, vol. 269, no. 20, pp. 4981–4984, 2002.

[35] J.-P. Issa, "CpG island methylator phenotype in cancer," *Nature Reviews Cancer*, vol. 4, no. 12, pp. 988–993, 2004.

[36] G. F. Crouse, "Non-canonical actions of mismatch repair," *DNA Repair*, vol. 38, pp. 102–109, 2016.

[37] M. T. Russo, G. De Luca, P. Degan, and M. Bignami, "Different DNA repair strategies to combat the threat from 8-oxoguanine," *Mutation Research/Fundamental and Molecular Mechanisms of Mutagenesis*, vol. 614, no. 1-2, pp. 69–76, 2007.

[38] K. A. Johnson, M. L. Mierzwa, S. P. Fink, and L. J. Marnett, "MutS recognition of exocyclic DNA adducts that are endogenous products of lipid oxidation," *The Journal of Biological Chemistry*, vol. 274, no. 38, pp. 27112–27118, 1999.

[39] L. A. VanderVeen, M. F. Hashim, Y. Shyr, and L. J. Marnett, "Induction of frameshift and base pair substitution mutations by the major DNA adduct of the endogenous carcinogen malondialdehyde," *Proceedings of the National Academy of Sciences of the United States of America*, vol. 100, no. 24, pp. 14247–14252, 2003.

[40] J. E. P. Loughery, P. D. Dunne, K. M. O'Neill, R. R. Meehan, J. R. McDaid, and C. P. Walsh, "DNMT1 deficiency triggers mismatch repair defects in human cells through depletion of repair protein levels in a process involving the DNA damage response," *Human Molecular Genetics*, vol. 20, no. 16, pp. 3241–3255, 2011.

[41] N. Ding, E. M. Bonham, B. E. Hannon, T. R. Amick, S. B. Baylin, and H. M. O'Hagan, "Mismatch repair proteins recruit DNA methyltransferase 1 to sites of oxidative DNA damage," *Journal of Molecular Cell Biology*, vol. 8, no. 3, pp. 244–254, 2016.

[42] E. B. Kurutas, "The importance of antioxidants which play the role in cellular response against oxidative/nitrosative stress: current state," *Nutrition Journal*, vol. 15, no. 1, p. 71, 2016.

[43] G. R. Drummond, S. Selemidis, K. K. Griendling, and C. G. Sobey, "Combating oxidative stress in vascular disease: NADPH oxidases as therapeutic targets," *Nature Reviews Drug Discovery*, vol. 10, no. 6, pp. 453–471, 2011.

[44] K. Koschutnig, S. Heikkinen, S. Kemmo, A.-M. Lampi, V. Piironen, and K.-H. Wagner, "Cytotoxic and apoptotic effects of single and mixed oxides of β-sitosterol on HepG2-cells," *Toxicology In Vitro*, vol. 23, no. 5, pp. 755–762, 2009.

[45] K.-H. Wagner, A. Jürß, B. Zarembach, and I. Elmadfa, "Impact of antiseptics on radical metabolism, antioxidant status and genotoxic stress in blood cells: povidone-iodine versus octenidine dihydrochloride," *Toxicology in Vitro*, vol. 18, no. 4, pp. 411–418, 2004.

[46] M. Spitzwieser, E. Holzweber, G. Pfeiler, S. Hacker, and M. Cichna-Markl, "Applicability of *HIN-1*, *MGMT* and *RASSF1A* promoter methylation as biomarkers for detecting field cancerization in breast cancer," *Breast Cancer Research*, vol. 17, no. 1, p. 125, 2015.

[47] F. Migheli, A. Stoccoro, F. Coppedè et al., "Comparison study of MS-HRM and pyrosequencing techniques for quantification of *APC* and *CDKN2A* gene methylation," *PLoS One*, vol. 8, no. 1, article e52501, 2013.

[48] O. V. Leontieva, Z. N. Demidenko, and M. V. Blagosklonny, "Rapamycin reverses insulin resistance (IR) in high-glucose medium without causing IR in normoglycemic medium," *Cell Death & Disease*, vol. 5, no. 5, article e1214, 2014.

[49] WHO, "Obesity: Preventing and Managing the Global Epidemic. Report of a WHO Consultation," WHO Technical Report Series 894, Geneva, Switzerland, 2000.

[50] S. Furukawa, T. Fujita, M. Shimabukuro et al., "Increased oxidative stress in obesity and its impact on metabolic syndrome," *The Journal of Clinical Investigation*, vol. 114, no. 12, pp. 1752–1761, 2004.

[51] P. Newsholme, E. P. Haber, S. M. Hirabara et al., "Diabetes associated cell stress and dysfunction: role of mitochondrial and non-mitochondrial ROS production and activity," *The Journal of Physiology*, vol. 583, no. 1, pp. 9–24, 2007.

[52] M. Remely, F. Ferk, S. Sterneder et al., "Vitamin E modifies high-fat diet-induced increase of DNA strand breaks, and changes in expression and DNA methylation of *Dnmt1* and *MLH1* in C57BL/6J male mice," *Nutrients*, vol. 9, no. 12, p. 607, 2017.

[53] E. Berger, N. Vega, M. Weiss-Gayet, and A. Géloën, "Gene network analysis of glucose linked signaling pathways and their role in human hepatocellular carcinoma cell growth and survival in HuH7 and HepG2 cell lines," *BioMed Research International*, vol. 2015, Article ID 821761, 19 pages, 2015.

[54] S. Yara, J.-C. Lavoie, and E. Levy, "Oxidative stress and DNA methylation regulation in the metabolic syndrome," *Epigenomics*, vol. 7, no. 2, pp. 283–300, 2015.

[55] N. Aykin-Burns, I. M. Ahmad, Y. Zhu, L. W. Oberley, and D. R. Spitz, "Increased levels of superoxide and H_2O_2 mediate the differential susceptibility of cancer cells versus normal cells to glucose deprivation," *The Biochemical Journal*, vol. 418, no. 1, pp. 29–37, 2009.

[56] D. Ahmed, P. W. Eide, I. A. Eilertsen et al., "Epigenetic and genetic features of 24 colon cancer cell lines," *Oncogene*, vol. 2, no. 9, article e71, 2013.

[57] O. J. Switzeny, E. Müllner, K.-H. Wagner, H. Brath, E. Aumüller, and A. G. Haslberger, "Vitamin and antioxidant rich diet increases *MLH1* promoter DNA methylation in DMT2 subjects," *Clinical Epigenetics*, vol. 4, no. 1, p. 19, 2012.

[58] S. Kishikawa, T. Murata, H. Ugai, T. Yamazaki, and K. K. Yokoyama, "Control elements of *Dnmt1* gene are regulated in cell-cycle dependent manner," *Nucleic Acids Symposium Series*, vol. 3, no. 1, pp. 307-308, 2003.

[59] R. Mjelle, S. A. Hegre, P. A. Aas et al., "Cell cycle regulation of human DNA repair and chromatin remodeling genes," *DNA Repair*, vol. 30, pp. 53–67, 2015.

[60] A. K. Smolarek, J. Y. So, B. Burgess et al., "Dietary administration of δ- and γ-tocopherol inhibits tumorigenesis in the animal model of estrogen receptor–positive, but not HER-2 breast cancer," *Cancer Prevention Research*, vol. 5, no. 11, pp. 1310–1320, 2012.

[61] J. H. Houtgraaf, J. Versmissen, and W. J. van der Giessen, "A concise review of DNA damage checkpoints and repair in mammalian cells," *Cardiovascular Revascularization Medicine*, vol. 7, no. 3, pp. 165–172, 2006.

[62] E. H. Sarsour, A. L. Kalen, and P. C. Goswami, "Manganese superoxide dismutase regulates a redox cycle within the cell cycle," *Antioxidants & Redox Signaling*, vol. 20, no. 10, pp. 1618–1627, 2014.

[63] S. Djelloul, M. E. Forgue-Lafitte, B. Hermelin et al., "Enterocyte differentiation is compatible with SV40 large T expression and loss of p53 function in human colonic Caco-2 cells. Status of the pRb1 and pRb2 tumor suppressor gene products," *FEBS Letters*, vol. 406, no. 3, pp. 234–242, 1997.

[64] W. Wongpaiboonwattana, P. Tosukhowong, T. Dissayabutra, A. Mutirangura, and C. Boonla, "Oxidative stress induces hypomethylation of LINE-1 and hypermethylation of the RUNX3 promoter in a bladder cancer cell line," *Asian Pacific Journal of Cancer Prevention*, vol. 14, no. 6, pp. 3773–3778, 2013.

[65] T. Arányi, A. Váradi, I. Simon, and G. E. Tusnády, "The BiSearch web server," *BMC Bioinformatics*, vol. 7, no. 1, p. 431, 2006.

[66] A. Yates, W. Akanni, M. R. Amode et al., "Ensembl 2016," *Nucleic Acids Research*, vol. 44, no. D1, pp. D710–D716, 2016.

[67] X. Li, Y. Wang, Z. Zhang, X. Yao, J. Ge, and Y. Zhao, "Correlation of MLH1 and MGMT methylation levels between peripheral blood leukocytes and colorectal tissue DNA samples in colorectal cancer patients," *Oncology Letters*, vol. 6, no. 5, pp. 1370–1376, 2013.

[68] P. Tannorella, A. Stoccoro, G. Tognoni et al., "Methylation analysis of multiple genes in blood DNA of Alzheimer's disease and healthy individuals," *Neuroscience Letters*, vol. 600, pp. 143–147, 2015.

[69] E. M. Wolff, H.-M. Byun, H. F. Han et al., "Hypomethylation of a LINE-1 promoter activates an alternate transcript of the MET oncogene in bladders with cancer," *PLoS Genetics*, vol. 6, no. 4, article e1000917, 2010.

Hindawi
Oxidative Medicine and Cellular Longevity
Volume 2018, Article ID 9156285, 11 pages
https://doi.org/10.1155/2018/9156285

Review Article

Critical Role of Zinc as Either an Antioxidant or a Prooxidant in Cellular Systems

Sung Ryul Lee

Department of Convergence Biomedical Science, Cardiovascular and Metabolic Disease Center, College of Medicine, Inje University, Busan, Republic of Korea

Correspondence should be addressed to Sung Ryul Lee; lsr1113@inje.ac.kr

Received 26 October 2017; Revised 9 January 2018; Accepted 16 January 2018; Published 20 March 2018

Academic Editor: Glenda Gobe

Zinc is recognized as an essential trace metal required for human health; its deficiency is strongly associated with neuronal and immune system defects. Although zinc is a redox-inert metal, it functions as an antioxidant through the catalytic action of copper/zinc-superoxide dismutase, stabilization of membrane structure, protection of the protein sulfhydryl groups, and upregulation of the expression of metallothionein, which possesses a metal-binding capacity and also exhibits antioxidant functions. In addition, zinc suppresses anti-inflammatory responses that would otherwise augment oxidative stress. The actions of zinc are not straightforward owing to its numerous roles in biological systems. It has been shown that zinc deficiency and zinc excess cause cellular oxidative stress. To gain insights into the dual action of zinc, as either an antioxidant or a prooxidant, and the conditions under which each role is performed, the oxidative stresses that occur in zinc deficiency and zinc overload in conjunction with the intracellular regulation of free zinc are summarized. Additionally, the regulatory role of zinc in mitochondrial homeostasis and its impact on oxidative stress are briefly addressed.

1. Introduction

Oxidative stress can be defined as an excessive production of reactive oxygen/nitrogen species (ROS/RNS), known as prooxidants, and/or a deficiency of enzymatic and nonenzymatic antioxidants, which are involved in the detoxification of ROS/RNS [1]. The occurrence of oxidative species is normal in a cell, but excess production occurs when the discharge of oxidants becomes too large for the cellular antioxidant defense mechanisms to detoxify or when the functioning of the antioxidant defense mechanisms is perturbed. Excessive oxidants cause alterations to the normal structure and function of DNA, lipids, and proteins, which trigger mutagenesis and oxidative damage in the cell. Therefore, excessive oxidative stress can generally be considered both a cause and an effect of numerous pathological conditions, such as cancer, neurodegeneration, cardiovascular diseases, diabetes, and kidney diseases, as discussed elsewhere [2–4]. It has been suggested that increased oxidative stress is involved in aging [5]. To combat excessive oxidative stress, various natural or synthetic antioxidants have been evaluated to prevent or attenuate the pathological transition [2, 6–8].

In living systems, various metals are involved in a wide variety of biological processes through their action as catalytic and structural components, as discussed elsewhere [7, 9]. Redox-active metals (e.g., copper and iron) participate in cycling reactions through the transfer of electrons between metals and as substrates to perform redox homeostasis in cellular biochemical reactions. Even these essential metals can cause uncontrolled oxidative stress when their regulation is disturbed [6, 10]. Toxic metals, such as arsenic and cadmium, which have no apparent biological function, can interact strongly with proteins and DNA [6, 7] and cause site-specific damage that results in the conformational change of the proteins and DNA and the excessive production of metal-mediated ROS and RNS [11]. Given the abundant anthropogenic influences in the environment, people may be exposed to these metals via the inhalation of contaminated air, the dietary intake of plant-derived food, and drinking water [12]. Industrial zinc use has increased over time; currently, it is used in galvanization, zinc-based

alloys, brass, and bronze [13]. Zinc is also used for dental, medical, and household purposes [13]. Previously, the importance of zinc in health and disease has been largely studied from the perspective of severe deficiency with obvious clinical signs [14, 15]. In contrast with iron, copper, mercury, cadmium, and other metals that accumulate in tissues and produce toxic effects [16], there are fewer disorders associated with the excessive accumulation of zinc [14]. In the long-term high-dose supplementation of zinc, many of the toxic effects associated with zinc are a result of copper deficiency [17, 18]. Zinc possesses bactericidal properties at low concentrations. This is known as the oligodynamic effect and was identified by Karl Wilhelm von Nägeli through the mechanisms of oxidation-reduction reactions and the intracellular accumulation of ions in bacteria [19]. Moreover, clinical evidence has emphasized the importance of zinc in autodebridement, anti-infective action, and the promotion of epithelialization [20]. It has also been proven that topical administration of zinc in ointments or in bandages was better for disinfection and stimulation of wound healing than oral administration [20].

Zinc belongs to the divalent metals in group 12 of the periodic table and is normally colorless. Unlike other bioactive metals such as iron (ferric state (Fe^{3+}) or ferrous state (Fe^{2+})) and copper (cuprous state (Cu^{+}) and cupric state (Cu^{2+})), zinc is stable as a divalent cation (Zn^{2+}) and does not directly undergo redox reactions owing to its filled *d* shell [21]. Compounds containing Zn^{1+} are rare and require bulky ligands to stabilize the low oxidation state. Zn^{2+} cannot donate or receive a free electron and it is therefore redox inert; it is not considered an antioxidant in the traditional sense. Instead, Zn^{2+} can function as an efficient Lewis acid and is often integrated with four ligands into a tetrahedral array with side chains of amino acids such as aspartic acid, glutamic acid, cysteine, and histidine [21, 22]. As indicated by reviews of chronological research events in zinc biology [23, 24], the reported biological roles of zinc in health and disease have rapidly increased. Adults have approximately 1.4–2.3 g of zinc in their body and its content varies significantly between tissues. In this review, Zn^{2+} refers to the reactive pool of zinc, but "zinc" refers to the total zinc content, which encompasses all forms of zinc including the protein-bound pool (54%), the exchangeable reactive pool (44.7%), and Zn^{2+} [25]. Numerous findings have linked the induction of the enzymes involved in antioxidant defenses and with antioxidant potentials to the action of free or labile forms of Zn^{2+} [22, 26]. However, it is not easily discriminable whether the identified actions are derived from zinc or Zn^{2+}. The antioxidant function of zinc was suggested previously [26] and the anti-inflammatory effects of zinc were thereafter rapidly discovered [27, 28]. Paradoxically, the oxidative stress mediated by zinc deficiency and Zn^{2+} overload has been suggested to be closely linked to neurodegeneration in Alzheimer's disease [29] and neuronal cultures [30, 31]. Neuronal death that results from excess Zn^{2+} did not occur because of exogenous zinc, but because of intracellular Zn^{2+} overload, which was mobilized and redistributed in the brain [32].

The role of zinc as either an antioxidant (Figure 1) or prooxidant (Figure 2) is not straightforward owing to the diversity and complexity of Zn^{2+} activity. The purpose of this review is to provide an insight into the dual action of zinc, which acts as either an antioxidant or a prooxidant, and the circumstances in which each function is active. First, we have briefly addressed the biochemical and nutritional aspects of zinc. Second, the underlying mechanisms of zinc homeostasis are outlined and the redox involvement of zinc is addressed in conjunction with metallothionein (MT), which is a low-molecular weight cysteine-rich protein with Zn^{2+}-binding capacity [33–35]. Third, the oxidative stresses that occur in zinc deficiency and zinc overload are summarized. Fourth, the regulatory role of zinc in mitochondrial homeostasis and its impact on the oxidative stress have been discussed. Finally, we discussed the role of zinc as either an antioxidant or a prooxidant in conjunction with the intracellular regulation of free zinc.

2. Biochemical and Nutritional Properties of Zinc

Zn^{2+} is an essential heavy metal required by approximately 2800 macromolecules and more than 300 enzymes to build their proper structure and develop their function [36, 37]. In prokaryotes, approximately 83% of zinc proteins conduct enzymatic catalysis [38]. Eukaryotes use Zn^{2+} in diverse biological functions: zinc-related proteins in catalytic reactions (47%), DNA transcription (44%), protein transport systems (5%), and signaling pathways (3%) [38]. Zn^{2+} is also involved in stabilization of the membrane structure [39–41], and its deficiency impairs the plasma membrane functions required for platelet aggregation, osmotic protection, and various other processes [41]. Therefore, the widespread deficiency of Zn^{2+} is likely to result in major health consequences such as severe defects in growth, development, and proper functioning of the reproductive, immune, and neurosensory systems and in behavior, as discussed elsewhere [15, 24, 42]. According to the TOXNET database of the US National Library of Medicine, the oral 50% lethal dose for zinc is approximately 3 g/kg body weight, which is over 10-fold higher than that for cadmium and 50-fold higher than that for mercury [43]. There are three major routes of entry by which zinc may reach a toxic level in the human body: through the inhalation of zinc oxide as dust or fume, through the skin, or by ingestion. Several studies have demonstrated that exposure to high concentrations of zinc (up to several millimolar) or industrial exposure did not produce severe health concerns [7, 44]. Excessive oral zinc intake (over 150 mg/day) for long periods may induce copper (Cu) deficiency-like symptoms owing to the resulting inhibition of Cu uptake [45].

Zn^{2+} is hydrophilic and cannot permeate across the cytoplasmic plasma membrane and the membranes of intracellular compartments. Cellular and whole-body Zn^{2+} levels are controlled by MTs, Zn^{2+} transporters (solute carrier family 30A, ZnTs), and Zn^{2+} importers (solute carrier family 39A, ZIPs) [46, 47]. The ZnT family facilitates the mobilization of Zn^{2+} in the opposite direction of ZIP (as discussed elsewhere [48]). In addition to the ZIP family,

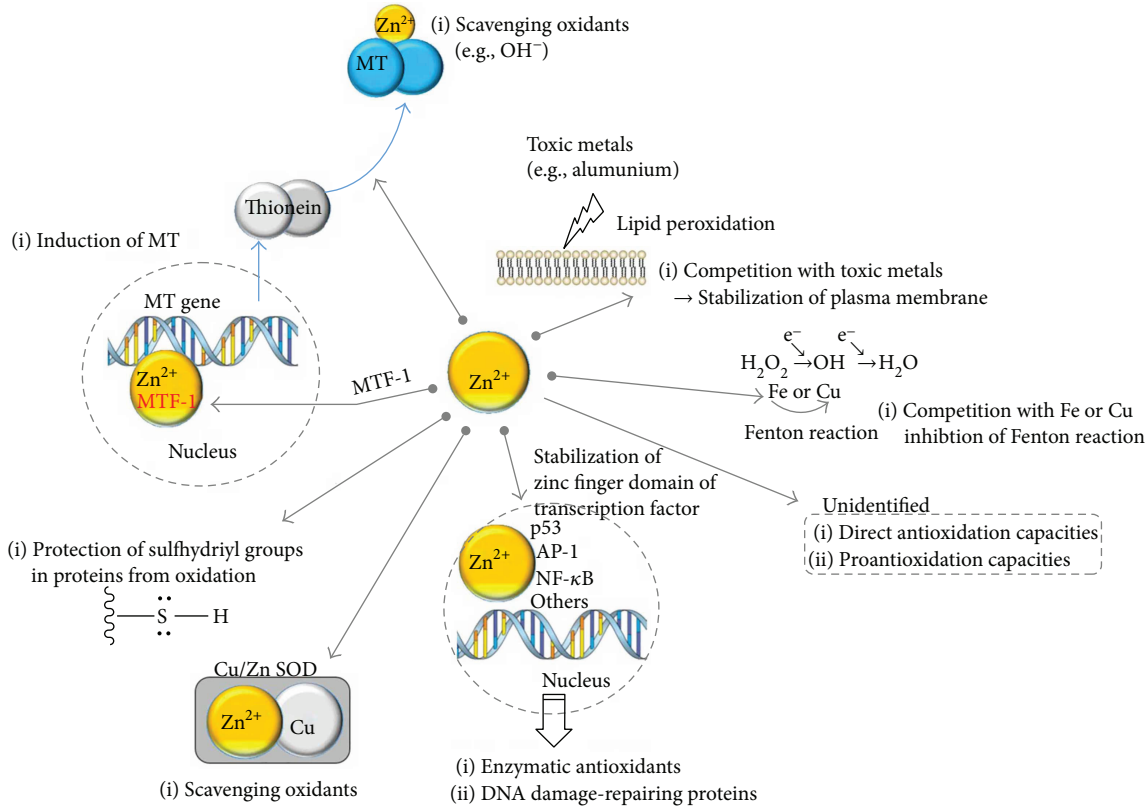

Figure 1: Involvement of zinc as an antioxidant. AP-1: activator protein 1; Cu: copper; Fe: iron; MT: metallothionein; MTF-1: metal-responsive transcription factor-1; NF-κB: nuclear factor kappa-B; p53: tumor suppressor p53; SOD: superoxide dismutase.

other membrane transporter proteins, including some types of voltage-gated calcium channels, the glutamate receptor, the acetylcholine receptor, and the transient receptor potential (TRP) channel are involved in mobilization of Zn^{2+} across the cellular membrane (as discussed elsewhere [49]). In the wound healing process, extracellular Zn^{2+} released from cellular injuries can be sensed by ZnR/GPR39, which can be triggered by nanomolar concentrations of Zn^{2+}, and promotes signaling that leads to epithelial repair [50]. The increased Zn^{2+} level in the cytosol will be recognized by the Zn^{2+}-sensitive transcription factor, MTF-1 [51]; once Zn^{2+} has been bound, MTF-1 translocates to the nucleus to upregulate the expression of MT and ZnTs, such as ZnT1 [52, 53]. Differently, Zn^{2+} can be buffered within a "zinc muffler" via a still unidentified Zn^{2+} transporter and is then translocated into an intracellular zinc store, such as the endoplasmic reticulum (ER), Golgi apparatus, lysosomes [54, 55], or mitochondria [55, 56]. However, there is no clearly identified mechanism through which the intracellular or extracellular level of Zn^{2+} is exactly sensed.

3. MT and Its Involvement in the Zinc-Mediated Redox Switch

MTs have four isoforms (MT I–IV), which show tissue-specific expression. MT I and MT II are ubiquitously expressed but are transcriptionally regulated by the metal-response element-binding transcription factor-1 (MTF-1); MT III is predominantly expressed in neurons; and MT IV is dominant in the brain and epithelial tissue (as discussed elsewhere [33, 57]). In contrast to MT I/MT II, both MT III and MT IV are not inducible. MT is located in various cellular compartments, such as the nucleus, cytosol, and cellular organelles [58–60]. MT binds Zn^{2+} more tightly and at a higher concentration in comparison with other zinc proteins [34]. Four and three zinc ions are captured via their formation of α and β clusters with different affinity in MT, respectively [35, 61, 62]. It has been suggested that the specific coordination of the zinc/thiolate clusters in MT [62] will react sensitively to the redox state and thus render flexibility either in cellular availability of Zn^{2+} or the redistribution of Zn^{2+} [35]. By contrast, MT can participate in redox chemistry that does not originally result from Zn^{2+} itself, but rather from its coordination of Zn(II)-thiolate moiety [62–64]. MT is able to scavenge the hydroxyl radical (OH^-) with 300-fold greater efficacy than glutathione [65, 66]. Moreover, the inherent activity of MT as an antioxidant may be involved in the protection against oxidative damage, such as radiation injury [66] or central nervous system pathology [67]. One of the pathways of MT degradation is its cleavage by lysosomal enzymes, such as cathepsin B, in lysosomes *in vivo* [52]. Compared with apo-MT, metal-bound MT species, such as Zn-MT and cadmium-MT, are extremely resistant to degradation. Metals protect MT against proteolysis, and the degradation of MT and metal release are likely to occur concomitantly [68].

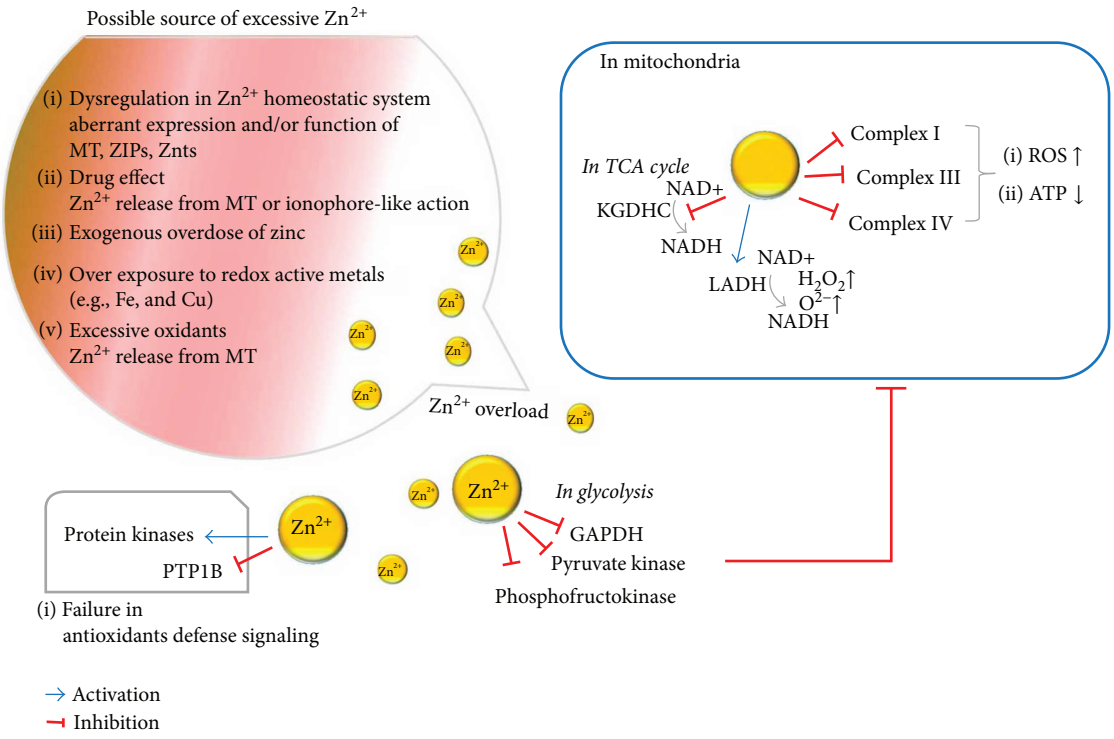

Figure 2: Involvement of zinc as a prooxidant. ATP: adenosine triphosphate; complex I: NADH:ubiquinone oxidoreductase; complex III: cytochrome bc1 complex; complex IV: cytochrome c oxidase; GAPDH: glyceraldehyde-3-phosphate dehydrogenase; KGDHC: alpha-ketoglutarate dehydrogenase complex; LADH: lipoamide dehydrogenase; MT: metallothionein; NADH: nicotinamide adenine dinucleotide; PTP1B: protein tyrosine phosphatase 1B; ROS: reactive oxygen species; TCA: tricarboxylic acid, (NADH); ZIP: zinc importer; ZnT: zinc transporter.

4. Impact of Zn^{2+} on Mitochondrial Homeostasis and Its Involvement in Oxidative Stress

Mitochondria are the major source of ROS production [69, 70]. Therefore, it is valuable to elucidate the role of Zn^{2+} in mitochondrial functions to obtain further insight into the role of Zn^{2+} as either an antioxidant or a prooxidant. In the model of ischemia/reperfusion (I/R) injury, the effect of Zn^{2+} differs between tissues. For example, brain damage during I/R can be attenuated by Zn^{2+} scavenging [71], but cardioprotectants require Zn^{2+}, as discussed elsewhere [28, 72]. Mitochondria are semiautonomous organelles capable of transcription and translation, and thus, the timely supply of Zn^{2+} must be supplied for these processes. A reduced content of Zn^{2+} can affect mitochondrial biogenesis, as matrix-localized metalloproteases that proteolytically cleave newly arrived proteins during their mitochondrial maturation require Zn^{2+} as a cofactor [73]. Zn^{2+} is a powerful inhibitor of the redox-regulated Mia40/Erv1 pathway, an essential component of the import pathway used by the small Tim proteins [74]. Thus, an aberrant level of cytosolic Zn^{2+} could suppress the correct positioning of the mitochondrial proteins required for mitochondrial biogenesis. In addition, zinc deficiency also induces ER stress response owing to accumulation of misfolded proteins that induce a vicious cycle of ER stress and oxidative stress [75, 76]. Improper supply of Zn^{2+} into mitochondria, for example, an insufficient level of ZnT6 [77] or alcoholic liver disease [78], may compromise many mitochondrial enzymes and proteins involved in mitochondrial protein processing, and thus mitochondrial ROS production can be enhanced owing to mitochondrial dysfunction.

4.1. Glycolysis and TCA Cycle. As shown in Figure 2, several Zn^{2+}-regulated enzymes involved in glycolysis have been identified [79–81]. In addition to zinc deficiency, a high level of Zn^{2+} can inhibit glycolysis via its inhibitory effects on glyceraldehyde-3-phosphate dehydrogenase (GAPDH) [79], phosphofructokinase [80], and muscle pyruvate kinase [81]; however, these effects can be reversed by a high level of histidine. A high Zn^{2+} concentration will interrupt the Krebs cycle and mitochondrial ATP production through a decrease in the production of a reduced form of nicotinamide adenine dinucleotide (NADH) [32]. The activity of GAPDH can be inhibited indirectly, because Zn^{2+} causes a reduction in nicotinamide-adenine dinucleotide (NAD^+) levels [82]. It should be noted that the Zn^{2+}-mediated inhibition of glycolysis is prominent only in cultured neurons because of their heavy reliance on glycolysis for ATP production compared with the brain [83]. In the tricarboxylic acid (TCA) cycle, the α-ketoglutarate dehydrogenase complex, which is an upstream of the bc1 complex (complex III), can be suppressed in the presence of a high Zn^{2+} level [84]. Mitochondrial lipoamide dehydrogenase (LADH), which catalyzes NADH oxidation by oxygen,

produces hydrogen peroxide as the major product and the superoxide radical as the minor product. As high Zn^{2+} level does not only activate LADH oxidase but also inhibits both the forward and reverse mode of LADH thiol oxidoreductase activity, abundant ROS production will occur [85].

4.2. Mitochondrial Respiratory Complexes. Zn^{2+} can bind slowly and progressively to the active state of complex I (NADH:ubiquinone oxidoreductase), whereas it binds rapidly and tightly to the resting state(s) [86]. At micromolar concentrations, Zn^{2+} inhibits complex I more strongly than Mg^{2+}, Ca^{2+}, Ba^{2+}, and Mn^{2+} to Cu^{2+} or Cd^{2+} through blocking of the proton transfer to bound quinone or proton translocation. Complex II (succinate dehydrogenase (SDH)), during both the forward and reverse electron transfers, will be suppressed by exposure to low micromolar concentrations of manganese (Mn), and this suppression results in the production of mitochondrial H_2O_2 in rat microglial cells, but not astroglial cells [87]. However, Zn^{2+} does not suppress complex II activity. The electron bifurcation at complex III (cytochrome bc1 complex) is believed to be the most critical electron transfer steps in the respiratory chain [88]. The Zn^{2+} binding to the bc1 complex does not interfere with the binding of either of the substrates, hydroquinone or cytochrome c, but at 100–200 nM, Zn^{2+} can bind to the hydroquinone center (QP Center) of Fe-S-depleted mitochondrial bc1 complexes with high affinity and in a reversible mode; thus, Zn binding can block a protonatable group in the bc1 complex [89]. Complex IV (cytochrome c oxidase) is a membrane-bound enzyme that catalyzes the reduction of O_2 to H_2O and uses part of the energy released in this reaction to pump protons across the membrane. Zn^{2+} could inhibit complex IV (cytochrome c oxidase) activity in a biphasic manner [90]. There is less evidence to suggest that Zn^{2+} is directly involved in changes in complex V (the F_0F_1 ATP synthase complex) [91].

The inhibition of ETC by high Zn^{2+} levels may lead to cellular death either via the dissipation of the mitochondrial transmembrane potential [83, 92, 93], reduced cellular ATP levels [94], or increased ROS production [92]. The mitochondrial permeability transition pore (MPTP) is sensitive to changes in thiol redox status, and thus, Zn^{2+} can stimulate MPTP opening via interference in thiol recycling [95]. However, it is controversial as to whether Zn^{2+} can directly induce MPTP opening. Mitochondrial dysfunction is not the sole source of Zn^{2+}-induced cell death, as neuronal cells can be damaged not only by compromised mitochondrial function but also by PI3K-mediated inhibition of mitochondrial movement [96]. In contrast, neuronal cell death was also mediated by H_2O_2-induced lysosomal membrane permeabilization owing to the intolerable accumulation of Zn^{2+} in the lysosome [97].

5. Role of Zinc as Either an Antioxidant or a Prooxidant in Conjunction with Regulation of Intracellular Free Zinc

Harmful effects of ROS/RNS can be prevented or slowed by nonenzymatic antioxidants (e.g., alpha-tocopherol, ascorbate, glutathione, and MT) and antioxidant enzymes (e.g., superoxide dismutase (SOD), catalase, and glutathione peroxidase) [98, 99]. The action of zinc as an antioxidant (Figure 1) is linked to zinc deficiency and disease. However, involvement of cellular zinc decreases in increased levels of ROS and that of RNS is still poorly understood. There is minimal evidence that excessive oxidation/peroxidation primarily occurs *in vivo* in tissues from zinc-deficient animals [26]. Indeed, a zinc-deficient diet will cause a reduction of food intake in rats [100, 101] and thus, multinutritional defects that result from low food intake will be included in the effects of pure zinc deficiency. Unexpectedly, dietary Zn deficiency does not impair the overall antioxidant defense capabilities in any tissue [102] and an uncompromised free radical defense system remains operational [26]. Zinc itself is not redox active, and thus, Zn^{2+} does not interact directly with ROS or with carbon-centered free radicals [26]. The possible sources of ROS in low zinc levels could be connected to (1) decreased activity of key antioxidant enzymes such as Cu/Zn-specific SOD. It is known that there is no positive correlation between Cu/Zn-SOD activity and dietary Zn intake or tissue zinc concentration. The decreased activity of SOD in zinc deficiency might not be a critical factor for oxidative stress, as the overexpression of SOD in yeast did not rescue the oxidative stress levels [103]. In conditions of nutritional stress, the change in Cu/Zn-SOD activity occurs not only through the concentration of Zn^{2+} but also through the concentration of Cu [102]. Alternatively, mismetallation in the absence of Zn^{2+} may be deleterious and yield either an inactive protein or a misfolded state prone to aggregation; (2) disturbance in the induction of MT by Zn^{2+}; (3) lower protection of the free sulfhydryl groups in proteins. Zn^{2+} can protect the sulfhydryl groups in proteins against oxidation, as shown in δ-aminolevulinate dehydratase, dihydroorotase, the cytoskeletal protein tubulin, and Zn finger DNA-binding proteins [26]. The interaction of Zn^{2+} with sulfhydryl groups can be involved in the regulation of enzymatic activity through the prevention of intramolecular disulfide formation, which causes steric hindrance and conformational changes [26]. It is noteworthy that Zn-MT does not protect all sulfhydryl groups against oxidative stress as since Zn^{2+} will be lost from Zn^{2+}-MT after reaction with OH^- and O_2^- [26]; (4) less competition with redox-active metal ions involved in oxidative reaction. The protein structure of MT can be modified by the reaction with L-homocysteine, and homocysteinylated-MT was reported to lose function and cause increased production of ROS, chronic inflammation, and atherothrombotic disease [104]. Zn^{2+} can compete with copper or iron for certain types of binding sites, owing to the similarities in their coordination chemistry [105], and thereby suppress their ability to transfer electrons in a particular environment and cause ROS production. For example, competition of Zn^{2+} with iron and copper in the cell membrane leads to an inhibition of the NADPH oxidase enzyme, another source of O_2^- and H_2O_2 production [106], and attenuates chronic inflammation and hyperglycemia [11, 12]; (5) dysfunction of the mitochondria and/or ER owing to an insufficiency of zinc; and (6) indirect involvement in oxidative reactions. Zn^{2+} binds selectively to

NADPH, but not to NADH. Therefore, Zn^{2+} can inhibit the NADPH-mediated drug-oxidizing system [107]. Zn^{2+} can impede the formation of Fe-oxygen-enoic acid complexes, which initiates lipid peroxidation [107]. In addition, Zn^{2+} can suppress the propagation step of lipid peroxidation at phosphatidylserine, which is where aluminum and related nonredox metals (Sc^{3+}, Ga^{3+}, In^{3+}, Be^{2+}, and Y^{3+}) bind preferentially [39]. Hence, Zn^{2+} performs the role of a stabilizer of macromolecules and biological membranes and minimizes their oxidative/peroxidative damage [40, 41]; although, there are some exceptions [108, 109]. The pharmacological intake of zinc can confer antioxidant-like functions, as shown in its alimentary effects against acute ethanol toxicity [110], whole-body radiation [111], isoproterenol-induced cardiac oxidative injury [112], and transition metal-mediated site-specific oxidative injury [113, 114]. It is assumed that zinc participates as an antioxidant [23], as several transcription factors [27, 115] can be upregulated by Zn^{2+} and the antioxidant, detoxifying molecules (glutathione, SOD, glutathione S-transferase, hemeoxygenase-1) and nuclear factor erythroid 2-related factor 2 (Nrf2) can be induced (Figure 1).

In addition to the antioxidant role of zinc (Figure 1), several prooxidant effects mediated by Zn^{2+} also exist and are highly associated with aberrant increases in Zn^{2+} levels (Figure 2). With the aberrant expression and function of Zn^{2+} influx and/or efflux system in conjunction with MT, intracellular Zn^{2+} overload or Zn^{2+} deficiency can occur as discussed elsewhere [48, 116–118]. In this type of Zn^{2+} overload, it will take some time until the detoxifying mechanisms in the cytosol and organelles (e.g., lysosomes and mitochondria) are compromised [119]. In the case of ischemia/reperfusion or the prevalence of oxidants such as peroxynitrite and methylisothiazolinone, the released Zn^{2+} from MT or other Zn^{2+}-bound proteins render Zn^{2+} as a prooxidant as a result of protein misfolding and the subsequent accumulation of these proteins that induces oxidative stress [35, 120]. Exogenous nitric oxide (NO) or N-methyl-D-aspartate (NMDA), which increase the production of endogenous NO via receptor activation leads to peroxynitrite ($ONOO^-$) formation and then Zn^{2+} release from intracellular stores, as shown in cerebrocortical neurons [121]. In cardiomyocytes, ROS and/or RNS provide major contributions to a rapid increase in intracellular Zn^{2+} levels, as a result of the mobilization of Zn^{2+} from intracellular stores. Moreover, during oxidative stress, including ultraviolet A irradiation, Zn^{2+} is released from MTs, either by nitrosylation or oxidation of the thiol ligands. Surgical injury or tissue damage, which releases Zn^{2+} from damaged cells, leads to a local increase in Zn^{2+} concentration in the neighboring cells. Certain drugs or metabolites can release Zn^{2+} from proteins, which will then cause cytotoxic effects. For example, ebselen, a selenium-containing redox drug that mimics the glutathione peroxidase, releases Zn^{2+} through the oxidation of Zn^{2+}-thiolate clusters in MTs [122]. It should be mentioned that release of Zn^{2+} from Keap1 by phase II inducers, such as oxidants and electrophiles, dissociates NRF2 from keap1; thus, this mechanism can function as a sensor for the induction of antioxidant responses [123].

Excessive Zn^{2+} stimulates mitochondrial ROS production, as described in Section 4. Zn^{2+}-ROS generation (produced by mitochondria, NADPH-oxidase (Nox), and other sources) can trigger further intracellular Zn^{2+} mobilization. Zn^{2+} appears to have other metabolic effects that are largely independent of the direct effects on mitochondria (Figure 2). In endothelial cells, aberrant increase in Zn^{2+} may lead to an increase in Nox1 expression, which contributes to the progression of vascular senescence [124]. Notably, senescent endothelial cells are labile to excess Zn^{2+} but are resistant to Zn^{2+} deficiency [125]. Considering the proapoptotic [126] or antiapoptotic role of Zn^{2+} [127–129], the prosenescence and proapoptotic effects of Zn^{2+} involved in vascular aging should be further elucidated in the future. In cultured neurons, Zn^{2+} has been found to trigger the activation of PKC, which results in the induction and activation of Nox1 [130] and also to induce nitric oxide synthase [131], with the resulting generation of O^{2-}, NO, and peroxynitrite [131]. In contrast, Zn^{2+} itself can induce protein kinase C- (PKC-) dependent MT phosphorylation, which results in the amplification of acute Zn^{2+} increases during in vitro brain ischemia [132]. Excessive Zn^{2+} distorts the signaling pathways, and this effect may lead to disruption of cellular homeostasis (Figure 2). For example, Zn^{2+} can inhibit the protein tyrosine phosphatase 1B (PTP 1B) and consequently activate the numerous kinases targeted by PTP 1B. This uncontrolled activation of kinases results in mitochondrial dysfunction and the activation of transcription factors such as Egr-1 or Elk-1, which leads to caspase-independent cell death [133].

6. Conclusion

Zn^{2+} performs versatile functions involved in the structural development and catalysis of enzymes and in signal mediation in biological system. One of these functions is that the important component of Zn^{2+} in redox regulation works as an essential component in Cu/Zn SOD and antioxidant via the control of cellular signal transduction, such as gene regulation (e.g., p53, NF-κB, and AP-1) and enzymatic activities. Numerous trials of Zn^{2+} supplements and topical delivery were indicated to provide beneficial impacts on health and the amelioration of pathological conditions. An adequate supply of zinc is considered essential in slowing the aging process, which in turn leads to improved cognitive functions, immune functions, stress response, and age-related neurodegenerative disorders [11]. In addition to alcoholism, zinc chelators were shown to facilitate some opioid-withdrawal signs in animals. Zinc deficiency, which affects more than 15% of the world's population, is also common among opioid consumers, and opioid-treated animals exhibit imbalances in zinc distribution [134]. As shown clinically, Zn^{2+} overload occurs in rare cases but its increase causes oxidative stress via the suppression of metabolism and mitochondrial functions. Several causes that lead to the increase of Zn^{2+} were addressed in the previous sections. Aberrant release from binding sites, such as MT, and/or from deposits in the organelles, such as mitochondria and lysosomes [55], will cause secondary oxidative stress initiated by mitochondrial

and oxidant-producing enzymes. Numerous findings have suggested that excessive Zn^{2+} caused oxidative stress owing to its role as a prooxidant and eventually caused cellular death. However, it should be mentioned that numerous biomedical studies have employed irrelevant Zn^{2+} conditions, including the use of the supraphysiological concentrations of zinc, and various forms of zinc [97]. In addition, when high levels of Zn are administered orally or by injection, there may be numerous differences in the tissue distribution, metabolism, excretion, interaction, and overall homeostasis of Zn in the whole animal system [26]. In understanding of the role of Zn^{2+} as either an antioxidant or a prooxidant, the time window of Zn^{2+} effects presents another concern, as the enzymatic antioxidant systems will have a lag time for their induction whereas nonenzymatic antioxidant systems are not largely affected by Zn^{2+}. In addition, an abrupt increase of Zn^{2+} will be caused either by highly oxidative conditions or by failure of Zn^{2+} homeostasis; therefore, its direct role in the antioxidant defense responses is unclear. When considering the inhibitory effect of Zn^{2+} on metabolic and mitochondrial function, augmentation of ROS production by Zn^{2+} will be more prominent. Many signaling pathways can be activated or inhibited by Zn^{2+} [24, 135, 136]. Currently, it is hard to predict where Zn^{2+} will drive a cellular response. The exclusive role of Zn^{2+} as a prooxidant cannot be separated from the innate oxidative stresses caused by other factors, as the existence of excessive oxidants exaggerates the increased Zn^{2+} in any given system. The putative effects of zinc supplementation or deficiency may be significantly affected by the concomitant changes in MT I/II expression. In addition to zinc transporters, the status of aberrant expression or mutation of MTs [48] will influence the expected antioxidant roles of Zn^{2+}, because various biological functions of Zn^{2+} are cooperated with MTs, which aid in controlling the concentration of Zn^{2+} at critical sites. Indeed, the optimal amount of free Zn^{2+} and the deleterious impact of Zn^{2+} on the cellular system are complex and frequently seem to be less responsive to nutritional supplement with zinc [7]. The precise measurement of total zinc and free zinc levels in either healthy or pathological conditions allows the decision of the dose and duration of optimal zinc supplementation and maintenance. Recently, the examination of metal ionophores (e.g., dithiocarbamates and pyrithione) is in progress in cancer cell biology for their potential clinical use [137]. Metal chelators, such as desferrioxamine and tetrathiomolybdate, will suppress the availability of Zn^{2+}, even at normal zinc levels. It is reasonable that more attention should be paid to the specific effects of Zn^{2+}-chelator or ionophores involved in the oxidative responses in conjunction with the behavior of Zn^{2+}.

In this review, we have briefly outlined why both Zn^{2+} deficiency and Zn^{2+} overload could contribute to oxidative stress. Zinc, an essential metal for life, plays important roles as an antioxidant to combat and suppress oxidative stress. In contrast, the excessive presence of Zn^{2+} triggers harmful oxidative stress. Therefore, strategies to enhance the antioxidant activity of Zn^{2+} while minimizing the induction of prooxidant effects should be the subject of future studies. Despite the numerous technical hurdles, the targeted and controlled delivery of Zn^{2+} and/or chelators to specific areas or tissues should be established for both clinical and scientific purposes.

Disclosure

The author apologizes for the vast number of outstanding publications that could not be cited owing to space limitations.

Conflicts of Interest

The author declares that there are no conflicts of interest.

Acknowledgments

This work was supported by the Basic Science Research Program (2015R1D1A3A 01015596) through the National Research Foundation of Korea (NRF) funded by the Ministry of Education, Science, and Technology.

References

[1] H. Sies, "Oxidative stress: from basic research to clinical application," *The American Journal of Medicine*, vol. 91, no. 3, Supplement 3, pp. S31–S38, 1991.

[2] A. M. Pisoschi and A. Pop, "The role of antioxidants in the chemistry of oxidative stress: a review," *European Journal of Medicinal Chemistry*, vol. 97, pp. 55–74, 2015.

[3] B. Poljsak, D. Suput, and I. Milisav, "Achieving the balance between ROS and antioxidants: when to use the synthetic antioxidants," *Oxidative Medicine and Cellular Longevity*, vol. 2013, Article ID 956792, 11 pages, 2013.

[4] P. I. Oteiza, G. G. Mackenzie, and S. V. Verstraeten, "Metals in neurodegeneration: involvement of oxidants and oxidant-sensitive transcription factors," *Molecular Aspects of Medicine*, vol. 25, no. 1-2, pp. 103–115, 2004.

[5] I. Korovila, M. Hugo, J. P. Castro et al., "Proteostasis, oxidative stress and aging," *Redox Biology*, vol. 13, pp. 550–567, 2017.

[6] S. J. S. Flora, "Structural, chemical and biological aspects of antioxidants for strategies against metal and metalloid exposure," *Oxidative Medicine and Cellular Longevity*, vol. 2, no. 4, pp. 191–206, 2009.

[7] K. Jomova and M. Valko, "Advances in metal-induced oxidative stress and human disease," *Toxicology*, vol. 283, no. 2-3, pp. 65–87, 2011.

[8] P. Poprac, K. Jomova, M. Simunkova, V. Kollar, C. J. Rhodes, and M. Valko, "Targeting free radicals in oxidative stress-related human diseases," *Trends in Pharmacological Sciences*, vol. 38, no. 7, pp. 592–607, 2017.

[9] M. Valko, K. Jomova, C. J. Rhodes, K. Kuča, and K. Musílek, "Redox- and non-redox-metal-induced formation of free radicals and their role in human disease," *Archives of Toxicology*, vol. 90, no. 1, pp. 1–37, 2016.

[10] C. W. Siah, D. Trinder, and J. K. Olynyk, "Iron overload," *Clinica Chimica Acta*, vol. 358, no. 1-2, pp. 24–36, 2005.

[11] E. Mocchegiani, L. Costarelli, R. Giacconi, F. Piacenza, A. Basso, and M. Malavolta, "Zinc, metallothioneins and immunosenescence: effect of zinc supply as nutrigenomic approach," *Biogerontology*, vol. 12, no. 5, pp. 455–465, 2011.

[12] S. Clemens and J. F. Ma, "Toxic heavy metal and metalloid accumulation in crop plants and foods," *Annual Review of Plant Biology*, vol. 67, no. 1, pp. 489–512, 2016.

[13] A. C. Tolcin, *2009 Minerals Yearbook*, United States Geological Survey, Washington, DC, USA, 2011.

[14] J. E. Cummings and J. P. Kovacic, "The ubiquitous role of zinc in health and disease," *Journal of Veterinary Emergency and Critical Care*, vol. 19, no. 3, pp. 215–240, 2009.

[15] K. Jurowski, B. Szewczyk, G. Nowak, and W. Piekoszewski, "Biological consequences of zinc deficiency in the pathomechanisms of selected diseases," *JBIC Journal of Biological Inorganic Chemistry*, vol. 19, no. 7, pp. 1069–1079, 2014.

[16] A. S. Prasad, "Essentiality and toxicity of zinc," *Scandinavian Journal of Work, Environment & Health*, vol. 19, Supplement 1, pp. 134–136, 1993.

[17] H. N. Hoffman II, R. L. Phyliky, and C. R. Fleming, "Zinc-induced copper deficiency," *Gastroenterology*, vol. 94, no. 2, pp. 508–512, 1988.

[18] S. R. Simon, R. F. Branda, B. H. Tindle, and S. L. Burns, "Copper deficiency and sideroblastic anemia associated with zinc ingestion," *American Journal of Hematology*, vol. 28, no. 3, pp. 181–183, 1988.

[19] M. Yasuyuki, K. Kunihiro, S. Kurissery, N. Kanavillil, Y. Sato, and Y. Kikuchi, "Antibacterial properties of nine pure metals: a laboratory study using *Staphylococcus aureus* and *Escherichia coli*," *Biofouling*, vol. 26, no. 7, pp. 851–858, 2010.

[20] A. B. G. Lansdown, U. Mirastschijski, N. Stubbs, E. Scanlon, and M. S. Ågren, "Zinc in wound healing: theoretical, experimental, and clinical aspects," *Wound Repair and Regeneration*, vol. 15, no. 1, pp. 2–16, 2007.

[21] K. L. Haas and K. J. Franz, "Application of metal coordination chemistry to explore and manipulate cell biology," *Chemical Reviews*, vol. 109, no. 10, pp. 4921–4960, 2009.

[22] T. Kochanczyk, A. Drozd, and A. Krezel, "Relationship between the architecture of zinc coordination and zinc binding affinity in proteins – insights into zinc regulation," *Metallomics*, vol. 7, no. 2, pp. 244–257, 2015.

[23] W. Maret, "Zinc biochemistry: from a single zinc enzyme to a key element of life," *Advances in Nutrition*, vol. 4, no. 1, pp. 82–91, 2013.

[24] T. Fukada and T. Kambe, Eds., *Zinc Signals in Cellular Functions and Disorders*, Springer, Tokyo, Japan, 2014.

[25] L. C. Costello, C. C. Fenselau, and R. B. Franklin, "Evidence for operation of the direct zinc ligand exchange mechanism for trafficking, transport, and reactivity of zinc in mammalian cells," *Journal of Inorganic Biochemistry*, vol. 105, no. 5, pp. 589–599, 2011.

[26] T. M. Bray and W. J. Bettger, "The physiological role of zinc as an antioxidant," *Free Radical Biology & Medicine*, vol. 8, no. 3, pp. 281–291, 1990.

[27] M. Jarosz, M. Olbert, G. Wyszogrodzka, K. Młyniec, and T. Librowski, "Antioxidant and anti-inflammatory effects of zinc. Zinc-dependent NF-κB signaling," *Inflammopharmacology*, vol. 25, no. 1, pp. 11–24, 2017.

[28] N. Efeovbokhan, S. K. Bhattacharya, R. A. Ahokas et al., "Zinc and the prooxidant heart failure phenotype," *Journal of Cardiovascular Pharmacology*, vol. 64, no. 4, pp. 393–400, 2014.

[29] Y. Yuan, F. Niu, Y. Liu, and N. Lu, "Zinc and its effects on oxidative stress in Alzheimer's disease," *Neurological Sciences*, vol. 35, no. 6, pp. 923–928, 2014.

[30] A. Clausen, T. McClanahan, S. G. Ji, and J. H. Weiss, "Mechanisms of rapid reactive oxygen species generation in response to cytosolic Ca^{2+} or Zn^{2+} loads in cortical neurons," *PLoS One*, vol. 8, no. 12, article e83347, 2013.

[31] Y. H. Kim, E. Y. Kim, B. J. Gwag, S. Sohn, and J. Y. Koh, "Zinc-induced cortical neuronal death with features of apoptosis and necrosis: mediation by free radicals," *Neuroscience*, vol. 89, no. 1, pp. 175–182, 1999.

[32] J. Y. Koh, S. W. Suh, B. J. Gwag, Y. Y. He, C. Y. Hsu, and D. W. Choi, "The role of zinc in selective neuronal death after transient global cerebral ischemia," *Science*, vol. 272, no. 5264, pp. 1013–1016, 1996.

[33] R. D. Palmiter, "The elusive function of metallothioneins," *Proceedings of the National Academy of Sciences of the United States of America*, vol. 95, no. 15, pp. 8428–8430, 1998.

[34] W. Maret, "The function of zinc metallothionein: a link between cellular zinc and redox state," *The Journal of Nutrition*, vol. 130, no. 5, pp. 1455S–1458S, 2000.

[35] W. Maret, "Metallothionein redox biology in the cytoprotective and cytotoxic functions of zinc," *Experimental Gerontology*, vol. 43, no. 5, pp. 363–369, 2008.

[36] C. Andreini, L. Banci, I. Bertini, and A. Rosato, "Counting the zinc-proteins encoded in the human genome," *Journal of Proteome Research*, vol. 5, no. 1, pp. 196–201, 2006.

[37] C. Andreini and I. Bertini, "A bioinformatics view of zinc enzymes," *Journal of Inorganic Biochemistry*, vol. 111, pp. 150–156, 2012.

[38] C. Andreini, I. Bertini, and A. Rosato, "Metalloproteomes: a bioinformatic approach," *Accounts of Chemical Research*, vol. 42, no. 10, pp. 1471–1479, 2009.

[39] S. V. Verstraeten, L. V. Nogueira, S. Schreier, and P. I. Oteiza, "Effect of trivalent metal ions on phase separation and membrane lipid packing: role in lipid peroxidation," *Archives of Biochemistry and Biophysics*, vol. 338, no. 1, pp. 121–127, 1997.

[40] M. Chvapil, "New aspects in the biological role of zinc: a stabilizer of macromolecules and biological membranes," *Life Sciences*, vol. 13, no. 8, pp. 1041–1049, 1973.

[41] B. L. O'Dell, "Role of zinc in plasma membrane function," *The Journal of Nutrition*, vol. 130, no. 5, pp. 1432S–1436S, 2000.

[42] M. Stefanidou, C. Maravelias, A. Dona, and C. Spiliopoulou, "Zinc: a multipurpose trace element," *Archives of Toxicology*, vol. 80, no. 1, pp. 1–9, 2006.

[43] L. M. Plum, L. Rink, and H. Haase, "The essential toxin: impact of zinc on human health," *International Journal of Environmental Research and Public Health*, vol. 7, no. 12, pp. 1342–1365, 2010.

[44] J. J. Langham Brown, "Zinc fume fever," *The British Institute of Radiology*, vol. 61, no. 724, pp. 327–329, 1988.

[45] A. S. Prasad, G. J. Brewer, E. B. Schoomaker, and P. Rabbani, "Hypocupremia induced by zinc therapy in adults," *JAMA*, vol. 240, no. 20, pp. 2166–2168, 1978.

[46] J. P. Liuzzi and R. J. Cousins, "Mammalian zinc transporters," *Annual Review of Nutrition*, vol. 24, no. 1, pp. 151–172, 2004.

[47] D. J. Eide, "Zinc transporters and the cellular trafficking of zinc," *Biochimica et Biophysica Acta (BBA) - Molecular Cell Research*, vol. 1763, no. 7, pp. 711–722, 2006.

[48] T. Kimura and T. Kambe, "The functions of metallothionein and ZIP and ZnT transporters: an overview and perspective,"

International Journal of Molecular Sciences, vol. 17, no. 12, p. 336, 2016.

[49] A. Bouron and J. Oberwinkler, "Contribution of calcium-conducting channels to the transport of zinc ions," *Pflügers Archiv*, vol. 466, no. 3, pp. 381–387, 2014.

[50] H. Sharir, A. Zinger, A. Nevo, I. Sekler, and M. Hershfinkel, "Zinc released from injured cells is acting via the Zn^{2+}-sensing receptor, ZnR, to trigger signaling leading to epithelial repair," *The Journal of Biological Chemistry*, vol. 285, no. 34, pp. 26097–26106, 2010.

[51] T. Kimura, N. Itoh, and G. K. Andrews, "Mechanisms of heavy metal sensing by metal response element-binding transcription factor-1," *Journal of Health Science*, vol. 55, no. 4, pp. 484–494, 2009.

[52] I. Bremner and N. T. Davies, "The induction of metallothionein in rat liver by zinc injection and restriction of food intake," *Biochemical Journal*, vol. 149, no. 3, pp. 733–738, 1975.

[53] G. K. Andrews, "Cellular zinc sensors: MTF-1 regulation of gene expression," *Biometals*, vol. 14, no. 3/4, pp. 223–237, 2001.

[54] I. Kukic, S. L. Kelleher, and K. Kiselyov, "Zn^{2+} efflux through lysosomal exocytosis prevents Zn^{2+}-induced toxicity," *Journal of Cell Science*, vol. 127, no. 14, pp. 3094–3103, 2014.

[55] Q. Lu, H. Haragopal, K. G. Slepchenko, C. Stork, and Y. V. Li, "Intracellular zinc distribution in mitochondria, ER and the Golgi apparatus," *International Journal of Physiology, Pathophysiology and Pharmacology*, vol. 8, no. 1, pp. 35–43, 2016.

[56] R. A. Colvin, A. I. Bush, I. Volitakis et al., "Insights into Zn^{2+} homeostasis in neurons from experimental and modeling studies," *American Journal of Physiology-Cell Physiology*, vol. 294, no. 3, pp. C726–C742, 2008.

[57] D. Juárez-Rebollar, C. Rios, C. Nava-Ruíz, and M. Méndez-Armenta, "Metallothionein in brain disorders," *Oxidative Medicine and Cellular Longevity*, vol. 2017, Article ID 5828056, 12 pages, 2017.

[58] Z. Zhou and Y. J. Kang, "Immunocytochemical localization of metallothionein and its relation to doxorubicin toxicity in transgenic mouse heart," *The American Journal of Pathology*, vol. 156, no. 5, pp. 1653–1662, 2000.

[59] B. Ye, W. Maret, and B. L. Vallee, "Zinc metallothionein imported into liver mitochondria modulates respiration," *Proceedings of the National Academy of Sciences of the United States of America*, vol. 98, no. 5, pp. 2317–2322, 2001.

[60] S. R. Hennigar and S. L. Kelleher, "Zinc networks: the cell-specific compartmentalization of zinc for specialized functions," *Biological Chemistry*, vol. 393, no. 7, pp. 565–578, 2012.

[61] A. H. Robbins, D. McRee, M. Williamson et al., "Refined crystal structure of Cd, Zn metallothionein at 2.0Åresolution," *Journal of Molecular Biology*, vol. 221, no. 4, pp. 1269–1293, 1991.

[62] A. Krezel and W. Maret, "Different redox states of metallothionein/thionein in biological tissue," *Biochemical Journal*, vol. 402, no. 3, pp. 551–558, 2007.

[63] W. Maret, "Metallothionein/disulfide interactions, oxidative stress, and the mobilization of cellular zinc," *Neurochemistry International*, vol. 27, no. 1, pp. 111–117, 1995.

[64] N. M. Giles, A. B. Watts, G. I. Giles, F. H. Fry, J. A. Littlechild, and C. Jacob, "Metal and redox modulation of cysteine protein function," *Chemistry & Biology*, vol. 10, no. 8, pp. 677–693, 2003.

[65] M. Sato and I. Bremner, "Oxygen free radicals and metallothionein," *Free Radical Biology & Medicine*, vol. 14, no. 3, pp. 325–337, 1993.

[66] P. J. Thornalley and M. Vasak, "Possible role for metallothionein in protection against radiation-induced oxidative stress. Kinetics and mechanism of its reaction with superoxide and hydroxyl radicals," *Biochimica et Biophysica Acta (BBA) - Protein Structure and Molecular Enzymology*, vol. 827, no. 1, pp. 36–44, 1985.

[67] M. Penkowa, "Metallothioneins are multipurpose neuroprotectants during brain pathology," *The FEBS Journal*, vol. 273, no. 9, pp. 1857–1870, 2006.

[68] C. D. Klaassen, S. Choudhuri, J. M. McKim, L. D. Lehman-McKeeman, and W. C. Kershaw, "In vitro and in vivo studies on the degradation of metallothionein," *Environ Health Perspect*, vol. 102, Supplement 3, pp. 141–146, 1994.

[69] J. F. Turrens, "Mitochondrial formation of reactive oxygen species," *The Journal of Physiology*, vol. 552, no. 2, pp. 335–344, 2003.

[70] F. L. Muller, Y. Liu, and H. Van Remmen, "Complex III releases superoxide to both sides of the inner mitochondrial membrane," *The Journal of Biological Chemistry*, vol. 279, no. 47, pp. 49064–49073, 2004.

[71] C. W. Shuttleworth and J. H. Weiss, "Zinc: new clues to diverse roles in brain ischemia," *Trends in Pharmacological Sciences*, vol. 32, no. 8, pp. 480–486, 2011.

[72] Z. Xu and J. Zhou, "Zinc and myocardial ischemia/reperfusion injury," *Biometals*, vol. 26, no. 6, pp. 863–878, 2013.

[73] A. B. Taylor, B. S. Smith, S. Kitada et al., "Crystal structures of mitochondrial processing peptidase reveal the mode for specific cleavage of import signal sequences," *Structure*, vol. 9, no. 7, pp. 615–625, 2001.

[74] B. Morgan, S. K. Ang, G. Yan, and H. Lu, "Zinc can play chaperone-like and inhibitor roles during import of mitochondrial small Tim proteins," *The Journal of Biological Chemistry*, vol. 284, no. 11, pp. 6818–6825, 2009.

[75] C. D. Ellis, F. Wang, C. W. MacDiarmid, S. Clark, T. Lyons, and D. J. Eide, "Zinc and the Msc2 zinc transporter protein are required for endoplasmic reticulum function," *The Journal of Cell Biology*, vol. 166, no. 3, pp. 325–335, 2004.

[76] J. D. Malhotra, H. Miao, K. Zhang et al., "Antioxidants reduce endoplasmic reticulum stress and improve protein secretion," *Proceedings of the National Academy of Sciences of the United States of America*, vol. 105, no. 47, pp. 18525–18530, 2008.

[77] E. Napoli, C. Ross-Inta, S. Wong et al., "Altered zinc transport disrupts mitochondrial protein processing/import in fragile X-associated tremor/ataxia syndrome," *Human Molecular Genetics*, vol. 20, no. 15, pp. 3079–3092, 2011.

[78] Q. Sun, W. Zhong, W. Zhang, and Z. Zhou, "Defect of mitochondrial respiratory chain is a mechanism of ROS overproduction in a rat model of alcoholic liver disease: role of zinc deficiency," *American Journal of Physiology-Gastrointestinal and Liver Physiology*, vol. 310, no. 3, pp. G205–G214, 2016.

[79] B. Krotkiewska and T. Banas, "Interaction of Zn^{2+}, and Cu^{2+}, ions with glyceraldehyde-3-phosphate dehydrogenase from bovine heart and rabbit muscle," *The International Journal of Biochemistry*, vol. 24, no. 9, pp. 1501–1505, 1992.

[80] T. Ikeda, K. Kimura, S. Morioka, and N. Tamaki, "Inhibitory effects of Zn^{2+} on muscle glycolysis and their reversal by

histidine," *Journal of Nutritional Science and Vitaminology*, vol. 26, no. 4, pp. 357–366, 1980.

[81] N. Tamaki, T. Ikeda, K. Kimura, and S. Morioka, "Inhibitory effect of Zn^{2+} on rabbit muscle pyruvate kinase and reactivation by histidine," *Journal of Nutritional Science and Vitaminology*, vol. 27, no. 2, pp. 107–116, 1981.

[82] C. T. Sheline, M. M. Behrens, and D. W. Choi, "Zinc-induced cortical neuronal death: contribution of energy failure attributable to loss of NAD^+ and inhibition of glycolysis," *The Journal of Neuroscience*, vol. 20, no. 9, pp. 3139–3146, 2000.

[83] K. E. Dineley, T. V. Votyakova, and I. J. Reynolds, "Zinc inhibition of cellular energy production: implications for mitochondria and neurodegeneration," *Journal of Neurochemistry*, vol. 85, no. 3, pp. 563–570, 2003.

[84] A. M. Brown, B. S. Kristal, M. S. Effron et al., "Zn^{2+} inhibits α-ketoglutarate-stimulated mitochondrial respiration and the isolated α-ketoglutarate dehydrogenase complex," *The Journal of Biological Chemistry*, vol. 275, no. 18, pp. 13441–13447, 2000.

[85] I. G. Gazaryan, B. F. Krasnikov, G. A. Ashby, R. N. F. Thorneley, B. S. Kristal, and A. M. Brown, "Zinc is a potent inhibitor of thiol oxidoreductase activity and stimulates reactive oxygen species production by lipoamide dehydrogenase," *The Journal of Biological Chemistry*, vol. 277, no. 12, pp. 10064–10072, 2002.

[86] M. S. Sharpley and J. Hirst, "The inhibition of mitochondrial complex I (NADH:ubiquinone oxidoreductase) by Zn^{2+}," *The Journal of Biological Chemistry*, vol. 281, no. 46, pp. 34803–34809, 2006.

[87] Y. Liu, D. S. Barber, P. Zhang, and B. Liu, "Complex II of the mitochondrial respiratory chain is the key mediator of divalent manganese-induced hydrogen peroxide production in microglia," *Toxicological Sciences*, vol. 132, no. 2, pp. 298–306, 2013.

[88] H. Nohl, L. Gille, A. Kozlov, and K. Staniek, "Are mitochondria a spontaneous and permanent source of reactive oxygen species?," *Redox Report*, vol. 8, no. 3, pp. 135–141, 2003.

[89] T. A. Link and G. von Jagow, "Zinc ions inhibit the Q_P center of bovine heart mitochondrial bc_1 complex by blocking a protonatable group," *The Journal of Biological Chemistry*, vol. 270, no. 42, pp. 25001–25006, 1995.

[90] S. S. Kuznetsova, N. V. Azarkina, T. V. Vygodina, S. A. Siletsky, and A. A. Konstantinov, "Zinc ions as cytochrome C oxidase inhibitors: two sites of action," *Biochemistry*, vol. 70, no. 2, pp. 128–136, 2005.

[91] W. Rouslin, C. W. Broge, and B. V. Chernyak, "Effects of Zn^{2+} on the activity and binding of the mitochondrial ATPase inhibitor protein, IF_1," *Journal of Bioenergetics and Biomembranes*, vol. 25, no. 3, pp. 297–306, 1993.

[92] S. L. Sensi, H. Z. Yin, S. G. Carriedo, S. S. Rao, and J. H. Weiss, "Preferential Zn^{2+} influx through Ca^{2+}-permeable AMPA/kainate channels triggers prolonged mitochondrial superoxide production," *Proceedings of the National Academy of Sciences of the United States of America*, vol. 96, no. 5, pp. 2414–2419, 1999.

[93] K. E. Dineley, L. L. Richards, T. V. Votyakova, and I. J. Reynolds, "Zinc causes loss of membrane potential and elevates reactive oxygen species in rat brain mitochondria," *Mitochondrion*, vol. 5, no. 1, pp. 55–65, 2005.

[94] K. E. Dineley, J. M. Scanlon, G. J. Kress, A. K. Stout, and I. J. Reynolds, "Astrocytes are more resistant than neurons to the cytotoxic effects of increased $[Zn^{2+}]_i$," *Neurobiology of Disease*, vol. 7, no. 4, pp. 310–320, 2000.

[95] V. Petronilli, P. Costantini, L. Scorrano, R. Colonna, S. Passamonti, and P. Bernardi, "The voltage sensor of the mitochondrial permeability transition pore is tuned by the oxidation-reduction state of vicinal thiols. Increase of the gating potential by oxidants and its reversal by reducing agents," *The Journal of Biological Chemistry*, vol. 269, no. 24, pp. 16638–16642, 1994.

[96] L. M. Malaiyandi, A. S. Honick, G. L. Rintoul, Q. J. Wang, and I. J. Reynolds, "Zn^{2+} inhibits mitochondrial movement in neurons by phosphatidylinositol 3-kinase activation," *The Journal of Neuroscience*, vol. 25, no. 41, pp. 9507–9514, 2005.

[97] J. J. Hwang, S. J. Lee, T. Y. Kim, J. H. Cho, and J. Y. Koh, "Zinc and 4-hydroxy-2-nonenal mediate lysosomal membrane permeabilization induced by H_2O_2 in cultured hippocampal neurons," *The Journal of Neuroscience*, vol. 28, no. 12, pp. 3114–3122, 2008.

[98] J. M. Mates, C. Perez-Gomez, and I. Nunez de Castro, "Antioxidant enzymes and human diseases," *Clinical Biochemistry*, vol. 32, no. 8, pp. 595–603, 1999.

[99] B. Halliwell, "Antioxidants in human health and disease," *Annual Review of Nutrition*, vol. 16, no. 1, pp. 33–50, 1996.

[100] T. Goto, M. Komai, H. Suzuki, and Y. Furukawa, "Long-term zinc deficiency decreases taste sensitivity in rats," *The Journal of Nutrition*, vol. 131, no. 2, pp. 305–310, 2001.

[101] J. K. Chesters and M. Will, "Some factors controlling food intake by zinc-deficient rats," *The British Journal of Nutrition*, vol. 30, no. 3, pp. 555–566, 1973.

[102] C. G. Taylor, W. J. Bettger, and T. M. Bray, "Effect of dietary zinc or copper deficiency on the primary free radical defense system in rats," *The Journal of Nutrition*, vol. 118, no. 5, pp. 613–621, 1988.

[103] N. Harris, M. Bachler, V. Costa, M. Mollapour, P. Moradas-Ferreira, and P. W. Piper, "Overexpressed Sod1p acts either to reduce or to increase the lifespans and stress resistance of yeast, depending on whether it is Cu^{2+}-deficient or an active Cu,Zn-superoxide dismutase," *Aging Cell*, vol. 4, no. 1, pp. 41–52, 2005.

[104] J. C. Barbato, O. Catanescu, K. Murray, P. M. DiBello, and D. W. Jacobsen, "Targeting of metallothionein by L-homocysteine: a novel mechanism for disruption of zinc and redox homeostasis," *Arteriosclerosis, Thrombosis, and Vascular Biology*, vol. 27, no. 1, pp. 49–54, 2007.

[105] K. Hegetschweiler, P. Saltman, C. Dalvit, and P. E. Wright, "Kinetics and mechanisms of the oxidation of myoglobin by Fe(III) and Cu(II) complexes," *Biochimica et Biophysica Acta (BBA) - Protein Structure and Molecular Enzymology*, vol. 912, no. 3, pp. 384–397, 1987.

[106] A. S. Prasad, "Zinc is an antioxidant and anti-inflammatory agent: its role in human health," *Frontiers in Nutrition*, vol. 1, p. 14, 2014.

[107] J. C. Ludwig, R. L. Misiorowski, M. Chvapil, and M. D. Seymour, "Interaction of zinc ions with electron carrying coenzymes NADPH and NADH," *Chemico-Biological Interactions*, vol. 30, no. 1, pp. 25–34, 1980.

[108] W. J. Bettger, T. J. Fish, and B. L. O'Dell, "Effects of copper and zinc status of rats on erythrocyte stability and superoxide dismutase activity," *Proceedings of the Society for Experimental Biology and Medicine*, vol. 158, no. 2, pp. 279–282, 1978.

[109] H. Pasantes-Morales and C. Cruz, "Protective effect of taurine and zinc on peroxidation-induced damage in photoreceptor outer segments," *Journal of Neuroscience Research*, vol. 11, no. 3, pp. 303–311, 1984.

[110] G. L. Floersheim, "Protection against acute ethanol toxicity in mice by zinc aspartate, glycols, levulose and pyritinol," *Agents and Actions*, vol. 16, no. 6, pp. 580–584, 1985.

[111] G. L. Floersheim and A. Bieri, "Further studies on selective radioprotection by organic zinc salts and synergism of zinc aspartate with WR 2721," *The British Journal of Radiology*, vol. 63, no. 750, pp. 468–475, 1990.

[112] P. K. Singal, K. S. Dhillon, R. E. Beamish, and N. S. Dhalla, "Protective effect of zinc against catecholamine-induced myocardial changes electrocardiographic and ultrastructural studies," *Laboratory Investigation*, vol. 44, no. 5, pp. 426–433, 1981.

[113] S. R. Powell, D. Hall, L. Aiuto, R. A. Wapnir, S. Teichberg, and A. J. Tortolani, "Zinc improves postischemic recovery of isolated rat hearts through inhibition of oxidative stress," *American Journal of Physiology-Heart and Circulatory Physiology*, vol. 266, no. 6, Part 2, pp. H2497–H2507, 1994.

[114] S. R. Powell, R. L. Nelson, J. M. Finnerty et al., "Zinc-bis-histidinate preserves cardiac function in a porcine model of cardioplegic arrest," *The Annals of Thoracic Surgery*, vol. 64, no. 1, pp. 73–80, 1997.

[115] M. M. Cortese, C. V. Suschek, W. Wetzel, K. D. Kröncke, and V. Kolb-Bachofen, "Zinc protects endothelial cells from hydrogen peroxide via Nrf2-dependent stimulation of glutathione biosynthesis," *Free Radical Biology & Medicine*, vol. 44, no. 12, pp. 2002–2012, 2008.

[116] T. Fukada, S. Yamasaki, K. Nishida, M. Murakami, and T. Hirano, "Zinc homeostasis and signaling in health and diseases: zinc signaling," *JBIC Journal of Biological Inorganic Chemistry*, vol. 16, no. 7, pp. 1123–1134, 2011.

[117] G. Lyubartseva and M. A. Lovell, "A potential role for zinc alterations in the pathogenesis of Alzheimer's disease," *BioFactors*, vol. 38, no. 2, pp. 98–106, 2012.

[118] K. Smidt and J. Rungby, "ZnT3: a zinc transporter active in several organs," *Biometals*, vol. 25, no. 1, pp. 1–8, 2012.

[119] S.-J. Lee and J.-Y. Koh, "Roles of zinc and metallothionein-3 in oxidative stress-induced lysosomal dysfunction, cell death, and autophagy in neurons and astrocytes," *Molecular Brain*, vol. 3, no. 1, p. 30, 2010.

[120] P. W. Land and E. Aizenman, "Zinc accumulation after target loss: an early event in retrograde degeneration of thalamic neurons," *The European Journal of Neuroscience*, vol. 21, no. 3, pp. 647–657, 2005.

[121] E. Bossy-Wetzel, M. V. Talantova, W. D. Lee et al., "Crosstalk between nitric oxide and zinc pathways to neuronal cell death involving mitochondrial dysfunction and p38-activated K^+ channels," *Neuron*, vol. 41, no. 3, pp. 351–365, 2004.

[122] C. Jacob, W. Maret, and B. L. Vallee, "Ebselen, a selenium-containing redox drug, releases zinc from metallothionein," *Biochemical and Biophysical Research Communications*, vol. 248, no. 3, pp. 569–573, 1998.

[123] A. T. Dinkova-Kostova, W. D. Holtzclaw, and N. Wakabayashi, "Keap1, the sensor for electrophiles and oxidants that regulates the phase 2 response, is a zinc metalloprotein," *Biochemistry*, vol. 44, no. 18, pp. 6889–6899, 2005.

[124] G. Salazar, J. Huang, R. G. Feresin, Y. Zhao, and K. K. Griendling, "Zinc regulates Nox1 expression through a NF-κB and mitochondrial ROS dependent mechanism to induce senescence of vascular smooth muscle cells," *Free Radical Biology & Medicine*, vol. 108, pp. 225–235, 2017.

[125] M. Malavolta, L. Costarelli, R. Giacconi et al., "Changes in Zn homeostasis during long term culture of primary endothelial cells and effects of Zn on endothelial cell senescence," *Experimental Gerontology*, vol. 99, pp. 35–45, 2017.

[126] A. Q. Truong-Tran, L. H. Ho, F. Chai, and P. D. Zalewski, "Cellular zinc fluxes and the regulation of apoptosis/gene-directed cell death," *The Journal of Nutrition*, vol. 130, no. 5, pp. 1459S–1466S, 2000.

[127] B. Hennig, P. Meerarani, P. Ramadass et al., "Zinc nutrition and apoptosis of vascular endothelial cells: implications in atherosclerosis," *Nutrition*, vol. 15, no. 10, pp. 744–748, 1999.

[128] D. K. Perry, M. J. Smyth, H. R. Stennicke et al., "Zinc is a potent inhibitor of the apoptotic protease, caspase-3. A novel target for zinc in the inhibition of apoptosis," *The Journal of Biological Chemistry*, vol. 272, no. 30, pp. 18530–18533, 1997.

[129] R. B. Franklin and L. C. Costello, "The important role of the apoptotic effects of zinc in the development of cancers," *Journal of Cellular Biochemistry*, vol. 106, no. 5, pp. 750–757, 2009.

[130] K. M. Noh and J. Y. Koh, "Induction and activation by zinc of NADPH oxidase in cultured cortical neurons and astrocytes," *The Journal of Neuroscience*, vol. 20, article Rc111, 2000.

[131] M. D. Pluth, E. Tomat, and S. J. Lippard, "Biochemistry of mobile zinc and nitric oxide revealed by fluorescent sensors," *Annual Review of Biochemistry*, vol. 80, no. 1, pp. 333–355, 2011.

[132] M. A. Aras, H. Hara, K. A. Hartnett, K. Kandler, and E. Aizenman, "Protein kinase C regulation of neuronal zinc signaling mediates survival during preconditioning," *Journal of Neurochemistry*, vol. 110, no. 1, pp. 106–117, 2009.

[133] H. Haase and W. Maret, "Intracellular zinc fluctuations modulate protein tyrosine phosphatase activity in insulin/insulin-like growth factor-1 signaling," *Experimental Cell Research*, vol. 291, no. 2, pp. 289–298, 2003.

[134] D. Ciubotariu, C. M. Ghiciuc, and C. E. Lupusoru, "Zinc involvement in opioid addiction and analgesia – should zinc supplementation be recommended for opioid-treated persons?," *Substance Abuse Treatment, Prevention, and Policy*, vol. 10, no. 1, p. 29, 2015.

[135] S. R. Lee, S. J. Noh, J. R. Pronto et al., "The critical roles of zinc: beyond impact on myocardial signaling," *The Korean Journal of Physiology & Pharmacology*, vol. 19, no. 5, pp. 389–399, 2015.

[136] S. Noh, S. R. Lee, Y. J. Jeong et al., "The direct modulatory activity of zinc toward ion channels," *Integrative Medicine Research*, vol. 4, no. 3, pp. 142–146, 2015.

[137] W. Q. Ding and S. E. Lind, "Metal ionophores – an emerging class of anticancer drugs," *IUBMB Life*, vol. 61, no. 11, pp. 1013–1018, 2009.

Hindawi
Oxidative Medicine and Cellular Longevity
Volume 2017, Article ID 3405089, 11 pages
https://doi.org/10.1155/2017/3405089

Research Article

Differential Susceptibility of Germ and Leydig Cells to Cadmium-Mediated Toxicity: Impact on Testis Structure, Adiponectin Levels, and Steroidogenesis

Marli C. Cupertino,[1] Rômulo D. Novaes,[2] Eliziária C. Santos,[3] Ana C. Neves,[1] Edson Silva,[4] Juraci A. Oliveira,[1] and Sérgio L. P. Matta[1]

[1]*Department of General Biology, Federal University of Viçosa, 36570-000 Viçosa, MG, Brazil*
[2]*Institute of Biomedical Sciences, Department of Structural Biology, Federal University of Alfenas, 37130-001 Alfenas, MG, Brazil*
[3]*School of Medicine, Federal University of Jequitinhonha and Mucuri Valleys, 39100-000 Diamantina, MG, Brazil*
[4]*Department of Basic and Health Sciences, Federal University of Jequitinhonha and Mucuri Valleys, 39100-000 Diamantina, MG, Brazil*

Correspondence should be addressed to Sérgio L. P. Matta; smatta@ufv.br

Received 4 August 2017; Accepted 25 October 2017; Published 20 December 2017

Academic Editor: Joseph Adeyemi

This study investigated the relationship between germ and Leydig cell death, testosterone, and adiponectin levels in cadmium-mediated acute toxicity. Cadmium chloride was administered in a single dose to five groups of rats: G1 (0.9% NaCl) and G2 to G5 (0.67, 0.74, 0.86, and 1.1 mg Cd/kg). After 7 days, the animals were euthanized, and the testosterone and testes were analyzed. Dose-dependent Cd accumulation in the testes was identified. At 0.86 and 1.1 mg/kg, animals exhibited marked inflammatory infiltrate and disorganization of the seminiferous epithelium. While Leydig cells were morphologically resistant to Cd toxicity, massive germ cell death and DNA oxidation and fragmentation were observed. Although numerical density of Leydig cells was unchanged, testosterone levels were significantly impaired in animals exposed to 0.86 and 1.1 mg Cd/kg, occurring in parallel with the reduction in total adiponectins and the increase in high-molecular weight adiponectin levels. Our findings indicated that Leydig and germ cells exhibit differential microstructural resistance to Cd toxicity. While germ cells are a primary target of Cd-induced toxicity, Leydig cells remain resistant to death even when exposed to high doses of Cd. Despite morphological resistance, steroidogenesis was drastically impaired by Cd exposure, an event potentially related to the imbalance in adiponectin production.

1. Introduction

As life-threatening inorganic pollutants are widely distributed in soil, water, and food, heavy metal poisoning is a serious public health problem worldwide [1]. Due to the long half-life (20–40 years) and low rate of excretion by organisms, cadmium (Cd) is an environmental toxicant with great potential to induce irreversible injuries in multiple organs, especially the liver, kidney, brain, lungs, and testes [2–4].

In the testes, besides inducing microstructural fragility (e.g., endothelial damage, vascular congestion, edema, hemorrhage, and testis calcification) [5, 6], Cd also disturbs the redox balance, eliciting proinflammatory and prooxidant events linked to genotoxicity, carcinogenesis, and cell death [1, 2]. Cadmium-mediated toxicity has also been associated with inhibition of expression of important regulatory molecules, such as focal adhesion kinase, Src kinases, and tyrosine phosphatase SHP2; these are essential for maintaining the morphofunctional integrity of the germinative epithelium, especially the Sertoli cell barrier and Sertoli-germ cell interactions [7–10]. These changes are related to molecular imbalance of the testis microenvironment and have a

negative impact on steroidogenesis and spermatogenesis; this results in severe consequences such as hypogonadal syndromes and disturbance of male fertility [11, 12].

There is consistent evidence relating oxidative stress and the inflammatory process to the microstructural and functional testis disturbances triggered by exposure to heavy metals [6, 13, 14]. Although poorly understood, adiponectins have been suggested to be immunomodulator molecules with important effects on testicular homeostasis [15–17]. Adiponectins are a class of hormones primarily produced by adipose tissue; their testis mRNA expression and protein levels have been associated with interstitial Leydig cells [15–17]. By interacting directly with Leydig cell receptors (Adipo-R1 and Adipo-R2), adiponectins act as potential endogenous regulators of steroidogenesis in animals and humans [17, 18]. As potent anti-inflammatory mediators, adiponectins also protect Leydig cells against cytokine-mediated cytotoxicity, acting as a testicular defense mechanism to attenuate the negative impact of proinflammatory molecules, particularly those released by macrophages (e.g., interleukin 1 [IL-1], tumor necrosis factor alpha [TNF-α], and interferon gamma [IFN-γ]), on steroidogenesis [19, 20]. To the best of our knowledge, the role of adiponectins in Cd-mediated toxicity of reproductive organs remains unexplored. Thus, investigation of the relationship between adiponectins, testis structure, and function can introduce a new perspective on the regulatory mechanisms activated in the testes in response to Cd toxicity.

Although the impact of Cd on the testis microstructure has been investigated [10, 21], the mechanisms related to the pathological reorganization of testis parenchyma and stroma remain poorly understood. Given that fertility disturbances have been reported after exposure to heavy metals, germ and Leydig cells have been considered the main testicular targets of Cd-mediated toxicity [12, 22]. However, it remains unclear if the heterogeneous distribution of germ and Leydig cells is also related to differential morphofunctional resistance or susceptibility to Cd toxicity. Thus, given the hypothesis that Cd acts as an endocrine disruptor [22, 23], this study investigated the relationship between testicular microstructural remodeling, cell death, steroidogenesis, and adiponectin levels in an experimental model of acute Cd-mediated toxicity.

2. Materials and Methods

2.1. Groups and Model of Cd-Induced Testicular Damage. Thirty male Wistar rats (9 weeks old) weighting 287.9 ± 14.14 g were maintained in animal facilities with controlled relative air humidity (60–70%), temperature (22 ± 2°C), and photoperiod (12/12 h). The animals received food and water ad libitum. The experimental protocol was approved by the Institutional Ethics Committee (protocol 030/2010).

The animals were randomized into five groups of six animals each: control (CT), 0.9% NaCl; Cd1, 0.67 mg Cd/kg (1.1 mg/kg $CdCl_2$); Cd2, 0.74 mg Cd/kg (1.2 mg/kg $CdCl_2$); Cd3, 0.86 mg Cd/kg (1.4 mg/kg $CdCl_2$); and Cd4, 1.1 mg Cd/kg (1.8 mg/kg $CdCl_2$). Cadmium chloride ($CdCl_2$, Sigma-Aldrich, MO, USA) was dissolved in distilled water and administered in a single intraperitoneal injection. Cadmium doses were determined considering the minimal dose (1.2 mg/kg $CdCl_2$) effective to induce testicular damage [24]. As low Cd doses are more realistic and consistent with environmental contaminations, we used one dose lower and two doses higher than minimally necessary to cause testicular effects [6].

2.2. Euthanasia and Organ Collection. Seven days after Cd exposure, the animals were weighed and euthanized under deep anesthesia (5 mg/kg xylazine and 45 mg/kg ketamine, i.p.). Blood samples (5 mL) were collected by cardiac puncture in glass test tubes, and testosterone plasma levels were quantified. The testes were removed and weighed. The right testis was used for the measurement of testicular Cd accumulation, genomic DNA extraction, analysis of oxidative damage, and adiponectin quantification. The left testis was immersed in histological fixative (1 M paraformaldehyde and 1 M glutaraldehyde in 0.1 M phosphate buffer, 1 : 1, *v*/*v*) for 24 h [6]. The tunica albuginea was excised by using a scalpel and surgical tweezers and weighed, and its weight was subtracted from the total testicle weight, providing the gonadal parenchyma weight [7]. Then, the testes were used for histopathological and stereological analyses in bright-field microscopy [6].

2.3. Testicular Cadmium Content. Testicular cadmium content was determined by atomic absorption spectrophotometry and by energy-dispersive X-ray spectroscopy (EDS) [6, 25]. Testis samples were weighed and dried at 70°C until a constant dry weight was achieved. Dried samples were digested (30 min) in Erlenmeyer flasks with 1.5 mL concentrated HNO_3 and 0.5 mL $HClO_4$ (70%) using a plate heater, where the temperature was gradually increased from 70°C to 90°C. After digestion, the samples were diluted in deionized water (25 mL) and filtered. Cadmium concentration in each sample was determined using an atomic absorption spectrophotometer (Varian 220FS SpectrAA, Palo Alto, California, USA).

Relative Cd dose-dependent testicular accumulation was investigated by EDS using a scanning electron microscope (Leo 1430VP, Carl Zeiss, Jena, Thuringia, Germany) with an attached X-ray detector system (Tracor TN5502, Middleton, Wisconsin, USA) [26]. Small pieces of the testis from each animal were dehydrated at 60°C and coated with a thin film of evaporated carbon (Quorum Q150 T, East Grinstead, West Sussex, England, UK). The EDS microanalysis was performed at ×1000 magnification, with an accelerating voltage of 20 kV and a working distance of 19 mm [6]. Cadmium distribution was normalized considering the mean distribution of reference minerals (Na, Ca, K, P, Mg, Fe, and S) [27, 28].

2.4. Histopathological and Stereological Analyses. After albuginea removal, fixed testis samples were dehydrated in ethanol and embedded in glycol methacrylate (Leica Microsystems, Wetzlar, Germany). Three-micrometer-thick semiserial sections were obtained in a rotary microtome. To avoid analyzing the same histologic area, one out of every

20 sections was collected and used. Testis slices were stained with 1% toluidine blue/sodium borate [6]. Stereological estimations were obtained from digital images captured at different magnifications using a light microscope (Olympus BX-60, Tokyo, Japan) equipped with a digital camera (Olympus QColor-3; Tokyo, Japan) [29]. Stereological principles [30] were applied to investigate the general testis microstructure. The volume densities (Vv) (%) of seminiferous tubules, intertubules, blood vessels, lymphatic vessels, and connective tissue were estimated in 10 histological fields per animal (200x magnification) using a point counting method and the equation $Vv = Pp/Pt$, where Pp is the number of test points hitting the structure of interest and Pt is the total points in the test system ($Pt = 266$).

2.5. Leydig Cell Histomorphometry and Stereology. Testicular number and volume distribution of Leydig cells (LC) were estimated from point counting, direct measures of nuclear volume, and the proportions between the nucleus and cytoplasm. The mean diameter of the LC nucleus was obtained by computational planimetry for 50 cells per animal. Only cells with evident nucleoli were used as the reference in all quantifications. The nuclear volume (LCnv) was obtained by calculating the mean nuclear diameter using the notation $4/3\ \pi R^3$, where R = nuclear diameter/2. Using ×100 objective lens (×1000 magnification), volume densities of the LC cytoplasm (Vvcy) (%) and nuclei (Vvnu) (%) were estimated by point counting, using the same formula previously described. Leydig cell cytoplasmic volume (LCcyv) was estimated as follows: $LCcyv = (Vvcy \times LCnv)/Vvnu$. These parameters were used to calculate the nucleus/cytoplasm ratio, which was estimated as LCnv/LCcyv. In addition, individual LC volume (LCV) was estimated as LCnv + LCcyv. Leydig cell volume was used to estimate the LC number per testis unity and testis mass. Leydig cell number per testis was estimated as LCV/gonadal volume, and LC number per mass unity was calculated as LCV/gonadal mass. All microstructural parameters were measured using the image analysis software Image-Pro Plus (Media Cybernetics, Rockville, Maryland, USA) [30].

2.6. In Situ Apoptosis Assay. Apoptosis was detected by the TUNEL (terminal deoxynucleotidyl transferase dUTP nick end labeling) assay (Calbiochem, Merck KGaA, Darmstadt, Germany). Testis samples were included in paraffin, and five-micrometer-thick sections were deparaffinized, rehydrated, and incubated with proteinase K for 20 min at room temperature. Sections were washed in distilled water and incubated with H_2O_2 plus methanol (5 min) to stop endogenous peroxidase activity. Preparations were incubated in a humid chamber with terminal transferase (Tdt) equilibrium buffer, at room temperature, for 20 min, followed by Tdt mix enzyme and dithiothreitol (DTT) for 60 min at 37°C. Apoptotic cells were detected from the formation of brown precipitate after incubation with 3,3-diaminobenzidine tetrahydrochloride (DAB) and H_2O_2 for 13 min. The terminal transferase enzyme was omitted for the negative control. Positive controls were incubated with 1.00 U/mL DNase I (Invitrogen, Waltham, Massachusetts, USA) in DNase buffer for 10 min. Tissue distribution of apoptotic cells was evaluated by computational analysis (Image-Pro Plus, Media Cybernetics, Rockville, Maryland, USA) determining the optical density of brown pixels in all images submitted to the TUNEL assay.

2.7. DNA Fragmentation Assay. Genomic DNA extraction was carried out according to [31]. Briefly, testis samples (100 mg) were macerated and treated with DNA extraction solution (100 mM Tris-HCl (pH 8.0), 50 mM EDTA, 500 mM NaCl, 30 μL 20% sodium dodecyl sulfate (SDS), and 20 μL proteinase K) at 65°C for 24 h. After inactivation in a dry bath at 95°C, 1.5 μL 20 mg/mL of RNAse was added and incubated at 37°C for 30 min. Proteins and cellular debris were precipitated with 300 μL 6 M NaCl at 4°C for 15 min. After centrifugation (25,000 ×g, 20 min), an equal volume of phenol : chloroform : isoamyl alcohol (25 : 24 : 1) was added and centrifuged, and the upper aqueous layer containing the nucleic acid was collected. Nucleic acid was precipitated with absolute ethanol and 10 M ammonium acetate solution (pH 5.2) at −20°C. Samples were washed with 70% ethanol, centrifuged at 3000 ×g for 15 min, dried, and then suspended in 50 μL Milli-Q water. DNA damage was evaluated in agarose gel electrophoresis [27]. Briefly, genomic DNA quantity and purity were determined in a NanoDrop system (Thermo Fisher Scientific, NanoDrop Products, Waltham, Massachusetts, USA). Finally, 1000 ng/μL DNA and molecular marker (1000 bp DNA ladder, New England BioLabs Inc., Ipswich, USA) was subjected to 1.5% agarose gel (containing 0.5 μg/mL gel red) electrophoresis (Advance, Tokyo, Japan). DNA ladder formation was visualized under a UV transilluminator (Vilber Lourmat, Cedex, France). The optical density of the agarose gels was determined by computational analysis (Image-Pro Plus, Media Cybernetics, Rockville, Maryland, USA).

2.8. Serum Testosterone Quantification. Plasma testosterone concentrations were obtained by chemiluminescence using a commercial diagnostic biochemical kit (Access Testosterone, Beckman Coulter, Brea, California, USA) and the instructions provided by the manufacturer. The measurements were obtained on Access II equipment (Beckman Coulter, Brea, California, USA). The results were expressed in ng/dL.

2.9. Enzyme-Linked Immunosorbent Assay (ELISA) for Adiponectins. Fragments of testicular tissue (100 mg) were homogenized (LabGEN YO 0427-09, Cole-Parmer, Vernon Hills, IL, USA) in a protease inhibitor (Sigma-Aldrich, USA) and centrifuged at 3000 ×g for 10 min. The supernatant was collected for the cytokine assay. The concentration of cytokines was measured by the sandwich ELISA [32]. Adiponectin and high-molecular weight (HMW) adiponectin were measured using commercial kits, according to the manufacturer's instructions (USCN Life Science Inc., Wuhan, China).

2.10. Statistical Analysis. Results were expressed as means and standard deviations (SD). Biochemical and molecular data were submitted to unifactorial one-way analysis of variance followed by the Tukey post hoc test for multiple comparisons. Morphological data were compared using the

Kruskal-Wallis test. All results with $p < 0.05$ were considered statistically significant.

3. Results

The mean weight of the animals was similar ($p > 0.05$) in all groups (CT: 304.1 ± 21.2 g; Cd1: 300.2 ± 10.3 g; Cd2: 285.5 ± 40.0 g; Cd3: 279.7 ± 19.3 g; and Cd4: 270.2 ± 22.6 g). All groups treated with $CdCl_2$ presented with increased testicular Cd concentration compared to CT animals ($p < 0.05$). The highest Cd concentration was identified in Cd4 animals, compared to all other groups ($p < 0.05$). After normalization by reference minerals, Cd accumulation showed a dose-dependent behavior, with the highest relative distribution of this metal in Cd4 animals ($p < 0.05$) (see Figure 1).

The testes from CT animals presented with well-delimited tubular and intertubular compartments (Figure 2). In these animals, regular seminiferous tubule profiles were observed and a thick and organized seminiferous epithelium, structured by well-defined and juxtaposed germ cells, was also noted. Animals treated with $CdCl_2$ showed dose-dependent histopathological manifestations. The tubular compartment, nuclear hyperchromasia, cytoplasmic vacuolization, inflammatory infiltrate, epithelial dissociation, and germ cell fragmentation were the main histopathological findings observed in all intoxicated animals, especially in Cd3 and Cd4 (Figure 2).

The testes exhibited reduced mass in all Cd-exposed animals, compared to the CT group ($p < 0.05$). Albuginea mass was similar in all groups ($p > 0.05$). No statistically significant differences in tubular and intertubular stereological parameters were identified among the groups ($p > 0.05$) (see Table 1).

The TUNEL assay revealed germ cell death in all Cd-intoxicated groups (Figure 3). Positive cells were clearly identified from a well-defined brown marking, considering the negative and positive internal controls applied in this technique. Diffuse and massive distribution of TUNEL-positive germ cells was evident in all groups exposed to Cd, especially in Cd3 and Cd4. All intertubular cells were negative in the TUNEL method (Figure 3).

From computational analysis, dose-dependent cell death was clearly observed in all groups exposed to Cd, especially in Cd3 and Cd4 animals ($p < 0.05$), which also presented marked DNA fragmentation compared to the other groups ($p < 0.05$) (Figure 4).

The testes from CT animals presented with well-delimited intertubular space, evident blood and lymphatic vessel profiles, homogeneous connective tissue distribution, reduced cellularity, and well-defined Leydig cells. Mononuclear and polymorphonuclear inflammatory infiltrate, vascular congestion, hemorrhage, and increased mast cell distribution were the main types of microstructural intertubular damage identified in Cd-intoxicated groups, especially in Cd3 and Cd4 (Figure 5).

Quantitative analysis indicated minor microstructural changes in Leydig cells. Only Cd3 and Cd4 animals presented with reduced nuclear diameter as well as reduced nuclear, cytoplasmic, and general cell volume, compared to the other groups ($p < 0.05$). The other microstructural variables presented similar results among the groups ($p > 0.05$) (see Table 2).

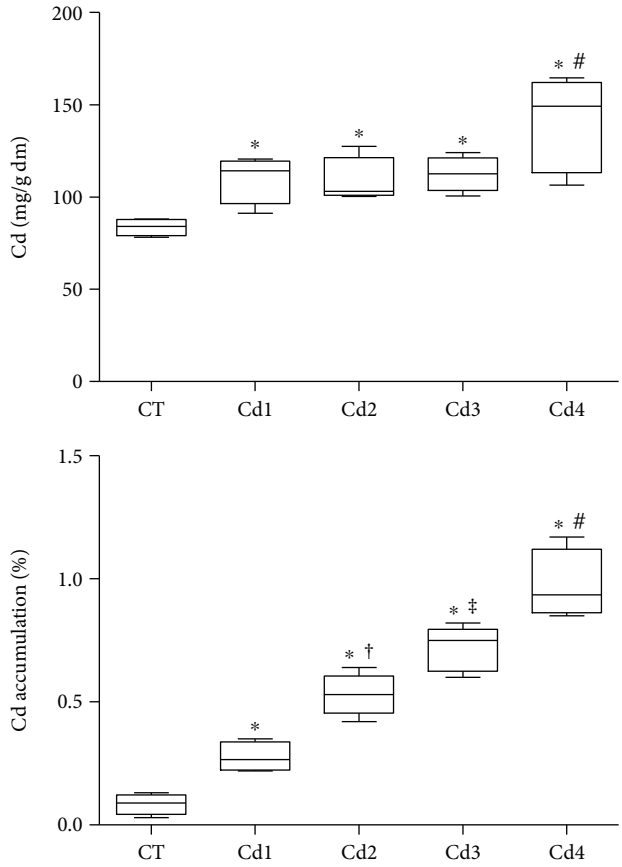

Figure 1: Cadmium (Cd) concentration (mg/g dry mass) and testicular dose-dependent accumulation (%) in rats. Cadmium accumulation was based on proportional distribution compared to the mean distribution of reference minerals (Na, Ca, K, P, Mg, S, Zn, Cu, and Se). Control (CT): 0.9% saline; Cd1: 0.67 mg Cd/kg; Cd2: 0.74 mg Cd/kg; Cd3: 0.86 mg Cd/kg; and Cd4: 1.1 mg Cd/kg. Statistical difference ($^{*}p < 0.05$ versus CT; $^{\dagger}p < 0.05$ versus Cd1; $^{\ddagger}p < 0.05$ versus CT, Cd1, and Cd2; and $^{\#}p < 0.05$ versus CT, Cd1, Cd2, and Cd3).

The groups CT, Cd1, and Cd2 presented with similar testosterone serum levels ($p > 0.05$). Testosterone was markedly reduced in Cd3 and Cd4 animals, compared to the other groups ($p < 0.05$) (see Figure 6).

While total adiponectin testicular levels were reduced ($p < 0.05$), high-molecular weight adiponectin was increased in all Cd-intoxicated groups, compared to CT animals ($p < 0.05$). These findings were also replicated when comparing Cd2, Cd3, and Cd4 groups with Cd1 animals ($p < 0.05$) (see Figure 7).

4. Discussion

Taken together, our findings indicate that the experimental model of Cd-mediated toxicity was effective in inducing morphological, biochemical, and molecular abnormalities in the testes. Consistent with an acute model, marked testis

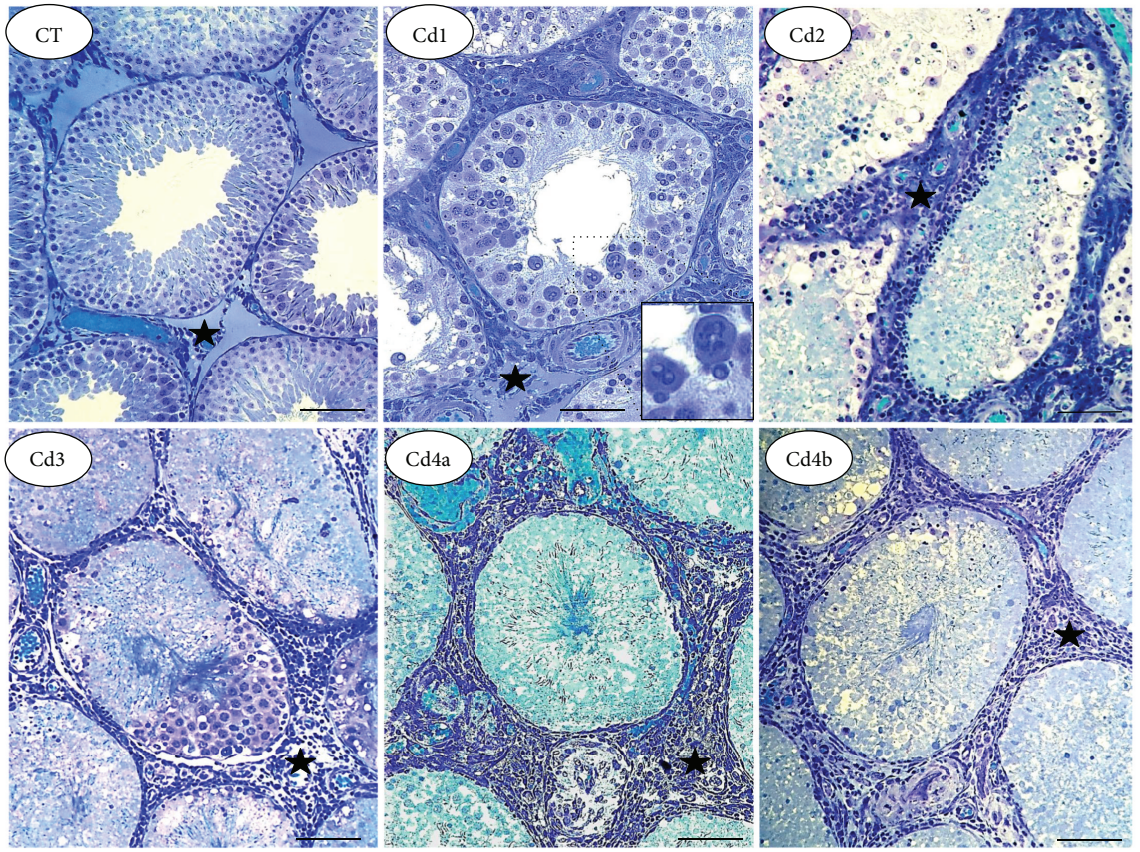

Figure 2: Representative microscopic images of the tubular compartment in the testis from control rats and those exposed to cadmium (Cd). Control (CT): 0.9% saline; Cd1: 0.67 mg Cd/kg; Cd2: 0.74 mg Cd/kg; Cd3: 0.86 mg Cd/kg; and Cd4: 1.1 mg Cd/kg. In CT, well-defined tubular structure with the preserved seminiferous epithelium is observed. In Cd1 to Cd4, dose-dependent epithelial damage is observed, with intense germ cell dissociation and reduced distribution. In Cd1, germ cells with abnormal nuclear morphology are highlighted. Marked inflammatory infiltrate is observed in intertubular compartment (star), especially in Cd2 to Cd4.

Table 1: Biometric and stereological testicular parameters in control rats and those exposed to cadmium (Cd).

Parameters	CT	Cd1	Cd2	Cd3	Cd4
Testis (g)	1.53 ± 0.09	0.89 ± 0.22*	0.83 ± 0.21*	1.0 ± 0.11*	0.94 ± 0.20*
Albuginea (g)	0.07 ± 0.01	0.05 ± 0.01	0.07 ± 0.03	0.1 ± 0.05	0.1 ± 0.07
Tubule (%)	92.9 ± 0.17	88.9 ± 7.5	79.7 ± 11.5	88.5 ± 7.6	85.8 ± 8.4
Intertubule (%)	7.1 ± 0.2	11.1 ± 7.5	20.4 ± 11.5	11.5 ± 7.6	14.2 ± 8.4
Blood vessels (%)	4.6 ± 2.9	5.6 ± 4.9	4.5 ± 2.1	3.4 ± 2.2	2.9 ± 0.7
Lymphatic vessels (%)	46.4 ± 2.6	39.2 ± 20.0	28.5 ± 19.6	54.9 ± 6.9	33.4 ± 22.4
Connective tissue (%)	14.1 ± 5.2	16.2 ± 9.0	47.3 ± 30.0	30.7 ± 32.3	40.3 ± 35.9

Control (CT): 0.9% saline; Cd1: 0.67 mg Cd/kg; Cd2: 0.74 mg Cd/kg; Cd3: 0.86 mg Cd/kg; and Cd4: 1.1 mg Cd/kg. Data are expressed as mean and standard deviation (mean ± SD). Statistical difference (*$p < 0.05$ versus CT).

damage was observed, particularly vascular congestion, intense inflammation, disorganization of the seminiferous epithelium, nuclear pleomorphism, cytoplasm vacuolization, and death of germ cells. Although reorganization of testis compartments was not achieved, the period of Cd exposure was enough to induce Cd accumulation and trigger genomic DNA fragmentation, antagonistic profiles of total adiponectin, and HMD adiponectin production, as well as disturbances in testosterone levels, which were associated with volumetric rather than numerical changes in Leydig cells.

As a typical model of heavy metal toxicity, Cd accumulation occurred in a dose-dependent manner [6]; this was consistent with morphological damage and molecular abnormalities in the testis (most severe in the groups Cd3 and Cd4). Although all groups exhibited testis hypotrophy, the proportions of tubular and intertubular components

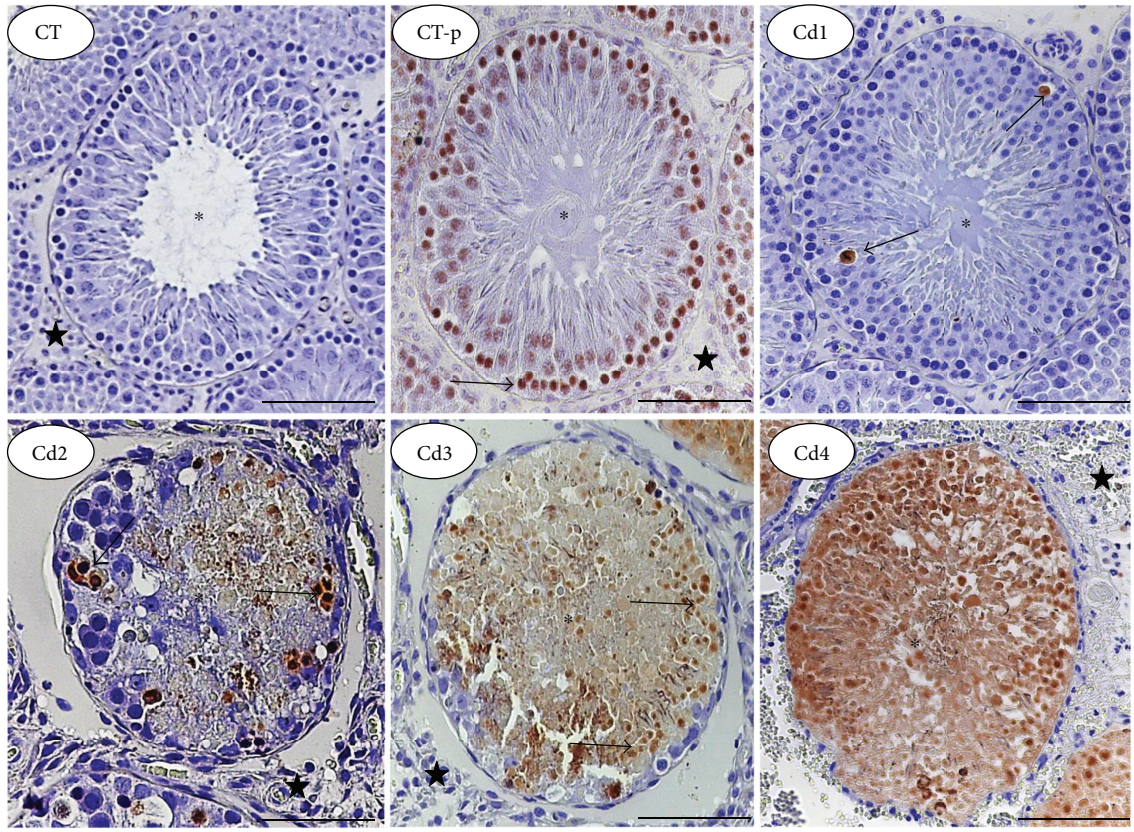

Figure 3: Distribution of apoptotic cells in the testes of control rats and those exposed to cadmium (Cd) (TUNEL technique, bars = 100 μm). Control (CT): 0.9% saline; CT-p (positive control for the TUNEL technique): 1.00 U/mL DNase I; Cd1: 0.67 mg Cd/kg; Cd2: 0.74 mg Cd/kg; Cd3: 0.86 mg Cd/kg; and Cd4: 1.1 mg Cd/kg. Cells with brown nuclei show positivity for apoptosis (arrows). Asterisks: seminiferous tubules; star: intertubular compartment.

remained unchanged. This indicates that Cd induced similar volumetric effects on both testicular components, with no evident change in the relative distribution of testis structures. Conversely, acute Cd exposure was associated with marked histopathological damage, especially mononuclear and polymorphonuclear inflammatory infiltrate and microstructural abnormalities in germ cells. Inside the broad spectrum of heavy metal toxicity [33, 34], the testes seem to be highly sensitive to divalent metals, especially Cd [35]. There is evidence that increased susceptibility to Cd is associated with molecular mimicry and competition with Ca, which is essential for the maintenance of the integrity of the Sertoli cell barrier [4, 10]. As Cd and Ca exhibit divergent functional properties, the Sertoli cell barrier becomes unstable and unable to control the adluminal molecular environment; this causes germ cell stress, accumulation of free calcium, and cell death [6, 10]. De Souza Predes et al. [24] showed that a single dose of cadmium chloride (1 to 1.2 mg/kg) is sufficient to cause testicular degeneration, which was compatible with severe inflammation, diffuse hemorrhage, and germ cell vacuolization. Beyond these pathological manifestations, Bekheet [36] pointed out that disorganization of the seminiferous epithelium and germ cell death are the most severe pathological manifestations of Cd-mediated toxicity.

In fact, marked dose-dependent germ cell death was observed in animals exposed to Cd, which was more evident and diffused in the groups receiving the highest doses of Cd (Cd3 and Cd4). Surprisingly, TUNEL marking was restricted to the seminiferous epithelium, and no positive intertubular cells were identified. This finding indicates that heterogeneous distribution of parenchymal cells is associated with different resistance profiles against aggression and that germ cells are primary targets of Cd-mediated toxicity. As clearly identified, all differentiation stages of germ cells were susceptible to Cd-induced death. A similar characteristic was reported by Zhou et al. [37] and Marettová et al. [5] who found that beyond aberrant morphology, there were reduced spermatogonium and spermatocyte numbers, as well as abnormal and immature cells in the tubular lumen.

Although the signaling pathways underlying testis damage are not completely understood, cell death has been associated with direct and indirect Cd-mediated cytotoxicity [35, 38]. *In vitro* models indicate that in fibroblasts [39] and human leukemia cells [40], caspase activation is closely correlated with cell death, so that caspase inhibitors are effective in attenuating Cd-induced cell death. Lemarie et al. [41] and Shih et al. [42] showed that cells exposed to Cd exhibit increased gene expression and release of apoptosis-inducing

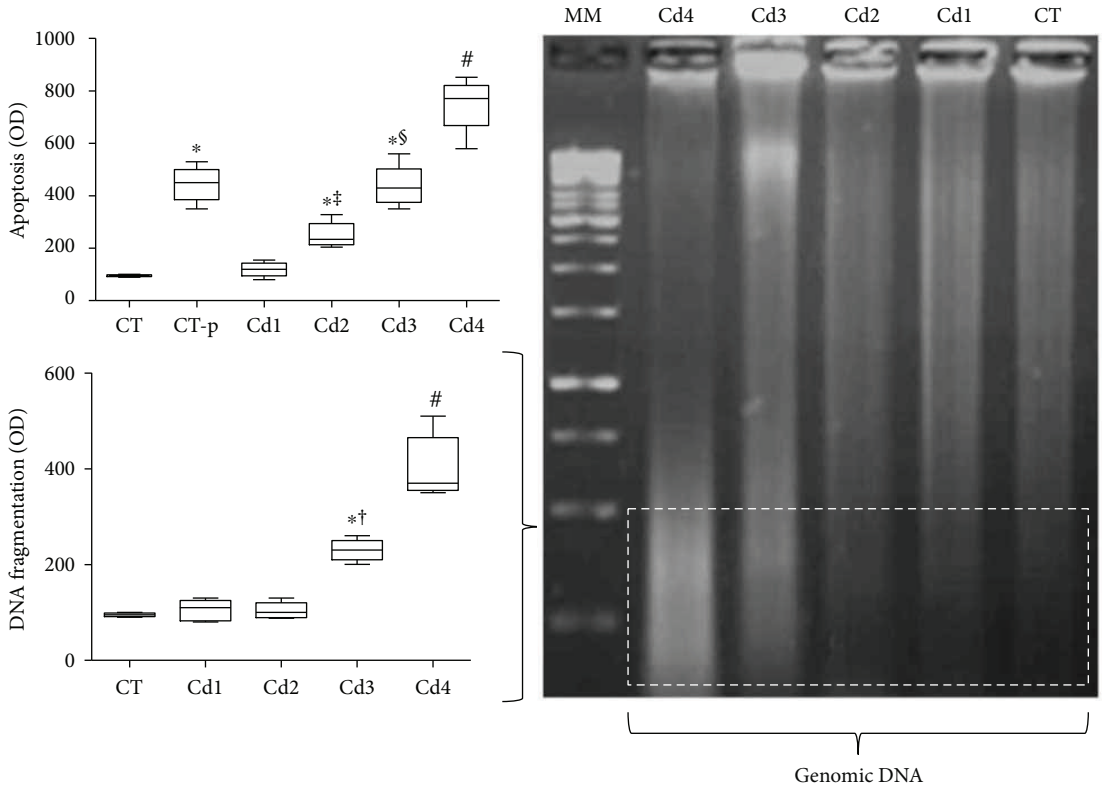

Figure 4: Genomic DNA oxidation and apoptotic index in the testis from control rats and those exposed to cadmium (Cd). DNA oxidation was evaluated by a ladder test using electrophoresis in agarose gel (left image). Optical density was computationally evaluated from the third tercile of agarose gel (dotted area). Apoptosis was evaluated by using microscopic images obtained from testis histological sections submitted to the TUNEL technique. In the graphics, DNA oxidation and apoptosis results were expressed as the difference in optical density (OD) compared to those of negative control animals (CT). MM: molecular marker. Control (CT): 0.9% saline; CT-p: 1.00 U/mL DNase I (positive control for the TUNEL technique); Cd1: 0.67 mg Cd/kg; Cd2: 0.74 mg Cd/kg; Cd3: 0.86 mg Cd/kg; and Cd4: 1.1 mg Cd/kg. In the graphics, data are expressed as mean and standard deviation (mean ± SD). Statistical difference ($^{*}p < 0.05$ versus CT; $^{\ddagger}p < 0.05$ versus CT-p and Cd1; $^{\S}p < 0.05$ versus CT-p, Cd1, and Cd2; $^{\#}p < 0.05$ versus CT, CT-p, Cd1, Cd2, and Cd3; and $^{\dagger}p < 0.05$ versus Cd1 and Cd2).

factor (AIF), which triggers cell death. This mechanism was also observed in the testes from Cd-exposed rats, in which germ cell death was associated with nuclear membrane damage [43] and translocation of AIF from mitochondria to the nucleus [38]. By interacting with cell DNA, AIF induces chromatin condensation and fragmentation through recruitment of downstream caspase-independent nucleases, causing an electrophoretic pattern of ladder-like DNA splitting [38, 44]. In fact, our findings indicate that cell death was consistent with DNA fragmentation, especially in the groups Cd3 and Cd4. Beyond direct Cd-induced AIF-DNA interaction, genotoxicity has also been associated with Cd-mediated redox imbalance [43, 45]. Together with direct inhibition of antioxidant enzymes (e.g., superoxide dismutase, catalase, and glutathione-S-transferase), Cd also stimulates inflammation and the secondary production of reactive oxygen metabolites (ROS) from recruited leucocytes (e.g., respiratory burst), inducing intense lipid, protein, and DNA oxidation [6, 46]. Although cell death is closely correlated with redox status, steroidogenesis is also sensitive to oxidative stress, which is dependent on dose, duration, and frequency of heavy metal exposure [46, 47].

Beyond low testosterone levels, animals exposed to the highest doses of Cd (Cd3 and Cd4) also exhibited a reduction in absolute morphological parameters of Leydig cells. As this finding was not associated with Leydig cell death, the impact of these microstructural changes on steroidogenesis remains poorly understood. However, it has been reported that downregulation of steroidogenesis can precede morphological abnormalities, especially in the initial stages of Cd poisoning [35, 48, 49]. In fact, our findings indicate that, despite the marked microstructural resistance of Leydig cells, as compared to germ cells, steroidogenesis is potentially sensitive to Cd-mediated toxicity. This proposition is corroborated by Laskey and Phelps [50] who suggested that viability of Leydig cells is achieved at the expense of inhibition of metabolic pathways not directly involved in cell survival, including steroidogenesis. In addition, Cd was proposed as a direct endocrine disruptor, with negative impacts on testosterone production [23]. Although poorly understood, Cd-induced steroid biosynthesis imbalance is potentially associated with downregulation of steroidogenic acute regulatory proteins (StAR), which participate in the conversion of cholesterol to

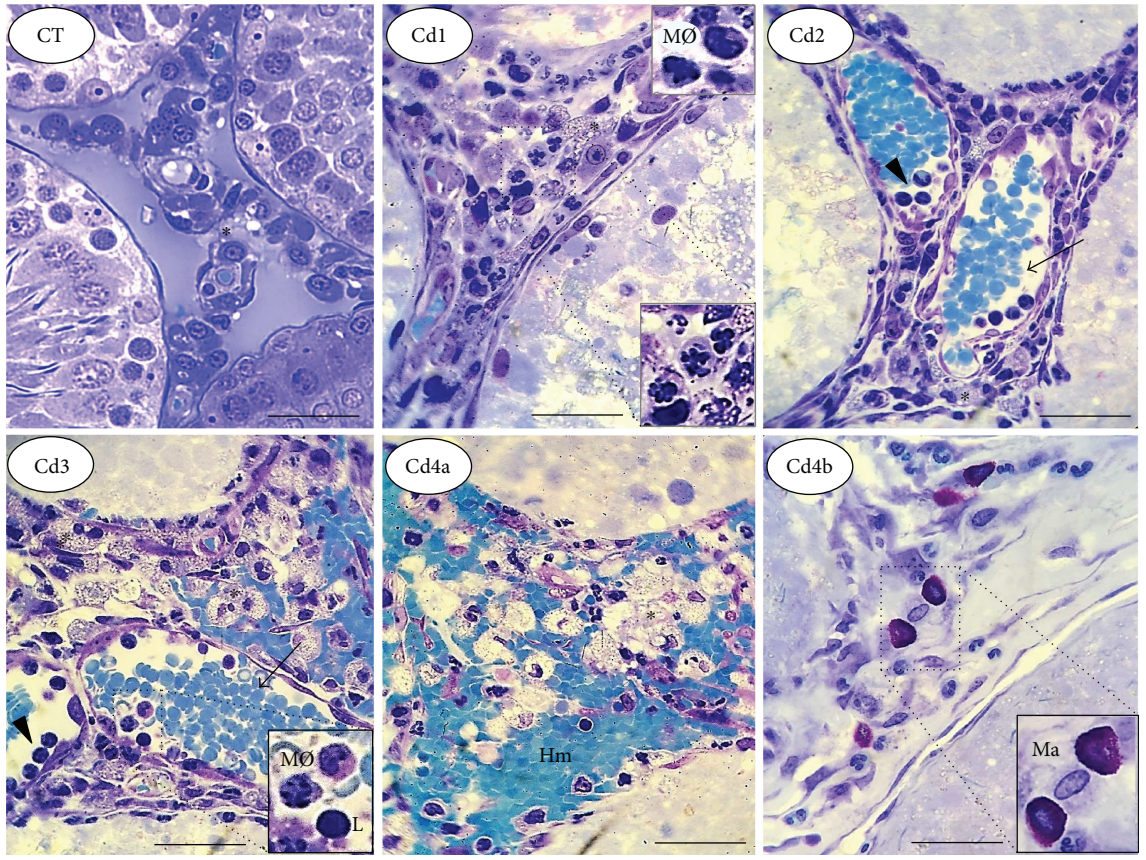

Figure 5: Representative microscopic images of the intertubular compartment in the testis from control rats and those exposed to cadmium (Cd). Control (CT): 0.9% saline; Cd1: 0.67 mg Cd/kg; Cd2: 0.74 mg Cd/kg; Cd3: 0.86 mg Cd/kg; and Cd4: 1.1 mg Cd/kg. In CT, well-defined intertubular structure with reduced cellularity and evident blood and lymphatic vessels is observed. In Cd1 to Cd4, dose-dependent damage is evident. In Cd-intoxicated animals, abnormal nuclear morphology in interstitial cells (Cd1, highlighted image), vascular congestion (Cd2 and Cd3), hemorrhage (Cd4a), and mast cell accumulation (Cd4b) were the main histopathological findings. The images of Cd4a and Cd4b indicate different and complementary morphological aspects of the same group of animals (Cd4). Arrows: blood vessels; arrowheads: leucocytes with marginal interaction; asterisk: Leydig cells; Hm: hemorrhagic foci; MØ: macrophages; L: lymphocytes; Ma: mast cells.

Table 2: Leydig cell absolute microstructural parameters obtained from the testis of control and exposed rats to four different Cd concentrations.

Parameters	Control	Cd1	Cd2	Cd3	Cd4
Nuclear diameter (μm)	6.4 ± 0.2	5.88 ± 0.3	5.6 ± 0.9	5.5 ± 0.3*	5.2 ± 0.3*
Nuclear volume (μm^3)	146.2 ± 20.6	121.1 ± 19.4	113.2 ± 26.2	108.3 ± 10.7	101.1 ± 9.1*
Cytoplasm volume (μm^3)	500.1 ± 105.1	394.6 ± 135.9	306.4 ± 108.1	268.2 ± 98.6*	201.0 ± 150.3*
Cell volume (μm^3)	646.3 ± 103.5	515.7 ± 149.9	419.6 ± 132.3	376.5 ± 105.4*	302.1 ± 152.4*
Cells per testis ($\times 10^8$)	7.6 ± 2.2	10.8 ± 5.9	6.1 ± 3.6	8.4 ± 4.4	12.2 ± 4.7
Cells per testis gram ($\times 10^8$)	6.1 ± 3.0	11.9 ± 6.7	7.0 ± 3.2	7.3 ± 3.5	13.4 ± 5.9
Nucleus/cytoplasm ratio	21.4 ± 1.2	23.98 ± 5.3	28.5 ± 10.8	28.4 ± 11.3	31.7 ± 12.4

Control (CT): 0.9% saline; Cd1: 0.67 mg Cd/kg; Cd2: 0.74 mg Cd/kg; Cd3: 0.86 mg Cd/kg; and Cd4: 1.1 mg Cd/kg. Data are expressed as mean and standard deviation (mean ± SD). Statistical difference (*$p < 0.05$ versus CT).

testosterone [51, 52]. It has been suggested that Cd also impairs the interaction between gonadotrophic luteinizing hormone (LH) and its receptor in Leydig cells [53]. However, this mechanism is controversial and requires further investigation.

Although the inhibitory effect of proinflammatory molecules, such as IL-1, IFN-γ, and TNF-α, on steroidogenesis is well known [15, 19], the testicular function of adiponectins is still poorly understood [17]. Even more obscure is the role adiponectins have in heavy metal poisoning. As a protective

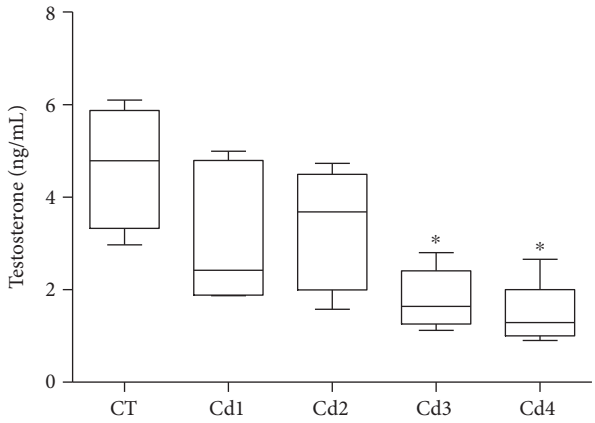

Figure 6: Testosterone serum levels in control rats and those exposed to cadmium (Cd). Control (CT): 0.9% saline; Cd1: 0.67 mg Cd/kg; Cd2: 0.74 mg Cd/kg; Cd3: 0.86 mg Cd/kg; and Cd4: 1.1 mg Cd/kg. Data are expressed as mean and standard deviation (mean ± SD). Statistical difference ($^{*}p < 0.05$ versus CT).

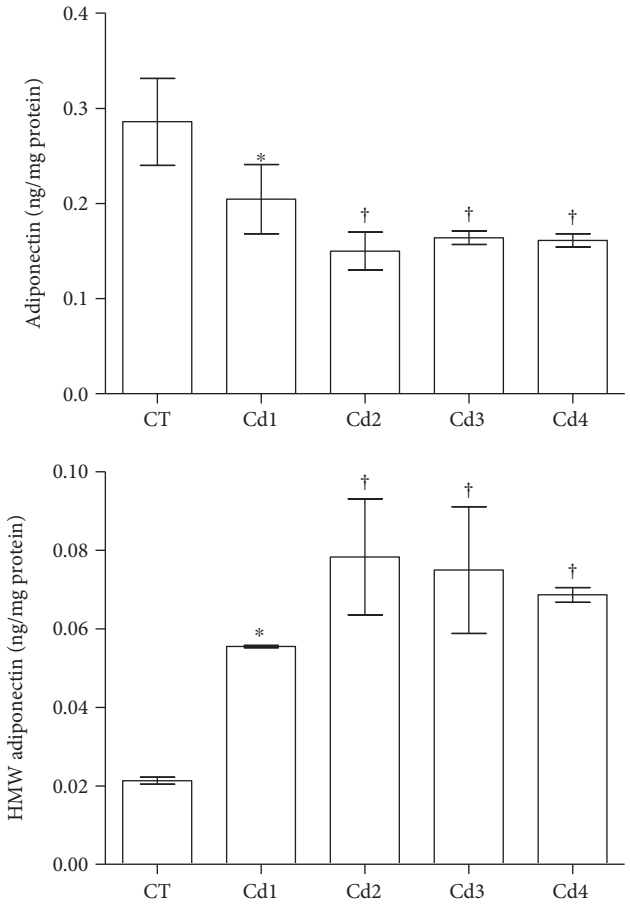

Figure 7: Testicular levels of adiponectin and high-molecular weight (HMW) adiponectin in control rats and those exposed to cadmium (Cd). Control (CT): 0.9% saline; Cd1: 0.67 mg Cd/kg; Cd2: 0.74 mg Cd/kg; Cd3: 0.86 mg Cd/kg; and Cd4: 1.1 mg Cd/kg. Data are expressed as mean and standard deviation (mean ± SD). Statistical difference ($^{*}p < 0.05$ versus CT; $^{\dagger}p < 0.05$ versus CT and Cd1).

contraregulatory reaction against Cd-induced toxicity, we expected a consistent increase in adiponectin in the testes from animals exposed to the highest doses of Cd, especially Cd3 and Cd4. However, while total adiponectin was reduced, HMW adiponectin isoform was detected in high levels in all Cd-exposed animals. Although adiponectins present with potent immunomodulation and antiapoptotic and antioxidant properties [54, 55], our findings suggest that testicular adiponectins can have a role other than attenuation of inflammatory damage and germ cell death. Thus, a potential relationship between adiponectin and its HMW isoforms with StAR proteins brings further perspectives for the control of steroidogenesis and testis functionality [15, 17, 56]. By regulating StAR expression, Pfaehler et al. [56] suggested that adiponectin modulates steroidogenesis in Leydig cells by direct inhibition of gene transcription. In this study, downregulation of StAR was associated with reduced adiponectin levels (10 and 100 ng/mL) and low testosterone production in rats. In fact, adiponectin and its receptors have been identified in Leydig cells from animals and humans [15, 16]. Considering the variable profile of total and HMW adiponectins, it is possible that this molecule acts in different testicular pathways, an issue that requires further investigation. Conversely, there is evidence that testosterone selectively inhibits gene expression and secretion of HMW adiponectins [57], a finding potentially related to the high levels of these molecules in the groups receiving the higher doses of Cd, especially Cd3 and Cd4.

5. Conclusions

Taken together, our findings indicate that Cd-mediated toxicity is associated with morphological and functional testis damage. Beyond a heterogeneous distribution, germ and Leydig cells exhibited divergent profiles of resistance to Cd. While germ cells are highly susceptible and constitute a primary target of Cd-induced genotoxicity, Leydig cells are resistant to cell death. Although Leydig cells are resistant to Cd-induced cell death, even in high doses of this metal, steroidogenesis is profoundly impaired. Despite their anti-inflammatory potential, total and HMW adiponectins are potentially involved in testis function, including steroidogenesis, instead of exerting a protective role against Cd-mediated microstructural damage and germ cell death.

Disclosure

This work was based on a PhD thesis entitled "Mineral and Inflammatory Disturbances on Reproductive System Triggered by Cadmium Exposure," developed at the Federal University of Viçosa, Brazil, 2016, by Marli Carmo Cupertino as the first author.

Conflicts of Interest

The authors indicate no potential conflicts of interest.

Acknowledgments

This work was supported by Universidade Federal de Viçosa (UFV), Fundação de Amparo à Pesquisa do Estado de Minas Gerais (FAPEMIG), and Conselho Nacional de Desenvolvimento Científico e Tecnológico (CNPq), Brazil.

References

[1] E. W. P. Wong and C. Y. Cheng, "Impacts of environmental toxicants on male reproductive dysfunction," *Trends in Pharmacological Sciences*, vol. 32, no. 5, pp. 290–299, 2011.

[2] C. Y. Cheng, E. W. P. Wong, P. P. Y. Lie et al., "Environmental toxicants and male reproductive function," *Spermatogenesis*, vol. 1, no. 1, pp. 2–13, 2011.

[3] H. T. Wan, D. D. Mruk, C. K. C. Wong, and C. Y. Cheng, "Targeting testis-specific proteins to inhibit spermatogenesis: lesson from endocrine disrupting chemicals," *Expert Opinion on Therapeutic Targets*, vol. 17, no. 7, pp. 839–855, 2013.

[4] X. Xiao, D. D. Mruk, E. I. Tang et al., "Environmental toxicants perturb human Sertoli cell adhesive function via changes in F-actin organization mediated by actin regulatory proteins," *Human Reproduction*, vol. 29, no. 6, pp. 1279–1291, 2014.

[5] E. Marettová, M. Maretta, and J. Legáth, "Changes in the peritubular tissue of rat testis after cadmium treatment," *Biological Trace Element Research*, vol. 134, no. 3, pp. 288–295, 2010.

[6] M. C. Cupertino, R. D. Novaes, E. C. Santos et al., "Cadmium-induced testicular damage is associated with mineral imbalance, increased antioxidant enzymes activity and protein oxidation in rats," *Life Sciences*, vol. 175, pp. 23–30, 2017.

[7] A. C. T. Morais, M. K. Balarini, E. O. Lopes et al., "The tubular compartment and the spermatogenic dynamics of the wild rodent *Oxymycterus nasutus* (Rodentia: Cricetidae)," *Animal Reproduction Science*, vol. 149, no. 3-4, pp. 249–258, 2014.

[8] Y. Gao, D. D. Mruk, and C. Y. Cheng, "Sertoli cells are the target of environmental toxicants in the testis – a mechanistic and therapeutic insight," *Expert Opinion on Therapeutic Targets*, vol. 19, no. 8, pp. 1073–1090, 2015.

[9] H. T. Wan, D. D. Mruk, C. K. C. Wong, and C. Y. Cheng, "The apical ES–BTB–BM functional axis is an emerging target for toxicant-induced infertility," *Trends in Molecular Medicine*, vol. 19, no. 7, pp. 396–405, 2013.

[10] C. Y. Cheng, "Toxicants target cell junctions in the testis: insights from the indazole-carboxylic acid model," *Spermatogenesis*, vol. 4, no. 2, article e981485, 2014.

[11] B. H. Y. Yeung, H. T. Wan, A. Y. S. Law, and C. K. C. Wong, "Endocrine disrupting chemicals: multiple effects on testicular signaling and spermatogenesis," *Spermatogenesis*, vol. 1, no. 3, pp. 231–239, 2011.

[12] Q. Zhang, P. Zou, H. Zhan et al., "Dihydrolipoamide dehydrogenase and cAMP are associated with cadmium-mediated Leydig cell damage," *Toxicology Letters*, vol. 205, no. 2, pp. 183–189, 2011.

[13] E. A. Taha, S. K. Sayed, N. M. Ghandour et al., "Correlation between seminal lead and cadmium and seminal parameters in idiopathic oligoasthenozoospermic males," *Central European Journal of Urology*, vol. 66, no. 1, pp. 84–92, 2013.

[14] H. Yuan, F. Qin, W. Guo, H. Gu, and A. Shao, "Oxidative stress and spermatogenesis suppression in the testis of cadmium-treated *Bombyx mori* larvae," *Environmental Science and Pollution Research*, vol. 23, no. 6, pp. 5763–5770, 2016.

[15] J. E. Caminos, R. Nogueiras, F. Gaytán et al., "Novel expression and direct effects of adiponectin in the rat testis," *Endocrinology*, vol. 149, no. 7, pp. 3390–3402, 2008.

[16] O. M. Ocon-Grove, S. M. Krzysik-Walker, S. R. Maddineni, G. L. Hendricks, and R. Ramachandran, "Adiponectin and its receptors are expressed in the chicken testis: influence of sexual maturation on testicular *ADIPOR1* and *ADIPOR2* mRNA abundance," *Reproduction*, vol. 136, no. 5, pp. 627–638, 2008.

[17] L. J. Martin, "Implications of adiponectin in linking metabolism to testicular function," *Endocrine*, vol. 46, no. 1, pp. 16–28, 2014.

[18] P. Roumaud and L. J. Martin, "Roles of leptin, adiponectin and resistin in the transcriptional regulation of steroidogenic genes contributing to decreased Leydig cells function in obesity," *Hormone Molecular Biology and Clinical Investigation*, vol. 24, no. 1, pp. 25–45, 2015.

[19] L. Wu, B. Xu, W. Fan, X. Zhu, G. Wang, and A. Zhang, "Adiponectin protects Leydig cells against proinflammatory cytokines by suppressing the nuclear factor-κB signaling pathway," *The FEBS Journal*, vol. 280, no. 16, pp. 3920–3927, 2013.

[20] K. L. Cerny, M. Van Fleet, A. Slepenkin, E. M. Peterson, and P. J. Bridges, "Differential expression of mRNA encoding cytokines and chemokines in the reproductive tract after infection of mice with Chlamydia trachomatis," *Reproductive System & Sexual Disorders*, vol. 4, no. 3, 2015.

[21] N. Li, D. D. Mruk, W. M. Lee, C. K. C. Wong, and C. Y. Cheng, "Is toxicant-induced Sertoli cell injury in vitro a useful model to study molecular mechanisms in spermatogenesis?," *Seminars in Cell & Developmental Biology*, vol. 59, pp. 141–156, 2016.

[22] C. A. Lamas, A. P. B. Gollücke, and H. Dolder, "Grape juice concentrate (G8000®) intake mitigates testicular morphological and ultrastructural damage following cadmium intoxication," *International Journal of Experimental Pathology*, vol. 96, no. 5, pp. 301–310, 2015.

[23] Z. Knazicka, Z. Forgacs, J. Lukacova, S. Roychoudhury, P. Massanyi, and N. Lukac, "Endocrine disruptive effects of cadmium on steroidogenesis: human adrenocortical carcinoma cell line NCI-H295R as a cellular model for reproductive toxicity testing," *Journal of Environmental Science and Health, Part A*, vol. 50, no. 4, pp. 348–356, 2015.

[24] F. De Souza Predes, M. A. S. Diamante, and H. Dolder, "Testis response to low doses of cadmium in Wistar rats," *International Journal of Experimental Pathology*, vol. 91, no. 2, pp. 125–131, 2010.

[25] M. C. Cupertino, K. L. C. Costa, D. C. M. Santos et al., "Long-lasting morphofunctional remodelling of liver parenchyma and stroma after a single exposure to low and moderate doses of cadmium in rats," *International Journal of Experimental Pathology*, vol. 94, no. 5, pp. 343–351, 2013.

[26] R. D. Novaes, I. R. S. C. Maldonado, A. J. Natali, C. A. Neves, and A. Talvani, "Elemental mapping of cardiac tissue by scanning electron microscopy and energy dispersive X-ray spectroscopy: proof of principle in Chaga's disease myocarditis model," *Canadian Journal of Cardiology*, vol. 29, no. 5, pp. 639.e3–639.e4, 2013.

[27] P. L. Sequetto, T. T. Oliveira, I. A. C. Soares et al., "The flavonoid chrysin attenuates colorectal pathological remodeling reducing the number and severity of pre-neoplastic lesions in rats exposed to the carcinogen 1,2-dimethylhydrazine," *Cell and Tissue Research*, vol. 352, no. 2, pp. 327–339, 2013.

[28] P. L. Sequetto, T. T. Oliveira, I. R. S. C. Maldonado et al., "Naringin accelerates the regression of pre-neoplastic lesions and the colorectal structural reorganization in a murine model of chemical carcinogenesis," *Food and Chemical Toxicology*, vol. 64, pp. 200–209, 2014.

[29] R. D. Novaes, A. R. Penitente, R. V. Gonçalves et al., "Effects of Trypanosoma cruzi infection on myocardial morphology, single cardiomyocyte contractile function and exercise tolerance in rats," *International Journal of Experimental Pathology*, vol. 92, no. 5, pp. 299–307, 2011.

[30] R. D. Novaes, A. R. Penitente, A. Talvani, A. J. Natali, C. A. Neves, and I. R. S. C. Maldonado, "Use of fluorescence in a modified disector method to estimate the number of myocytes in cardiac tissue," *Arquivos Brasileiros de Cardiologia*, vol. 98, no. 3, pp. 252–258, 2012.

[31] N. Coombs, A. C. Gough, and J. N. Primrose, "Optimisation of DNA and RNA extraction from archival formalin-fixed tissue," *Nucleic Acids Research*, vol. 27, no. 16, article e12, 1999.

[32] E. C. Santos, R. D. Novaes, D. S. S. Bastos et al., "Modulation of oxidative and inflammatory cardiac response by nonselective 1- and 2-cyclooxygenase inhibitor and benznidazole in mice," *Journal of Pharmacy and Pharmacology*, vol. 67, no. 11, pp. 1556–1566, 2015.

[33] A. W. Obianime and I. I. Roberts, "Antioxidants, cadmium-induced toxicity, serum biochemical and the histological abnormalities of the kidney and testes of the male Wistar rats," *Nigerian Journal of Physiological Sciences*, vol. 24, no. 2, pp. 177–185, 2009.

[34] A. Sarkar, G. Ravindran, and V. Krishnamurthy, "A brief review on the effect of cadmium toxicity: from cellular to organ level," *International Journal of Biotechnology*, vol. 3, no. 1, pp. 17–36, 2013.

[35] E. Marettová, M. Maretta, and J. Legáth, "Toxic effects of cadmium on testis of birds and mammals: a review," *Animal Reproduction Science*, vol. 155, pp. 1–10, 2015.

[36] S. H. M. Bekheet, "Cadmium chloride rapidly alters both BTB tight junction proteins and germ cells in young rat testes," *Egyptian Academic Journal of Biological Sciences*, vol. 2, no. 1, pp. 59–74, 2010.

[37] T. Zhou, X. Jia, R. E. Chapin et al., "Cadmium at a non-toxic dose alters gene expression in mouse testes," *Toxicology Letters*, vol. 154, no. 3, pp. 191–200, 2004.

[38] J. Kim and J. Soh, "Cadmium-induced apoptosis is mediated by the translocation of AIF to the nucleus in rat testes," *Toxicology Letters*, vol. 188, no. 1, pp. 45–51, 2009.

[39] M. S. Kim, B. J. Kim, H. N. Woo et al., "Cadmium induces caspase-mediated cell death: suppression by Bcl-2," *Toxicology*, vol. 145, no. 1, pp. 27–37, 2000.

[40] M. Kondoh, S. Araragi, K. Sato, M. Higashimoto, M. Takiguchi, and M. Sato, "Cadmium induces apoptosis partly via caspase-9 activation in HL-60 cells," *Toxicology*, vol. 170, no. 1-2, pp. 111–117, 2002.

[41] A. Lemarie, D. Lagadic-Gossmann, C. Morzadec, N. Allain, O. Fardel, and L. Vernhet, "Cadmium induces caspase-independent apoptosis in liver Hep3B cells: role for calcium in signaling oxidative stress-related impairment of mitochondria and relocation of endonuclease G and apoptosis-inducing factor," *Free Radical Biology & Medicine*, vol. 36, no. 12, pp. 1517–1531, 2004.

[42] C. M. Shih, W. C. Ko, J. S. Wu et al., "Mediating of caspase-independent apoptosis by cadmium through the mitochondria-ROS pathway in MRC-5 fibroblasts," *Journal of Cellular Biochemistry*, vol. 91, no. 2, pp. 384–397, 2004.

[43] O. H. El-Habit and A. E. Abdel Moneim, "Testing the genotoxicity, cytotoxicity, and oxidative stress of cadmium and nickel and their additive effect in male mice," *Biological Trace Element Research*, vol. 159, no. 1–3, pp. 364–372, 2014.

[44] J. Thompson and J. Bannigan, "Cadmium: toxic effects on the reproductive system and the embryo," *Reproductive Toxicology*, vol. 25, no. 3, pp. 304–315, 2008.

[45] X. Li, P. Yin, and L. Zhao, "Effects of individual and combined toxicity of bisphenol A, dibutyl phthalate and cadmium on oxidative stress and genotoxicity in HepG 2 cells," *Food and Chemical Toxicology*, vol. 105, pp. 73–81, 2017.

[46] A. Djuric, A. Begic, B. Gobeljic et al., "Oxidative stress, bioelements and androgen status in testes of rats subacutely exposed to cadmium," *Food and Chemical Toxicology*, vol. 86, pp. 25–33, 2015.

[47] L. Yuan, A. K. Dietrich, Y. S. Ziegler, and A. M. Nardulli, "17β-Estradiol alters oxidative damage and oxidative stress response protein expression in the mouse mammary gland," *Molecular and Cellular Endocrinology*, vol. 426, no. 426, pp. 11–21, 2016.

[48] M. Takiguchi and S. Yoshihara, "New aspects of cadmium as endocrine disruptor," *Environmental Science and Technology*, vol. 13, no. 2, pp. 107–116, 2006.

[49] A. C. A. Dankers, M. J. E. Roelofs, and A. H. Piersma, "Endocrine disruptors differentially target ATP-binding cassette transporters in the blood-testis barrier and affect Leydig cell testosterone secretion *in vitro*," *Toxicological Sciences*, vol. 136, no. 2, pp. 382–391, 2013.

[50] J. W. Laskey and P. V. Phelps, "Effect of cadmium and other metal cations on *in vitro* Leydig cell testosterone production," *Toxicology and Applied Pharmacology*, vol. 108, no. 2, pp. 296–306, 1991.

[51] D. Gunnarsson, M. Svensson, G. Selstam, and G. Nordberg, "Pronounced induction of testicular $PGF_{2\alpha}$ and suppression of testosterone by cadmium—prevention by zinc," *Toxicology*, vol. 200, no. 1, pp. 49–58, 2004.

[52] S. G. Haider, "Cell biology of Leydig cells in the testis," *International Review of Cytology*, vol. 233, pp. 181–241, 2004.

[53] A. S. Midzak, H. Chen, and V. Papadopoulos, "Leydig cell aging and the mechanisms of reduced testosterone synthesis," *Molecular and Cellular Endocrinology*, vol. 299, no. 1, pp. 23–31, 2009.

[54] P. Bobbert, C. Scheibenbogen, A. Jenke et al., "Adiponectin expression in patients with inflammatory cardiomyopathy indicates favourable outcome and inflammation control," *European Heart Journal*, vol. 32, no. 9, pp. 1134–1147, 2011.

[55] T. Wang, X. Mao, H. Li et al., "*N*-Acetylcysteine and allopurinol up-regulated the Jak/STAT3 and PI3K/Akt pathways via adiponectin and attenuated myocardial postischemic injury in diabetes," *Free Radical Biology & Medicine*, vol. 63, pp. 291–303, 2013.

[56] A. Pfaehler, M. K. Nanjappa, E. S. Coleman et al., "Regulation of adiponectin secretion by soy isoflavones has implication for endocrine function of the testis," *Toxicology Letters*, vol. 209, no. 1, pp. 78–85, 2012.

[57] A. Xu, K. W. Chan, R. L. C. Hoo et al., "Testosterone selectively reduces the high molecular weight form of adiponectin by inhibiting its secretion from adipocytes," *Journal of Biological Chemistry*, vol. 280, no. 18, pp. 18073–18080, 2005.